APPLICATION OF STRUCTURAL MONITORING IN MANAGEMENT DECISIONS FOR LARGE INFRASTRUCTURE

by

Joshua A. Levy

Submitted in partial fulfilment of the requirements
for the degree of Master of Applied Science

at

Dalhousie University
Halifax, Nova Scotia
November 2011

DALHOUSIE UNIVERSITY

DEPARTMENT OF CIVIL AND RESOURCE ENGINEERING

The undersigned hereby certify that they have read and recommend to the Faculty of Graduate Studies for acceptance a thesis entitled “Application of Structural Monitoring in Management Decisions for Large Infrastructure” by Joshua A. Levy in partial fulfillment of the requirements for the degree of Master of Applied Science.

Dated: November 18, 2011

Supervisor: __________________________________

Readers: __________________________________

____

DALHOUSIE UNIVERSITY

DATE: November 18, 2011

AUTHOR: Joshua A. Levy

TITLE: Application of Structural Monitoring in Management Decisions for Large Infrastructure

DEPARTMENT OR SCHOOL: Department of Civil and Resource Engineering

DEGREE: MASc CONVOCATION: May YEAR: 2012

Signature of Author

Table of Contents

List of Tables ix
List of Figures x
Abstract xiii
List of Abbreviations and Symbols Used xiv
Acknowledgements xvii
Chapter 1. Introduction 1
  1.1 Halifax Harbour Crossing 1
  1.2 Project Purpose 2
  1.3 Methodology 2
    1.3.1 Instrumentation of Selected Bridge Members 2
    1.3.2 Calibration of Existing Numerical Model 3
    1.3.3 Long-Term Data Collection 3
    1.3.4 Comparison with Canadian Code Loads 3
Chapter 2. Relevant Literature 4
  2.1 Bridge Management 4
    2.1.1 Time/Age-Based Methods 4
    2.1.2 Visual Inspection 4
    2.1.3 Semi-Analytical Methods 5
    2.1.4 Structural Health Monitoring 5
  2.2 Long-Span Bridge Lane Loads 5
    2.2.1 Published Literature – Buckland et al. 1978 & Buckland et al. 1980 6
    2.2.2 American Standards – ASCE (1981) 7
    2.2.3 American Standards – AASHTO (2007) 8
    2.2.4 Canadian Standards – CAN/CSA S6-88 9
    2.2.5 Canadian Standards – OHBDC 1991 9

2.2.6 Canadian Standards – CHBDC 2006 10

2.2.7 European Standards – BS 5400-2:1978 11

2.2.8 European Standards – Eurocode 1 (2002) 12

2.2.9 Published Literature – Lutomirska 2009 13

Chapter 3. Description of A. Murray MacKay Bridge and Existing Evaluation 15

3.1 Structural Description 15

3.1.1 Main Towers 15

3.1.2 Cables 16

3.1.3 Deck System 16

Chapter 4. Project Objective 18

4.1 Numerical Model 18

4.2 Model Calibration 20

4.3 Code-Based Bridge Evaluation 21

Chapter 5. MacKay Bridge Monitoring System 22

5.1 Gauge Locations 22

5.2 Gauge Installation 25

5.3 System Wiring 27

5.4 Data Acquisition 28

5.5 Instrument Scaling Factor 28

5.5.1 Equipment 29

5.5.2 Procedure 29

5.5.3 Discussion 29

Chapter 6. Gauge Type Correction 31

6.1 Small-Scale Laboratory Testing 31

6.2 Full-Scale Laboratory Testing 32

6.3 Full-Scale Field Testing 35

Chapter 7. System Testing 39
7.1 Full-Scale Calibration Testing... 39
7.1.1 Calibration Truck 39
7.1.2 Static Testing 40
7.2 Repeatability of Data 42
7.3 Influence Lines 43
7.4 Impact of Opposing Traffic 44
7.5 Scan Rate Suitability 45
Chapter 8. Impact of Surface Preparation.. 49
8.1 Experimental Testing 50
8.2 Surface Preparation 50
8.2.1 Preparation Depth 51
8.2.2 Laboratory Specimen 53
8.2.3 Testing Procedure 55
8.2.4 Discussion 56
8.3 Numerical model of laboratory specimen 56
8.3.1 Theoretical and Laboratory Test Comparison 59
8.4 Parametric Investigation.. 60
8.4.1 Single Sided Surface Preparation.. 61
8.4.2 Double Sided Surface Preparation 61
8.4.3 Transition Zone 62
8.4.4 Diameter of Prepared Area 63
8.4.5 Interpretation of Model Results 64
8.4.6 Discussion 65
Chapter 9. Numerical Model Correction Factor 67
Chapter 10. Long-Term Data Collection 69

10.1 Data Management 69

10.2 Post-Processing 69

10.2.1 Zeroing 69

10.2.2 Temperature Correction 70

10.2.3 Traffic Event Identification 71

10.3 Interpretation 73

10.4 Characterization of Peak Traffic Events 75

10.4.1 Visual Examination of Peak Traffic Events 79

10.4.2 Comparison of Peak Pairs with Calibration Data 84

10.5 Data Errors and Plausible Data Problem 86

Chapter 11. Application of Collected Data 88

11.1 Identification of Influence Zones 88

11.2 CHBDC 2006 Strain Predictions 89

11.3 Probable Extreme Data 91

11.4 Comparison of Predicted Extreme Strain with Design Strain 95

Chapter 12. Conclusions and Recommendations 97

12.1 Fine Calibration of Existing Numerical Model 97

12.2 Comparison of Live Load Effects with Code Requirements 97

12.3 Instrumentation and Data Validation 97

12.4 Recommendations 99

References 100

Appendix I – Gauge Repeatability December 2009 - March 2010 102

Appendix II – Influence Lines From Slow Speed Tests 114

Appendix III – Gauge Comparison March 2010 – Numerical Model 126

Appendix IV – Long-Term Data Histograms 138

Appendix V – Peak Gauge Pair Examination 163

Appendix VI – Influence Zones From Calibration Test Data 176

Appendix VII – Summary of Detailed Calculations for CHBDC Live Load 179
Appendix VIII – Gumbel Probability Plots 181

List of Tables

Table 2-1 : OHBDC number of design lanes 10

Table 2-2 : OHBDC lane load modification factors 10

Table 5-1 : Datalogger gauge naming scheme 25

Table 5-2 : Calibrated gauge factors and conversion factors 30

Table 6-1 : Gauge placement dimensions 37

Table 7-1: Static positions from HMT 40

Table 8-1 : Comparison of web gauges on diagonals 49

Table 8-2 : Grinding versus time 52

Table 8-3 : Lab specimen surface preparation 54

Table 10-1 : Temperature corrections 71

Table 10-2 : Extreme strain readings (mm/mm x 10^{-6}) 75

Table 10-3 : Peak traffic event dates 76

Table 10-4 : Approximate speed of vehicle causing peak traffic event 83

Table 10-5 : Comparison of peak and calibration strains 85

Table 10-6 : Comparison of top versus bottom gauges for calibration and peak pairs..... 86

Table 11-1 : Peak strain ratios 88

Table 11-2 : Unfactored CHBDC design strains 91

Table 11-3 : Gumbel constants 93

Table 11-4 : Calculated values for N_T, top gauges 94

Table 11-5 : Calculated values for N_T, bottom gauges 94

Table 11-6 : Probable extreme data 95

Table 11-7 : Ratio of extreme predicted strain versus unfactored CHBDC design strain 95

Table 11-8 : Ratio of extreme predicted strain versus unfactored CHBDC design strain 96

List of Figures

Figure 2-1 : Traffic loading for long-span bridges (Buckland et al. 1978) 7
Figure 2-2 : AASHTO design truck (AASHTO 2007) 8
Figure 2-3 : Design truck 9
Figure 2-4 : OHBDC design truck 10
Figure 2-5 : CHBDC design truck 11
Figure 2-6 : CHBDC lane load with 80% design truck (CHBDC 2006) 11
Figure 2-7 : Lane load (adapted from BS 1978) 12
Figure 2-8 : North American multilane distribution (adapted from Lutomirska 2009) 14
Figure 2-9 : Eurocode multilane load distribution (adapted from Lutomirski 2009) 14
Figure 2-10 : Actual multilane distribution (adapted from Lutomirski 2009) 14
Figure 3-1 : MacKay layout (adapted from B&T) 15
Figure 3-2 : Main tower cruciform layout (adapted from B&T) 16
Figure 3-3 : Main cable hexagonal layout (adapted from B&T) 16
Figure 3-4 : Orthotropic deck and transverse stiffening trusses (adapted from B&T) 17
Figure 3-5 : Longitudinal stiffening truss layout 17
Figure 4-1: Global bridge model (courtesy of Buckland and Taylor) 18
Figure 4-2: Local bridge model (courtesy of Buckland and Taylor) 18
Figure 4-3: Modeled deck system (adapted from B&T) 20
Figure 5-1: Instrumented section (adapted from B&T) 22
Figure 5-2 : Longitudinal stiffening truss 22
Figure 5-3 : Longitudinal stiffening truss profile (adapted from B&T) 23
Figure 5-4 : Lateral stiffening truss 23
Figure 5-5 : Lateral stiffening truss plan (adapted from B&T) 23
Figure 5-6 : Flange gauge pair next to diagonal gusset plate 24
Figure 5-7: Strain gauge positioning on web and flanges 24
Figure 5-8 : Full bridge completion terminal (Campbell Scientific 2007) 25
Figure 5-9 : Foil type weldable strain gauge 26
Figure 5-10 : Welding pattern (Vishay 2010) 26
Figure 5-11 : Dummy gauge 27

Figure 5-12 : Logger A completed wiring 28
Figure 6-1: Dogbone tensile specimen 31
Figure 6-2 : Tensile testing results 32
Figure 6-3: Instrumented lab specimen 33
Figure 6-4: Lab specimen cross-section 34
Figure 6-5 : Full-scale laboratory compression test specimen 34
Figure 6-6 : Gauge type comparison - laboratory testing - stepped load 35
Figure 6-7 : Profile of diagonal with new gauges 36
Figure 6-8 : Gauge type comparison - bridge member 36
Figure 6-9 : Section A-A (from Figure 6-7) 37
Figure 7-1 : Calibration truck profile 39
Figure 7-2 : Calibration truck footprint 40
Figure 7-3 : Jersey barrier placement 40
Figure 7-4 : Lane numbering 41
Figure 7-5 : Lateral truck positions, lanes 1 through 4 42
Figure 7-6 : Positioning of calibration truck for static testing 42
Figure 7-7 : Gauge comparison Dec versus Mar 43
Figure 7-8 : Sample influence line 44
Figure 7-9: Comparison of truck behaviour in normal travel and opposing direction 45
Figure 7-10 : Calibration truck COM 45
Figure 7-11 : Slow speed versus fast speed 46
Figure 7-12 : Fast speed data 46
Figure 7-13 : Slow speed curve fit 47
Figure 7-14 : Actual versus calculated peaks 48
Figure 8-1 : Mismatched strain readings 50
Figure 8-2 : Prepared area and transition zone 51
Figure 8-3 : Diameter of the prepared surfaces 51
Figure 8-4 : Grinder and sanding wheel in field 52
Figure 8-5 : Pitting corrosion 53
Figure 8-6 : Cross-section comparison 54
Figure 8-7 : Cross-section through web 55

Figure 8-8 : Laboratory testing results 56
Figure 8-9 : Isotropic view of web through centreline of mesh 57
Figure 8-10 : Sample finite element mesh 58
Figure 8-11 : Qualitative sample finite element strain profile 59
Figure 8-12 : Comfirmation with theory 60
Figure 8-13 : Single-sided surface preparation 61
Figure 8-14: Normalized strain for 1.5 mm double sided preparation 62
Figure 8-15 : Normalized transition zone 63
Figure 8-16 : Normalized preparation area 63
Figure 8-17 : Relating gauge difference to total preparation 64
Figure 8-18 : Relating gauge average to total preparation 65
Figure 9-1 : Model vs static results 67
Figure 9-2: Global average fit 68
Figure 10-1 : Sample of weekly data file 69
Figure 10-2 : 60 second sample of strain deviation during zero recording 70
Figure 10-3 : Increasing data trend flowchart 72
Figure 10-4 : Decreasing data trend flowchart 73
Figure 10-5 : Sample long-term histogram (gauge #1 D-T) 74
Figure 10-6 : Matching peak event pairs 77
Figure 10-7 : Extended matching peak event pairs 78
Figure 10-8 : Slow speed traffic event 80
Figure 10-9 : Mixed traffic event 81
Figure 10-10 : Fast speed traffic event 82
Figure 10-11 : Sample strain reversal 83
Figure 10-12 : Comparison of top versus bottom gauges for calibration and peak pair ... 86
Figure 10-13 : Plausible data 87
Figure 11-1 : Sample slow speed lane comparison 89
Figure 11-2 : Influence zones for diagonal #4 89
Figure 11-3 : Manual curve fit 90
Figure 11-4 : Gumbel distribution curve fit 92

Abstract

The traditional bridge evaluation process contains uncertainty that affects management decisions. Numerical models require assumptions regarding structural response, and code load models are inherently conservative to ensure uniform applicability.

This research investigated how structural monitoring could reduce uncertainty in the evaluation and management process. Targeted instrumentation was implemented on the MacKay Bridge. Controlled load testing was conducted to refine an existing numerical model. Long-term monitoring was completed to compare extreme in-situ traffic effects with the Canadian Highway Bridge Design Code. Throughout the project, accuracy of information collected was a priority; deviation from code recommendations requires absolute confidence in the data.

Outputs from controlled testing indicated that the existing numerical model for load distribution and structural response required minimal tuning. Long-term testing indicated that actual load effects are less than code requirements.

Results from this thesis show that structural monitoring can reduce uncertainty in structural evaluation and management decisions for infrastructure.

List of Abbreviations and Symbols Used

AASHTO	American Association of State Highway and Transportation Officials
ASCE	American Society of Civil Engineers
BS	British Standard
B&T	Buckland & Taylor Ltd.
CAN/CSA	Canadian Standards Association
CDF	cumulative distribution function
CHBDC	Canadian Highway Bridge Design Code
COM	centre of mass
CS-W	CAN/CSA design truck of weight W
C/L	centreline
DAL	Dalhousie University
DMT	Dartmouth main tower
D-B	diagonal, bottom of web
D-T	diagonal, top of web
FHWA	Federal Highway Administration
FLBN	flange, lower node, bottom of web, North side
FUTS	flange, upper node, top of web, South side
HHB	Halifax Harbour Bridges
HMT	Halifax main tower
HRM	Halifax Regional Municipality
ISIS	Intelligent Sensing for Innovative Structures
KEL	knife edge load
LRFD	load and resistance factor design
MVE	multi-vehicle event

NSTIR	Nova Scotia Department of Transportation and Infrastructure Renewal
OHBDC	Ontario Highway Bridge Design Code
OHBDCC	Ontario Highway Bridge Design Code Commentary
Opp	opposing
PVC	polyvinyl chloride
RAT	Remote Access Technology
SHM	structural health monitoring
TC	thermocouple
UDL	uniformly distributed load
WIM	weigh in motion

A	depth of preparation on side A (mm)
B	depth of preparation on side B (mm)
D/C	demand versus capacity ratio
F	remaining live load capacity (N)
FG	system gauge factor
$F_{xn}(X)$	Gumbel approximation
ℓ	dynamic load allowance
n	number of data points
N_T	number of traffic events
R_C	shunt resistance (Ω)
R_G	initial circuit resistance (Ω)
s	standard extremal variate
SSE	sum of squared errors
u_n	the characteristic largest value of X

UR_r	factored member capacity (N)
w	web thickness (mm)
W	weight of design truck (kN)
X	model correction factor
X, X_n	CDF of collected data
$\alpha_A A$	factored loads other than dead or live loads (N)
$\alpha_D D$	factored dead load (N)
$\alpha_L L$	factored live load (N)
α_n	an inverse measure of the dispersion of X_n
$\varepsilon_{m\ max}$	maximum expected strain (ε)
ε_s	expected strain (ε)
$\varepsilon_{n\ year}$	maximum expected strain in n years (ε)

Acknowledgements

Without the permission of Halifax Harbour Bridges, this project would not have been possible; thank you for giving me this opportunity. Similarly, Buckland & Taylor's cooperation and assistance were crucial to the success of the project. Halifax Harbour Bridges and Buckland & Taylor provided reports, drawings and modeling information/output that are not available to the public; these have been referenced in the text as (courtesy of B&T) or (courtesy of HHB). Where drawings have been modified in the text, they have been referenced as (adapted from B&T).

I would like to thank Mr. Brian Liekens and the staff at Remote Access Technologies for their aid in the field; Cherubini Metal Works, for their donation of the laboratory test specimen; Mr. John Everick, for his aid in developing software for data analysis; and the students and staff at Dalhousie University that assisted in other ways.

I express appreciation to my advisory committee, Dr. Jane Thorburn and Dr. Muhammad Habib for their input into the development and outcome of this thesis.

Finally, I would like to express my gratitude to Dr. John Newhook for his advice, guidance, and encouragement throughout this project.

Chapter 1. Introduction

As much of our significant infrastructure continues to age, the importance of infrastructure management is coming to the forefront. Decisions must be made based on the best possible information to effectively make use of limited resources. Combining engineering mechanics with structure-specific information can play a significant role in removing uncertainty in these management decisions. Combining loads and behaviours found through structural monitoring with numerical models augments what was traditionally a theoretical exercise to develop an accurate representation of the structure.

1.1 Halifax Harbour Crossing

One of the realities of developing cities in the vicinity of harbours is the necessity to cross water. Shortly after the founding of Halifax in the 1749, and the subsequent establishment of the community of Dartmouth in 1750, a continuous ferry service was begun to transport people, as well as goods, across the harbour. The service grew to what it has become today, the oldest continuously operational salt-water ferry service in North America (HRM 2011).

As Halifax and Dartmouth grew, it became apparent that the ferry service was insufficient. Halifax Harbour Bridges (HHB, formerly Halifax Dartmouth Bridge Commission) was created in 1950 by a statute of the province of Nova Scotia. In 1955 the Angus L. Macdonald Bridge became the first permanent link across the harbour. The bridge quickly became a key point of access to peninsular Halifax, and in 1970, the A. Murray MacKay Bridge (MacKay Bridge) was opened at the northern end of the Narrows. Demand on the bridges continued to grow and in 1999, the Macdonald Bridge was widened to accept a third lane.

Access to peninsular Halifax from the north side is limited by two suspension bridges however; all heavy truck traffic must cross the A. Murray MacKay Bridge. The bridge sees a daily average of 52,000 crossings; a maximum 116,000 daily crossings was recorded December 17th 2009.

1.2 Project Purpose

As part of the continuing maintenance plan for the harbour bridges, HHB contracted Buckland & Taylor Ltd. (B&T) of Vancouver to conduct a structural evaluation of the MacKay Bridge. This evaluation involved a comprehensive assessment of the stiffening trusses which support the bridge deck. To supplement the evaluation, Remote Access Technologies and Dalhousie University (RAT/DAL) were contracted to supply and install a structural monitoring system on select members of the stiffening trusses.

The purpose of this thesis was to investigate how structural monitoring can be used to improve traditional bridge evaluation and management methods. The research included two principle components: 1) the fine calibration of B&T's numerical model for load distribution, and 2) the verification of live load traffic models used in the numerical model.

The modeling of any structure requires assumptions regarding the behaviour of the structure. If a high degree of confidence in the model can be established through targeted instrumentation, all components of the model can be used with certainty; not just the instrumented members.

The load input models (in this case, traffic models) are a statistical extrapolation based on studies completed elsewhere and are developed to ensure a target level of reliability wherever a given code may be implemented. This leads to conservative decisions being made in the majority of situations. Site-specific traffic data will allow the engineer to understand the stresses placed on the structure in question, thereby removing excess conservatism required in a general load model.

1.3 Methodology

The project contained four distinct phases; these are briefly described below, and more extensively later in the thesis.

1.3.1 Instrumentation of Selected Bridge Members

Data collection was made possible by the instrumentation of selected members on the MacKay Bridge. This instrumentation process is described in Section Chapter 5.

1.3.2 Calibration of Existing Numerical Model

The second phase of the project was the fine calibration of B&T's numerical model. This was accomplished through the development of a calibration factor based on controlled testing. The calibration factor is described in Section 5.5 and Chapter 9.

1.3.3 Long-Term Data Collection

Fourteen months of continuous live load data were collected. The collection process and results are described in Chapter 10.

1.3.4 Comparison with Canadian Code Loads

Results from long-term testing are compared with Canadian design loads in Section 11.4.

Chapter 2. Relevant Literature

2.1 Bridge Management

Traditionally, decisions relating to bridge management and maintenance have been performed based on experience. These methods include time or age-based methods, visual inspections and semi-analytical methods. These methods make various assumptions regarding bridge conditions while few have attempted to determine the actual state of the bridge. Still fewer examine the specific traffic crossing the bridge under evaluation. In more recent times, structural health monitoring has been employed more frequently to monitor the long-term behavior of new materials, as well as aiding in the management process (ISIS 2006).

2.1.1 Time/Age-Based Methods

Based on experience in similar structures, decisions can be made as to the state of a bridge prior to construction. It is accepted that materials degrade over time in a predictable manner assuming that unexpected damage does not occur. Therefore preventative maintenance or replacement can be conducted with age (or use) as the principle variable (Neves et al. 2006). For example, concrete wearing surfaces could be expected to degrade over a period of time. If left unaltered, the deck would become unusable after 25 years. Therefore one could repair the deck after 20 years, extending the life without the lost use or expense of complete replacement.

2.1.2 Visual Inspection

Traditionally bridge condition data has been collected by visual inspection. Assumptions about the state of a bridge are made based on visual changes to the surface conditions; deterioration, damage and distress (Testa & Yanev 2002). Any internal changes remain unobserved resulting in an incomplete picture of the structure. In addition, visual inspections inherently contain many subjective judgments about the condition or severity of visible deterioration and hence are highly dependent on the skill, training and experience of the inspector.

Annual inspections are conducted on the highway bridges in Nova Scotia (NSTIR 2011). Following inspection, maintenance or replacement is prioritized based on several criteria including extent of degradation and the use of the structure. Other jurisdictions use similar inspection protocol and ranking systems. The Federal Highway Administration (FHWA) has traditionally used a system based on the 'current' state of a bridge (Arora 2009); following inspections, the information is used to grade each bridge against the initial designed state – once a threshold condition is reached (70% for example) the bridge is scheduled for repair or replacement.

Many highway agencies are becoming more proactive in their network management, favouring preventative maintenance based on early signs discovered during inspections. This allows the region as a whole to better manage all bridges. On a local scale, addressing degradation early extends the useful life of a structure (Arora 2009).

2.1.3 Semi-Analytical Methods

When questions arise as to the suitability of a bridge for increased loads, visual inspections may be used in conjunction with analytical methods to determine the bridge capacity. Combining in-situ observations based on the experience of the inspector for 'design' data, analyses can be completed. While dimensional degradation of members can be quantified based on field measurements, internal condition is still unobserved. Analyses must account for uncertainty in the field condition.

2.1.4 Structural Health Monitoring

Structural Health Monitoring (SHM) permits decisions to be made based on quantifiable, unbiased data. The structural monitoring techniques permit access to information about the condition and performance of a structure based on structural response to applied load (ISIS 2006).

Long-term monitoring allows the behavior of a bridge to be examined over time, providing the ability to effectively maintain the structure, improve future designs and identify damaged or degraded states (Catbas et al. 2008).

2.2 Long-Span Bridge Lane Loads

The majority of bridges can be considered short-span or medium-span bridges. The codes developed to assist engineers in designing these shorter bridges generally do not include specific provisions for long-span bridges. As a result, there is little guidance regarding traffic load patterns for long-span bridges.

This section presents the lane loads and accompanying vehicular loads (or point) loads outlined in the ASCE (1981), AASHTO (2007), CAN/CSA S6 (1988), OHBDC (1991), CHBDC (2006), BS 5400-2 (1978) and Eurocode 1 (2002), to represent closely packed, slow-moving traffic. This is accompanied by reference to two relevant publications by Buckland et al. (1978 & 1980) and Lutomirska (2009).

2.2.1 Published Literature – Buckland et al. 1978 & Buckland et al. 1980

Buckland et al. (1978 & 1980) published the results of a traffic analysis conducted in Vancouver, Canada. To gain an understanding of both regular traffic (few trucks) and mixed traffic, counts were conducted on both the Lions Gate Bridge (2.4% trucks – weight restriction) and the Second Narrows Bridge (7.4% trucks) in Vancouver. Data from the traffic counts was input into a numerical model which simulated three months of traffic.

The study produced a set of curves (Figure 2-1) which prescribe a uniform load per unit length (u), dependent on the loaded length on the bridge. While the percent of heavy trucks within the traffic pattern does affect the uniform load, the authors conclude that the maximum load was not overly sensitive to the truck intensity. Associated with the prescribed uniform load is a point load (P), which increases with loaded length.

In the recommendations, it is noted that the loaded length should be taken as the length of the influence line which would increase the load on the component in question, not necessarily the total length of the bridge, or the span.

To apply Figure 2-1, the loaded length is selected on the horizontal axis. Moving vertically to the curves representing the appropriate truck percentages, values for uniform load can be read off the inner vertical axis while those for the concentrated load (P) can be found on the outer vertical axis. For example, a loaded length of 61 m and a truck concentration of 7.4% would give u = 13 kN/m and P = 240 kN.

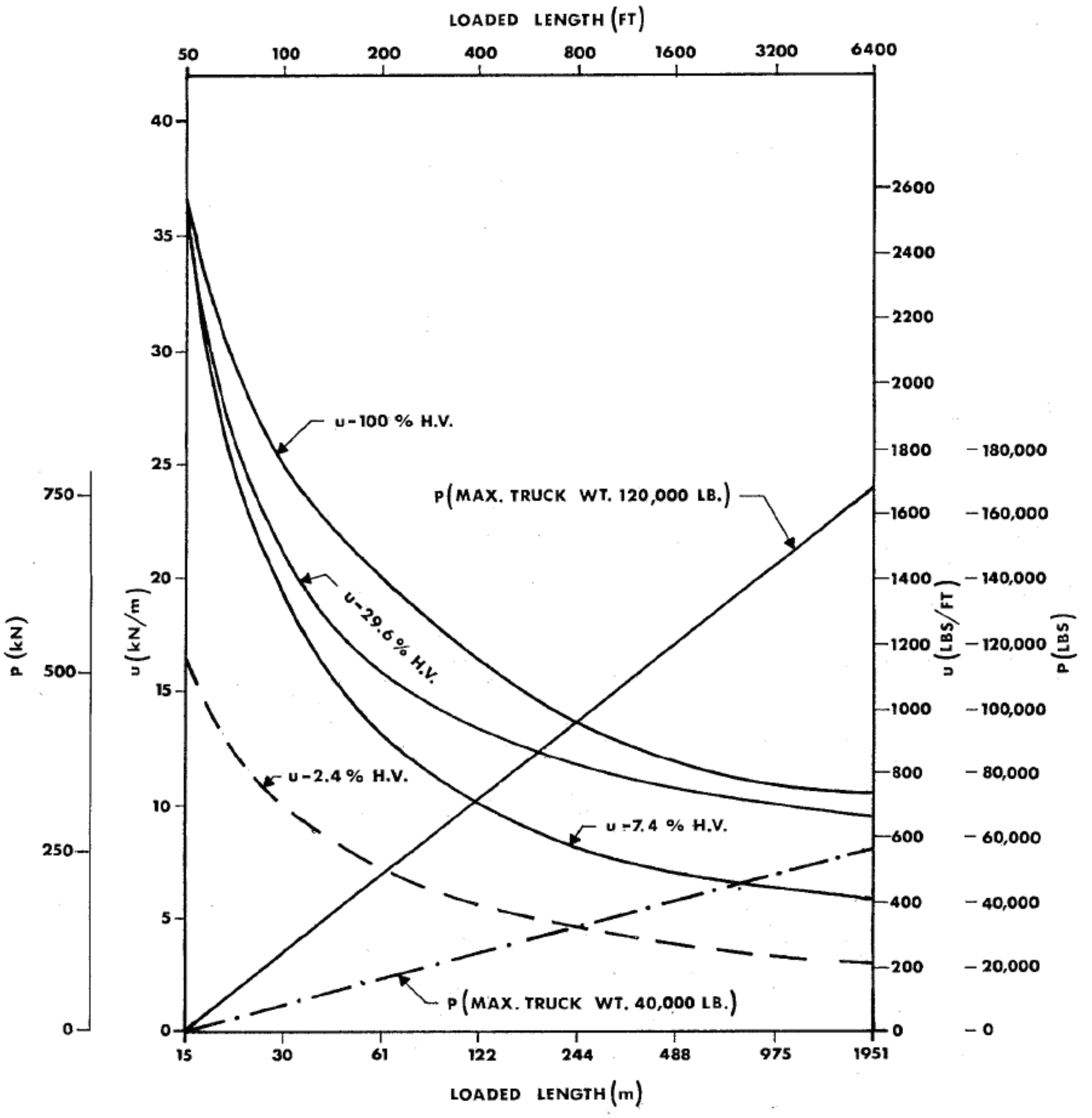

Figure 2-1 : Traffic loading for long-span bridges (Buckland et al. 1978)

2.2.2 American Standards – ASCE (1981)

Shortly after the publication of the study by Buckland et al. (1978, 1980), the results were adopted by the American Society of Civil Engineers as a recommendation for long-span bridge loads. While the curves were adopted, the lesser curves representing 2.4% traffic and the smaller truck, from the Lions Gate weight restriction, were removed. It was recognized that the uniform loads depended on closely spaced traffic which is generally slow moving; therefore no dynamic load factor was recommended.

Some additional guidance to the use of u and P was provided in the commentary. The worst-case load for the component in question is to be determined using the uniform load (u) by placing the load in the positive regions of the influence lines. After this, a single point load (P) is to be applied. This removes the possibility of unnecessarily large values of P.

It should be noted that the ASCE recommendations were not design codes – they were guidelines to best-practice.

2.2.3 American Standards – AASHTO (2007)

The Association of American State Highway and Transportation Officials (AASHTO) makes no reference to span limits when discussing live loads, however; Section 6.1 specifically states that 'The LRFD provisions have no span limit'. This is furthered by discussion in Section 4 by providing methods for designing various configurations of long-span bridges.

The AASHTO standard requires a combination of lane load and a fraction of the design truck, not a single point load. The lane load is 0.64 klf (9.4 kN/m) and is distributed laterally over a 10ft (3.0 m) design lane. The truck is a three axle configuration (Figure 2-2), with a total weight of 72 kip (320 kN). The design truck is to be applied in conjunction with the lane load to determine the worst-case load effect. Truck axles are to be ignored if they reduce the effect on the structure.

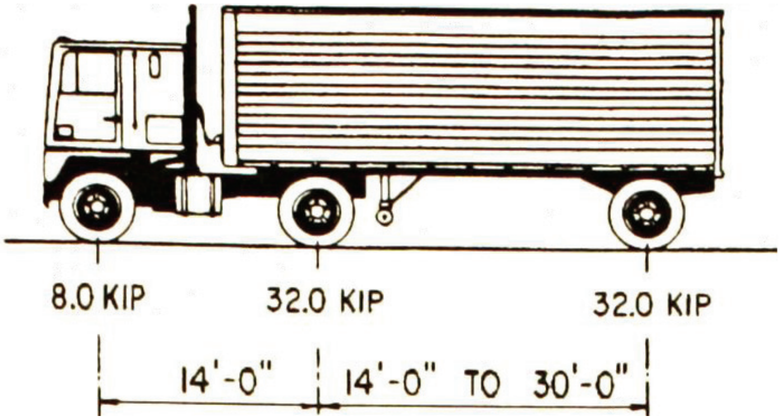

Figure 2-2 : AASHTO design truck (AASHTO 2007)

2.2.4 Canadian Standards – CAN/CSA S6-88

CAN/CSA S6-88 is specified as being applicable to bridges with a span of less than 100 m. Prior to the amalgamation with the OHBDC, a lane load of 0.02W was specified where the design truck weighed 600 kN (therefore 12 kN/m). This lane load was applied along with a fraction of the design truck shown in Figure 2-3.

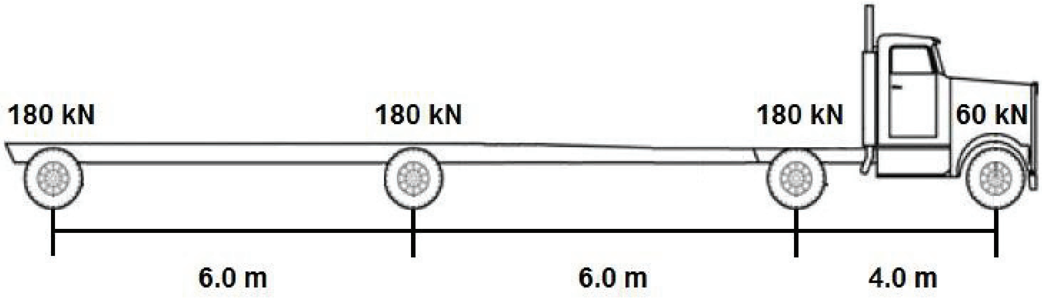

Figure 2-3 : Design truck

Design lanes and multi-lane reduction factors are identical to those found in the Ontario Highway Bridge Design Code (OHBDC), shown in Table 2-1 and Table 2-2.

The S6 commentary describes the lane load as representing multiple CS-W trucks with a minimum spacing of 10 m.

2.2.5 Canadian Standards – OHBDC 1991

The forward in the 3rd edition of the OHBDC (1991) stated that the code has been extended to cover bridges up to 150 m in span.

The uniform load specified is 10 kN/m, in addition to 70% of the OHBDC truck, where axles not contributing to a maximum load shall be ignored. The OHBDC truck weighs 740 kN and is shown in Figure 2-4. The number of design lanes is specified based on the deck width and shown in Table 2-1. When more than one design lane is to be loaded, a reduction factor shall be applied to the load, as specified in Table 2-2.

.

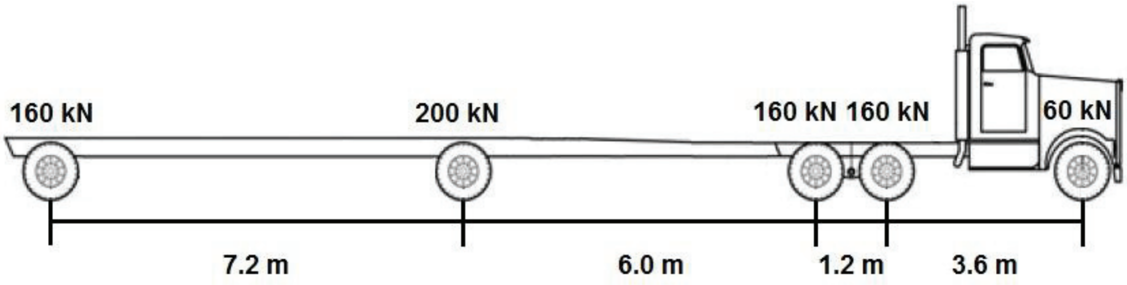

Figure 2-4 : OHBDC design truck

The commentary (OHBDCC 1991) explained that the lane load was developed based on placing up to three OHBDC trucks in a lane, with a minimum of 10 m between them.

Table 2-1 : OHBDC number of design lanes

Design Lane Width	Number of Lanes
6.0 m or less	1
over 6.0 m to 10.0 m	2
over 10.0 m to 13.5 m	3
over 13.5 m to 17.0 m	4
over 17.0 m to 20.5 m	5
over 20.5 m to 24.0 m	6
over 24.0 m to 27.5 m	7
over 27.5 m	8

Table 2-2 : OHBDC lane load modification factors

Number of Loaded Design Lanes	Modification Factor
1	1.00
2	0.90
3	0.80
4	0.70
5	0.60
6 or more	0.55

2.2.6 Canadian Standards – CHBDC 2006

The Canadian Highway Bridge Design Code (CHBDC) is the result of the amalgamation of the OHBDC (1991) and CAN/CSA (1988). The code does not specify a maximum length of bridge, however designers are warned that the code does not necessarily apply in full to long-span bridges – long-span bridge is then defined as having any single span longer than 150 m.

Similar to other current codes, the CHBDC prescribes a lane load and a truck load to be used in tandem. The base lane load is 9 kN/m, this is used with 80% of the CHBDC truck, where the design truck weighs 625 kN. The CHBDC design truck is shown in Figure 2-5 and the combined truck and lane load are shown in Figure 2-6.

When multiple lanes are loaded, the modification factors from Table 2-2 are to be used.

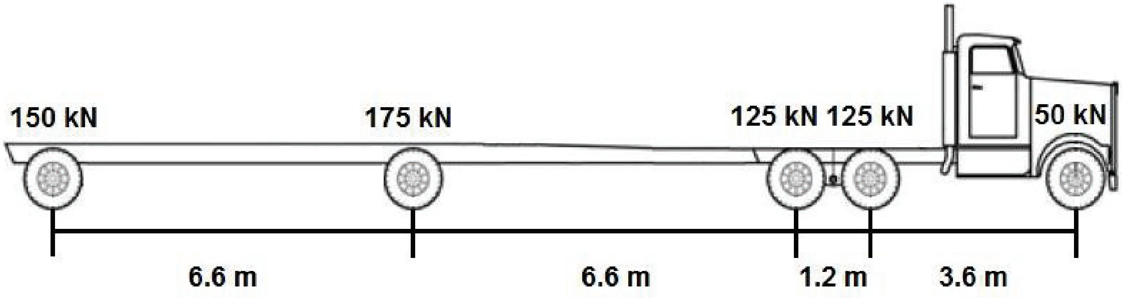

Figure 2-5 : CHBDC design truck

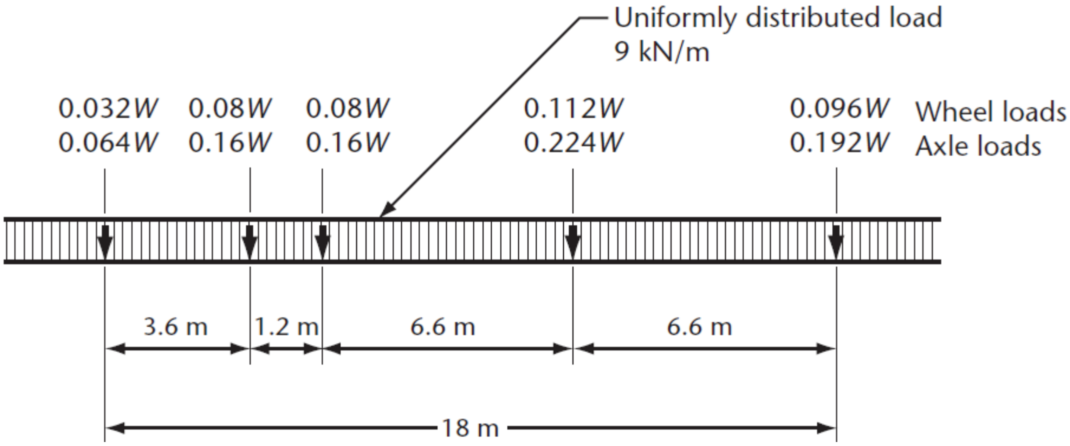

Figure 2-6 : CHBDC lane load with 80% design truck (CHBDC 2006)

2.2.7 European Standards – BS 5400-2:1978

The British Standard (BS) laid out a lane-load for bridges that was extended to long-span bridges. The uniformly distributed load (UDL) is to be applied in the positive section of the influence line. The magnitude of the applied line load depends on the loaded length of the component in question. Figure 2-7 shows the continuous function that was prescribed. For loaded lengths greater than 380 m, the lane load is 9 kN/m.

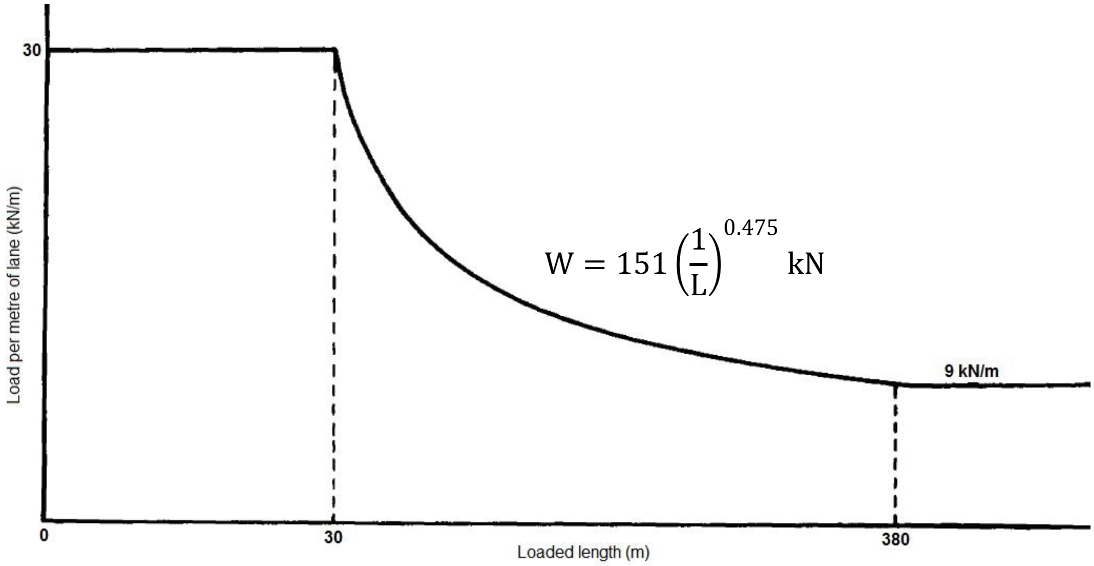

Figure 2-7 : Lane load (adapted from BS 1978)

Accompanying the uniform lane load is a knife edge load (KEL) of 120 kN applied in the positive region of the influence line.

For this load scenario, the bridge deck is divided into notional lanes where the lanes are between 2.8 m and 3.0 m. The UDL and KEL are applied in full to two adjacent notional lanes and the remaining notional lanes receive 1/3 of the load.

2.2.8 European Standards – Eurocode 1 (2002)

Replacing the aging British Standard, Eurocode provides guidance that is applicable to all of Europe. While the code was calibrated for load lengths of less than 200 m, the committee notes that the traffic loads are ‘safe-sided’ for lengths over 200 m.

Eurocode 1, Part 1-2 gives a traffic lane load of 9 kN/m^2 for use on bridges in the positive area of the influence line. The lane load is applied to the primary notional lane while the others receive a load of 2.5 kN/m^2. The notional lanes are 3.0 m wide; any remaining deck receives the reduced UDL.

Two axle loads are applied 1.2 m apart in the notional lanes; the wheels are spaced at 2.0 m. The axle loads in lanes 1 through 3 are 300 kN, 200 kN and 100 kN respectively. Other lanes receive no axle loads.

2.2.9 Published Literature – Lutomirska 2009

Lutomirska (2009) makes the most recent attempt to compare existing live load models, and to develop a new live load model for long-span bridges in North America. His efforts examined data from across the United States using video recordings and Weigh in Motion (WIM) data, along with statistical models, to conduct a study very similar to that of Buckland et al. (1978, 1980). The goal of the study was to develop a code-based approach for traffic loads; therefore calibration factors, multi-lane distribution and dynamic factors were examined. This would allow decisions to be based on reliability of the system.

It was concluded that a uniform lane load of 0.64 k/ft and the HL-93 Design Truck described by AASHTO were to be used. This recommendation is identical to the current AASHTO codes. The results of the study are not surprising because much of the data used was supplied by the FHWA.

Lutomirska (2009) makes a point of graphically comparing multi-lane distribution for various international codes against that found in his research. It was found that the codes tend to simplify the actual multilane distribution. In North America a uniform reduction factor is applied (Figure 2-8). By contrast, Eurocode 1 implements a factor for the primary lane, and a second factor for all remaining lanes (Figure 2-9). The actual distribution requires unique factors for all lanes being loaded (Figure 2-10).

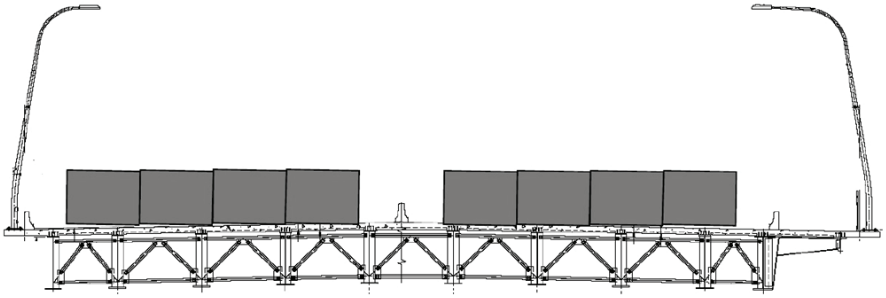

Figure 2-8 : North American multilane distribution (adapted from Lutomirska 2009)

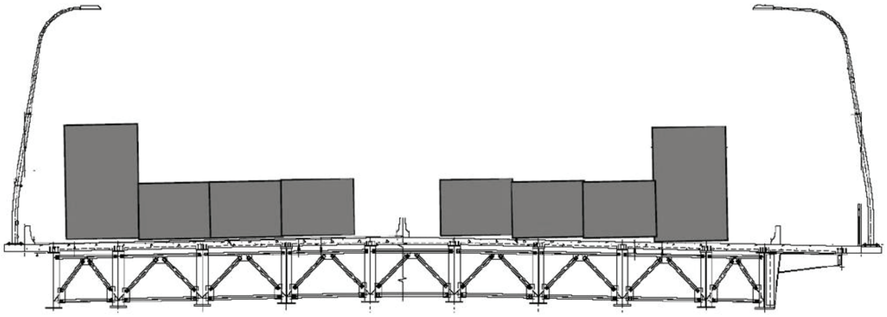

Figure 2-9 : Eurocode multilane load distribution (adapted from Lutomirski 2009)

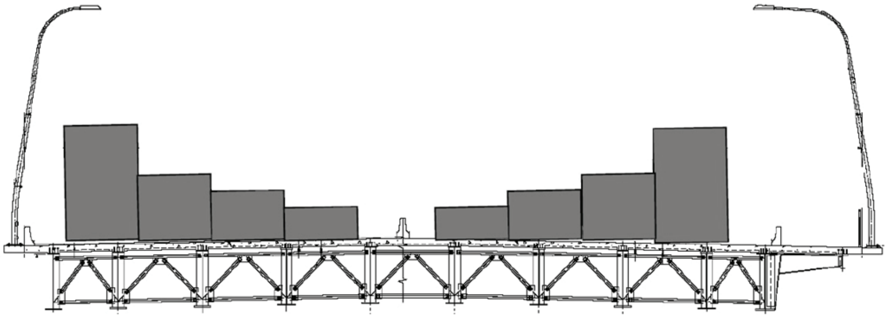

Figure 2-10 : Actual multilane distribution (adapted from Lutomirski 2009)

Chapter 3. Description of A. Murray MacKay Bridge and Existing Evaluation

3.1 Structural Description

The MacKay Bridge (Figure 3-1) consists of two steel box-girder approach spans totaling 460 m. The remaining 740 m of the bridge is encompassed by the suspended spans. Altogether, the MacKay Bridge is approximately 1200 m long.

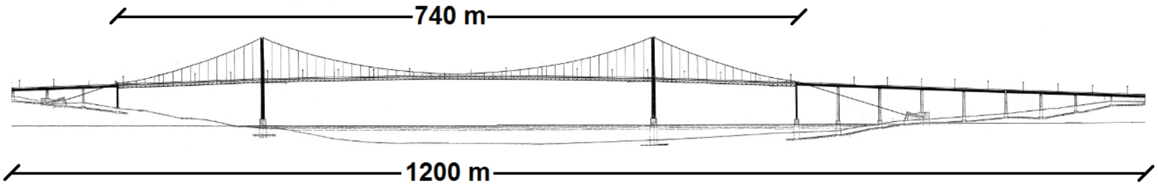

Figure 3-1 : MacKay layout (adapted from B&T)

The MacKay Bridge carries 4 lanes of mixed traffic with no pedestrian access. Maintenance access walkways along the bridge are found at deck level on the north side and at the bottom chord of the longitudinal stiffening truss along the south side of the bridge. A moveable maintenance platform is supported between the longitudinal stiffening trusses below the deck level.

3.1.1 Main Towers

The suspended sections of the bridge are supported by the Halifax Main Tower (HMT) and the Dartmouth Main Tower (DMT). These towers are formed from tubular structures constructed in a cruciform (Figure 3-2); two smaller cells outside of a larger central cell form each of a tower's two legs. The tower legs are joined be four sets of diagonal bracing, with horizontal members below the deck and at the tops of the main towers; almost 95 m above sea level.

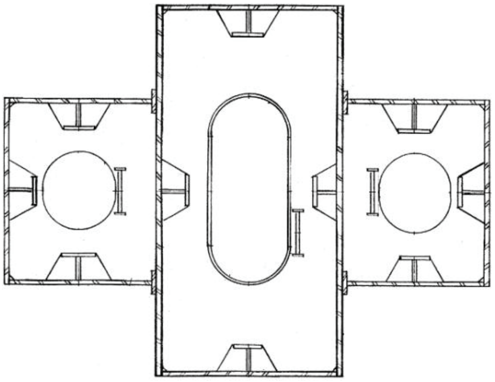

Figure 3-2 : Main tower cruciform layout (adapted from B&T)

3.1.2 Cables

The main cables of the MacKay Bridge consist of 61 strands of 40 mm diameter galvanized wire, laid in a hexagonal form (Figure 3-3). The circular form is completed with cedar filler and the entire cable is wrapped with galvanized wire prior to painting.

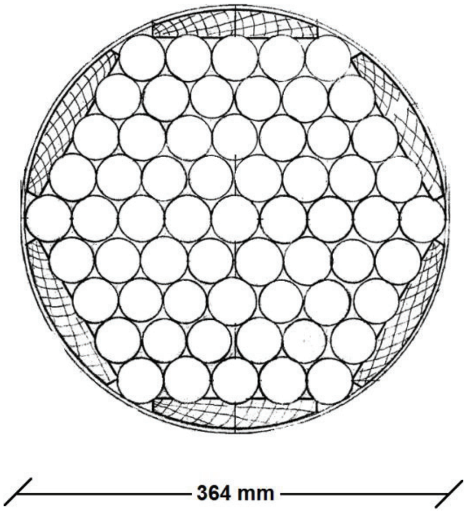

Figure 3-3 : Main cable hexagonal layout (adapted from B&T)

The hanger (suspender) cables consist of 6 galvanized strands twisted together forming a 54 mm cable. These hangers pass over the main cables via a custom cast cable band, allowing each hanger to be anchored only at deck level.

3.1.3 Deck System

Traffic on the MacKay Bridge is supported by an orthotropic steel deck, consisting of a steel flat-plat stiffened with longitudinal ribs. The deck spans between transverse stiffening trusses (Figure 3-4) located at the hangers. Further stiffening is provided by two below-deck longitudinal stiffening trusses (Figure 3-5) and a lateral stiffening truss. The behavior of the longitudinal and lateral stiffening trusses is the focus of this thesis.

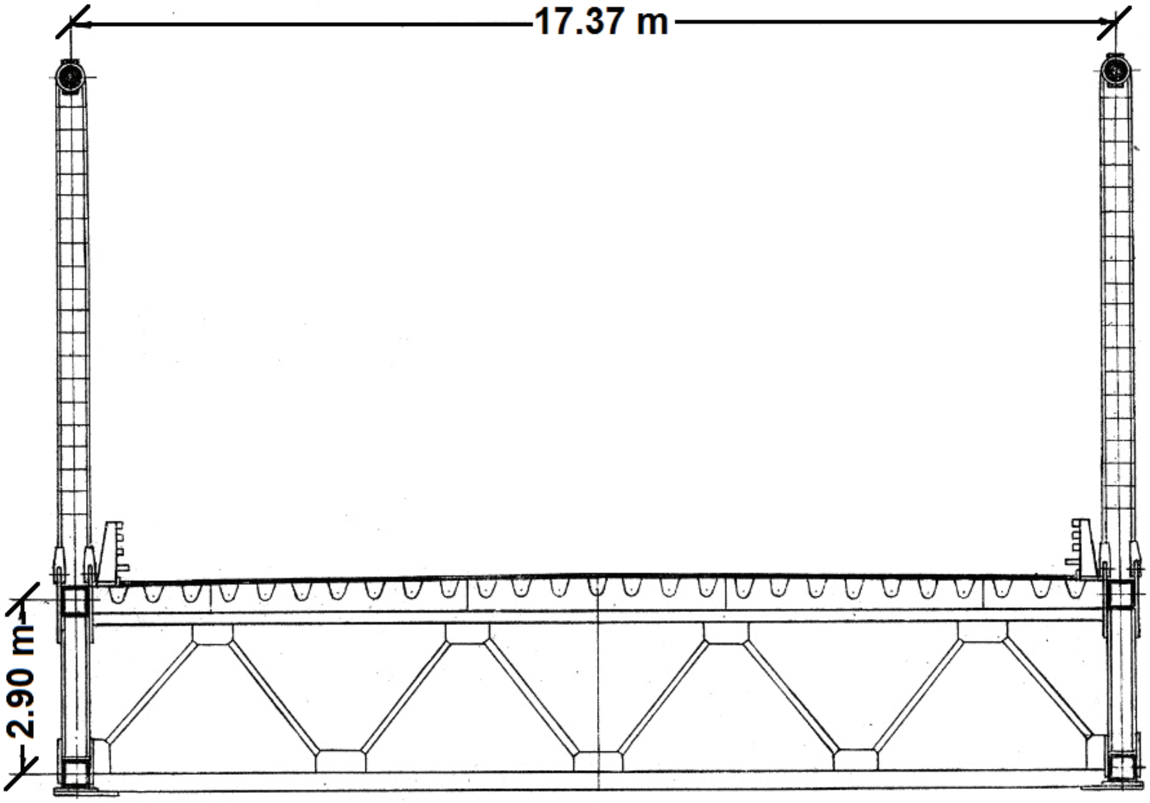

Figure 3-4 : Orthotropic deck and transverse stiffening trusses (adapted from B&T)

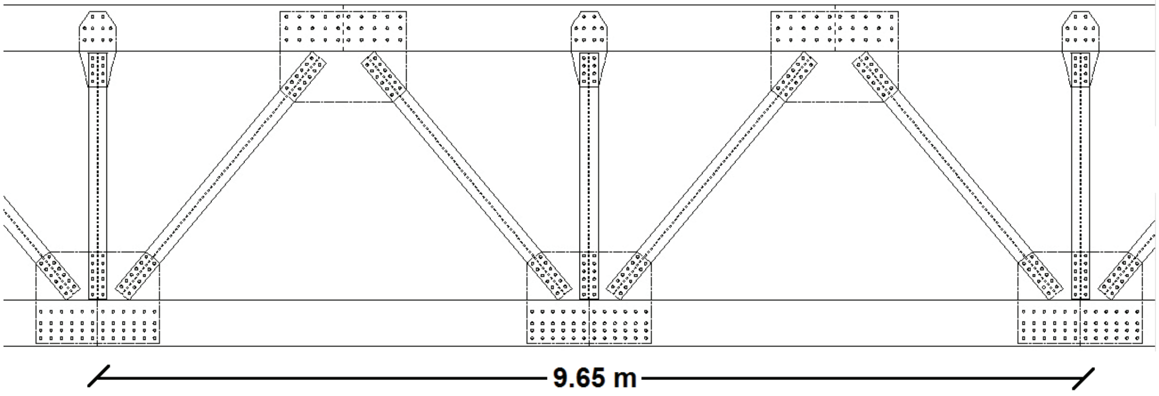

Figure 3-5 : Longitudinal stiffening truss layout

Chapter 4. Project Objective

4.1 Numerical Model

To determine the demands on individual components in the structure, B&T updated an existing three-dimensional numerical model for the MacKay Bridge. The model was developed for use with B&T's in-house structural analysis software which forms a stiffness matrix based on user input geometries. The global model (Figure 4-1) encompasses the suspended span superstructure of the bridge; this includes the main towers, cable bents, main cables, hanger cables and stiffening trusses.

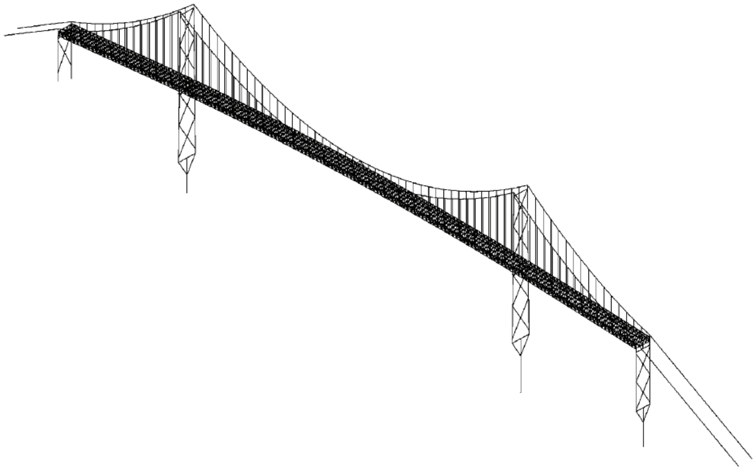

Figure 4-1: Global bridge model (courtesy of Buckland and Taylor)

While the existing model was sufficient for most global member effects, a second model (Figure 4-2) was required to examine the transverse stiffening trusses because of simplifications in the modeled deck system.

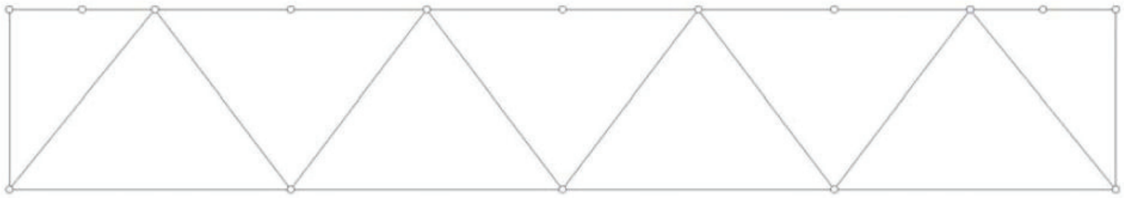

Figure 4-2: Local bridge model (courtesy of Buckland and Taylor)

All members in the structure were represented as beam elements, except for the main cables and hangers which were represented as non-linear cable elements. The cable elements are considered non-linear because the software uses the deflected position of the cable is used in the formation of the stiffness matrix. The foundations were not modeled; the cables and towers were instead assumed to be fixed at the interface.

As a result of the elements used, the global model can be considered partially linear; the dead and temperature loads are treated as non-linear, and the stiffness matrix for other loads is taken from the dead load model and treated linearly.

To facilitate modeling, several simplifying assumptions were made; these are described in the following section.

i. The mass of the deck and the distributed live load were included in modified top chords of the stiffening trusses. A third massless longitudinal member (Figure 4-3) was placed at the centerline of the bridge deck to incorporate the torsional stiffness, the lateral stiffness, and the vertical stiffness of the orthotropic deck system.
ii. The top chords of the stiffening trusses are collinear with the bridge deck in the model, whereas the truss chords are below the deck on the bridge. This simplification results in the stiffening trusses being slightly taller in the model, therefore the as-built dimensions are used to calculate member resistance.
iii. The vertical components of the stiffening trusses are vertical in the model; the members on the bridge are perpendicular to the deck. This was done to greatly simplify the geometry of the model.
iv. The top chords of the stiffening trusses were permitted to rotate to remove any effects resulting from combining the top chords with the deck system. The deck-bearing members at the main towers were permitted to translate and rotate, and those at the cable bents were permitted rotation only. All other components were considered to have fixed (no translation or rotation) connections at either end.

v. A separate local model (Figure 4-2) was constructed to examine the buckling and post-buckling behavior of several stiffening truss diagonals. Due to the large dimensions of the gusset plates used in the truss members, the plates were modeled as very short, very stiff members.

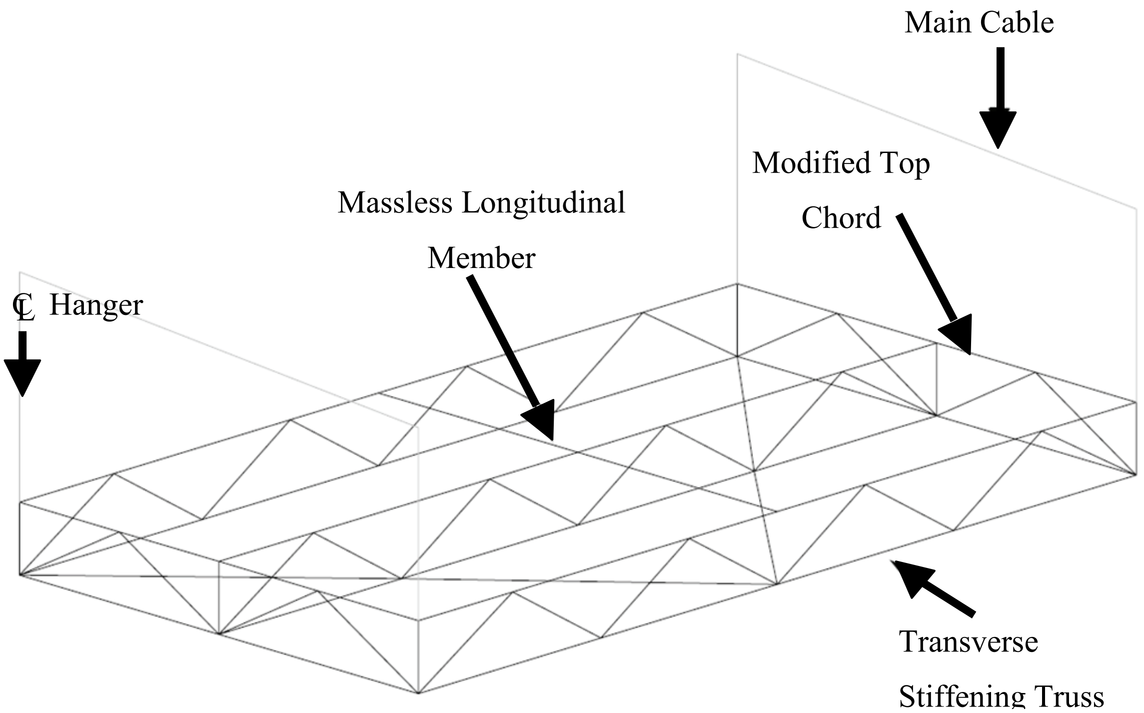

Figure 4-3: Modeled deck system (adapted from B&T)

4.2 Model Calibration

The model was initially developed to match Pratley and Dorton's as-built drawings and calculations. Looking at the deflected profile of the centre span under live and temperature loads, as well as horizontal wind load, B&T determined that their global model and the as-built design calculations agreed within 1% and 3% respectively (courtesy of B&T) based on the initial design loads.

Following a survey of the bridge in November of 2005, it was found that the long-term movement of the bridge has resulted in sag of the deck system, of approximately 500mm at midspan (courtesy of B&T). As a result, B&T updated their model to reflect the current state of the bridge by using cable sag as an additional load case.

4.3 Code-Based Bridge Evaluation

A quantitative approach used to identify members that require a more thorough examination employed demand to capacity ratios (D/C). Simply put, if the demand on a given member is less than or equal to the capacity of that member, the member is satisfactory. The inclusion of load and resistance factors allows the ratio to be compared to target reliability. Therefore a D/C ratio less than or equal to 1.0 implies that there is a satisfactory level of reliability. Similarly, a D/C ratio greater than 1.0 implies the target reliability was not met – this does not mean the member will fail. Members on the MacKay Bridge that returned D/C ratios close to 1.0 were identified and selected for instrumentation in this project.

The D/C ratio approach is sufficient if the member in question will see no increase in load; however, it is commonly desirable to know what increase in live load is acceptable for a bridge. The CHBDC (2006) was not developed for use with long-span bridges such as the MacKay Bridge however; the evaluation criteria are transferable because they are based on target reliabilities for a given member. This reliability is built into the codified equations set out in Section 14 which will determine the remaining live load capacity (F), as determined by the following:

$$\mathrm{F} = \frac{\mathrm{UR_r} - \sum \alpha_\mathrm{D} \mathrm{D} - \sum \alpha_\mathrm{A} \mathrm{A}}{\alpha_\mathrm{L} \mathrm{L}(1+\ell)} \qquad [4\text{-}1]$$

where:

$\mathrm{UR_r}$ = Factored member capacity

$\Sigma\alpha_\mathrm{D}\mathrm{D}$ = Factored dead load

$\Sigma\alpha_\mathrm{A}\mathrm{A}$ = Factored loads other than dead or live loads

$\alpha_\mathrm{L}\mathrm{L}(1+\ell)$ = Factored live load with dynamic load allowance

Chapter 5. MacKay Bridge Monitoring System

5.1 Gauge Locations

Following the preliminary analysis by B&T, several members of interest were identified close to both the Halifax and Dartmouth towers on either side of the deck. While these members were not predicted to fail, available information suggests that they may not meet the target reliabilities set out by the CHBDC (2006). The instrumented section shown in Figure 5-1 was selected to be representative of this group and was located close to a convenient power supply for the monitoring equipment. Ten diagonal members of the longitudinal stiffening trusses (Figure 5-2 and Figure 5-3), as well as two members of the lateral stiffening trusses (Figure 5-4 and Figure 5-5) were determined to be representative and were selected for instrumentation.

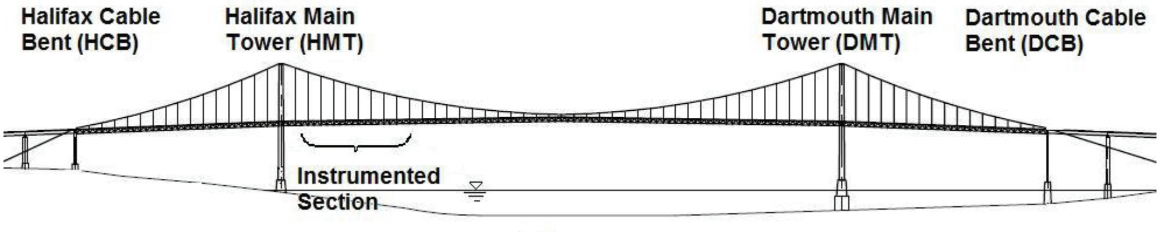

Figure 5-1: Instrumented section (adapted from B&T)

Figure 5-2 : Longitudinal stiffening truss

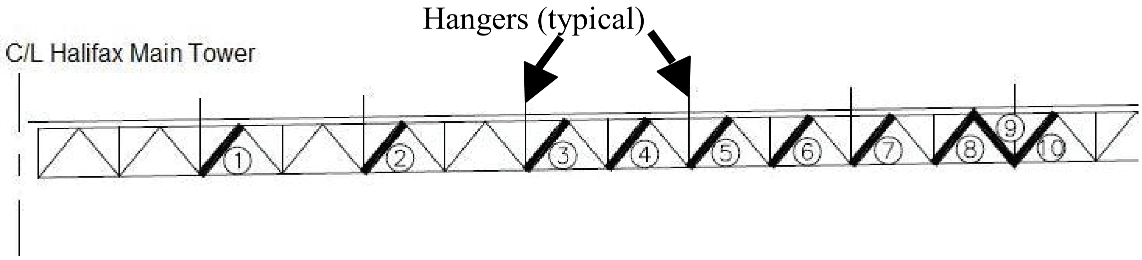

Figure 5-3 : Longitudinal stiffening truss profile (adapted from B&T)

Figure 5-4 : Lateral stiffening truss

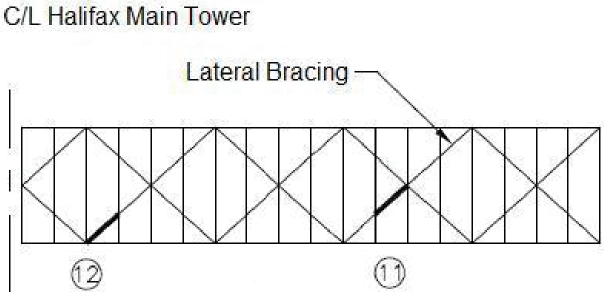

Figure 5-5 : Lateral stiffening truss plan (adapted from B&T)

Each instrumented truss member has two gauges located on the web. Diagonal #3 was further instrumented with two sets of four flange gauges (Figure 5-6) at both the upper and lower nodes. Paired gauges are located on opposite sides of the webs to provide redundancy (see Figure 5-7)

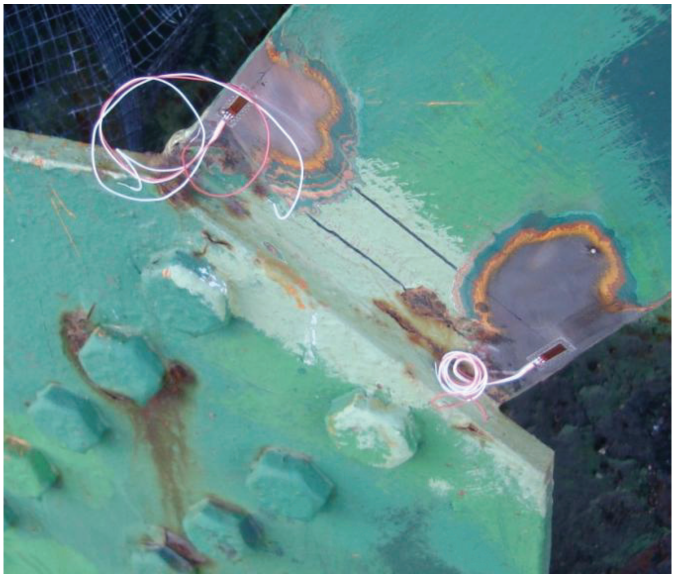

Figure 5-6 : Flange gauge pair next to diagonal gusset plate

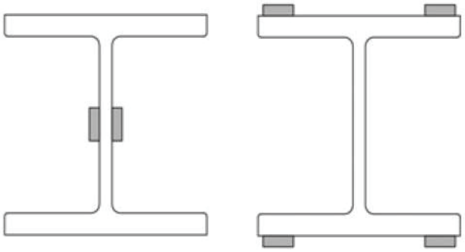

Figure 5-7: Strain gauge positioning on web and flanges

Table 5-1 provides a list of the gauges with their corresponding datalogger channels. These channels were used to identify the raw data within spreadsheets while any plotted data will be referenced by the member name and gauge location.

Gauges on the diagonal members were located in the middle of the member span (± 6 mm), using the bolted connections at the top and bottom as the reference. The flange gauges for diagonal #3 were located 50 mm from the edge of the gusset plates and 10 mm from the edge of the flange, as shown in Figure 5-6.

Table 5-1 : Datalogger gauge naming scheme

Channel	Logger A	Logger B	Channel	Logger A	Logger B
1	#1 D-T	#1 D-B	11	#7 D-T	#7 D-B
2	#2 D-T	#2 D-B	12	#8 D-T	#8 D-B
3	#3 D-T	#3 D-B	13	#9 D-T	#9 D-B
4	#3 F-U-T-S	#3 F-U-T-N	14	#10 D-T	#10 D-B
5	#3 F-U-B-S	#3 F-U-B-N	15	#11 D-T	#11 D-B
6	#3 F-L-T-S	#3 F-L-T-N	16	#12 D-T	#12 D-B
7	#3 F-L-B-S	#3 F-L-B-N	17	#1 D-Dumb	Box Dummy
8	#4 D-T	#4 D-B	18	#3 Dumb1	#3 Dumb2
9	#5 D-T	#5 D-B	19	#11 D-Dumb	#6 D-Dumb
10	#6 D-T	#6 D-B	20	TC	TC

D = Diagonal T = Top U = Upper N = North
F = Flange B = Bottom L = Lower S = South

5.2 Gauge Installation

A quarter-bridge configuration was used to measure strain. Linear pattern weldable strain gauges (Vishay Micro-Measurements General Purpose Strain Gauges type LWK-06-W250B-350) were installed. The full bridge was completed with a Campbell Scientific 4 Wire Full Bridge Terminal shown in Figure 5-8. The gauges are single axis ‘foil-type’ weldable strain gauges as shown in Figure 5-9. The gauges are bonded to weldable steel tabs in the factory and have pre-soldered lead wires. The field installation was completed by RAT according to the welding pattern specified by the manufacturer (see Figure 5-10). The gauges are internally thermally compensated for the steel substrate. The surface of the structure was ground smooth prior to installation of the gauges to ensure a proper bond.

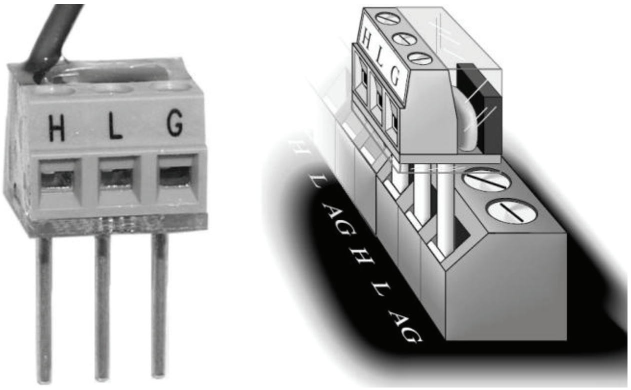

Figure 5-8 : Full bridge completion terminal (Campbell Scientific 2007)

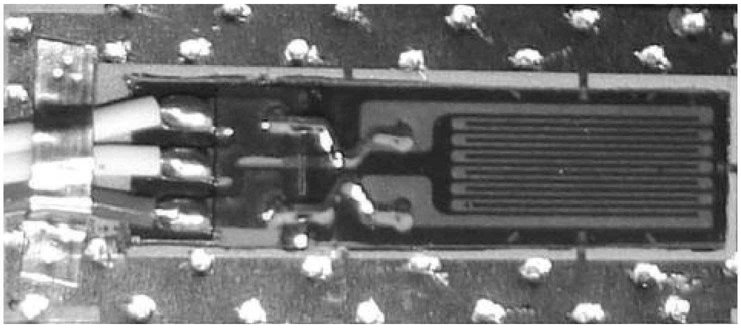

Figure 5-9 : Foil type weldable strain gauge

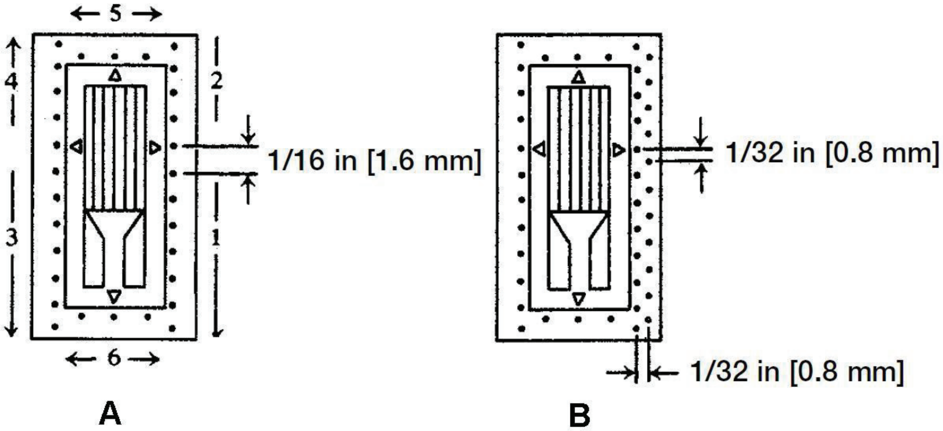

Figure 5-10 : Welding pattern (Vishay 2010)

A) initial weld pass B) second weld pass

Following initial installation, each gauge was protected by a system of nitrile rubber, Teflon and butyl rubber compounds (Vishay M-Coat F) to provide a moisture barrier and other environmental protection. Mechanical protection was provided by PVC plates which were installed to protect against any physical damage.

Supplemental 'dummy gauges' were installed at several representative locations on the bridge. These gauges are identical to the primary gauges, but they are mechanically isolated from bridge loads (see Figure 5-11). These gauges are sensitive solely to temperature strains and can be used to correct for thermal effects if necessary, and to assess any tendency for the system to drift with time.

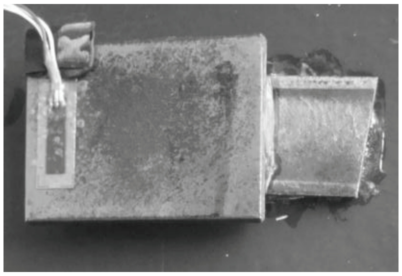

Figure 5-11 : Dummy gauge

5.3 System Wiring

The cable used was a three conductor, jacketed and shielded cable. The three conductor arrangement reduces noise and thermal influence on the gauge readings due to the long lengths of cable required to connect the gauges to the dataloggers. Slack in the wire was provided at the location of the gauges and at the dataloggers to prevent damage to the gauge or connections from accidental pulls on the cable. The cable was run in a conduit secured to the bridge.

Connections from the gauges to the cables were completed in the laboratory based on predetermined lengths. Each conducting wire was soldered and the final assembly sealed with heat-shrink tubing. Field splices were completed in a similar manner.

After installation, the shielding wires were individually grounded to the tower structure to eliminate any electromagnetic interference. Figure 5-12 shows the completed wiring of Logger A, Logger B is similar.

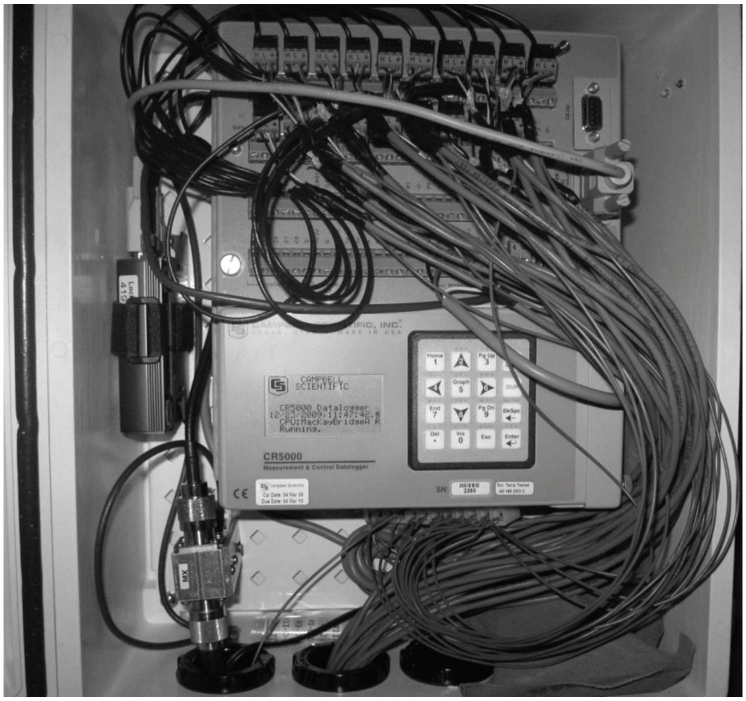

Figure 5-12 : Logger A completed wiring

5.4 Data Acquisition

Data was acquired and stored using two Campbell Scientific CR-5000 dataloggers (Logger A and Logger B). Both of the dataloggers are contained in water-resistant enclosures. Data collected is stored on-site on 2.0GB compact flash cards. The Campbell Scientific datalogger software was used to control data collection and data transfer from the unit. Data is copied to Dalhousie servers automatically once per hour. Transfer of data is completed using wireless modems found at each datalogger. Strain data is collected from the datalogger in micro-strain. Automatic measurements are taken at a rate of 1 Hz.

5.5 Instrument Scaling Factor

A manual electronic shunt calibration procedure was completed December 23rd, 2009. Shunt calibration is performed to determine that all the electronics are functioning and establish an instrument scaling factor for the system. The strain gauge circuitry is shunted with a large resistor that will simulate the equivalent effect of a known strain. The instrument readings are then compared against the known strain and adjustments can be made to gain settings or gauge factors such that each strain gauge is calibrated for instrument, installation and wiring effects. Strain gauges as manufactured have a gauge factor for the gauge only, not the full instrument and system. More details can be found in sources such as Vishay Micro-Measurements Tech Note TN-514 (Vishay 2007).

5.5.1 Equipment

To complete the calibration of the strain gauges, a 100 kΩ variable resistor was used. This was set to 85.64 kΩ which should have produced a 2005 micro-strain reading for the gauges used in this project.

5.5.2 Procedure

The calibration shunt resistor was applied to the dummy arm of the bridge at the datalogger. The displayed strain was recorded before and during the application to ensure that the proper range of values was achieved. This information was time stamped for future reference. This procedure was completed for the 38 channels that were active at the time of calibration.

5.5.3 Discussion

To determine the expected test result, Equation [5-1], provided by Vishay Micro-Measurements (2007) is used:

$$\varepsilon_s = \frac{-R_G}{FG\,(R_G + R_C)} \qquad [5\text{-}1]$$

where:

ε_s = Expected strain = 2005 $\mu\varepsilon$
R_G = Initial circuit resistance = 350 Ω
FG = System gauge factor = 2.03
R_C = Shunt resistance = 85.64 kΩ

After examination of the strain data and initial voltages collected during the shunting, it was determined that the relationship between the voltage and strain is linear with respect to the gauge factor (as indicated by Vishay). A calibrated system gauge factor (and conversion factor for existing data) was determined for each gauge/channel using the linear relationship. The factor was changed in the dataloggers basic program to be the average of those shown in Table 5-2 (1.98). The shunt calibration process resulted in a strain correction of less than 2% indicating that the gauges and instruments were functioning within the expected range. Data acquired prior to January 12, 2010 was collected using the manufacturer's suggested gauge factor of 2.03. Table 5-2 lists conversion factors which can be used to convert data collected prior to January 12, 2010 to the shunt calibrated values.

Table 5-2 : Calibrated gauge factors and conversion factors

	Logger A		**Logger B**	
Channel	Gauge Factor	Conversion Factor	Gauge Factor	Conversion Factor
1	1.974	1.028	1.979	1.026
2	1.974	1.028	1.964	1.034
3	1.972	1.030	1.972	1.029
4	1.972	1.029	1.960	1.036
5	1.972	1.029	1.983	1.023
6	1.971	1.030	1.965	1.033
7	1.979	1.026	1.967	1.032
8	1.964	1.034	1.968	1.032
9	1.963	1.034	1.968	1.031
10	1.968	1.031	1.958	1.037
11	2.001	1.014	1.993	1.019
12	1.991	1.020	1.993	1.019
13	1.997	1.017	2.000	1.015
14	2.007	1.011	1.994	1.018
15	1.987	1.021	1.995	1.018
16	1.997	1.016	1.976	1.027
17	1.980	1.025	1.978	1.026
18	1.989	1.021	1.984	1.023
19	1.996	1.017	1.986	1.022

Chapter 6. Gauge Type Correction

Following initial calibration of the instrumentation system the gauge type correction was examined to address the impact on strain gauge readings.

6.1 Small-Scale Laboratory Testing

Gauges were installed on a tensile specimen to compare the readings of bondable strain gauges and weldable strain gauges.

All gauges were installed as per manufacturer instructions in a laboratory setting by an experienced technician. The gauge factor provided by the manufacturer was used to convert the change in resistance into a strain value for both gauge types. Redundant gauges were installed on opposite sides of the specimen as shown in Figure 6-1.

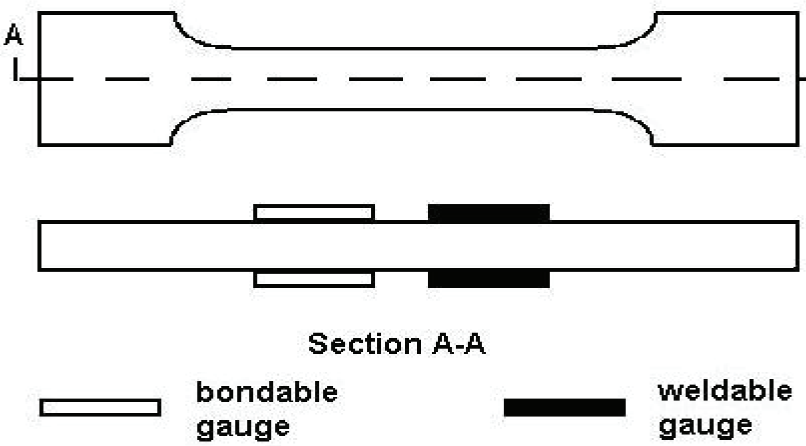

Figure 6-1: Dogbone tensile specimen

The cross-section of the specimen was measured at three separate locations and resulted in average of cross-sectional dimensions of 12.66 mm x 6.23 mm. The specimen was preloaded to 10 kN (127 MPa) and then the load was increased in increments of 500 N. During the loading sequence, the strains were recorded manually for all four gauges. The recorded strain from the tensile testing was zeroed (taking the preload as a permanent load). Theoretical values were determined using fundamental mechanics of materials equations for axially loaded members, the member cross-section and an assumed modulus of elasticity of 200000 MPa. Figure 6-2 shows a plot of recorded strain to applied load, with curves for theoretical, weldable, and bondable gauges.

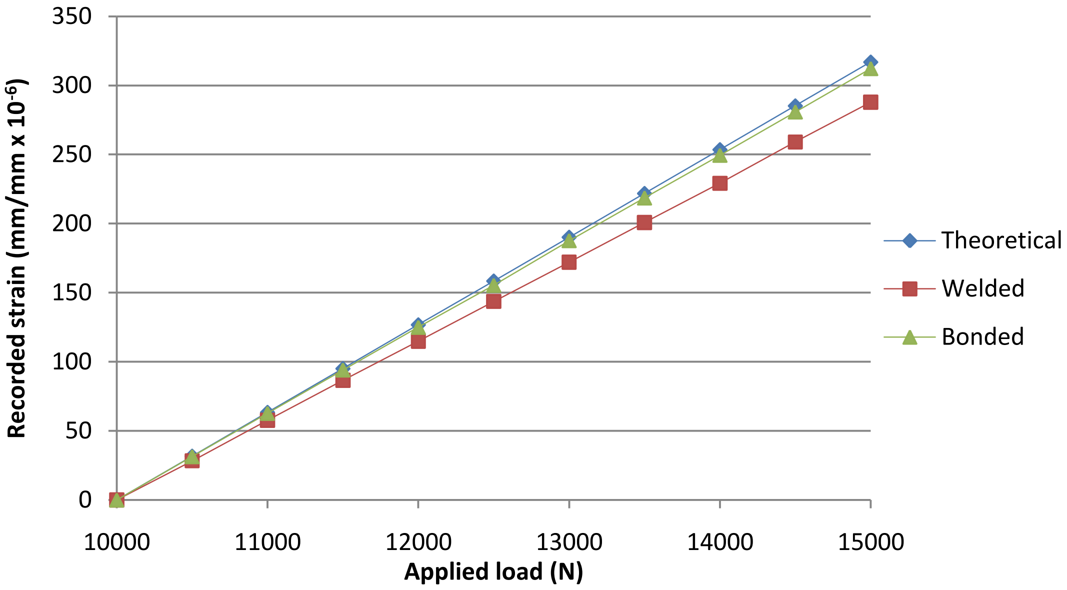

Figure 6-2 : Tensile testing results

Using the factory supplied gauge factors, the bondable gauges record 99% of the theoretical strain, whereas the weldable gauges record ~94% of the theoretical strain. This difference does not indicate a difference in accuracy; rather, it highlights the need for proper calibration to determine the correct gauge factor for installed weldable gauges.

6.2 Full-Scale Laboratory Testing

Further to the tensile coupon testing, a full-scale compression sample was prepared. A W460x52 section was selected as being the closest available section to that indicated in the original MacKay Bridge superstructure drawings. The specimen was 1219 mm long with 25.4 mm thick plates fully welded at either end.

All web gauges were attached along the vertical axis of the specimen. Welded gauges were placed 44 mm from mid-height and bondable gauges were placed 19 mm from mid-height. This is shown in Figure 6-3.

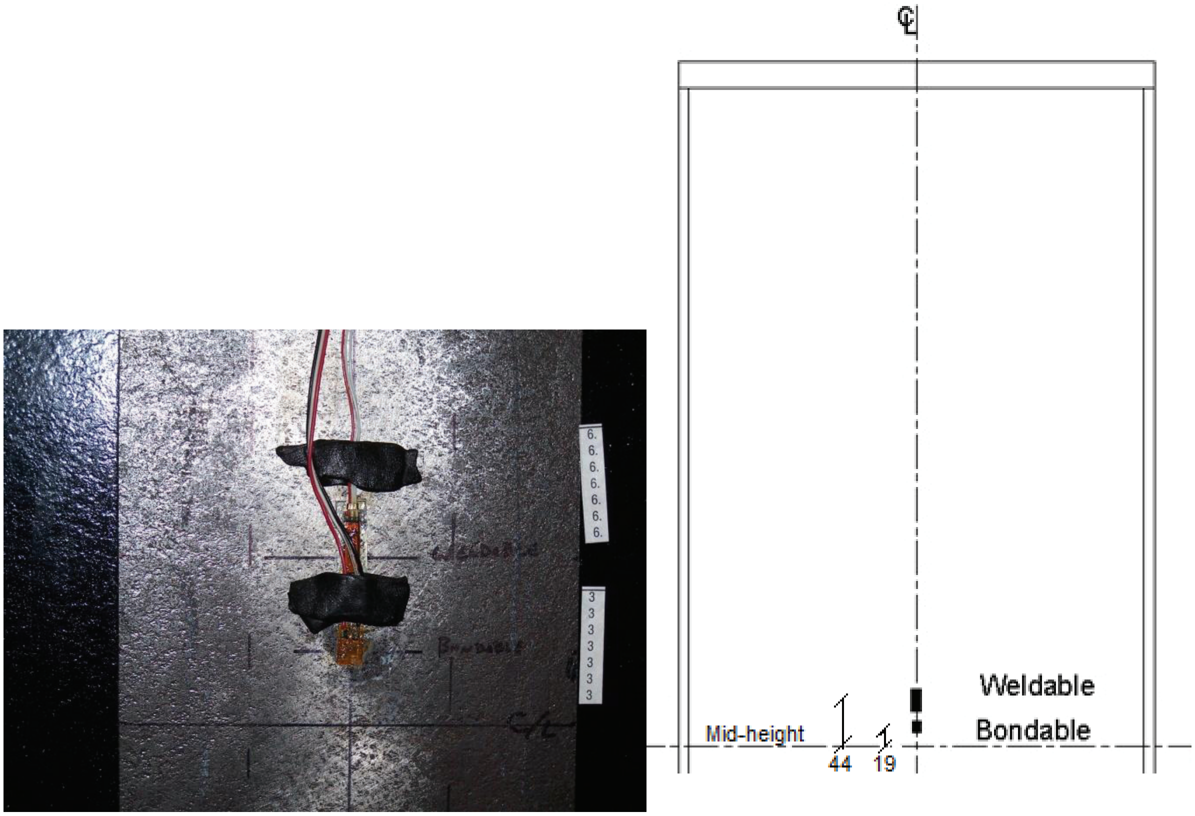

A) Photograph of specimen B) Elevation of specimen

Figure 6-3: Instrumented lab specimen

Bondable gauges were also installed on all flanges at the mid-height (Figure 6-4) to capture bending strain of the specimen. These were located ~10mm from the edge of the flanges in the same plane as the bondable web gauges. The flange gauge readings were used as a control during testing to ensure a minimum of testing eccentricity in the boundary conditions. The flange gauge readings were then averaged to produce an equivalent axial strain in the cross-section for comparison with web readings. The prepared specimen is shown in Figure 6-5.

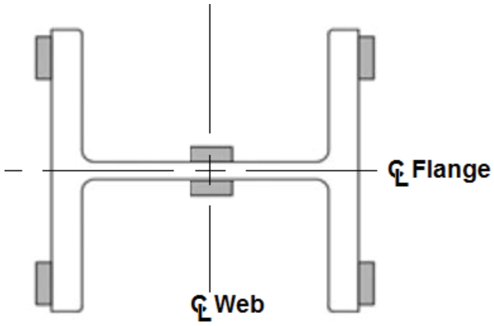

Figure 6-4: Lab specimen cross-section

Figure 6-5 : Full-scale laboratory compression test specimen

A step-like load function was applied to the specimen in nine equal intervals up to 300 kN. This loading pattern was performed with the specimen loaded axially as well as with a weak-axis eccentricity of 10 mm.

The results from axial testing show that there is good correlation between the web gauges and the flange gauges. The values recorded by the weldable gauges are approximately 91% of the bondable gauges. This is also similar to the results found from tensile testing. Figure 6-6 is a record of recorded strain versus time.

Results from eccentric loading also show strong correlation between calculated axial strain from flange gauges and web gauges. For these tests, the weldable gauges record 91% of the bondable gauges; still within the range of previous testing.

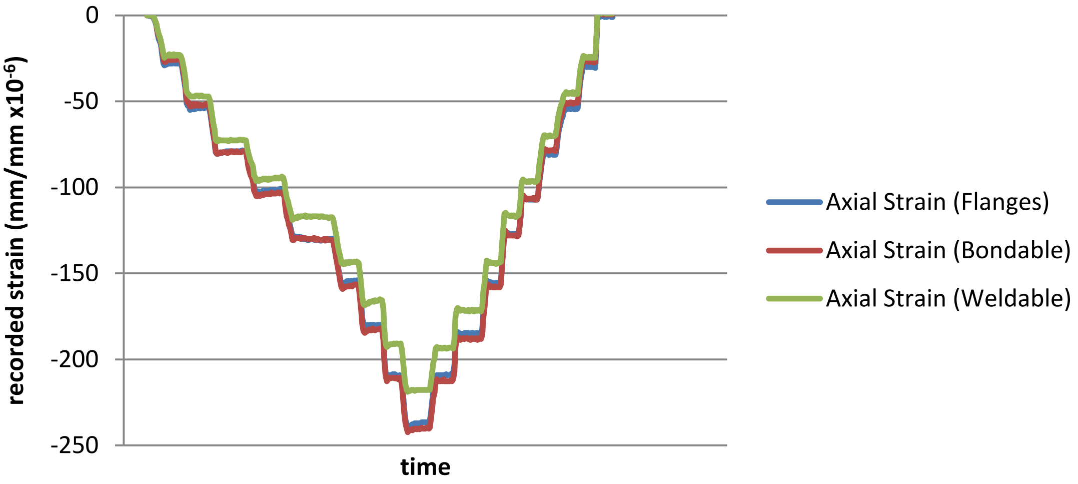

Figure 6-6 : Gauge type comparison - laboratory testing - stepped load

6.3 Full-Scale Field Testing

To confirm laboratory findings, two diagonal members on the MacKay Bridge were instrumented. Additional gauges were installed on diagonals #4 and #5 to investigate the large difference between top and bottom gauge readings found during field testing. The gauge recording lower strain was identified on each of these members and a weldable gauge was installed above the existing weldable gauge, as close as possible without damaging the existing gauges. A bondable gauge was also installed on both faces of each member to determine the actual strain thereby providing a calibration factor for the weldable gauges. The placement of these gauges is shown in Figure 6-7, Figure 6-8 and Figure 6-9. The location of gauges on each member is defined by the dimensions A and B listed in Table 6-1.

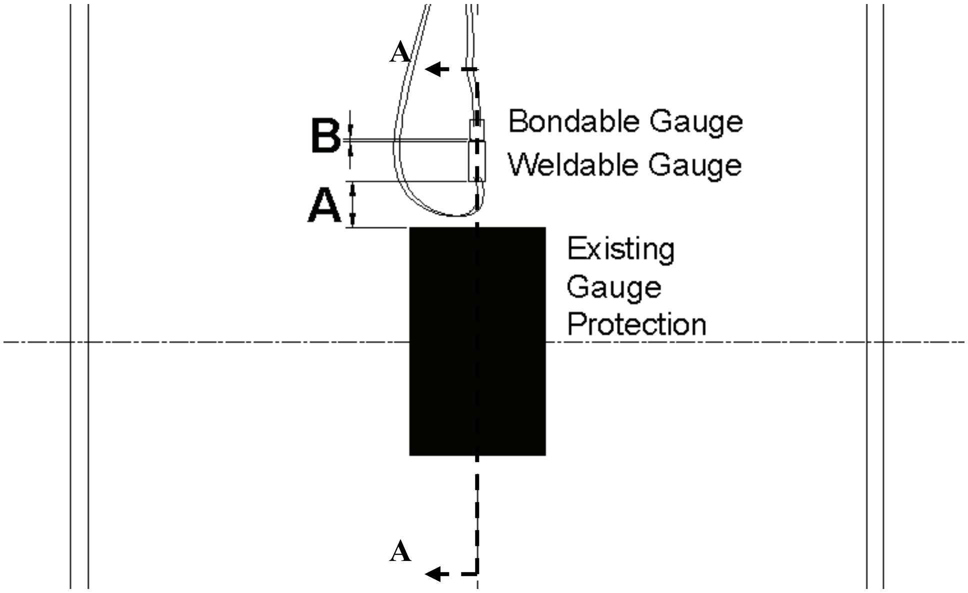

Figure 6-7 : Profile of diagonal with new gauges

Figure 6-8 : Gauge type comparison - bridge member

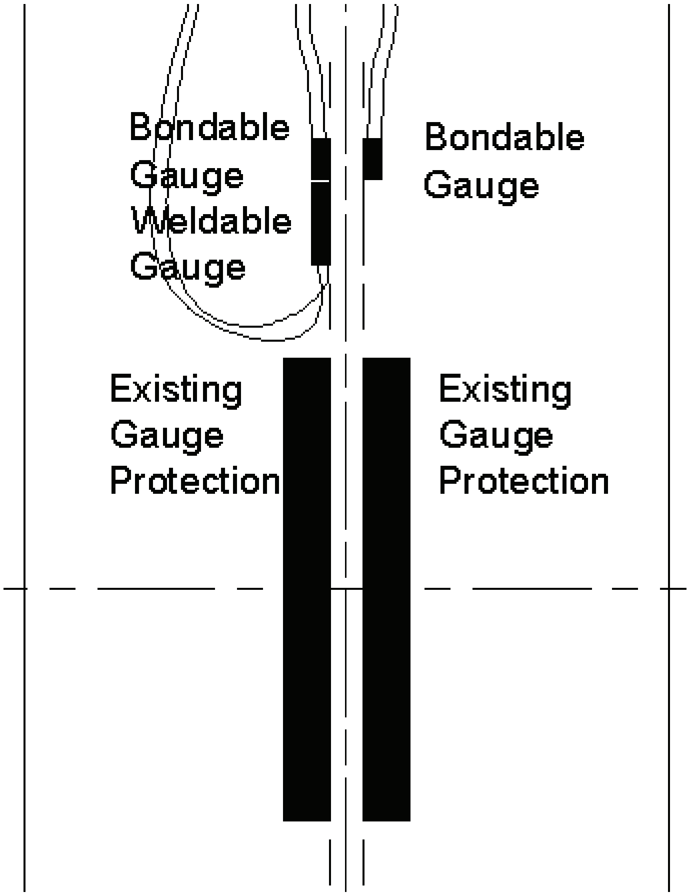

Figure 6-9 : Section A-A (from Figure 6-7)

Table 6-1 : Gauge placement dimensions

	Dimension A	Dimension B
Diagonal #4	25 mm	35 mm
Diagonal #5	3 mm	17 mm

The results from static calibration testing in August 2010 (see Section 7.1.2) show that the weldable gauges record 89% and 90% of the bondable gauges. Based on the actual testing, as well as the laboratory testing, a factor of 1.11 (1/0.90) was determined to be most appropriate as a correction factor for the weldable gauges. This adjustment could have been employed by changing the gauge factor in the data acquisition system, similar to the adjustment completed after the shunt calibration, such that the recorded results produced accurate strain values. However, the timing of the project meant that a significant portion of the field data had already been recorded with the manufacturer supplied gauge factor. The application of a new gauge factor part way through the data record would have introduced significant differences in post-processing protocol and potential for error. Due to the linear nature of this gauge type correction, the factor was applied following post-processing, simplifying the process. It is recommended however that gauge type calibration be conducted to determine appropriate gauge factors prior to commencing the field data acquisition whenever possible.

Chapter 7. System Testing

Following the installation of the data collection system, testing for functionality was required. This was achieved through a combination of full-scale calibration testing, as well as controlled laboratory testing and finite element modeling.

7.1 Full-Scale Calibration Testing

It was desirable to have the system tested at least twice throughout the testing period. To accomplish this, the MacKay Bridge was closed to all traffic for the period between midnight and 5:30am on two occasions; December 17th/18th 2009 and March 23rd/24th 2010. An additional test was completed on August 7th/8th 2010 with a different truck configuration during a separate bridge closure.

During these closures, testing was conducted at three different travel speeds: static (0 km/hr), slow speed (10 km/hr), and fast speed (40 km/hr). Static testing was used to compare known loads to the B&T numerical model behaviour; slow speed testing was completed to develop influence lines which were used to examine entire bridge behaviour; and fast speed testing was conducted to examine possible dynamic effects from vehicles travelling at the posted speed limit.

7.1.1 Calibration Truck

A heavily loaded truck was constructed using two trailers loaded with jersey barriers. The dimensions and loadings of this truck are shown in Figure 7-1 and Figure 7-2.

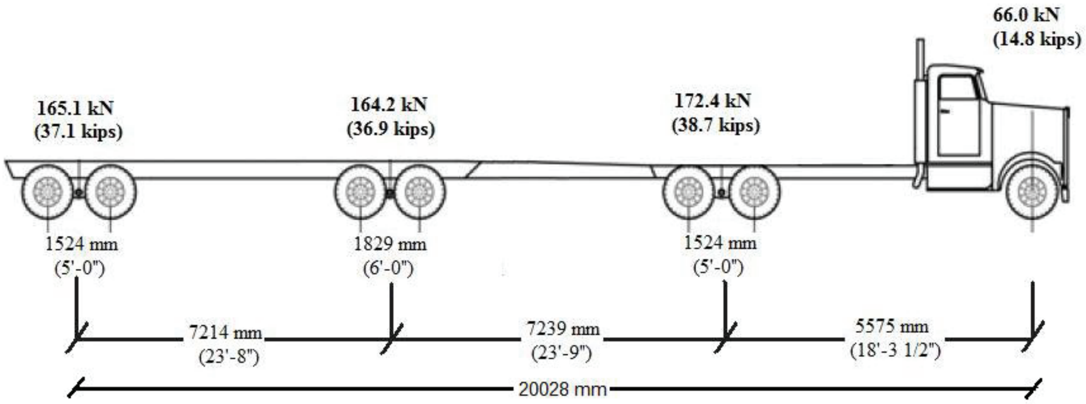

Figure 7-1 : Calibration truck profile

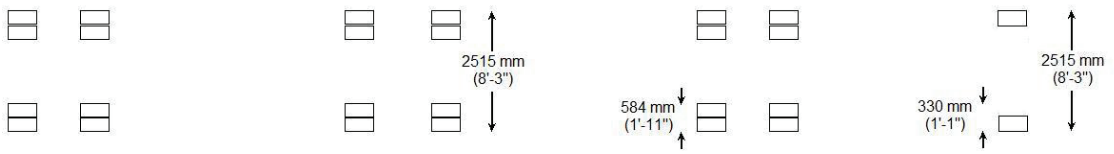

Figure 7-2 : Calibration truck footprint

The calibration truck was weighed the night of the calibration testing (December 17, 2009) at the provincial scales on Highway 102 near the airport industrial park exit. The layout of the jersey barriers on the trailers is shown in Figure 7-3.

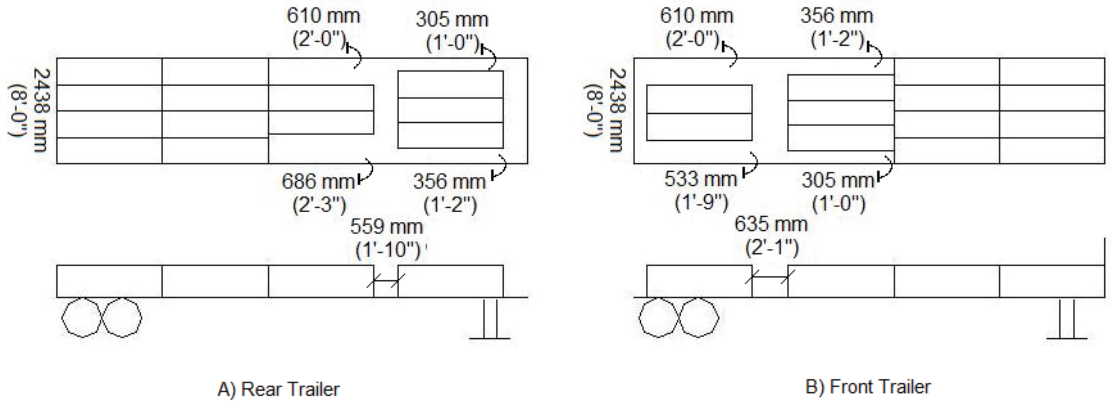

A) Rear Trailer

B) Front Trailer

Figure 7-3 : Jersey barrier placement

7.1.2 Static Testing

B&T provided ten truck positions for static testing. The positions and corresponding locations relative to the HMT are shown in Table 7-1.

Table 7-1: Static positions from HMT

Position ID	Distance from C/L HMT
1	36530 mm
2	46620 mm
3	50660 mm
4	55710 mm
5	60760 mm
6	65810 mm
7	69840 mm
8	74890 mm
9	79940 mm
10	84990 mm

The centreline of the Halifax Main Tower was agreed to be considered to be coincident with the centre of the expansion joint for the purposes of measuring truck locations. The front axle of the calibration truck was centered in the test lane and the engine shut off.

Testing was completed with the truck in similar positions in the four travel lanes shown in Figure 7-4. While every attempt was made to place the truck in the centre of the lanes, Figure 7-5 shows the actual position of the truck relative to the south guardrail kick plate. Figure 7-6 shows the positioning of the truck for testing. During all static tests, the truck was travelling towards Dartmouth as directed by B&T and the engine was shut off for data recording to avoid any possible dynamic interaction from truck vibrations.

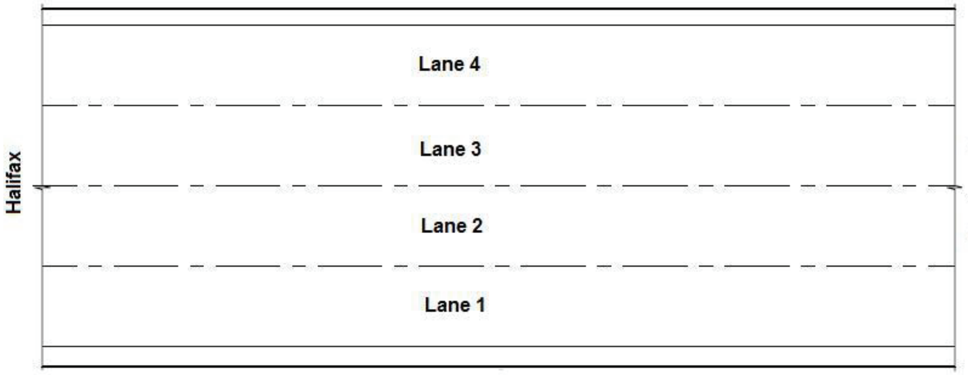

Figure 7-4 : Lane numbering

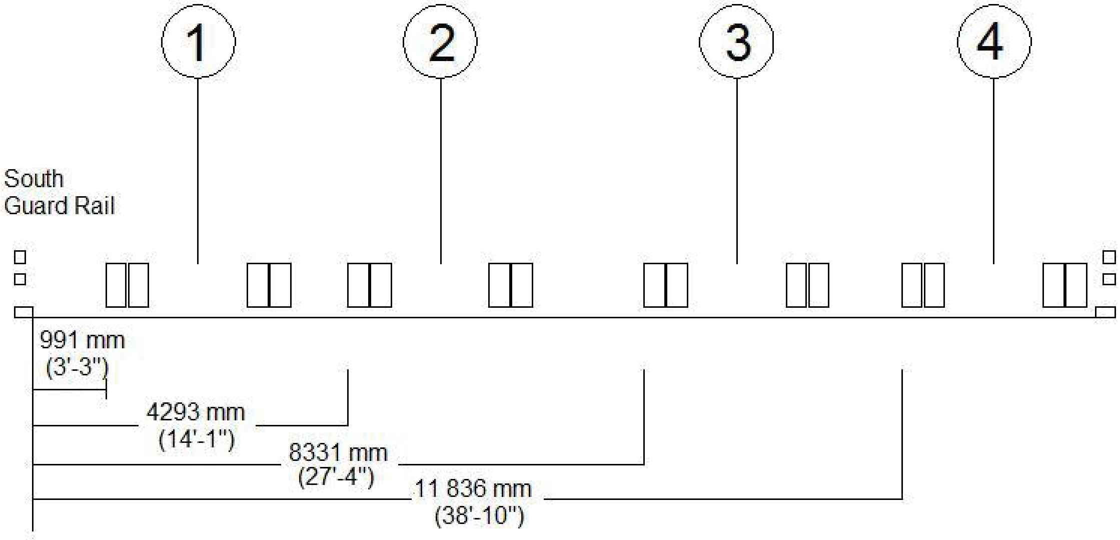

Figure 7-5 : Lateral truck positions, lanes 1 through 4

Figure 7-6 : Positioning of calibration truck for static testing

7.2 Repeatability of Data

To ensure stability of the system, as well as repeatability of data, calibration testing results from December 2009 and March 2010 were compared. Throughout the individual calibration tests, temperatures remained constant resulting in a stable response. Figure 7-7 shows the results of static testing in all four travel lanes in both December (solid lines) and March (dashed lines) for a sample gauge. The shape of the gauge response is consistent in all four travel lanes from both the December and March calibration testing – this provides a high level of confidence in the functionality of the system, as well as the reliability of the data. The complete set of gauge comparisons is shown in Appendix I – Gauge Repeatability December 2009 - March 2010.

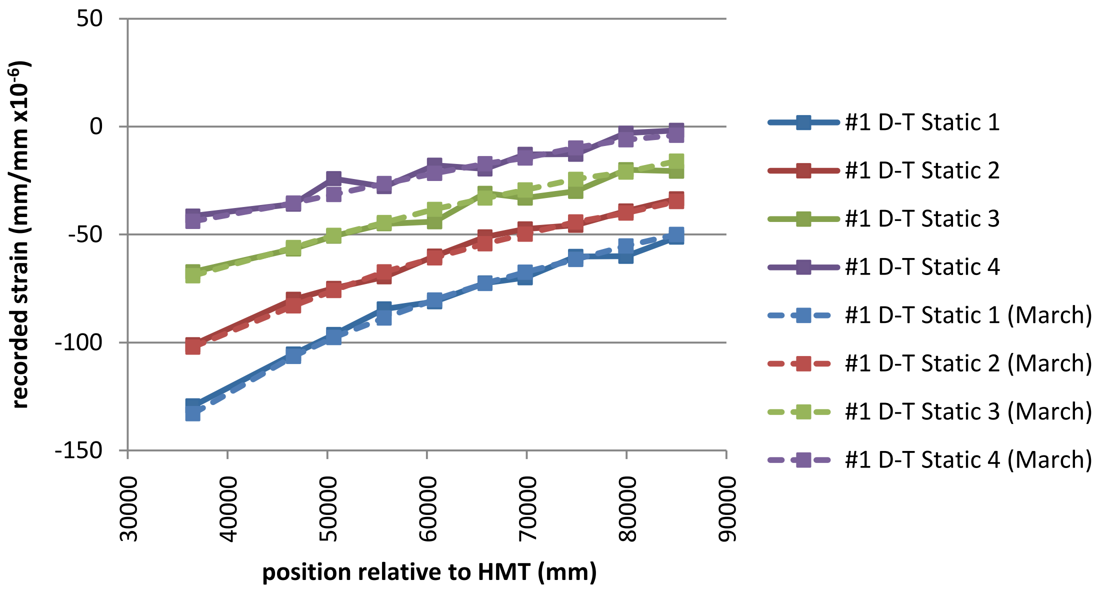

Figure 7-7 : Gauge comparison Dec versus Mar

7.3 Influence Lines

To develop influence lines for each instrumented diagonal, the calibration truck was driven at slow speed (10 km/hr) along the length of the bridge. Data was collected continuously and plotted for each gauge. A sample influence line is shown in Figure 7-8 with the entire set from December 2009 shown in Appendix II – Influence Lines From Slow Speed Tests.

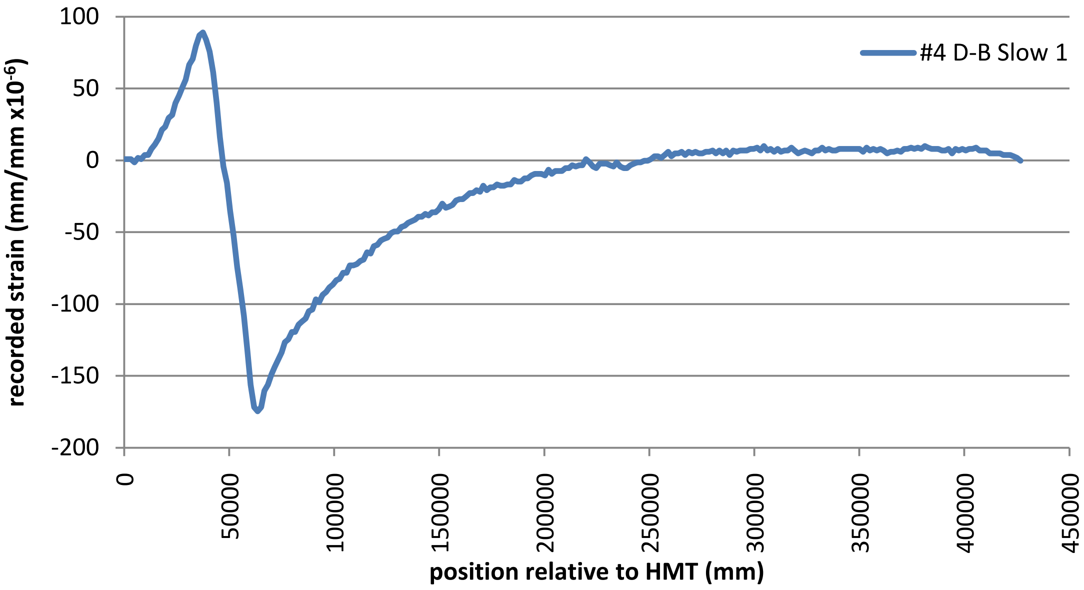

Figure 7-8 : Sample influence line

7.4 Impact of Opposing Traffic

An assumption made during the development of the influence lines described in Section 7.3 was that the calibration truck could be treated as a single point load; this assumption would seem appropriate for a relatively small truck (20 m) on a long-span bridge (740 m suspended span).

To confirm the assumption that the calibration truck could be treated as a unit load, plots were produced using static test data with the truck travelling in both normal travel and opposing directions, labeled #8 D-T and #8 D-T Opp in Figure 7-9. Static results were compared because of uncertainties in instantaneous truck position due to variable speed within the slow-speed and fast-speed testing.

The centre of mass (COM) of the truck was determined using first moment of axle weights and used as the locator for the truck position for the comparisons. The COM is shown on the calibration truck in Figure 7-10.

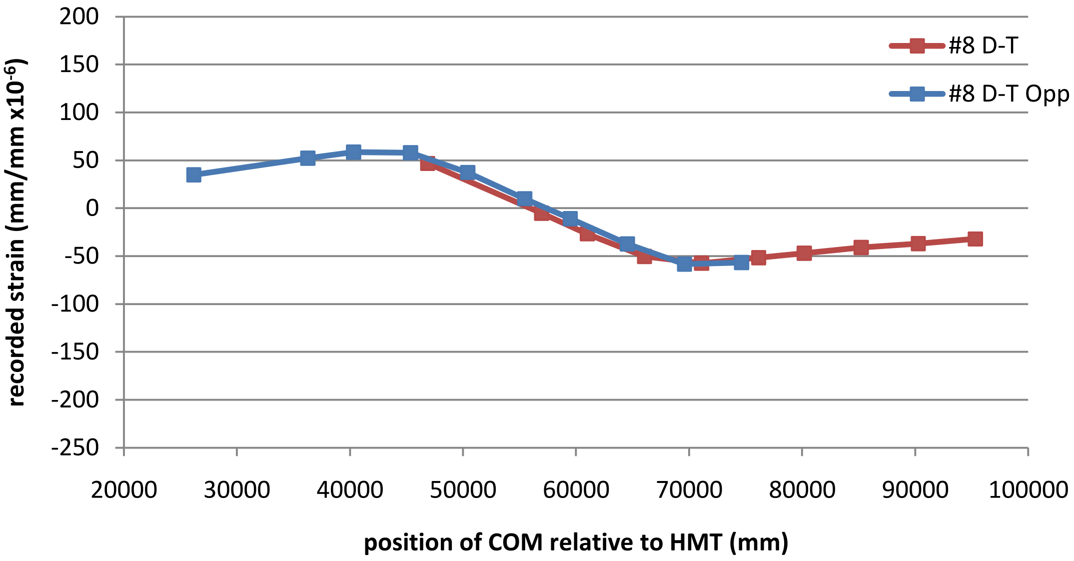

Figure 7-9: Comparison of truck behaviour in normal travel and opposing direction

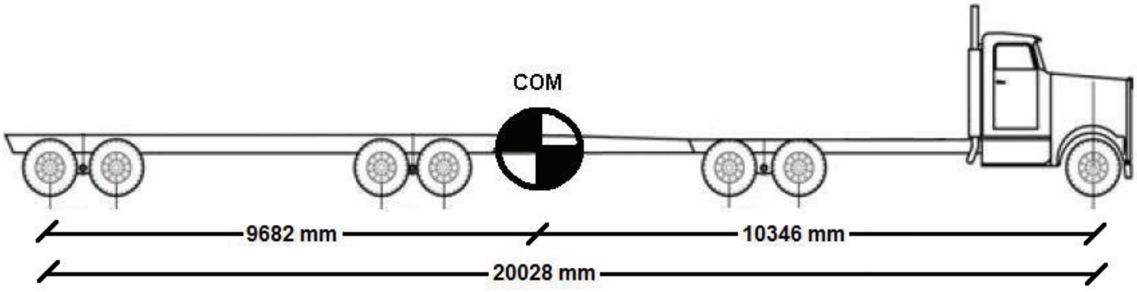

Figure 7-10 : Calibration truck COM

Upon examination of the graphical results based on COM, it becomes apparent that the load response pattern is identical regardless of the direction of travel, so long as the centre of mass is used to locate the truck. This indicates that the difference in truck geometry about the COM has minimal effect on bridge response; therefore the truck can be treated as a point load and the influence lines are valid. The important aspects of any truck, regardless of axle configuration, are the gross vehicle weight and the location of the COM.

7.5 Scan Rate Suitability

Based on the results of Calibration Tests #1 and #2, it was identified that select pairs of gauges are not recording the same peak data values under slow speed and fast speed traffic (Figure 7-11). Oddly, the fast speed has a lesser effect than the slow speed which is contrary to the expected behaviour where fast moving traffic would result in apparent load amplification due to dynamic interaction. Due to differences in test speed, fast-speed data contains four times the data of slow speed data. Figure 7-12 shows the data points for Lane 1 during the fast speed test recorded by Gauge #10 D-T.

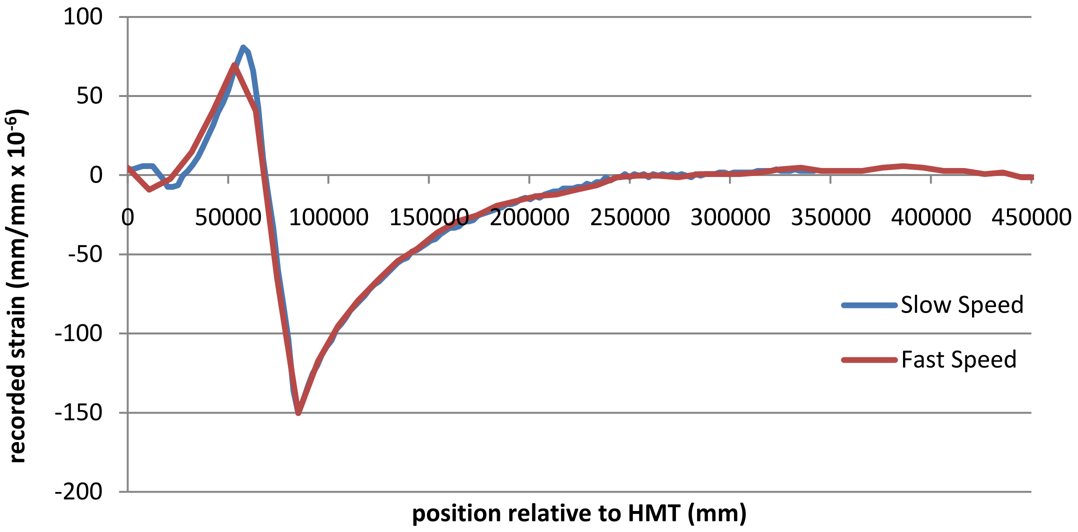

Figure 7-11 : Slow speed versus fast speed

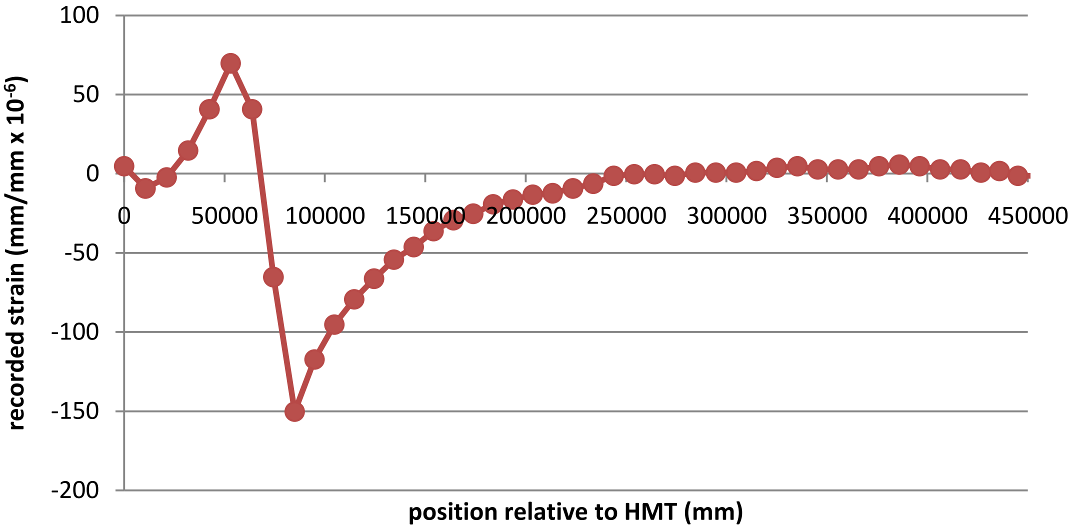

Figure 7-12 : Fast speed data

It is noted that the area of interest, directly adjacent to the peaks, holds relatively few data points to form the rapidly changing strain data curve. As a result, the potential lateral movement of these data points was examined. A series of linear curve fits were set to match the peaks of the slow speed curve for #10 D-T (Figure 7-13). The basic assumption is that the slow speed data (10 km/hr) is correct.

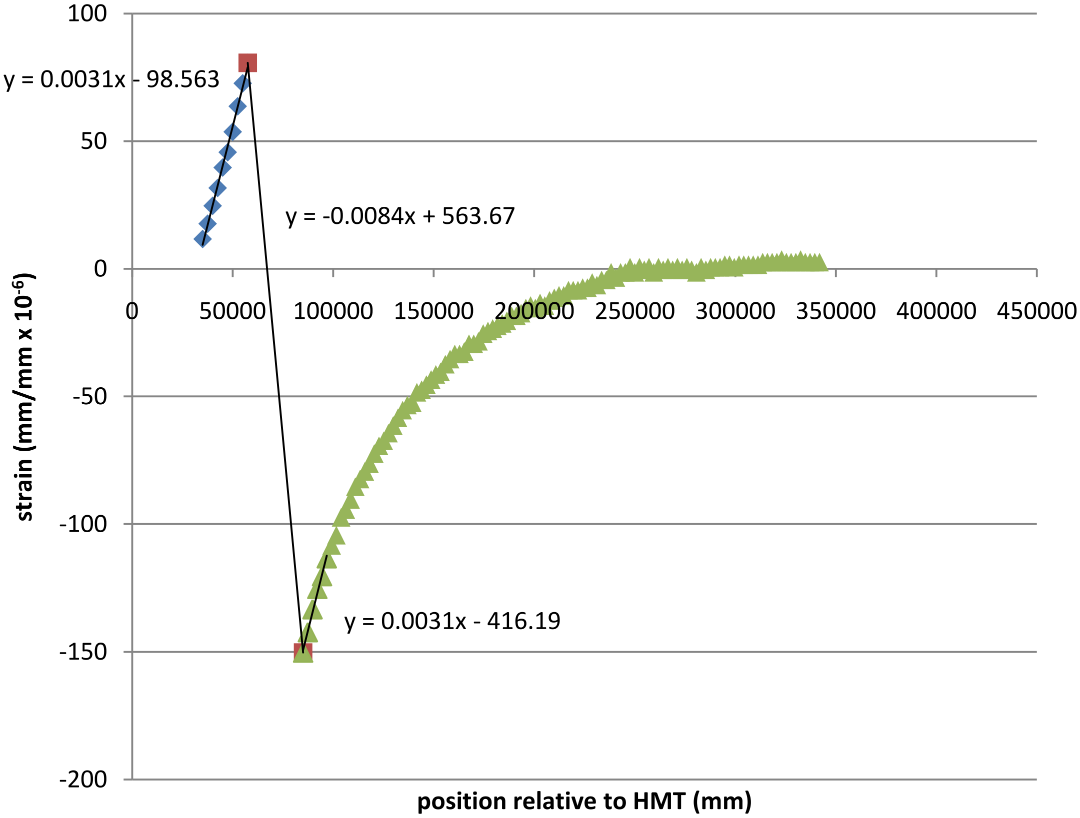

Figure 7-13 : Slow speed curve fit

Based on travel speed of 40 km/hr (fast speed), the distance travelled by the truck between readings was found to be 11.1 m. For the purposes of comparison, 20 different theoretical starting positions (horizontal offsets) were selected by equally dividing the time step into 0.05 second intervals.

These peak data readings are calculated based on the progressive position of the truck to examine the issue of the scan rate not being in synchronization with the position of the truck which causes maximum strain. Figure 7-14 is one of a series of plots were constructed; this shows that there is potential for the peak readings to be upwards of 30%

less than the actual peak at this scan rate for a truck travelling at 40 km/hr. This difference will diminish with truck travel speed.

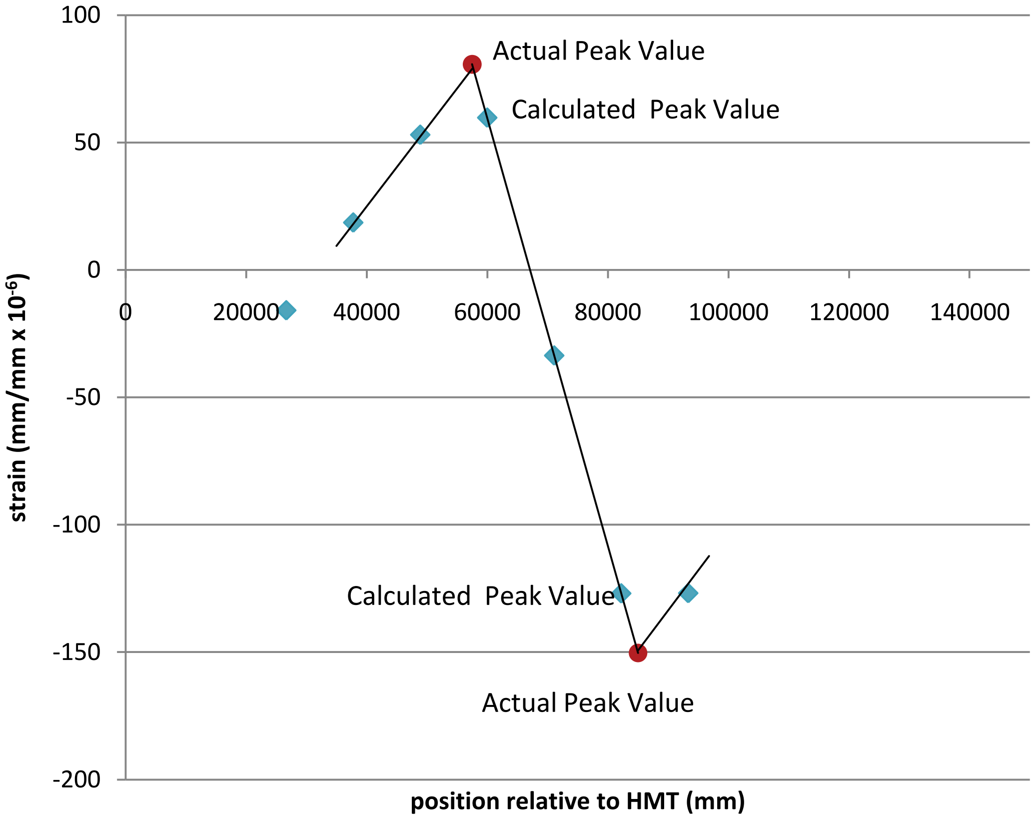

Figure 7-14 : Actual versus calculated peaks

Vehicular spacing is related to travel speed – slow moving (or stopped) traffic are believed to cause the largest loads on long-span bridges (Buckland et al. 1978). Therefore, the potential 'missed' peaks caused by a relatively slow scan rate are unlikely to negatively affect the outcome of this project.

Chapter 8. Impact of Surface Preparation

Following controlled calibration testing it was noted that some pairs of web strain gauges (top and bottom of the same web) were not producing the same strain readings (Figure 8-1). A member under pure axial loading should have uniform stress throughout the cross-section; some gauge readings indicated otherwise. Furthermore, these gauges were placed very close to the neutral axis of the section and hence should have very little sensitivity to any incidental moments on the member. Table 8-1 shows the difference in peak strain results, as well as the average reading for each web gauge pair from the March 2010 calibration testing.

Table 8-1 : Comparison of web gauges on diagonals

	Absolute Difference (mm/mm x10^{-6})	Average (mm/mm x10^{-6})	Absolute $\frac{\text{Difference}}{\text{Average}}$
Diagonal #1	20	-143	0.14
Diagonal #2	10	-153	0.06
Diagonal #3	74	-154	0.48
Diagonal #4	62	-149	0.41
Diagonal #5	41	-157	0.26
Diagonal #6	4	-148	0.03
Diagonal #7	3	-139	0.02
Diagonal #8	22	-141	0.16
Diagonal #9	14	152	0.09
Diagonal #10	8	-95	0.09
Diagonal #11	7	163	0.04
Diagonal #12	23	173	0.13

A major difference between field conditions and laboratory conditions was the increased amount of surface preparation required to reach solid metal in the field to install strain gauges. It was proposed that surface preparation prior to gauge installation could cause local strain changes, resulting in an impact on the individual gauge readings.

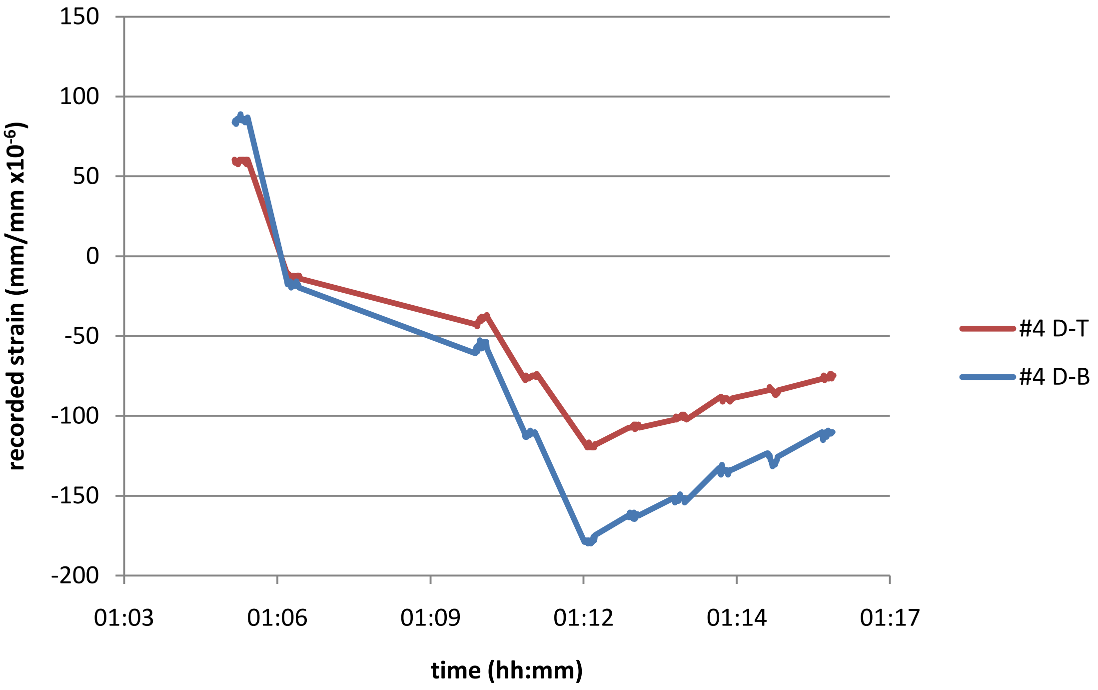

Figure 8-1 : Mismatched strain readings

8.1 Experimental Testing

In conjunction with the work completed to determine a conversion factor relating weldable and bondable gauges, a study was completed to look at the impact caused by varying degrees of surface preparation on gauge readings. The experimental testing was conducted in an attempt to reproduce the phenomena found in the field under controlled laboratory conditions.

8.2 Surface Preparation

To determine a typical surface preparation area, photographs of 16 gauges installed on the MacKay Bridge were examined. Using the known size of the strain gauges as a reference, the diameter of the prepared surface, as well as the transition zone to the rough surface was determined. Figure 8-2 shows a typical gauge and Figure 8-3 shows the distribution of field measured surface preparation diameters from the data set. An average diameter of 37 mm (rounded to 40 mm) and 50 mm were determined for the prepared surface (shown in blue) and transition zone (shown in red) respectively.

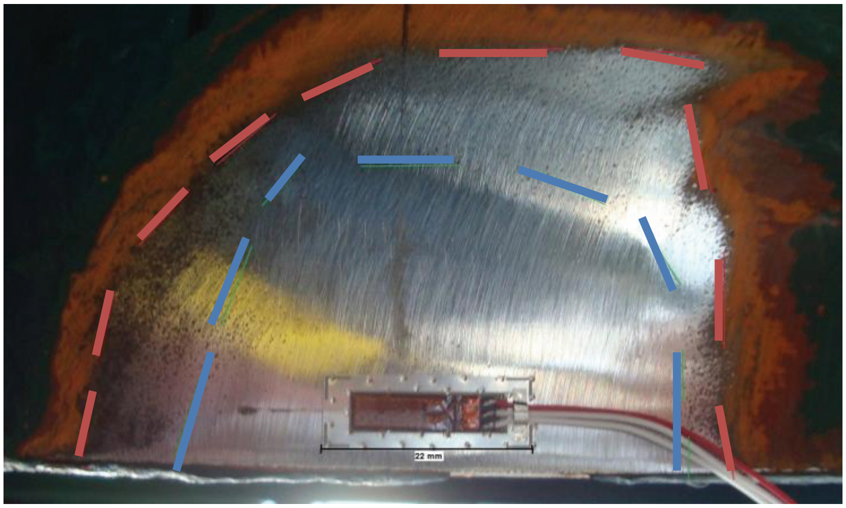

Figure 8-2 : Prepared area and transition zone

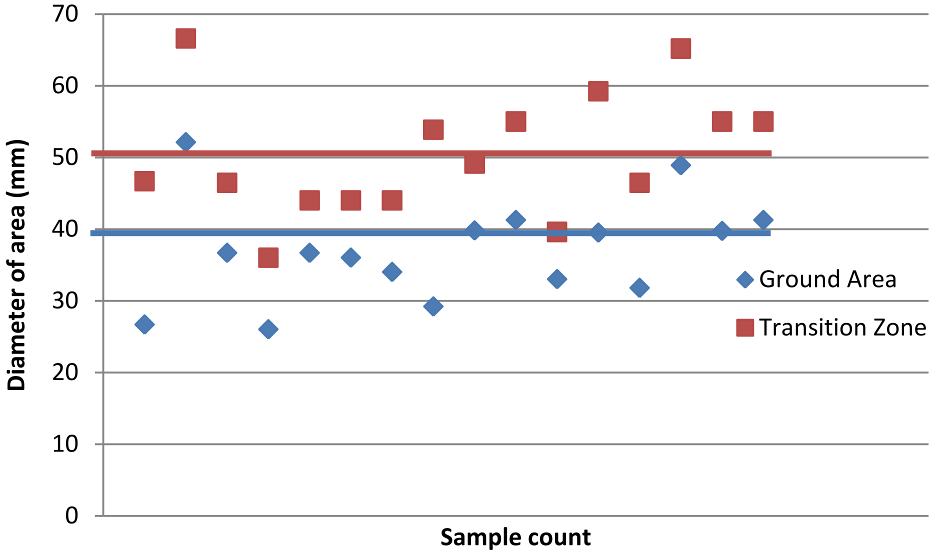

Figure 8-3 : Diameter of the prepared surfaces

8.2.1 Preparation Depth

To determine a reasonable depth of preparation, tools similar to those used in the field (Figure 8-4) were tested on a piece of steel plate in the lab. These tools consisted of a handheld grinder, with a 60 grit sanding wheel. Thirty second intervals were used to relate depth of preparation to time. Four trials were completed: heavy grind, soft grind, soft grind and heavy grind. This allowed the heavy grind to be attempted with both a new and a used sanding wheel. The results of the trials can be seen in Table 8-2. Based on these results, it is reasonable to have 1.0 mm or 1.5 mm of steel removed if pitting is particularly bad at a given gauge location.

The pitted steel (Figure 8-5) must be removed to provide a consistent surface for the gauge installation. Pitted surfaces will cause localized strain changes leading to data that is not representative of the member.

Figure 8-4 : Grinder and sanding wheel in field

Table 8-2 : Grinding versus time

Trial	Average material removed
Heavy Grinding (new wheel)	0.35 mm / 30s
Easy Grinding	0.08 mm / 30s
Easy Grinding	0.08 mm / 30s
Heavy Grinding (used wheel)	0.15 mm / 30s

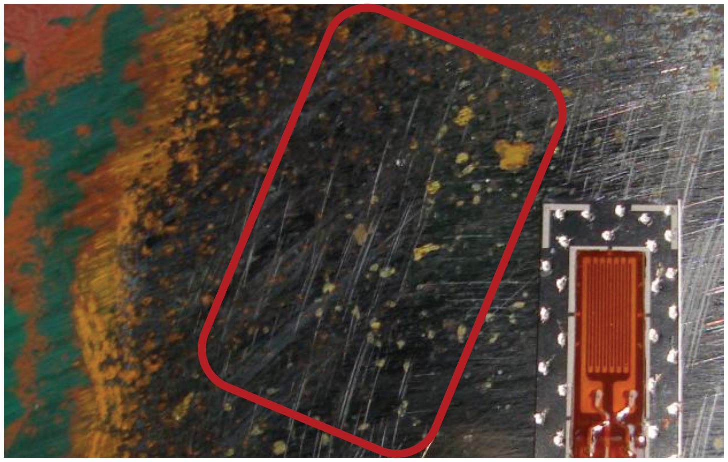

Figure 8-5 : Pitting corrosion

8.2.2 Laboratory Specimen

A rolled steel section (W460x52) was chosen to represent the built-up sections that comprise the MacKay Bridge because the web thickness and depth of section are comparable. A comparison of both sections can be seen in Figure 8-6. The section is 1220 mm long with a 25 mm plate shop-welded to the both ends. Three regions were prepared along the centreline of the section to examine the impact of varying surface preparation on the gauge readings. Table 8-3 shows details of the relative vertical position and preparation depth, Figure 8-7 shows the cross-section through the web. All gauges were single-axis bondable strain gauges, installed with M-Bond 200 Adhesive Kit by Vishay Micro-Measurements.

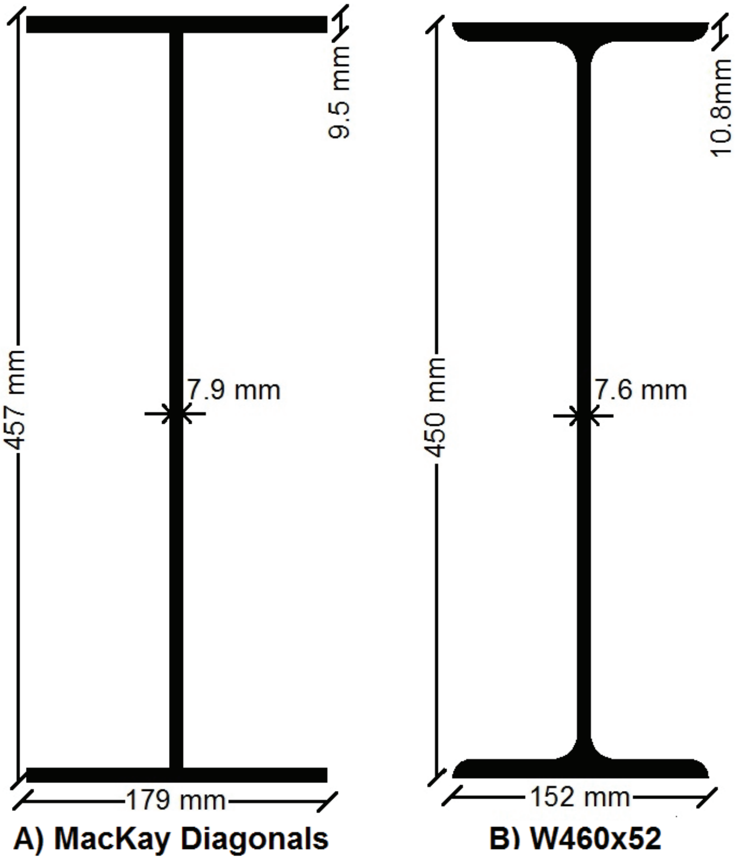

Figure 8-6 : Cross-section comparison

Table 8-3 : Lab specimen surface preparation

Gauge	Depth of Preparation	Vertical Position from C/L
A	0.0 mm	+37.5 mm
B	0.0 mm	+37.5 mm
AA	1.7 mm	+112.5 mm
BB	0.0 mm	+112.5 mm
AAA	1.3 mm	-37.5 mm
BBB	0.5 mm	-37.5 mm

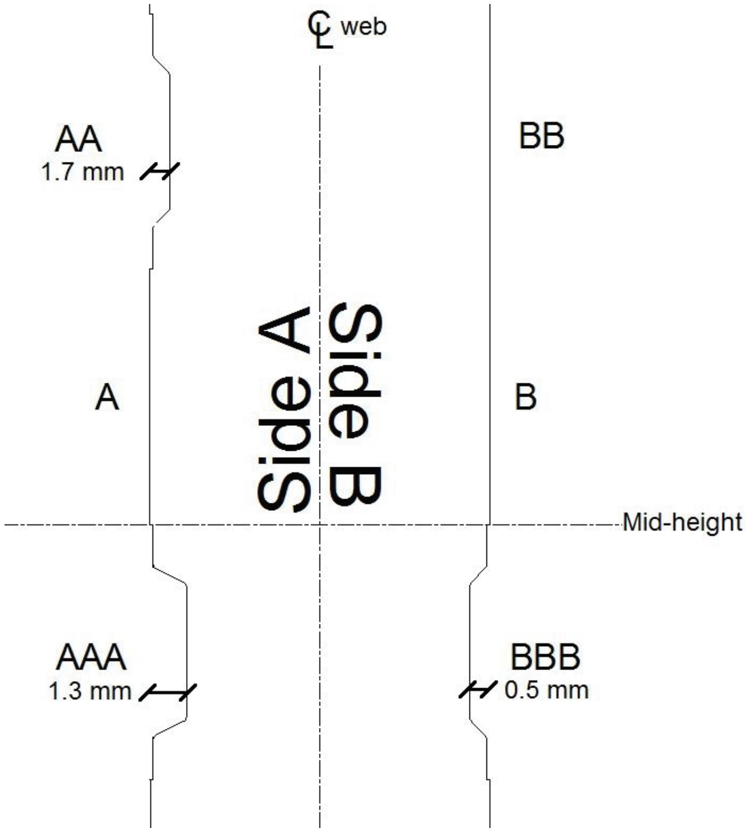

Figure 8-7 : Cross-section through web

8.2.3 Testing Procedure

To ensure a uniform stress was applied to the ends of the section, an additional 50 mm plate was added to either end. To monitor (and avoid) bending strains that would impact readings, 4 additional flange gauges were installed at the mid-height.

Figure 8-8 is a plot of section depth versus gauge strain readings for a compressive load of 300 kN; the nominal (theoretical) section strain is shown, as well as the separation between gauge pairs. The output of the series of six web gauges indicated localized reverse bending of the web in the gauge preparation zone.

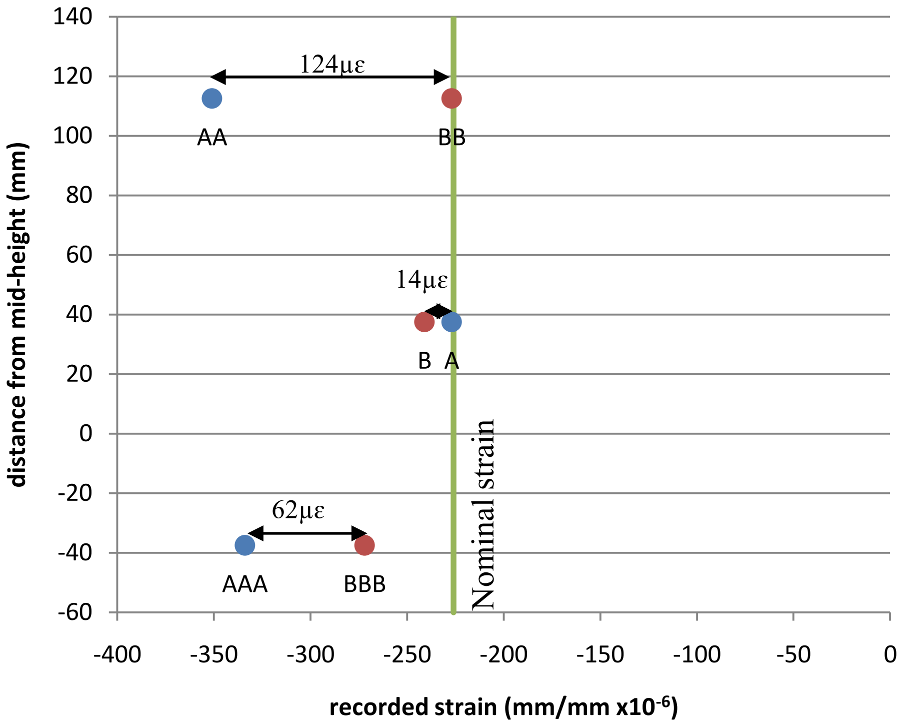

Figure 8-8 : Laboratory testing results

8.2.4 Discussion

The three pairs of gauges on the laboratory specimen are distinctly different from each other. The three combinations of surface preparation also show distinctly different trends. The difference in gauge readings for pairs with (some) surface preparation is quite similar to the ranges observed in the MacKay Bridge data, demonstrating that a surface preparation can cause the gauge reading separation.

8.3 Numerical model of laboratory specimen

To support the laboratory testing which showed that multiple surface preparations could potentially affect the gauge readings, a finite element model was developed.

The model was developed using ADINA software. Using 8-noded isotropic elements in a linear-elastic model, the laboratory specimen was recreated. To model the variations in thickness of the prepared areas, the web was separated into several elements. Nodes defining the surface preparation zone were then adjusted for preparation on both sides of the web. Figure 8-9 shows an isotropic view of a prepared area, with a cut face along the centerline. For clarity, Side A is shown outlined in blue and Side B outlined in red.

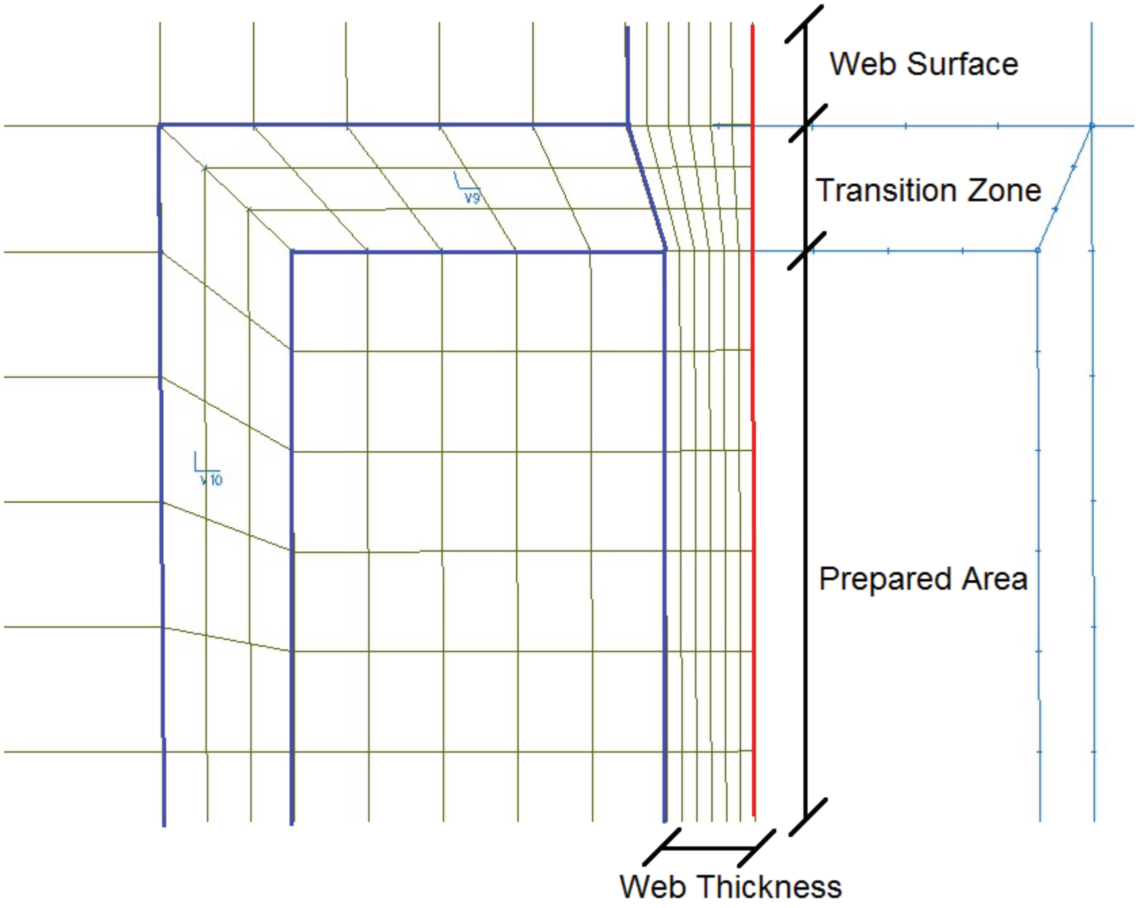

Figure 8-9 : Isotropic view of web through centreline of mesh

A linear variation in web thickness was used to define the transition zone. Six elements were used through the web thickness; the depth of all elements and nodal coordinates were adjusted to achieve a change in preparation depth.

The section was placed in axial compression with the load being applied as a uniform pressure. The boundary conditions for the model were applied to the base, restraining the model in the vertical direction. Images of the mesh and a sample strain profile can be seen in Figure 8-10 and Figure 8-11. It is very interesting to note that the axial strain over the majority of the member area is uniform (the green zone of Figure 8-11) and consistent with the nominal axial strain predicted by fundamental mechanics. The disturbed region is localized to surface prepared area where gauges would be applied.

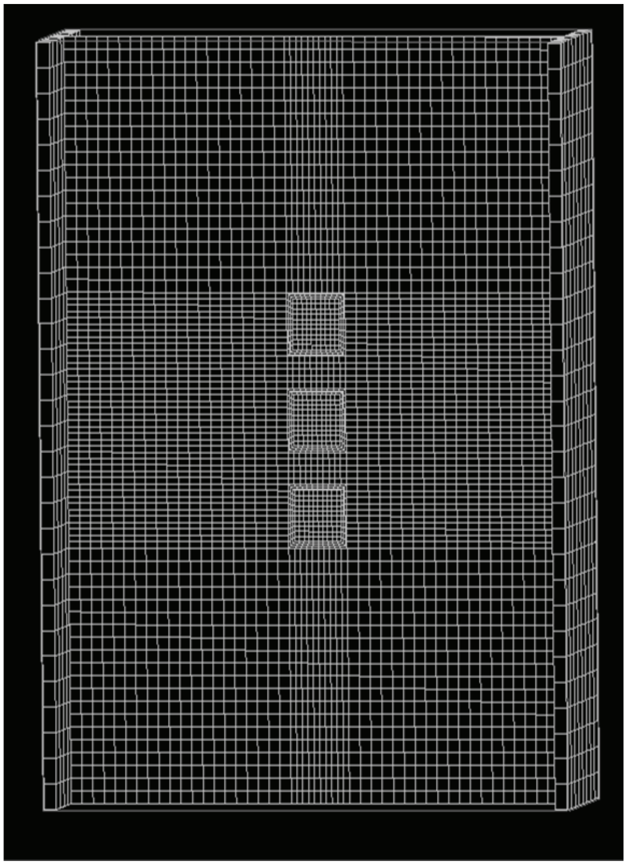

Figure 8-10 : Sample finite element mesh

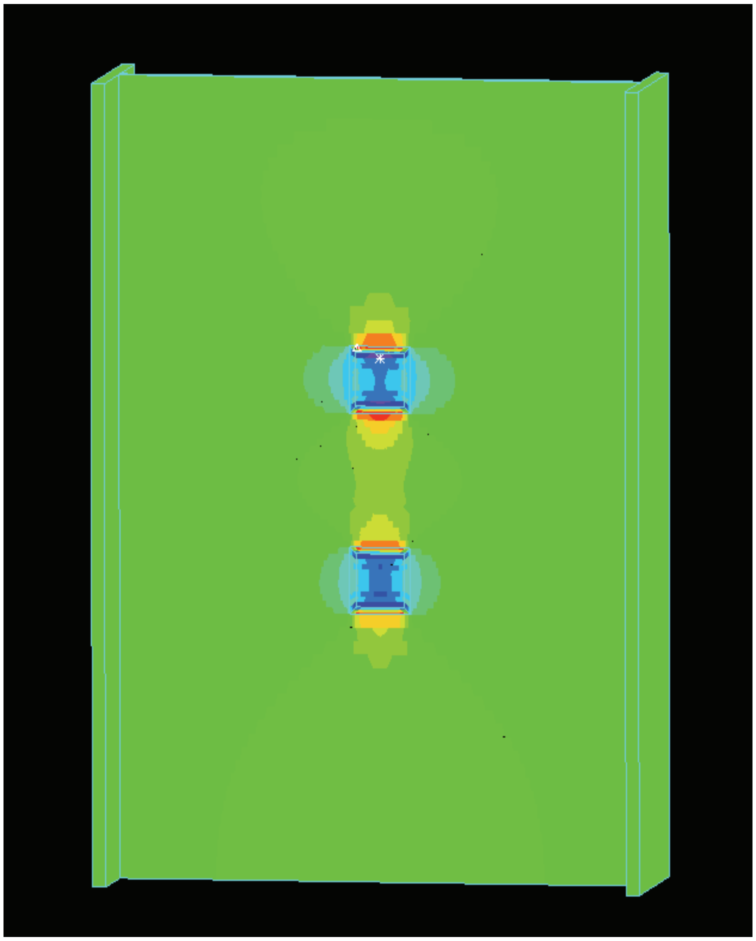

Figure 8-11 : Qualitative sample finite element strain profile

8.3.1 Theoretical and Laboratory Test Comparison

The results from the model are shown compared with the lab specimen in Figure 8-12. For this variation of the model, the depth of preparation required to reproduce the laboratory results were estimated based on Figures Figure 8-17 and Figure 8-18, presented later in this Section. While the gauge values are not identical, it is immediately apparent that the trends are comparable to those from the laboratory testing; gauges with no preparation are close to the nominal strain, and gauge with large surface preparation indicate more strain.

Despite the controls used in laboratory testing, there are still uncertainties; surface preparation is not precise, and there is always the possibility that material inconsistencies could change the outcome.

To summarize, the impact of gauge surface preparation observed in lab test data was corroborated using a linear elastic finite element model of the test section. While strain values computed were not identical to those found in the laboratory, trends were repeated, showing that surface preparation does affect the local strain measurements. This is believed to be the main cause of strain difference in web pairs observed in the field monitoring measurements.

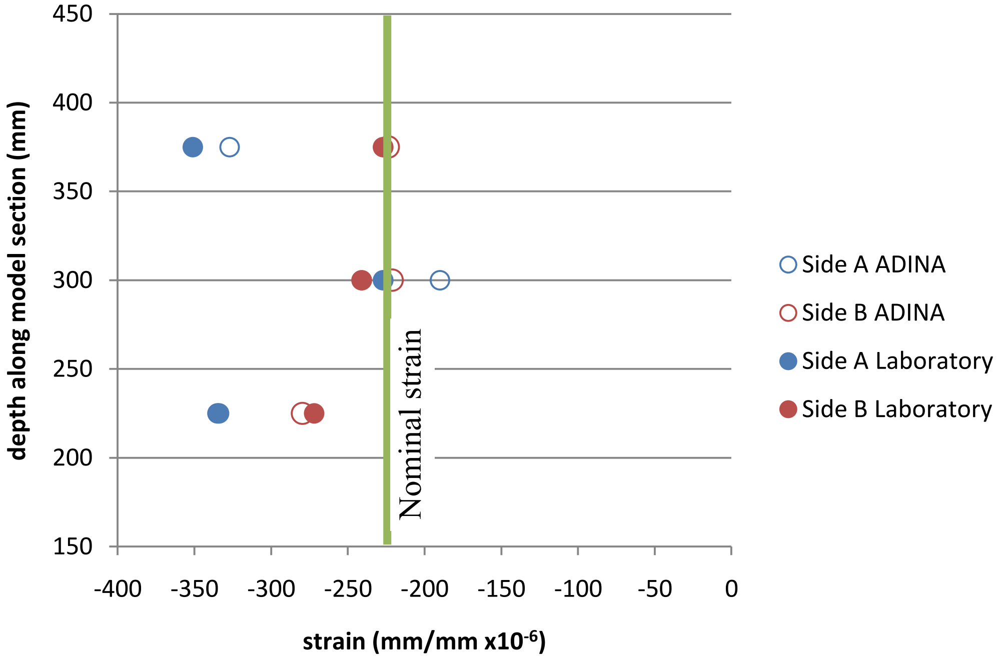

Figure 8-12 : Comfirmation with theory

8.4 Parametric Investigation

To further explore the effects of surface preparation on local gauge readings from the compression diagonals monitored on the MacKay Bridge, a numerical parametric study was completed using several parameters; depth of surface preparation, diameter of the prepared area, and width of the transition zone. Throughout the parametric investigation, the gross section geometry was held constant, with a web thickness of 7.6 mm.

For these parameters, a single gauge preparation area was placed at the centre of the model, similar to those used in the field. A load was applied which resulted in a nominal strain of 500 με.

8.4.1 Single Sided Surface Preparation

Single sided surface preparation was examined by varying the depth of preparation on side A from 0.0 mm to 1.5 mm. Side B had no surface preparation (or a depth of preparation of zero). By extracting the strain at the centre of the prepared region (where the gauge is located) and plotting strain against depth of preparation (Figure 8-13), the impact of surface preparation on measured strain is apparent. The strain values in Figure 8-13 have been normalized against the nominal strain of 500 με which would have occurred if no surface preparation had been done. It is important to observe that the influence is not the same on both gauges, hence the change in strain is not as simple as the ratio of thickness of a prepared web to an unprepared web.

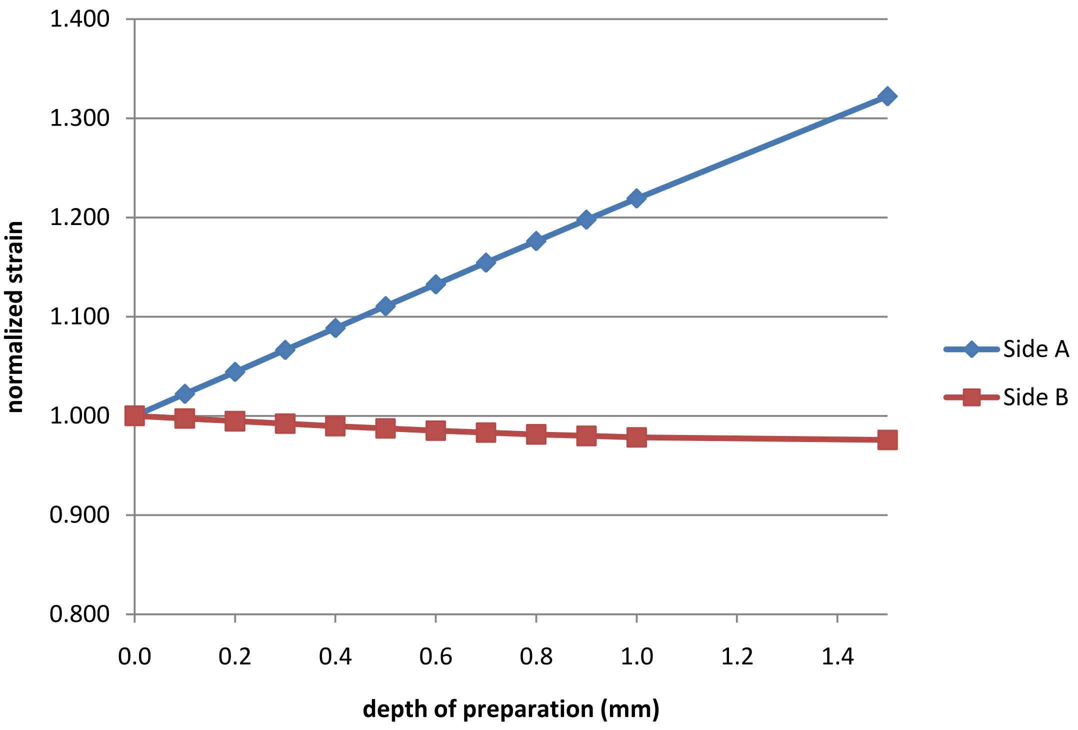

Figure 8-13 : Single-sided surface preparation

8.4.2 Double Sided Surface Preparation

Similarly, double sided surface preparation was examined by maintaining a total depth of web thickness removed. Three separate cases were examined; 0.5 mm, 1.0 mm and 1.5 mm of total surface preparation. For example, 0.1 mm preparation on side A and

0.4 mm preparation on side B would be a total of 0.5 mm. The study began with all preparation on side A and transitioned to a state of even preparation in 0.1 mm intervals.

The analysis shows that the measured strain behaves in a linear fashion when related to the depth of preparation on side A. Figure 8-14 shows the normalized strain distribution for 1.5 mm of total preparation, similar plots were produced for the other two scenarios. It is noted that when both sides had equal surface preparation (0.75 mm each), the strain readings for side A and B were equal but approximately 15% greater than the nominal web strain.

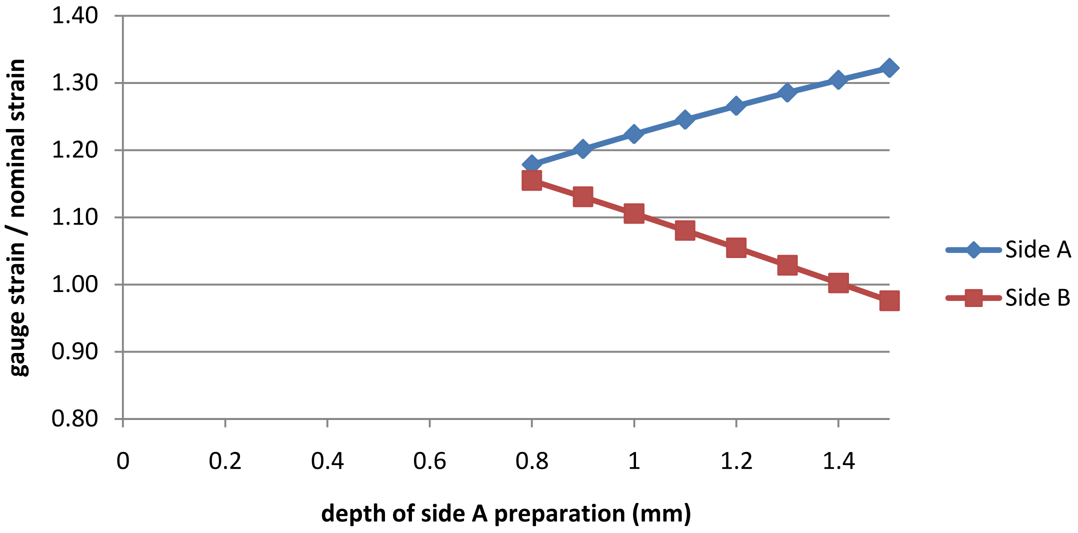

Figure 8-14: Normalized strain for 1.5 mm double sided preparation

8.4.3 Transition Zone

The diameter of the transition zone was examined to determine the extent of the effect it had on gauge readings at the centre of the prepared area. Using a preparation depth of 1.0 mm on a single preparation surface, the width of the transition zone was varied from 5 mm to 25 mm. The plot shown in Figure 8-15 was developed by normalizing the gauge strain based on the initial transition zone width of 5 mm.

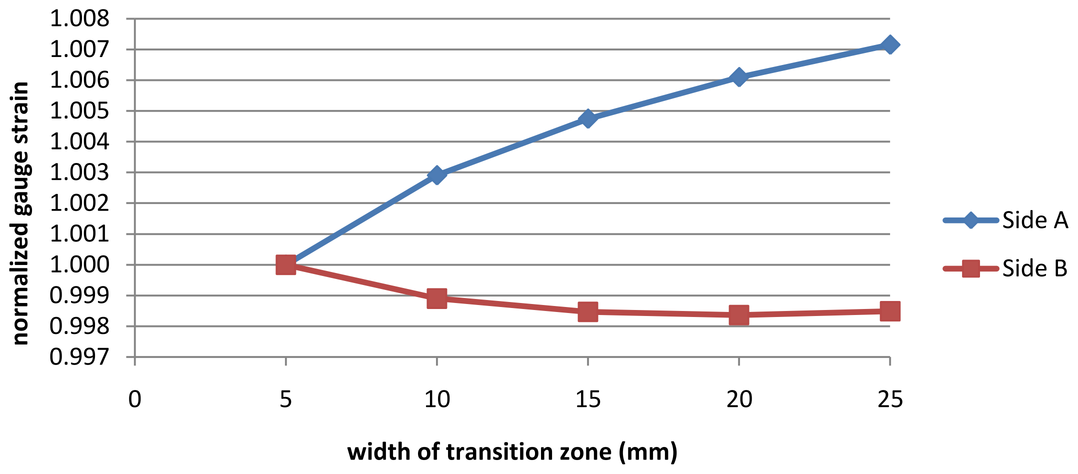

Figure 8-15 : Normalized transition zone

It was found that the strain changed by less than 1% due to the changes in transition zone diameter.

8.4.4 Diameter of Prepared Area

The final parameter examined is the diameter of the prepared area itself. Using a preparation depth of 1.0 mm on a single preparation surface, the diameter of the prepared area was varied from 20 mm to 60 mm. The plot shown in Figure 8-16 was produced by normalizing the gauge strain based on the initial 40 mm diameter.

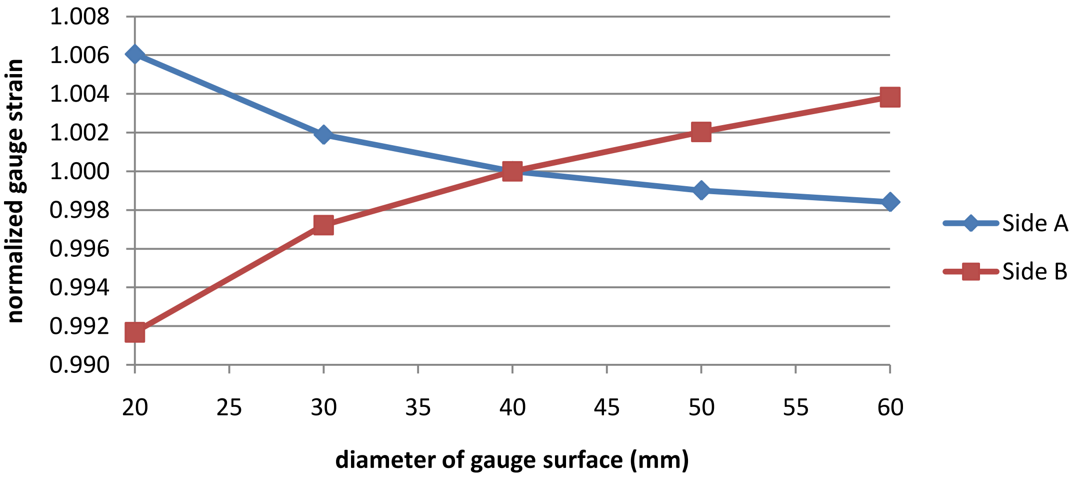

Figure 8-16 : Normalized preparation area

The size of the prepared area changed the strain by less than 1%. Therefore the depth of surface preparation is the most significant of the geometric parameters.

8.4.5 Interpretation of Model Results

Using the information developed from the parametric study, two plots were developed which relate the difference in readings between sides A and B , the average of A and B readings, and the total depth of preparation. These two plots are shown in Figure 8-17 and Figure 8-18. For these figures, 'A' and 'B' is depth of preparation on side A and side B, and 'w' is the web thickness.

Using Figure 8-17, for a given difference between strain readings of 15% of the nominal strain, a minimum total depth of preparation of ~8% of the nominal web thickness can be found. Similarly, using Figure 8-18, one can see that the average strain relies primarily on the total depth of preparation, regardless of whether that preparation is on Side A or Side B.

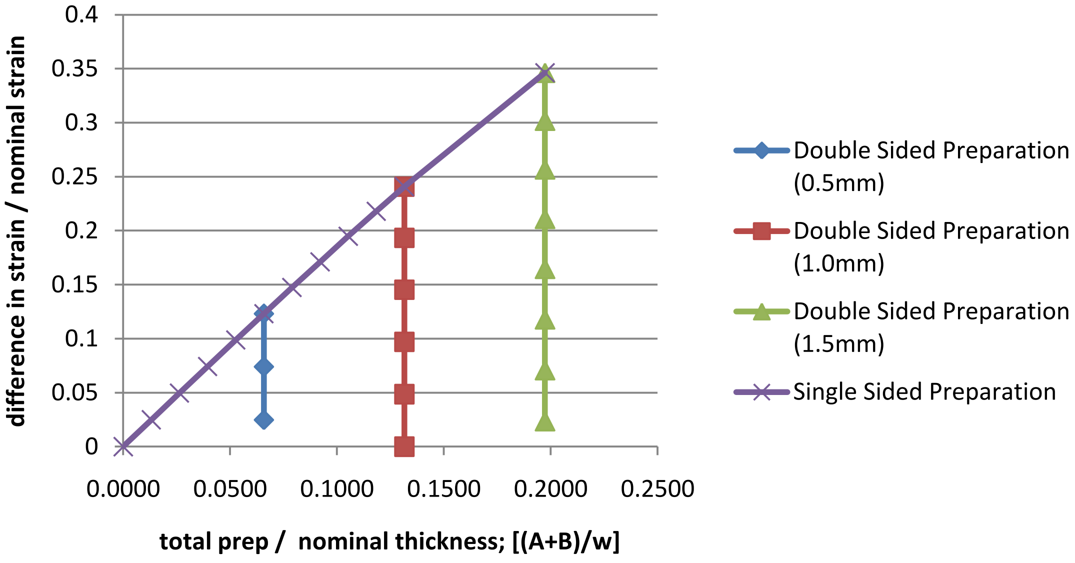

Figure 8-17 : Relating gauge difference to total preparation

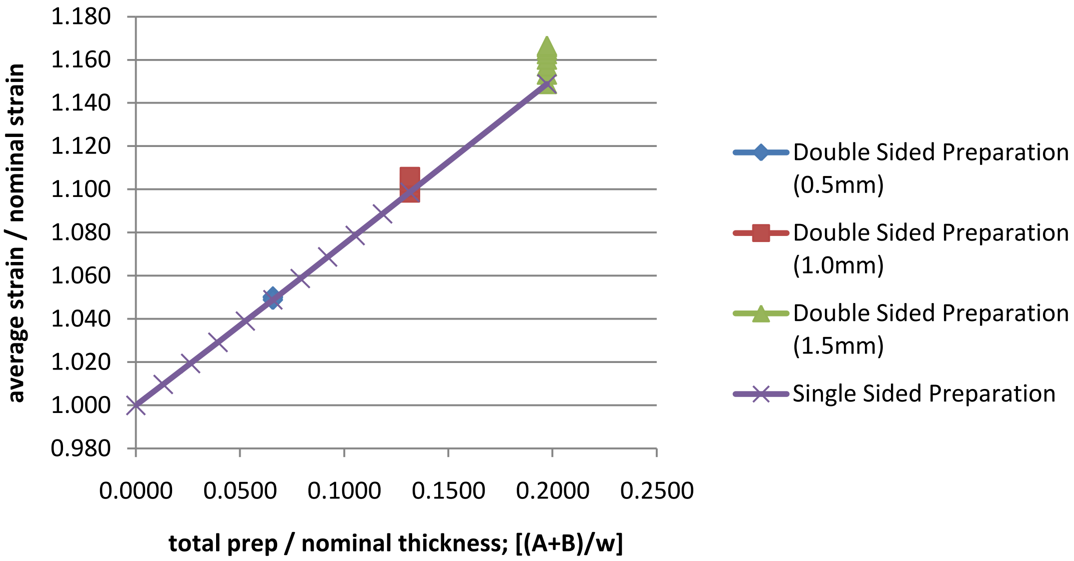

Figure 8-18 : Relating gauge average to total preparation

While these two findings indicate a minimum prepared surface, they cannot be used to determine the actual field conditions. As a result, the nominal strain cannot be determined from the gauge readings without knowing the depth of surface preparation a priori.

8.4.6 Discussion

Based on the parametric work done, it became obvious that there was a significant increase in local stresses (read gauge stresses) with increased depth of preparation. The magnitudes of the results presented above are specific to the diagonal members of the longitudinal and lateral stiffening trusses on the MacKay Bridge. It is recommended that a similar procedure be employed when surface preparation effects are being considered on members with different geometry.

It was determined that single sided surface preparation creates the most obvious difference between gauge readings, with the prepared side (Side A in the study) showing a large increase over the nominal strain, while the opposite side (Side B) shows a slight decrease. While not specifically shown, the large increase and minor decrease implies that the average of the two gauges is higher than the nominal strain. Figure 8-18 supports this conclusion; hence, the average of the gauge pairs should always be conservative compared to the nominal strain.

Finally, the average of Side A and Side B is more reliant on the total of the surface preparation, not the individual sides, implying that any additional bending strains introduced are minimal.

It is understood that some amount of surface preparation is required for a strain gauging project being implemented on existing steel. While the gauge reading of greater magnitude in any given pair is the most conservative selection, it may be too conservative. There is potential for the value to be 20% greater than the nominal strain with only 1.0 mm total preparation.

Based on the parametric study, it was found that any surface preparation will cause a decrease in cross-sectional area, resulting in an increase in the average local strain due to both section loss and local bending. As a result, it is recommended that the average of a pair of gauges be taken as the best estimate of actual strain. This value is either greater than the nominal member strain.

Chapter 9. Numerical Model Correction Factor

The recorded strains from the calibration testing were generally found to be lower than those predicted by the B&T numerical model. Figure 9-1 shows a representative sample, the entire set is in Appendix III – Gauge Comparison March 2010 – Numerical Model.

As a result of the difference, a model correction factor (multiplier) was sought to adjust the model results to more closely match with testing results. Curve fitting was completed using a simple linear modifier:

$$(\text{Test Data}) = \text{X} \cdot (\text{Model Results}) \qquad [9\text{-}1]$$

where:

X = Model correction factor

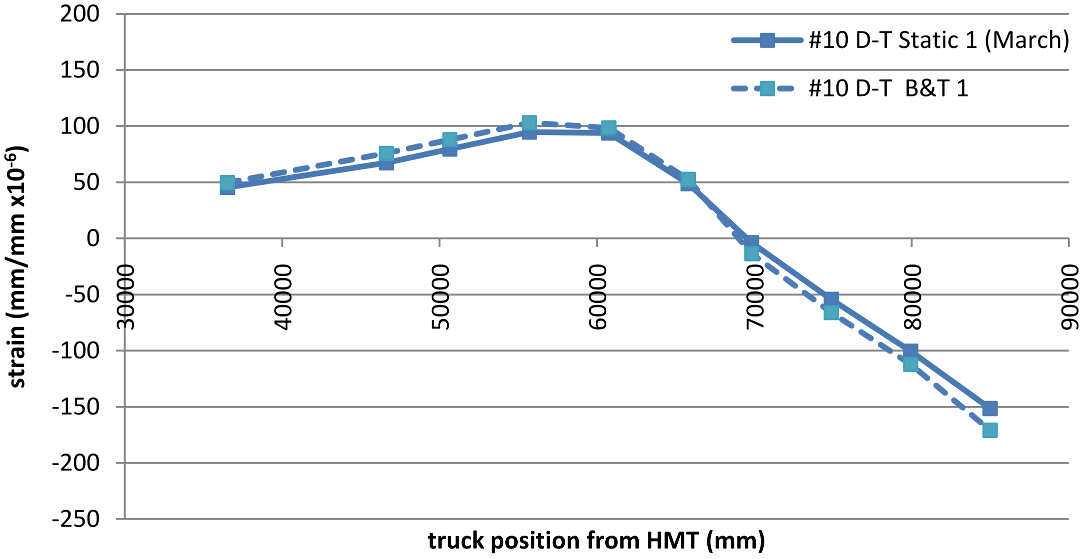

Figure 9-1 : Model vs static results

To fit a curve, the Sum of Squared Errors (SSE) was minimized for the data set to determine a best fit for the data (often referred to as the method of least squares).

$$\text{SSE} = \sum [\text{X}(\text{Model Results}) - \text{Test Data}]^2 \qquad [9\text{-}2]$$

While individual gauge fits would provide better correlation with the data, a single global correction factor was preferred because it would simplify interpretation of model results.

To determine the global correction, only diagonal gauges were examined, within these, #3 D-T was omitted because it was replaced during the year. Using data collected from the ten positions in the calibration testing, a global correction factor of 0.98 was determined. Figure 9-2 shows a sample global curve fit.

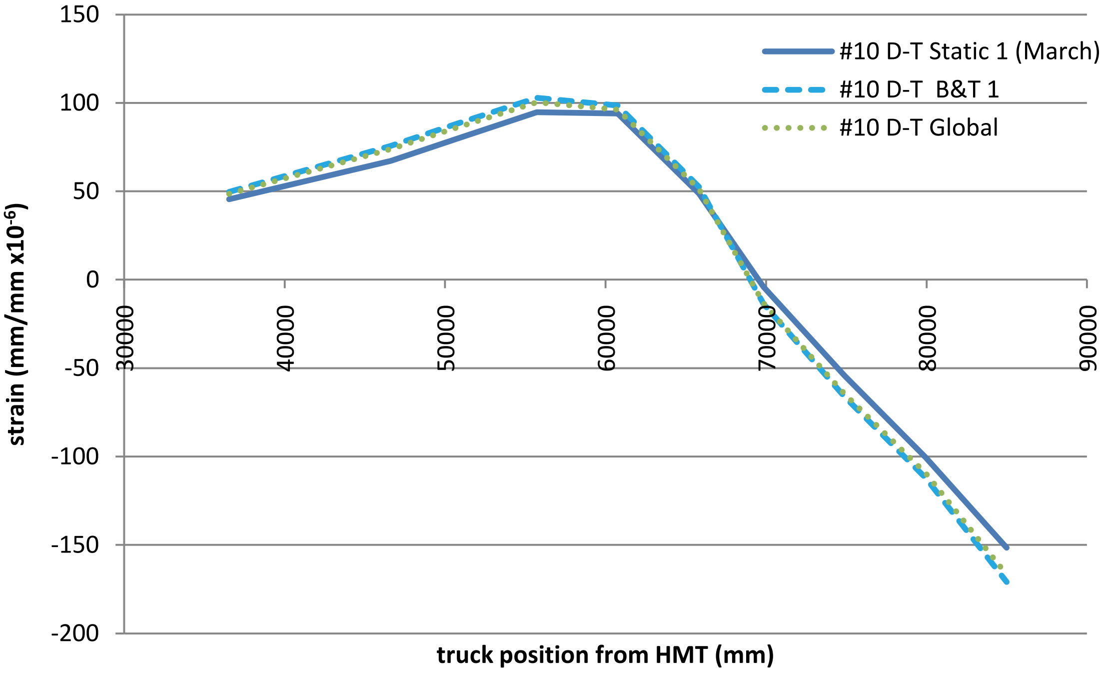

Figure 9-2: Global average fit

Chapter 10. Long-Term Data Collection

10.1 Data Management

Data was collected and stored in files averaging seven days in length; this permitted visual scans of the collected data to identify changes in trends that may indicate system or component failure. A sample of a weekly data file for a single gauge is shown in Figure 10-1. By separating the data into smaller portions, the potential for corruption of data was reduced.

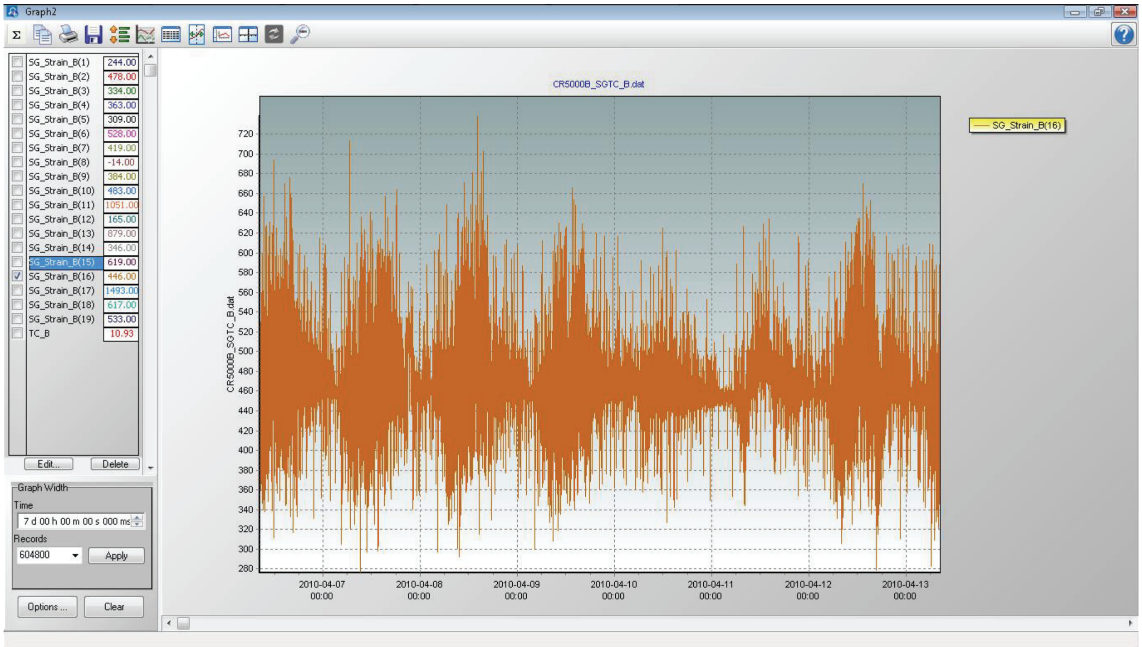

☐	SG_Strain_B(1)	244.00
☐	SG_Strain_B(2)	478.00
☐	SG_Strain_B(3)	334.00
☐	SG_Strain_B(4)	363.00
☐	SG_Strain_B(5)	309.00
☐	SG_Strain_B(6)	528.00
☐	SG_Strain_B(7)	419.00
☐	SG_Strain_B(8)	-14.00
☐	SG_Strain_B(9)	384.00
☐	SG_Strain_B(10)	483.00
☐	SG_Strain_B(11)	1051.00
☐	SG_Strain_B(12)	165.00
☐	SG_Strain_B(13)	879.00
☐	SG_Strain_B(14)	346.00
☐	SG_Strain_B(15)	619.00
☑	SG_Strain_B(16)	446.00
☐	SG_Strain_B(17)	1493.00
☐	SG_Strain_B(18)	617.00
☐	SG_Strain_B(19)	533.00
☐	TC_B	10.93

Time: 7 d 00 h 00 m 00 s 000 ms
Records: 604800

Figure 10-1 : Sample of weekly data file

10.2 Post-Processing

Three components were required in the post-processing phase of the data management; zeroing, temperature correction and traffic event isolation.

10.2.1 Zeroing

During strain gauge installation a residual strain is imparted on the system. This residual strain was removed from the gauge readings by identifying a point where no live load effect was present; the March 2010 calibration test was selected. This ‘zero’ reading is subtracted from all subsequent readings to determine the live load effect. The zero readings were developed during a period of bridge closure; therefore no vehicle live load effect was ensured. Figure 10-2 is a plot showing deviation in strain from the average zero reading for a period of 60 seconds during calibration testing. This shows there is little variation in strain during the zero readings period due to ambient vibrations.

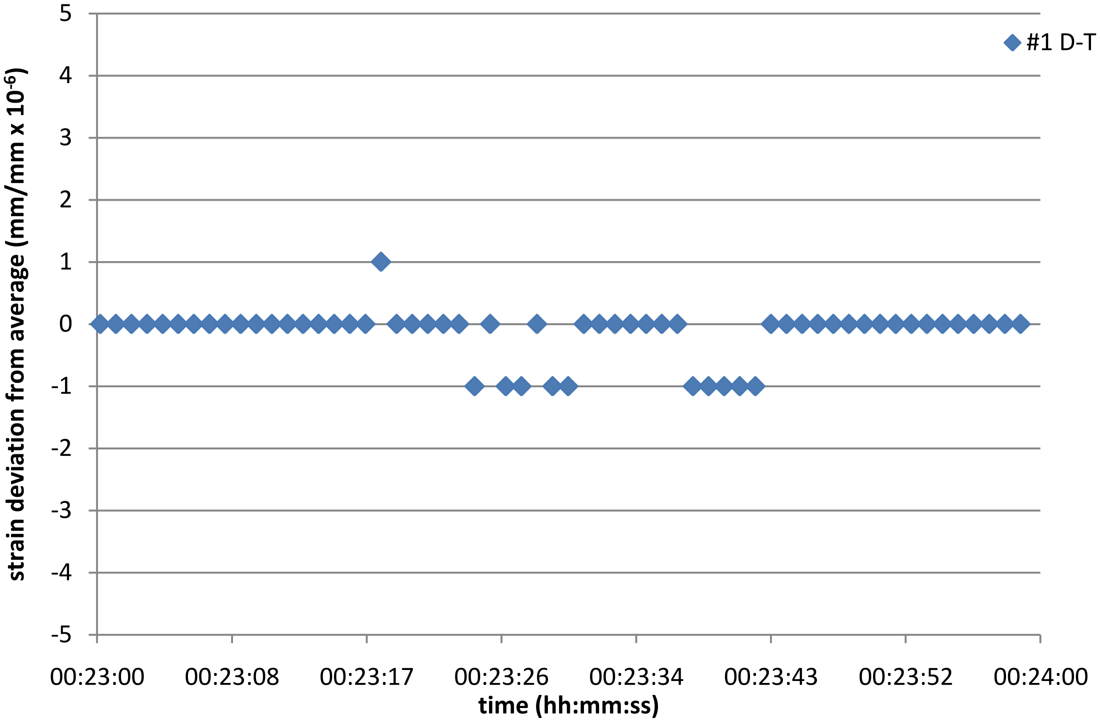

Figure 10-2 : 60 second sample of strain deviation during zero recording

10.2.2 Temperature Correction

As discussed in Section Chapter 5, several dummy gauges were installed on the bridge. These gauges were used to correct for temperature induced changes in the gauge readings. The gauges were selected to be thermally compensated for a steel substrate. This compensation is near perfect at room temperature but can be vary with the temperature range seen in field application. Similar to the 'zero' correction, a temperature correction is applied to all readings based on the dummy gauges that best represent the gauge of interest; #1 D-Dumb & #3 Dumb1 are on top of a truss chord, the average of these two gauges correct all gauges on the top of diagonals. Conversely, #3 Dumb2 is on the bottom of a diagonal and shielded from the sun, this better represents the gauges on the bottom of the diagonals (and below the deck). Table 10-1 lists the appropriate gauge-dummy pairs.

Table 10-1 : Temperature corrections

Gauge	Temperature Correction	Gauge	Temperature Correction
#1 D-T	#1 D-Dumb & #3 Dumb1	**#1 D-B**	#3 Dumb2
#2 D-T	#1 D-Dumb & #3 Dumb1	**#2 D-B**	#3 Dumb2
#3 D-T	#1 D-Dumb & #3 Dumb1	**#3 D-B**	#3 Dumb2
#3 F-U-T-S	#1 D-Dumb & #3 Dumb1	**#3 F-U-T-N**	#3 Dumb2
#3 F-U-B-S	#1 D-Dumb & #3 Dumb1	**#3 F-U-B-N**	#3 Dumb2
#3 F-L-T-S	#1 D-Dumb & #3 Dumb1	**#3 F-L-T-N**	#3 Dumb2
#3 F-L-B-S	#1 D-Dumb & #3 Dumb1	**#3 F-L-B-N**	#3 Dumb2
#4 D-T	#1 D-Dumb & #3 Dumb1	**#4 D-B**	#3 Dumb2
#5 D-T	#1 D-Dumb & #3 Dumb1	**#5 D-B**	#3 Dumb2
#6 D-T	#1 D-Dumb & #3 Dumb1	**#6 D-B**	#3 Dumb2
#7 D-T	#1 D-Dumb & #3 Dumb1	**#7 D-B**	#3 Dumb2
#8 D-T	#1 D-Dumb & #3 Dumb1	**#8 D-B**	#3 Dumb2
#9 D-T	#1 D-Dumb & #3 Dumb1	**#9 D-B**	#3 Dumb2
#10 D-T	#1 D-Dumb & #3 Dumb1	**#10 D-B**	#3 Dumb2
#11 D-T	#11 D-Dumb	**#11 D-B**	#3 Dumb2
#12 D-T	#11 D-Dumb	**#12 D-B**	#3 Dumb2

10.2.3 Traffic Event Identification

To simplify the data collection process, strain was recorded on a continuous basis at a frequency of 1 Hz. The result is an excess of data which represents all states of strain during the recorded period. For example in Figure 10-1, all strains for every second during that seven day period were recorded. Hence the complete data file includes many readings when there was no traffic within the influence zone of a particular gauge as well as many strain values associated with ‘ramping up’ to a peak reading and ‘ramping down’ from a peak reading. The desired outcome of the final stage of post-processing was the reduction of the data to contain only the peak strain caused by individual traffic events. A traffic event was identified as a change in strain culminating in a peak.

To separate true peaks (traffic events) from ambient noise, a filter was applied to the data ignoring changes in readings less than 5 $\mu\varepsilon$.

The flowcharts shown in Figure 10-3 and Figure 10-4 show the process used by the post-processing software for increasing and decreasing data trends.

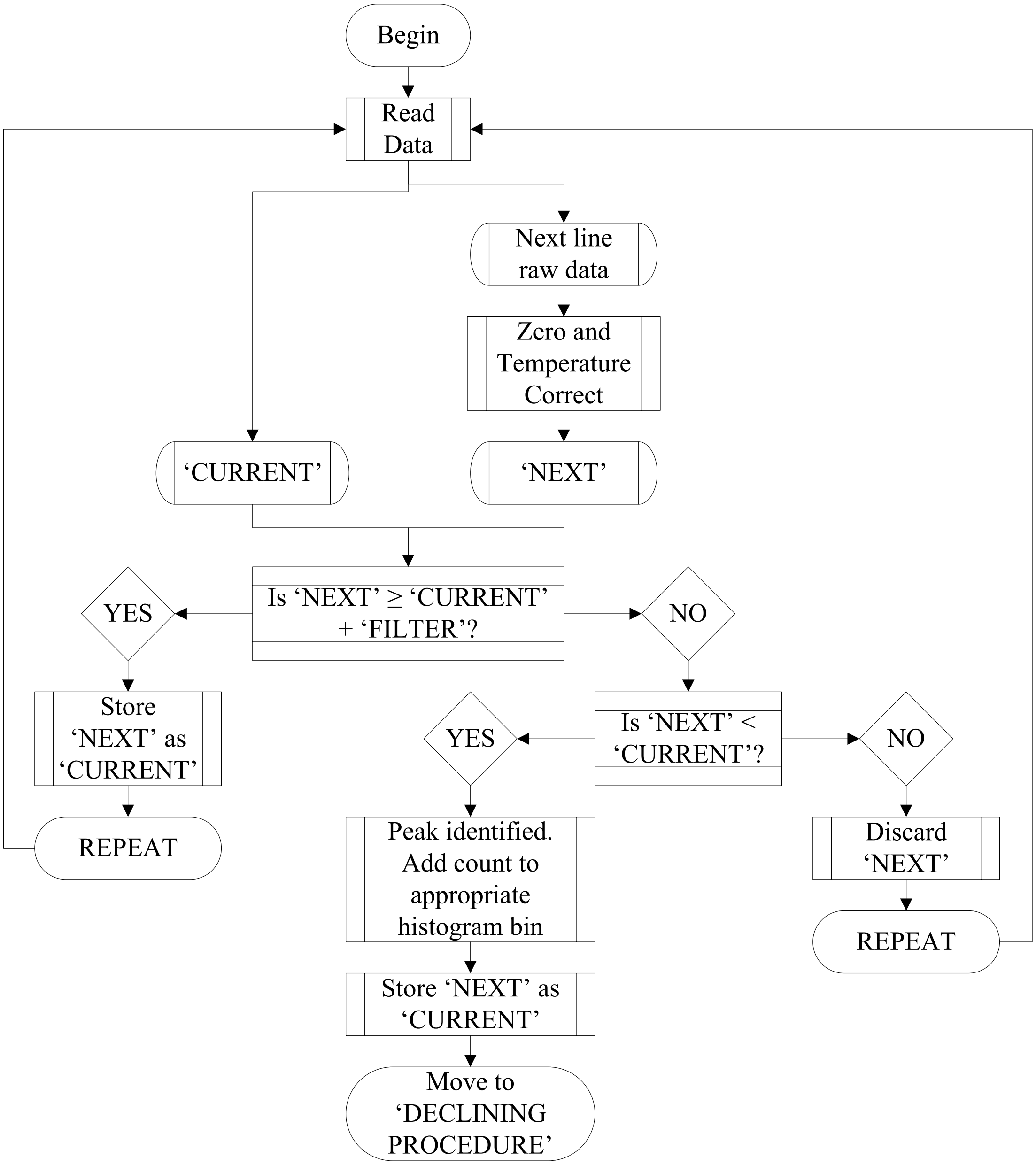

Figure 10-3 : Increasing data trend flowchart

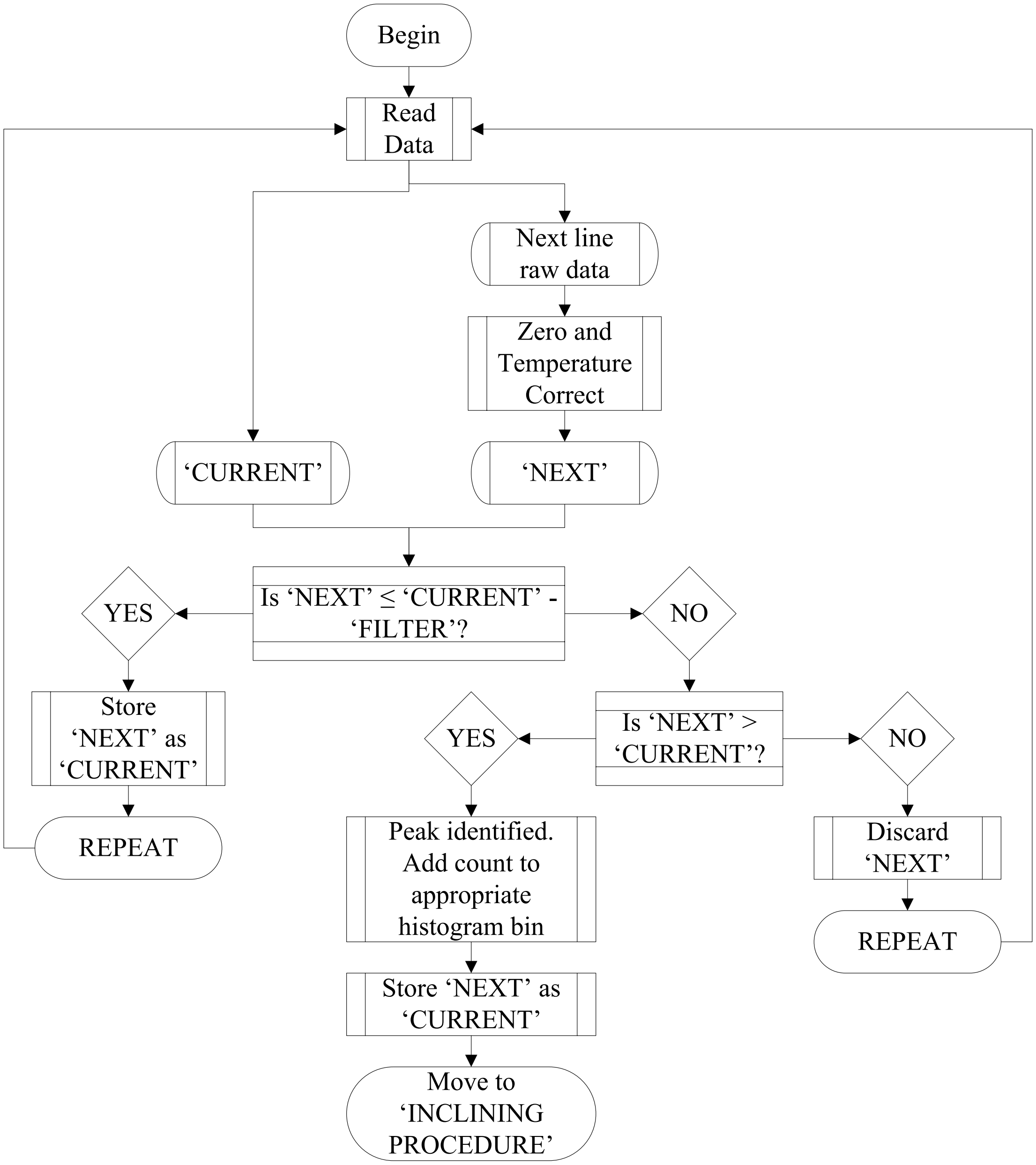

Figure 10-4 : Decreasing data trend flowchart

10.3 Interpretation

Following post-processing of the data to extract the live load peaks, histograms were developed to visualize the traffic event distribution for each gauge. The monitored period was from January 13, 2010 to March 15, 2011. A sample histogram of peak load effects is shown in Figure 10-5 for gauge #1 D-T with the entire set shown in Appendix IV – Long-Term Data Histograms. Negative values on the histogram indicate compressive strain, positive values indicate tensile strain. The same histogram is displayed on two vertical scales; linear and logarithmic. The linear scale is used to view trends in the entire data set while the logarithmic scale enables viewing of the extreme data values. From the logarithmic scale, it is easily seen that there is one peak strain of -217 με for gauge #1 D-T during the monitoring period. Table 10-2 shows the extreme values for all gauges.

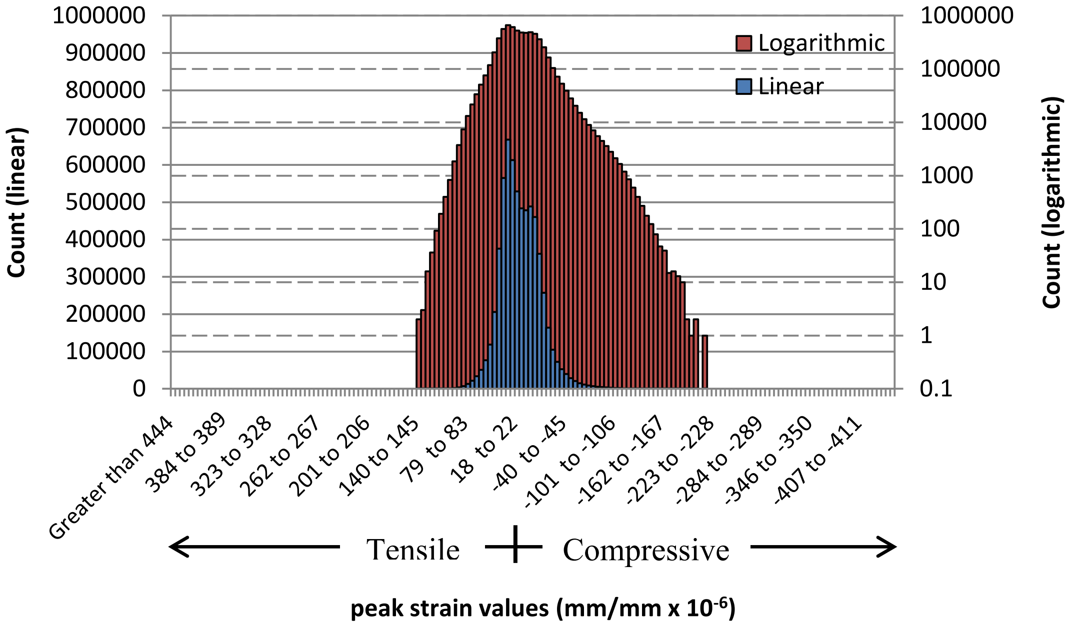

Figure 10-5 : Sample long-term histogram (gauge #1 D-T)

Table 10-2 : Extreme strain readings (mm/mm x 10^{-6})

Gauge	Maximum Strain	Minimum Strain	Gauge	Maximum Strain	Minimum Strain
#1 D-T	145	-217	**#1 D-B**	178	-245
#2 D-T	128	-245	**#2 D-B**	139	-256
#3 D-T (I)	111	-183	**#3 D-B**	206	-350
#3 D-T (N)	156	-339			
#3 F-U-T-S	156	-306	**#3 F-U-T-N**	178	-295
#3 F-U-B-S	278	-383	**#3 F-U-B-N**	295	-395
#3 F-L-T-S	239	-444	**#3 F-L-T-N**	261	-389
#3 F-L-B-S	172	-356	**#3 F-L-B-N**	233	-322
#4 D-T	161	-183	**#4 D-B**	222	-295
#5 D-T	222	-300	**#5 D-B**	189	-217
#6 D-T	217	-317	**#6 D-B**	228	-228
#7 D-T	189	-222	**#7 D-B**	200	-233
#8 D-T	183	-233	**#8 D-B**	228	-245
#9 D-T	273	-150	**#9 D-B**	283	-172
#10 D-T	200	-228	**#10 D-B**	217	-233
#11 D-T	322	-289	**#11 D-B**	339	-295
#12 D-T	288	-350	**#12 D-B**	422	-306

10.4 Characterization of Peak Traffic Events

Following identification of the peak traffic effects in Table 10-2, the characteristics of the peak traffic events were examined by focusing on the shape and duration of the strain data around the peak event. The traffic events causing the peak effects were identified using the histogram generation process. The largest events (approximately six per gauge) were identified – the data files corresponding to these events are listed in Table 10-3. From this table, Figure 10-6 was generated to determine which (if any) of the traffic effects were caused by a single event.

The plot shows time on the horizontal axis with the vertical axis representing each gauge in turn, alternating between top and bottom gauges in a pair. It was hypothesized that the largest event (peak reading) in a member would register on both top (shown in blue) and bottom (shown in red) gauges; therefore, points were plotted sequentially, following histogram bins, until a pair was registered for each member – those pairs are circled.

Table 10-3 : Peak traffic event dates

Gauge	1st Histogram Bin	2nd Histogram Bin	3rd Histogram Bin	4th Histogram Bin	5th Histogram Bin	6th Histogram Bin
#1 D-T	Jun22/10	Feb 16/10 Mar 9/10	Feb 9/10	Feb 9/10 Aug 31/10		
#1 D-B	Mar 22/10	Apr 27/10 May 18/10	Mar 9/10	Mar 2/10 Jun 22/10 Aug 31/10		
#2 D-T	Mar 22/10 May 18/10 Nov 10/10	Feb 16/10 Mar 22/10 Jan 5/11 Jan 12/11				
#2 D-B	Aug 31/10 Nov 10/10	Jun 29/10 May 18/10	Aug 31/10 Sept 14/10 Jan 5/11			
#3 D-T	Jun 29/10	May 18/10	Oct 5/10	Jun 1/10	Jan 5/11	Apr 20/10 May 4/10 Aug 31/10 Oct 5/10
#3 D-B	Jun 29/10	Mar 15/10	Aug 31/10	Aug 24/10 Aug 31/10	Apr 27/10	
#4 D-T	Feb 9/10 Mar 22/10 May 18/10	Jan 19/10 Feb 16/10 Jun 15/10 Mar 15/11				
#4 D-B	Aug 31/10	May 18/10	Mar 22/10	Apr 13/10 Aug 24/10		
#5 D-T	Mar 22/10 Aug 31/10 Oct 5/10	Oct 26/10	Feb 16/10 Sept 7/10			
#5 D-B	Mar 22/10 Apr 27/10	Jun 8/10	Feb 16/10			
#6 D-T	Apr 6/10	Oct 5/10	Mar 22/10	Feb 16/10	Jun 8/10	
#6 D-B	Aug 31/10 Jan 12/11	Aug 24/10 Aug 31/10	Mar 22/10 Apr 27/10 May 11/10 May 18/10			
#7 D-T	May 11/10 Jun 8/10 Jan 12/11	Mar 22/10 Jun 15/10 Aug 31/10				
#7 D-B	May 11/10	Aug 31/10	Mar 22/10 Jun 22/10 Jan 5/11			
#8 D-T	Jan 12/11	Jan 5/11 Jan 12/11	May 18/10 Aug 31/10 Oct 5/10 Oct 26/10			
#8 D-B	Feb 16/10	Mar 22/10	Apr 16/10 Aug 17/10			

Gauge	1st Histogram Bin	2nd Histogram Bin	3rd Histogram Bin	4th Histogram Bin	5th Histogram Bin	6th Histogram Bin
			Jan 12/11			
#9 D-T	Mar 15/11	Mar 22/10 Jun 8/10 Oct 26/10	Sept 28/10			
#9 D-B	Mar 15/11	Mar 15/11	Nov 3/10 Dec 14/10 Jan 12/10 Mar 15/11			
#10 D-T	May 18/10	Apr 13/10 Apr 16/10	Apr 27/10 May 11/10			
#10 D-B	Aug 17/10 Jan 5/11 Jan 12/11	May 18/10 Aug 17/10				
#11 D-T	Oct 19/10 May 15/11	Oct 19/10	Jun 1/10	Aug 31/10 Oct 19/10		
#11 D-B	Jun 1/10 Jun 22/10	Jun 8/10 Jun 22/10 Jul 27/10 Mar 15/11				
#12 D-T	Jul 27/10	Jul 27/10	Jul 27/10 Aug 31/10			
#12 D-B	Jul 27/10	Jul 27/10	Jul 27/10			

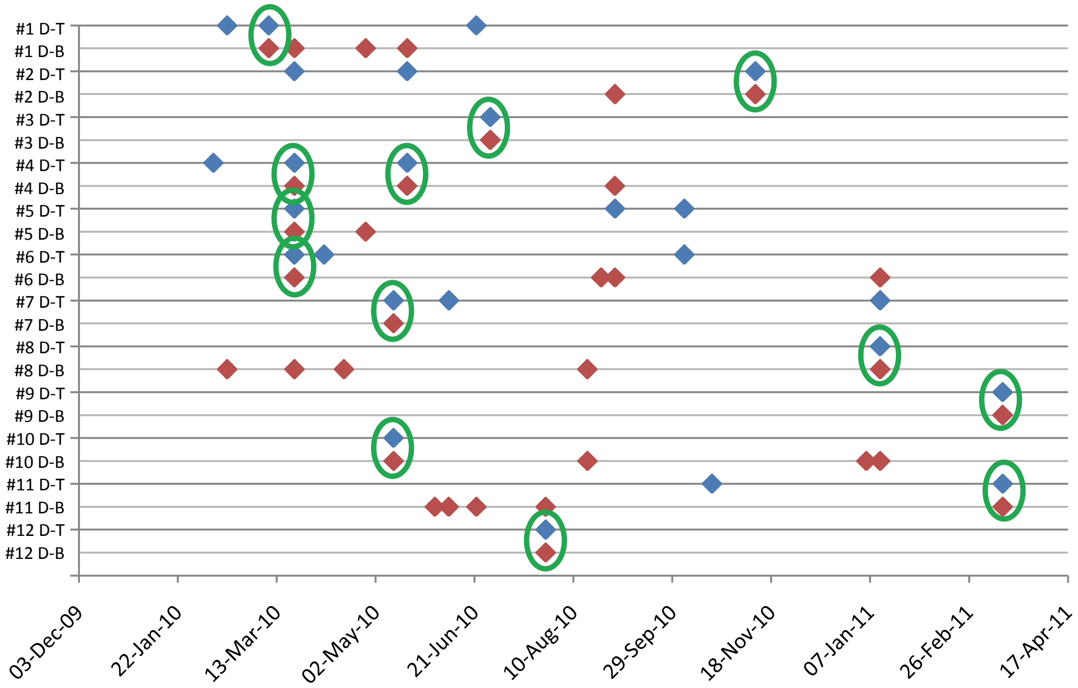

Figure 10-6 : Matching peak event pairs

It was noted that there were many points identified without a ‘match’ from the paired gauge. In other words, the event associated with a peak reading in the top gauge was not the same event which led to the peak reading in the bottom gauge. This led to an extension of the graph to include all of the events listed in Table 10-3. The data files were also visually examined to further examine the traffic events.

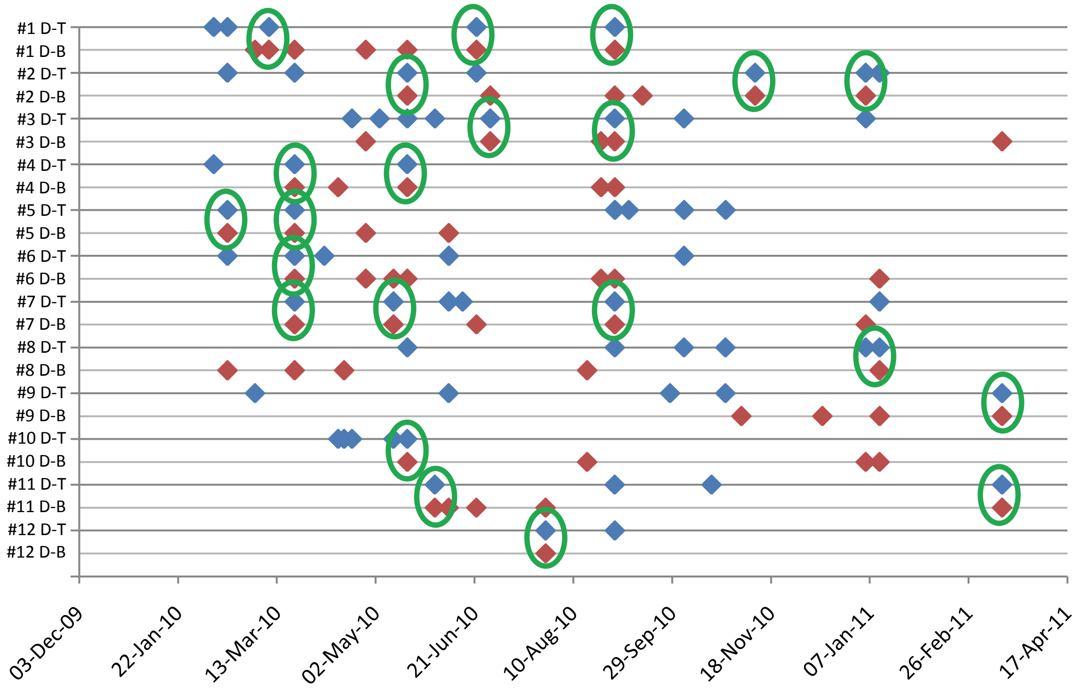

Figure 10-7 : Extended matching peak event pairs

From the extended data, it is noted that Diagonals #4 - #7 were affected by a large event the week of March 22nd, 2010, similarly Diagonals #1, #3 and #7 saw a large event the week ending August 31st, 2010. Despite these patterns, it is also apparent that the other diagonals were affected by individual events occurring during different times throughout the recorded period, suggesting that peak effects were caused by traffic events that did not span the entire bridge.

It is noted that while there are matching pairs for several large traffic effects, there are many data points that do not have a paired gauge.

10.4.1 Visual Examination of Peak Traffic Events

Traffic events of decreasing magnitude were visually examined until the matching pair was found; the plots of the matching pairs are shown in Appendix V – Peak Gauge Pair Examination. Three types of traffic events were discovered when examining the peak events: slow speed traffic events, mixed traffic events, and fast speed traffic events. The three event types are shown in Figure 10-8, Figure 10-9, and Figure 10-10 respectively. For clarity, the absolute values of recorded strain have been removed as these require correction for thermal effects and instrument offsets.

The horizontal axis in Figure 10-8 and Figure 10-9 is time with major division lines in 10 second increments (Figure 10-10 uses 5 second increments) and the vertical axis is recorded strain with major increment lines of 10 με (for Figure 10-8 and Figure 10-9) or 5 με (for Figure 10-10) increments This permits the viewing of the overall shape of the events, the relative magnitude and the duration of the events.

The point of interest is that the peak effects appear to be composed primarily of single vehicle events, with the vehicle travelling at a reasonable speed, similar to Figure 10-10. This observation is contrary to the initial assumption that peak traffic effects would be caused by slow moving (or stopped) traffic.

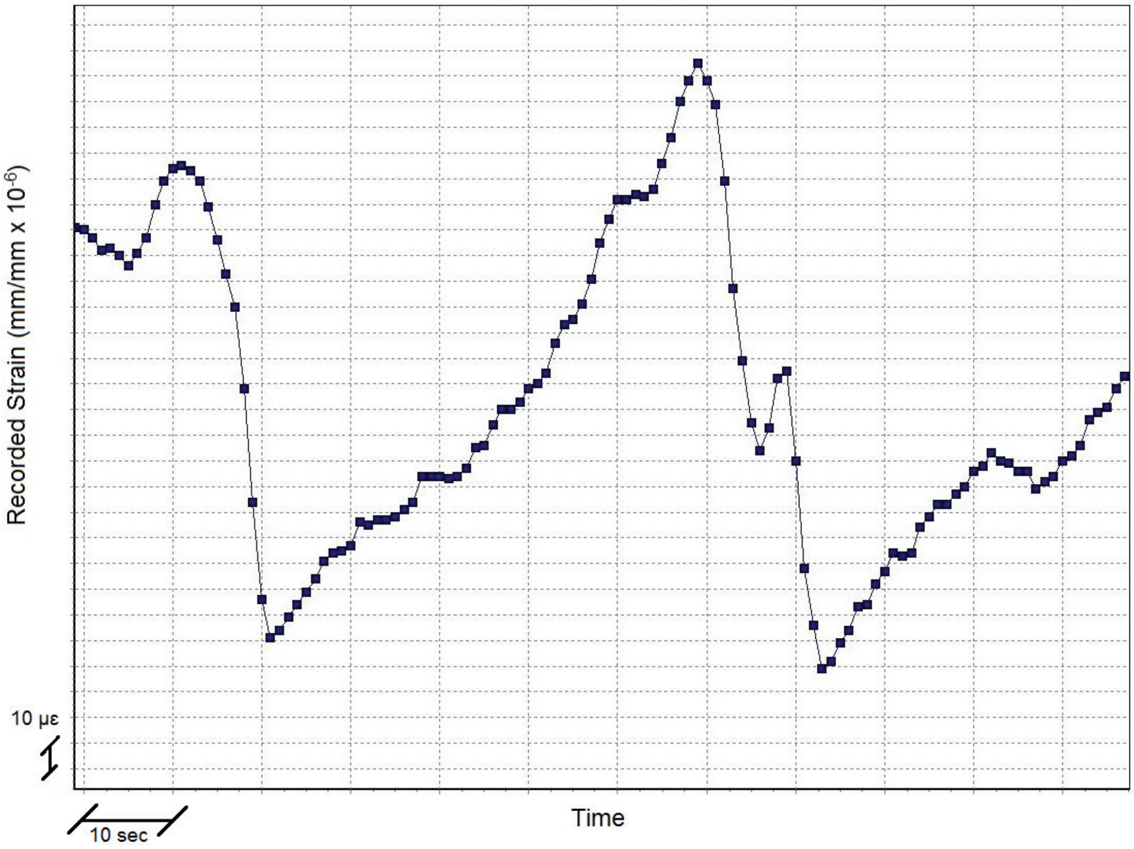

Figure 10-8 : Slow speed traffic event

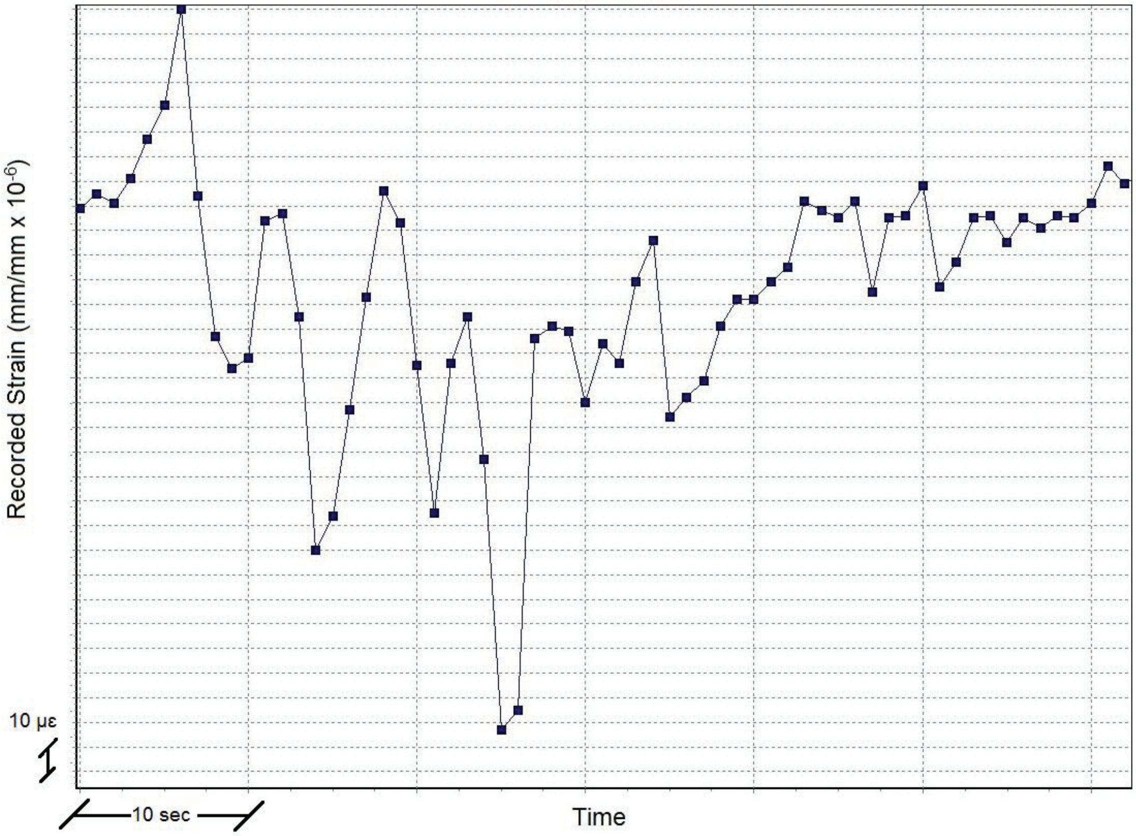

Figure 10-9 : Mixed traffic event

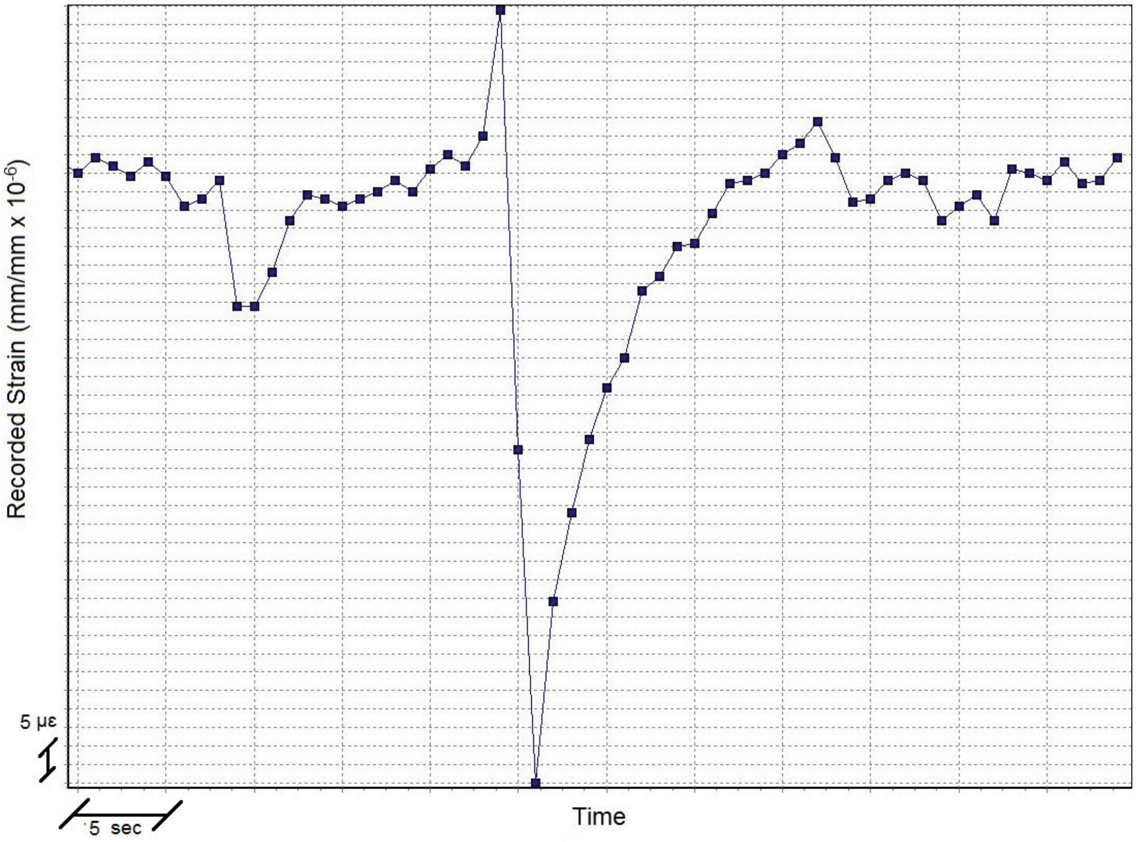

Figure 10-10 : Fast speed traffic event

To quantitatively compare vehicular speed, the influence lines for each diagonal were examined. A distinct feature of Diagonals #2 - #10 is the strain reversing section highlighted in Figure 10-11. This is the region where strains change from positive to negative (or negative to positive). Based on the slow speed testing, this reversal was determined to occur in Lane #1 over an average distance of 26.5 m.

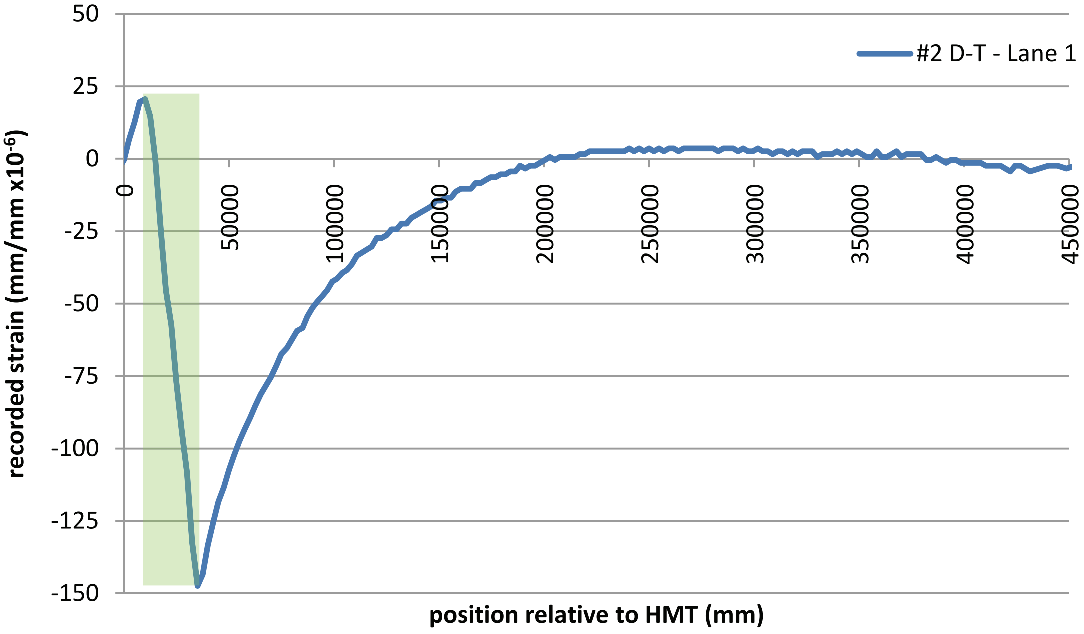

Figure 10-11 : Sample strain reversal

Data points which define the reversal section from the largest peak pair (from Table 10-3) were counted (data points are collected once per second). This provides a time period over which the reversal occurs. Dividing distance (26.5 m) by time (number of points), and converting to km/hr provides the results in Table 10-4. For Diagonals #7 and #8, no distinct reversal of strain was found in the peak event. These events were likely caused by a complex combination of traffic and are noted as multi-vehicle events (MVE).

Table 10-4 : Approximate speed of vehicle causing peak traffic event

Diagonal	Number of Points in Reversal	Calculated Speed (km/hr)
#1	7	14
#2	2	48
#3	8	12
#4	3 ½	27
#5	4	24
#6	4	24
#7	MVE	-
#8	MVE	-
#9	2	48
#10	4	24

Recalling the results from Section 7.5 – if traffic travels at 40 km/hr there is potential for the peak effect to be ‘missed’ by up to 30%, the peak effects shown in Figure 10-6 become more clear if the recorded vehicles are travelling between 12 km/hr and 48 km/hr. The likelihood of both gauges being perfectly synchronized is doubtful; therefore the pair is recording two different sections of the same traffic effect. The result is the potential for one gauge to record event X as the largest occurrence while the paired gauge records event Y as the largest. This explains the separation (or visibly singular) points in Figure 10-6 and Figure 10-7.

10.4.2 Comparison of Peak Pairs with Calibration Data

It was noted that many of the peak traffic events appear similar to the influence lines developed in Section 7.3. To provide some perspective to the peak load effects recorded, comparisons were made assuming that the peak events recorded were caused by either a single large truck, or two equal trucks in adjacent lanes. This comparison was possible using a linear ratio (for truck weights) because it was shown in Section 7.4 that the truck axle spacing had little effect on bridge response, therefore trucks could be treated as point loads on a long bridge. Table 10-5 shows a comparison between the peak recorded strains and the known calibration strain.

The average ratio of peak recorded strain versus calibration strain was used directly to determine that the gross vehicle weight(s) associated with the event was 1.48 times the calibration truck weight or approximately 870 kN for loading in lane 1 only. It is likely that there were either several large vehicles traveling at the same speed, or a single very heavy overload on the bridge – minimal additional traffic is likely to have been present.

Table 10-5 : Comparison of peak and calibration strains

Gauge	Recorded Calibration Strain (με)	Corrected Calibration Strain (με)	Peak Recorded Strain (με)	Peak / Calibrated
#1 D-T	-133	-148	-206	1.39
#1 D-B	-153	-170	-222	1.31
#2 D-T	-148	-164	-245	1.49
#2 D-B	-157	-174	-256	1.47
#3 D-T	-117	-130	-183	1.41
#3 D-B	-191	-212	-350	1.65
#4 D-T	-118	-131	-183	1.40
#4 D-B	-180	-200	-289	1.45
#5 D-T	-178	-198	-300	1.52
#5 D-B	-137	-152	-217	1.43
#6 D-T	-150	-167	-272	1.63
#6 D-B	-146	-162	-211	1.30
#7 D-T	-141	-157	-222	1.42
#7 D-B	-138	-153	-233	1.52
#8 D-T	-130	-144	-233	1.61
#8 D-B	-152	-169	-233	1.38
#9 D-T	-83	-92	-150	1.63
#9 D-B	-93	-103	-172	1.66
#10 D-T	-136	-151	-228	1.51
#10 D-B	-151	-168	-228	1.36
			Average	1.48

In Chapter 8 the phenomena of the top and bottom gauges recording different strains under controlled loading was discussed in detail. Using the matching peak pairs shown in Figure 10-6, the ratios of gauge pairs (top versus bottom) for the measured peaks were compared against the ratios produced from calibration test results. The comparison is presented in Table 10-6 and shown graphically in Figure 10-12. Diagonal #3, #10 and #12 are not shown because gauges were replaced during the recording period, resulting in an incomplete data set.

The results are qualitatively consistent but not identical; this difference is likely the result of a combination of event speed and the impact of scan synchronization, as discussed previously.

Table 10-6 : Comparison of top versus bottom gauges for calibration and peak pairs

Gauge (top)	**Matching Peak Pair (με)**	**Gauge (bottom)**	**Matching Peak Pair (με)**	**Matching Peak Pair (top/bottom)**	**Calibration Testing (top/bottom)**
#1 D-T	-206	**#1 D-B**	-245	0.84	0.87
#2 D-T	-245	**#2 D-B**	-256	0.96	0.94
#4 D-T	-183	**#4 D-B**	-295	0.62	0.66
#5 D-T	-300	**#5 D-B**	-217	1.38	1.30
#6 D-T	-272	**#6 D-B**	-228	1.19	1.03
#7 D-T	-222	**#7 D-B**	-233	0.95	1.02
#8 D-T	-233	**#8 D-B**	-245	0.95	0.86
#9 D-T	-150	**#9 D-B**	-172	0.87	0.91
#11 D-T	-289	**#11 D-B**	-283	1.02	0.96

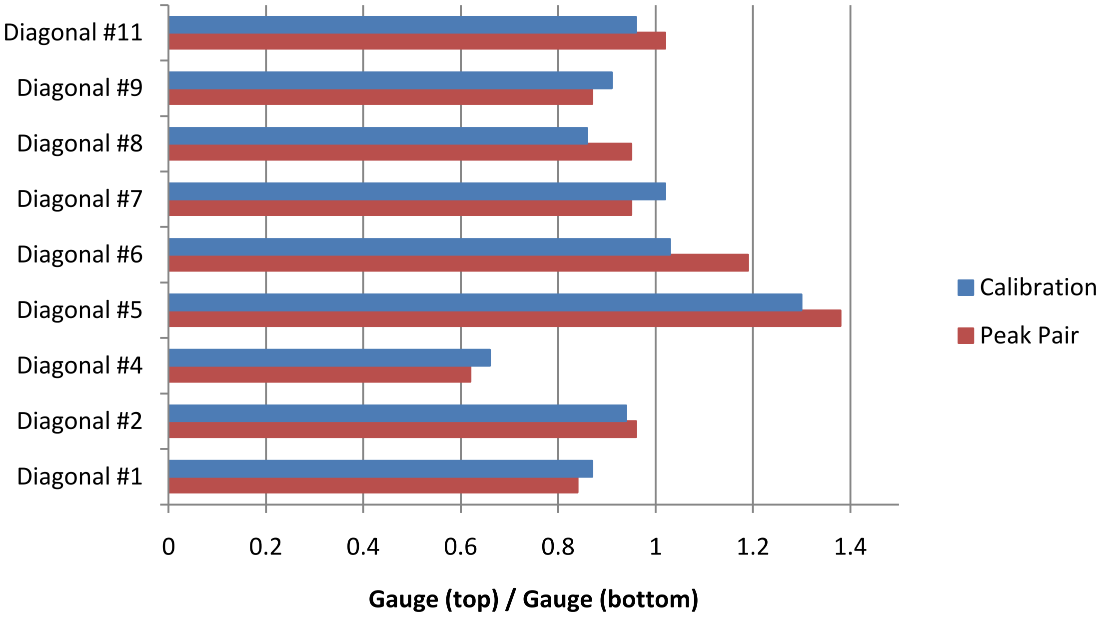

Figure 10-12 : Comparison of top versus bottom gauges for calibration and peak pair

10.5 Data Errors and Plausible Data Problem

During long-term data collection, it is expected that some unavoidable errors will occur resulting in erroneous data. While many of these occurrences are mitigated with periodic visual review of data, some are much more difficult to identify. Plausible data is a term used to define erroneous data that may appear to be real data as the magnitude of the readings is within the data range of other expected results. These plausible data errors can only be identified by careful examination and comparison with expected trends. One such piece of plausible data is shown in Figure 10-13. While the magnitude of this data is within the expected range of large traffic event data, it is unlikely that it is correct. The sudden change in trend, and subsequent return to that initial trend over a single reading, is an indicator that an error has occurred.

While not included in the current post-processing software, a procedure with an appropriate algorithm to remove these plausible data points would be helpful in future projects.

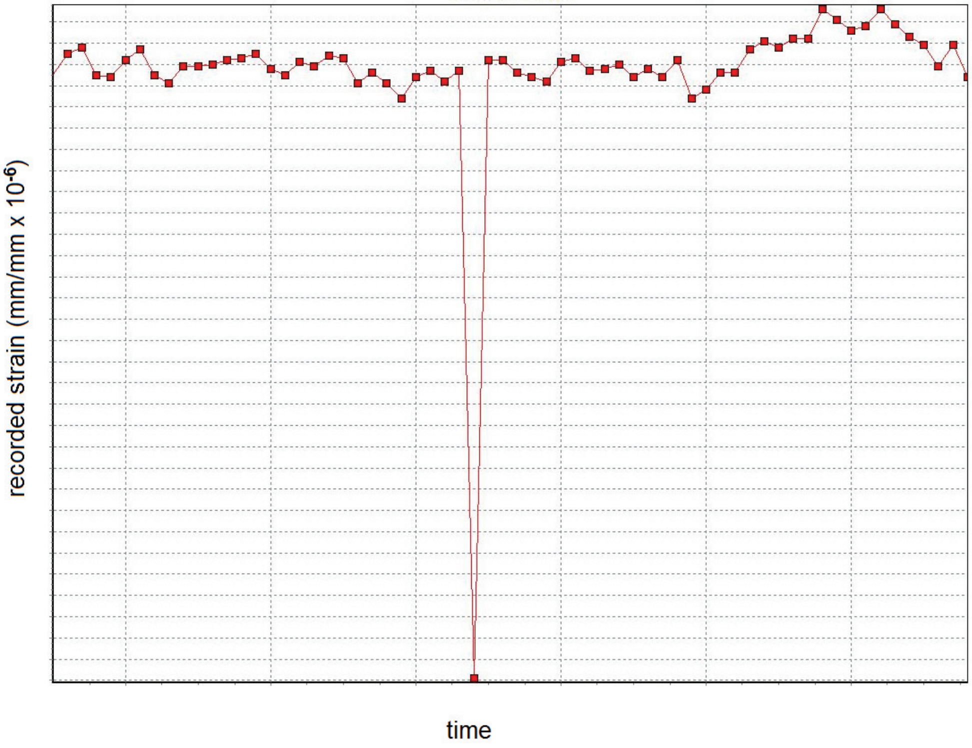

Figure 10-13 : Plausible data

Chapter 11. Application of Collected Data

11.1 Identification of Influence Zones

Using results from the slow-speed testing described in Section 7.1.2, influence zones were developed for the members of interest. The influence zones were identified as regions where an applied load would cause an increase in compressive strain; a sample of the slow-speed testing results is shown in Figure 11-1 and a sample of the influence zone, overlaid on a plan of the bridge, is shown in Figure 11-2. The value in the shaded region is a ratio of the peak strain, from the truck in that lane, with respect to Lane 1. These ratios are reported for all gauges in Table 11-1. Appendix II – Influence Lines From Slow Speed Tests shows the comparison of the slow speed data for lanes 1 through 4 and the influence zone for diagonals 1 through 12 can be found in Appendix VI – Influence Zones From Calibration Test Data.

Table 11-1 : Peak strain ratios

Diagonal	**$\frac{\text{Lane 1}}{\text{Lane 1}}$**	**$\frac{\text{Lane 2}}{\text{Lane 1}}$**	**$\frac{\text{Lane 3}}{\text{Lane 1}}$**	**$\frac{\text{Lane 4}}{\text{Lane 1}}$**
#1	1.00	0.77	0.52	0.33
#2	1.00	0.75	0.47	0.27
#3	1.00	0.74	0.46	0.24
#4	1.00	0.74	0.45	0.23
#5	1.00	0.74	0.44	0.22
#6	1.00	0.75	0.47	0.26
#7	1.00	0.74	0.45	0.22
#8	1.00	0.74	0.44	0.23
#9	1.00	0.75	0.47	0.25
#10	1.00	0.75	0.45	0.23
#11	1.00	0.64	-	-
#12	1.00	0.58	-	-

The diagonal members of the longitudinal stiffening trusses showed similar trends, with the exception of diagonal #9 which is oriented in the opposing direction in the truss.

The CHBDC lane load, described in Section 2.2.6, can be applied to these influence zones to determine the worst-case code-based loading.

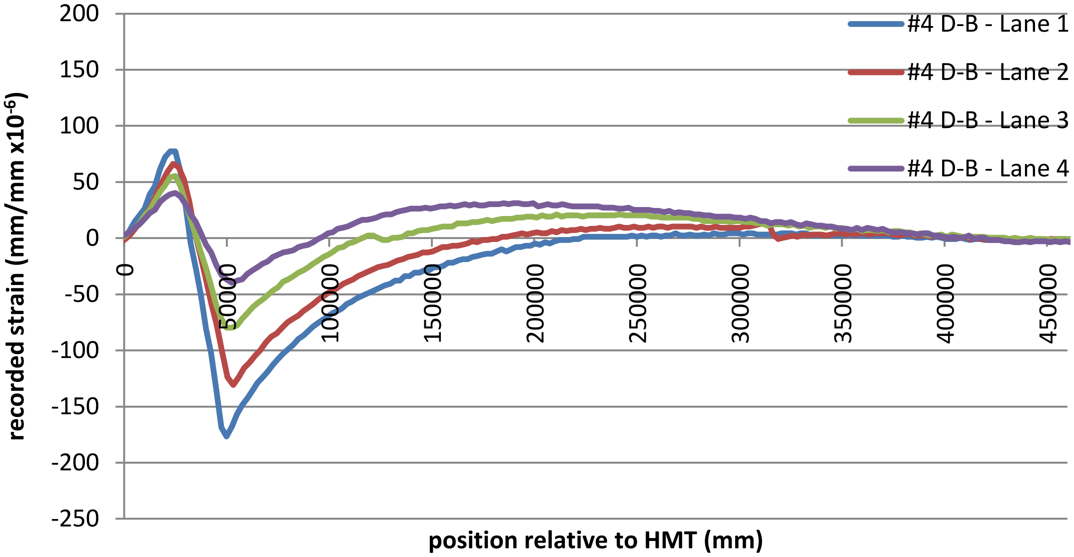

Figure 11-1 : Sample slow speed lane comparison

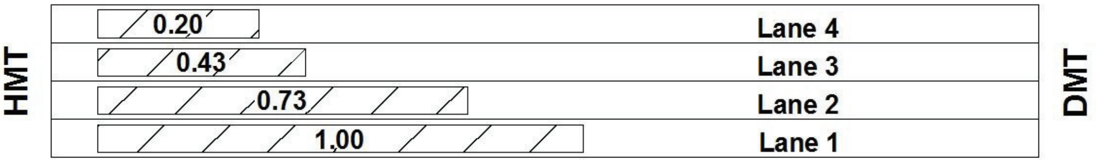

Figure 11-2 : Influence zones for diagonal #4

11.2 CHBDC 2006 Strain Predictions

To effectively use the influence zones, the curves from the slow-speed calibration plots shown in Appendix II – Influence Lines From Slow Speed Tests were manually fit with linear curves, as shown in Figure 11-3. The linear curves were then integrated to determine the area below the curve. This area was corrected for the gauge type and divided by the weight of the calibration truck, which is effectively a point load, used to develop the influence line. The procedure was repeated for all lanes. When comparing four lanes associated with a single diagonal, differences in loaded length are attributed to how the bridge distributes load.

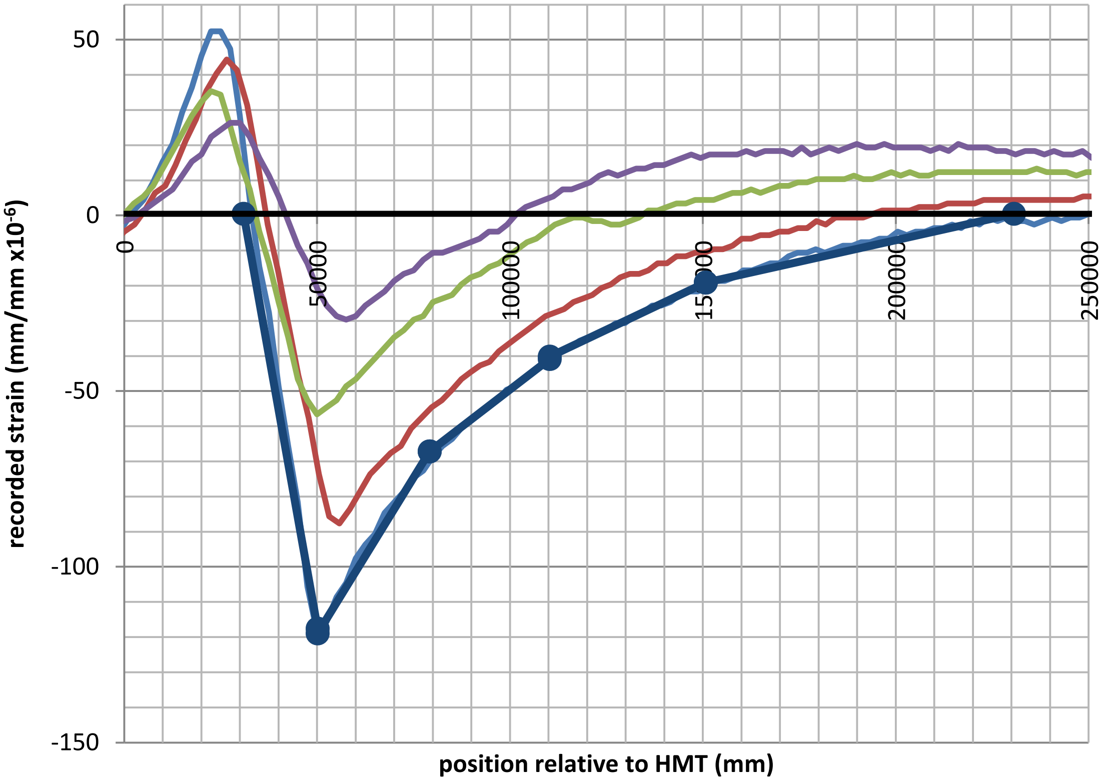

Figure 11-3 : Manual curve fit

Applying the CHBDC (2006) lane load of 9 kN/m to the influence line, as well as the 80% design truck, lane combinations were examined. It was found that the largest unfactored compressive design strain (-525 με) for diagonal members #1 - #10 is developed when three lanes are loaded. Diagonal #11 and #12 have an unfactored design strain of -503 με when only two lanes are loaded. Table 11-2 shows the calculated strains for various combinations of loaded lanes; detailed calculation results can be found in Appendix VII – Summary of Detailed Calculations for CHBDC .

Table 11-2 : Unfactored CHBDC design strains

	1 Loaded Lane	2 Loaded Lanes	3 Loaded Lanes	4 Loaded Lanes
Diagonal #1	-275	-440	-492	-488
Diagonal #2	-299	-465	-513	-496
Diagonal #3	-311	-479	-520	-499
Diagonal #4	-314	-480	-519	-494
Diagonal #5	-311	-478	-519	-494
Diagonal #6	-293	-451	-492	-478
Diagonal #7	-294	-450	-486	-461
Diagonal #8	-295	-454	-488	-463
Diagonal #9	-141	-246	-345	-418
	-166	-292	-365	-418
Diagonal #10	-319	-481	-525	-500
Diagonal #11	-376	-503	-474	-421
Diagonal #12	-400	-496	-452	-402

11.3 Probable Extreme Data

Several methods exist to approximate collected data. The approach described by Liu et al. (2009) and applied to strain readings on the Lehigh River Bridge (four-span continuous truss) in Pennsylvania was adapted to the MacKay Bridge data in this thesis. The method consists of the following steps:

1) identification of peak data;
2) development of histograms (with only peak data);
3) curve fitting of collected data;
4) extreme value prediction.

Liu et al. (2009) investigate several possible distributions for modeling the strain response. In their work, a log-normal distribution provided a better approximation for collected data. The Gumbel Approximation also provided an acceptable fit and results in a more convenient for for extreme data prediction. Therefore the Gumbel distribution was used to model the strain data distribution from the MacKay Bridge project. The Gumbel Distribution (Gumbel 1958) was used in this work in the form presented in Equation [11-1].

$$F_{X_n}(x) = \exp(e^{-\alpha_n(x-u_n)}) \quad [11\text{-}1]$$

where:

α_n is an inverse measure of the dispersion of X_n

u_n is the characteristic largest value of X

While mathematical methods exist to approximate the Gumbel constants, the graphical approach outlined in Ang and Tang (1984) was utilized. In this approach, the cumulative distribution function (CDF) of X_n is plotted on Gumbel Probability Paper. The slope of a linear best-fit (when calculated using the vertical and 's' axes is α_n. Likewise, the value read off the vertical axis at the point where the best-fit line intercepts the s-axis value of zero is equal to u_n. A sample of the Gumbel Probability chart is shown in Figure 11-4, with the plots for all twelve diagonals shown in Appendix VIII – Gumbel Probability Plots. Calculated values for α_n and u_n are listed in Table 11-3.

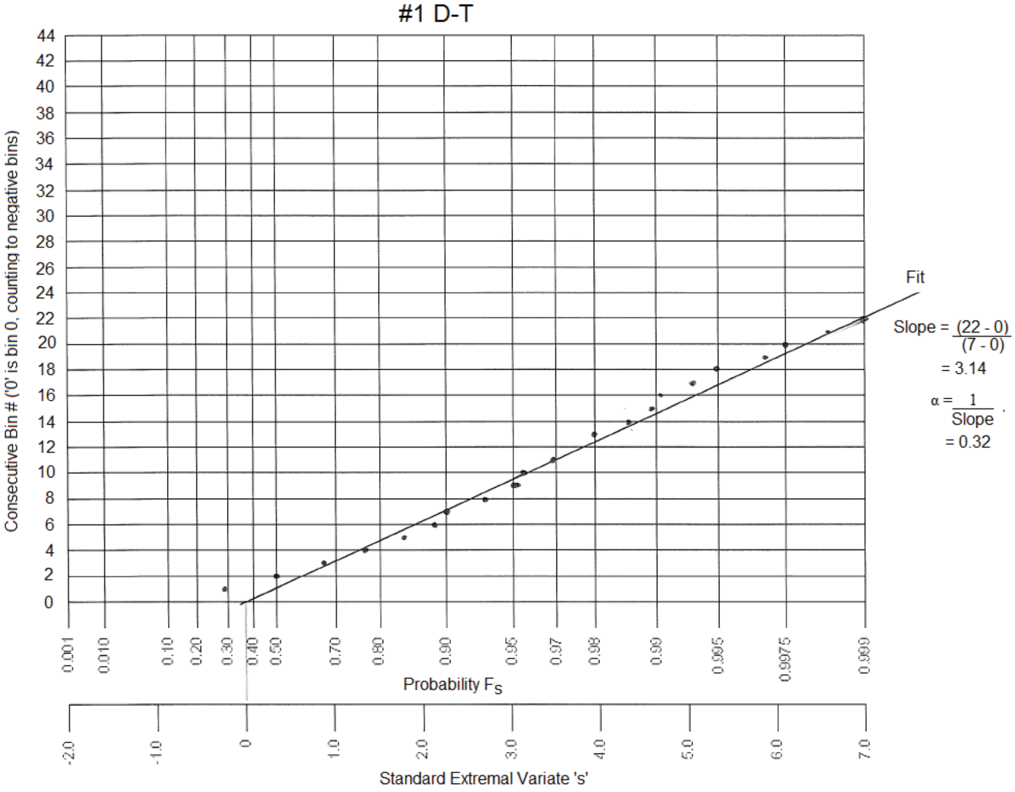

Figure 11-4 : Gumbel distribution curve fit

Table 11-3 : Gumbel constants

	α_n	u_n		α_n	u_n
#1 D-T	0.32	0.0	**#1 D-B**	0.29	0.0
#2 D-T	0.28	0.0	**#2 D-B**	0.27	-1.0
#3 D-T	0.25	1.0	**#3 D-B**	0.22	-2.0
#4 D-T	0.35	0.0	**#4 D-B**	0.23	-2.0
#5 D-T	0.23	1.0	**#5 D-B**	0.30	-1.0
#6 D-T	0.28	0.0	**#6 D-B**	0.28	-1.0
#7 D-T	0.30	0.0	**#7 D-B**	0.29	-1.0
#8 D-T	0.33	0.0	**#8 D-B**	0.28	-1.0
#9 D-T	0.47	1.0	**#9 D-B**	0.41	0.0
#10 D-T	0.30	0.0	**#10 D-B**	0.26	-3.0
#11 D-T	0.25	0.0	**#11 D-B**	0.23	-1.0
#12 D-T	0.23	6.0	**#12 D-B**	0.21	-1.0

Once Gumbel distributions have been constructed for all strain gauges, extreme data can be predicted by assuming future traffic counts based on the recorded period. In the case of the MacKay project, it was assumed that traffic events will remain constant. The Gumbel Approximation in Equation [11-1] can be rearranged to result in a maximum expected strain, shown in Equation [11-2].

$$\varepsilon_{\text{m max}} = u_n - \frac{1}{\propto_n}\ln\left[-\ln\left(1-\frac{1}{N_T}\right)\right] \tag{11-2}$$

where:

N_T is the number of traffic events for the selected period

The values for N_T for the recorded period were summed from the histogram data. The recorded period for each gauge was known, therefore traffic events were related to time. The value N_T was adjusted to reflect the cumulative number of events expected in the future years, calculated values for N_T are shown in Table 11-4 and Table 11-5. The assumption that the number of traffic events remains constant with time was chosen because no real understanding of the traffic itself is known. Applying this rearrangement to all strain gauges, and averaging the largest expected strain for each gauge pair results in the values shown in Table 11-6 in which probable extreme measurements are determined for 5 through 25 years into the future.

Table 11-4 : Calculated values for N_T, top gauges

	$N_{14\text{ months}}$	$N_{5\text{ years}}$	$N_{10\text{ years}}$	$N_{15\text{ years}}$	$N_{20\text{ years}}$	$N_{25\text{ years}}$
#1 D-T	1.63E+06	5.98E+06	1.20E+07	1.79E+07	2.39E+07	2.99E+07
#2 D-T	3.01E+06	1.11E+07	2.21E+07	3.32E+07	4.42E+07	5.53E+07
#3 D-T	5.61E+06	2.06E+07	4.13E+07	6.19E+07	8.25E+07	1.03E+08
#4 D-T	1.86E+06	6.84E+06	1.37E+07	2.05E+07	2.74E+07	3.42E+07
#5 D-T	3.69E+06	1.36E+07	2.71E+07	4.07E+07	5.42E+07	6.78E+07
#6 D-T	2.93E+06	1.07E+07	2.15E+07	3.22E+07	4.30E+07	5.37E+07
#7 D-T	2.21E+06	8.12E+06	1.62E+07	2.44E+07	3.25E+07	4.06E+07
#8 D-T	3.88E+06	1.42E+07	2.85E+07	4.27E+07	5.70E+07	7.12E+07
#9 D-T	2.54E+06	9.33E+06	1.87E+07	2.80E+07	3.73E+07	4.67E+07
#10 D-T	1.08E+06	3.95E+06	7.91E+06	1.19E+07	1.58E+07	1.98E+07
#11 D-T	5.15E+06	1.89E+07	3.78E+07	5.67E+07	7.56E+07	9.45E+07
#12 D-T	5.77E+06	2.12E+07	4.24E+07	6.36E+07	8.48E+07	1.06E+08

Table 11-5 : Calculated values for N_T, bottom gauges

	$N_{14\text{ months}}$	$N_{5\text{ years}}$	$N_{10\text{ years}}$	$N_{15\text{ years}}$	$N_{20\text{ years}}$	$N_{25\text{ years}}$
#1 D-B	1.25E+06	4.60E+06	9.21E+06	1.38E+07	1.84E+07	2.30E+07
#2 D-B	4.90E+06	1.80E+07	3.60E+07	5.40E+07	7.20E+07	9.00E+07
#3 D-B	3.24E+06	1.19E+07	2.38E+07	3.57E+07	4.76E+07	5.95E+07
#4 D-B	2.47E+06	9.06E+06	1.81E+07	2.72E+07	3.63E+07	4.53E+07
#5 D-B	1.92E+06	7.05E+06	1.41E+07	2.11E+07	2.82E+07	3.52E+07
#6 D-B	1.65E+06	6.05E+06	1.21E+07	1.82E+07	2.42E+07	3.03E+07
#7 D-B	3.06E+06	1.12E+07	2.25E+07	3.37E+07	4.49E+07	5.62E+07
#8 D-B	2.03E+06	7.44E+06	1.49E+07	2.23E+07	2.98E+07	3.72E+07
#9 D-B	4.71E+06	1.73E+07	3.46E+07	5.19E+07	6.91E+07	8.64E+07
#10 D-B	3.42E+06	1.26E+07	2.51E+07	3.77E+07	5.03E+07	6.29E+07
#11 D-B	4.84E+06	1.78E+07	3.56E+07	5.33E+07	7.11E+07	8.89E+07
#12 D-B	1.28E+06	4.71E+06	9.41E+06	1.41E+07	1.88E+07	2.35E+07

Table 11-6 : Probable extreme data

	Diagonal											
	#1	**#2**	**#3**	**#4**	**#5**	**#6**	**#7**	**#8**	**#9**	**#10**	**#11**	**#12**
$\varepsilon_{5\text{ year}}$	-270	-289	-289	-281	-284	-278	-281	-284	-289	-278	-295	-284
$\varepsilon_{10\text{ year}}$	-283	-301	-303	-292	-295	-289	-292	-295	-301	-289	-306	-295
$\varepsilon_{15\text{ year}}$	-292	-309	-312	-298	-301	-301	-303	-301	-306	-295	-311	-303
$\varepsilon_{20\text{ year}}$	-298	-314	-314	-303	-306	-303	-309	-306	-312	-300	-317	-309
$\varepsilon_{25\text{ year}}$	-298	-317	-317	-309	-312	-306	-309	-312	-317	-306	-322	-311

11.4 Comparison of Predicted Extreme Strain with Design Strain

Comparing the probable extreme data from Table 11-6 with predictions using loads and load patterns from CHBDC, it is immediately apparent that there is conservatism in the code when used for spans longer than those specified. Table 11-7 shows a ratio of largest predicted strain from monitoring to unfactored CHBDC design strain for each gauge.

Table 11-7 : Ratio of extreme predicted strain versus unfactored CHBDC design strain

	Diagonal											
	#1	**#2**	**#3**	**#4**	**#5**	**#6**	**#7**	**#8**	**#9**	**#10**	**#11**	**#12**
$\varepsilon_{5\text{ year}}$	0.55	0.56	0.56	0.54	0.55	0.57	0.58	0.58	0.69	0.53	0.59	0.57
$\varepsilon_{10\text{ year}}$	0.58	0.59	0.58	0.56	0.57	0.59	0.60	0.60	0.72	0.55	0.61	0.59
$\varepsilon_{15\text{ year}}$	0.59	0.60	0.60	0.57	0.58	0.61	0.62	0.62	0.73	0.56	0.62	0.61
$\varepsilon_{20\text{ year}}$	0.61	0.61	0.64	0.58	0.59	0.62	0.64	0.63	0.75	0.57	0.63	0.62
$\varepsilon_{25\text{ year}}$	0.61	0.62	0.65	0.59	0.60	0.62	0.64	0.64	0.76	0.58	0.64	0.63

While technically possible, it is unlikely that all diagonals would be optimized for the design loads required. Similarly, it is likely that diagonals in a similar configuration would respond to similar loadings. As a result, the largest predicted compressive strains and the largest CHBDC design strains were examined for groupings of similar diagonals: Diagonals #1 - #10 in the longitudinal stiffening trusses, and Diagonals #11 and #12 in the lateral stiffening trusses. This comparison is shown in Table 11-8, which gave the probable design ratios. Regardless of how the data is examined, it is apparent that the design codes are conservative for this particular element in the bridge. It is also evident that load capacity evaluations for these diagonals may produce distinctly different decisions depending whether the conservative code based methods or the structure-specific monitoring information is used.

Table 11-8 : Ratio of extreme predicted strain versus unfactored CHBDC design strain

	Diagonals	
	#1 - #10	**#11 & #12**
$\varepsilon_{5\ year}$	0.55	0.59
$\varepsilon_{10\ year}$	0.58	0.61
$\varepsilon_{15\ year}$	0.59	0.62
$\varepsilon_{20\ year}$	0.60	0.63
$\varepsilon_{25\ year}$	0.60	0.64

Chapter 12. Conclusions and Recommendations

This thesis described the work completed to collect and interpret structure-specific information for use in management decisions regarding the future use of the structure. The two main functions of the project were a) the fine calibration of the existing numerical model and b) the comparison of the actual live load response with that required by CHBDC (2006) live load patterns. These two components represent areas of uncertainty in the evaluation and management process.

12.1 Fine Calibration of Existing Numerical Model

Controlled load calibration testing was conducted to compare actual bridge response to that predicted by the existing numerical model. Using pre-determined positions, the actual bridge response was compared with predictions from the numerical model.

- A global linear modifier was developed using the sum of squared errors (least squares) method to correct model strain. Results indicate that model strains should be corrected with a multiplier of 0.98.

12.2 Comparison of Live Load Effects with Code Requirements

Long-term testing allowed the collection and examination of 14 months of continuous data.

- Diagonal members of the longitudinal stiffening trusses have similar values for peak recorded compressive strain, ranging from -228 με to 272 με. Diagonal #9 (-161 με) is inclined in the opposite direction. Diagonal members of the lateral stiffening truss recorded values of -292 με and -328 με. Recorded maxima for all instrumented members are all less than 64% of the design strains required by the CHBDC (2006).

12.3 Instrumentation and Data Validation

Throughout the project, emphasis was placed on the rigorous verification of data. A thorough understanding of the instrumentation system was developed through various means including: shunt calibration, gauge-type calibration, and repeated controlled-load calibration testing.

The results of the instrumentation examination are:

- Factory labeled, individual gauge factors are correct for the gauge – they do not represent the installed gauge system. For those gauges installed on the MacKay Bridge, the gauge factor was revised from 2.03 (as per factory label) to 1.98 based on shunt calibration.

- The strain gauges used in the MacKay project are affected by the weldable backing plates on which they are installed. Laboratory and full-scale testing indicate a gauge-type correction factor of 1.11 need be applied to all gauge readings to correct for the linear deviation from actual strain.

- Due to pitting corrosion on the existing truss members, surface preparation is required prior to gauge installation - surface preparation impacts the recorded strain. Through laboratory testing, as well as numerical modeling, it was shown that the difference between two gauges installed on opposite sides of a web was found to be up to 20% for a total depth of preparation of 1.5 mm. This is consistent with actual readings observed in the field.

- Any surface preparation prior to installation of a gauge will cause local stress concentrations resulting in an increase in average strain recorded by a pair of strain gauges on the web. While the lesser reading from any given pair is likely closer to the nominal strain, the average of the two gauges is recommended for data interpretation.

From controlled load calibration testing several comparisons were made, these indicate the following:

- Gauge response is repeatable. Controlled testing conducted over a broad temperature range (~-20ºC to ~+20ºC) and over a long time-frame (December

2009, March 2010 and August 2010) showed identical behaviour in all four travel lanes.

- The scan rate selected permits capture of the influence line under slow-speed conditions; however, traffic travelling at the posted speed limits (70 km/hr) has potential for 'missing' peak effects.

- Vehicles travelling in opposing directions (east to west vs west to east) cause identical behaviour in the bridge system when examined from the centre of mass.

12.4 Recommendations

Based on the goals and outcomes described in this thesis, several areas for future work are proposed:

- Further work in the area of long-span bridge loads is required. This thesis concluded that the CHBDC live load requirements appear to be conservative for stiffening trusses on the MacKay Bridge – this conclusion cannot be extended to other bridges (or other components of the MacKay Bridge) until more extensive data is gathered. As a result, targeted instrumentation of other bridges in several regions throughout the country is recommended to remove uncertainty in traffic pattern approximations.
- Current methods allow only traffic effects to be recorded, leaving little opportunity for understanding of the load. Therefore future instrumentation work should not be limited to structural instrumentation. The addition of Weigh-in-Motion sensors and video monitoring should be used to confirm assumptions of traffic location and vehicle type during loading.
- Additional preparation prior to implementation of instrumentation systems is also recommended. Gauge factors would be better implemented during data collection, rather than during post-processing. Similarly, peak identification would be better implemented during data collection to vastly reduce file sizes.
- For future algorithms, account should be made for erroneous readings.

References

AASHTO. 2007. AASHTO LRFD Bridge Design Specifications: Special P.E. Exam Edition. American Association of State Highway and Transportation Officials. Washington, United States.

ADINA R&D, 2008. Adina Theory and Modeling Guide – Volume 1: Solids & Structures. ADINA R&D Inc. Watertown, MA.

Ang, A., and Tang, W. 1984. Probability Concepts in Engineering Planning and Design: Vol. II. John Wiley & Sons, New York. 562 pp.

Arora, 2009. Scan 07-05: Better Practices in Bridge Management Decision-Making. Arora and Associates, Lawrenceville, NJ. 256 pp.

ASCE. Committee on Bridges of the Structural Division. 1981. Recommended Design Loads for Bridges. ASCE Structural Division Journal. 107(7): 1161.

Buckland, P., McBryde, P., Navin, F. and Zidek, J. 1978. Traffic Loading of Long Span Bridges. Transportation Research Record. 665(2): 146.

Buckland, P., Navin, P., Zidek, V., and McBryde, J. 1980. Proposed Vehicle Loading of Long-Span Bridges. ASCE Journal of the Structural Division. 106(4): 915

BS 5400-2. 1978. Steel, concrete and composite bridges – Part 2: Specification for loads. British Standards Institute. London, United Kingdom.

Campbell Sci, 2007. 4WfB120, 4WFB350, 4WFB1K 4 Wire Full Bridge Terminal Input Modules Revision 5/07: Instruction Manual. Retrieved December 2009 from http://www.campbellsci.ca/literature_docs.html.

CAN/CSA S6-06. 2006. Canadian Highway Bridge Design Code. Canadian Standards Association. Mississauga, Canada.

CAN/CSA S6.1-06. 2006. Canadian Highway Bridge Design Code Commentary. Canadian Standards Association. Mississauga, Canada.

CAN/CSA S6-88. 1988. Design of Highway Bridges. Canadian Standards Association. Toronto, Canada.

Catbas, F., Susoy, M. and Frangopol, D., 2008. Structural Health Monitoring and Reliability Estimation: Long-Span Truss Bridge Application with Environmental Monitoring Data. Engineering Structures, Vol 30:2347.

Eurocode, 2002. Eurocode 1: Part 2: Traffic Loads on Bridges. European Committee for Standardization. Brussels.

Gumbel, E. 1958. Statistics of Extremes. Columbia University Press. 375 pp.

Halifax Regional Municipality, 2011. A Brief History of HRM. Retrieved June 2011from http://www.halifax.ca/community/history.html.

ISIS 2006. Education Module 5: An Introduction to Structural Health Monitoring. ISIS Canada Research Network, Winnipeg, MB. 39 pp.

Liu, M., Frangopol, D., and Kim, S. 2009. Bridge Safety Evaluation Based on Monitored Live Load Effects. ASCE Journal of Bridge Engineering, 14(4): 257.

Lutomirska, M. 2009. Live Load Models for Long Span Bridges. Civil Engineering Thesis, Dissertations, and Student Research, University of Nebraska – Lincoln.

Neves, L., Frangopol, D. and Petcherdchoo, A. 2006. Probabilistic Lifetime Oriented Multiobjective Optimization of Bridge Maintenance: Combination of Maintenance Types. ASCE Journal of Structural Engineering 132(11):1821.

NSTIR 2011. 5-Year Highway Improvement Plan: 2011-12 Edition. Nova Scotia Department of Transportation and Infrastructure Renewal. Retrieved July 2011 from http://www.gov.ns.ca/tran/highways/5yearplan.

OHBDC 1991. Ontario Highway Bridge Design Code: 3rd Edition. Ministry of Transportation of Ontario. Downsview, Canada.

OHBDCC 1991. Ontario Highway Bridge Design Code Commentary. Ministry of Transportation of Ontario. Downsview, Canada.

Testa, R. and Yanev, B., 2002. Bridge Maintenance Level Assessment. Computer-Aided Civil and Infrastructure Engineering, 17:358.

Vishay, 2007. Tech Note TN-514: Shunt Calibration of Strain Gage Instrumentation. Vishay Micro-Measurements. Retrieved December 2009 from www.vishaypg.com/micro-measurements/stress-analysis-strain-gages/technotes-list/.

Vishay, 2010. Instruction Bulletin B-131-5: Attachment Techniques for Weldable Strain Gages and Temperature Sensors. Vishay Precision Group. Retrieved November 2011 from http://www.vishaypg.com/micro-measurements/stress-analysis-strain-gages/instruction-list/.

Appendix I – Gauge Repeatability December 2009 - March 2010

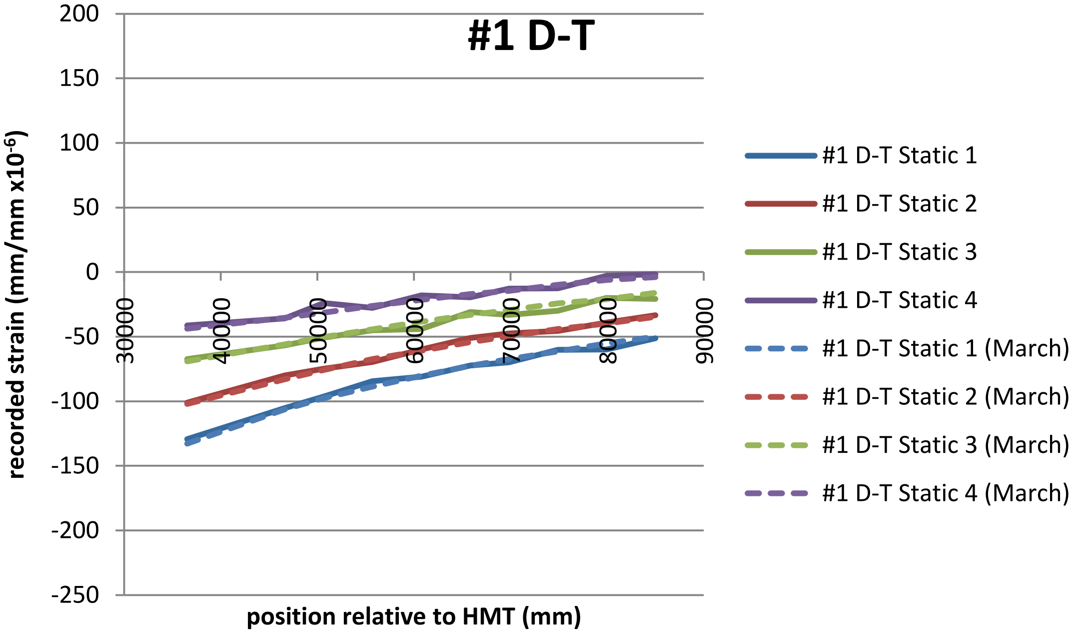

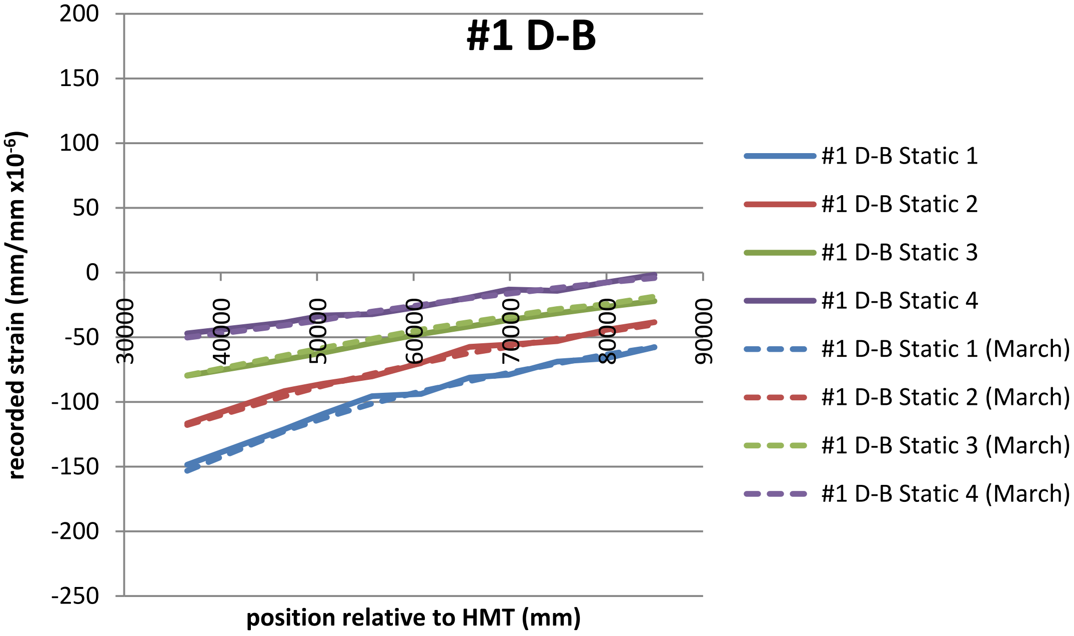

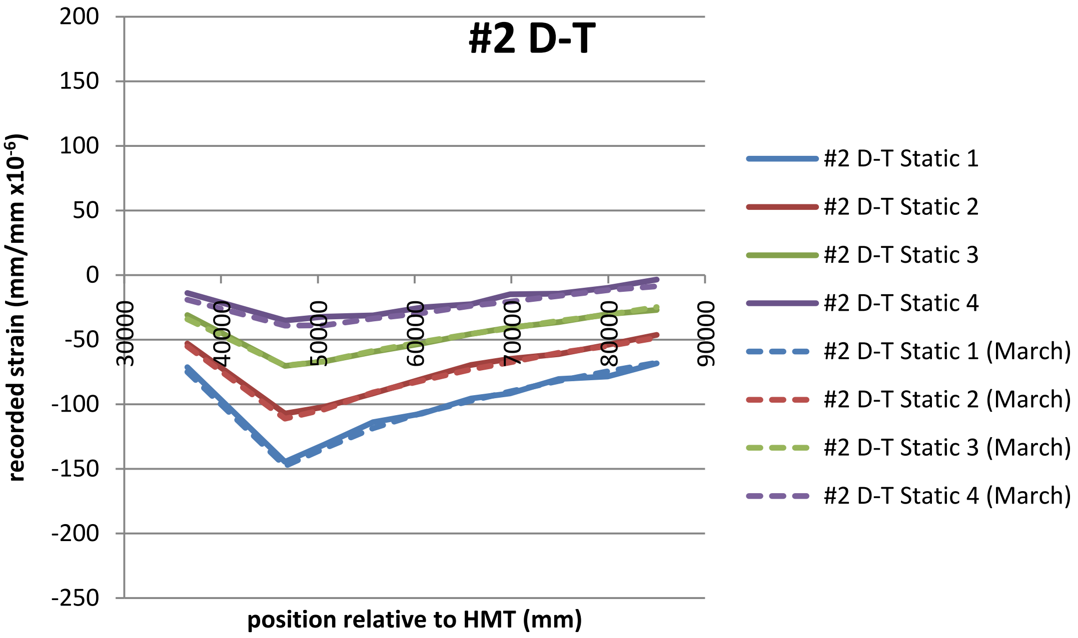
#2 D-T
200
150
100
50
0
-50
-100
-150
-200
-250
recorded strain (mm/mm x10^{-6})
30000
40000
50000
60000
70000
80000
90000
position relative to HMT (mm)
#2 D-T Static 1
#2 D-T Static 2
#2 D-T Static 3
#2 D-T Static 4
#2 D-T Static 1 (March)
#2 D-T Static 2 (March)
#2 D-T Static 3 (March)
#2 D-T Static 4 (March)

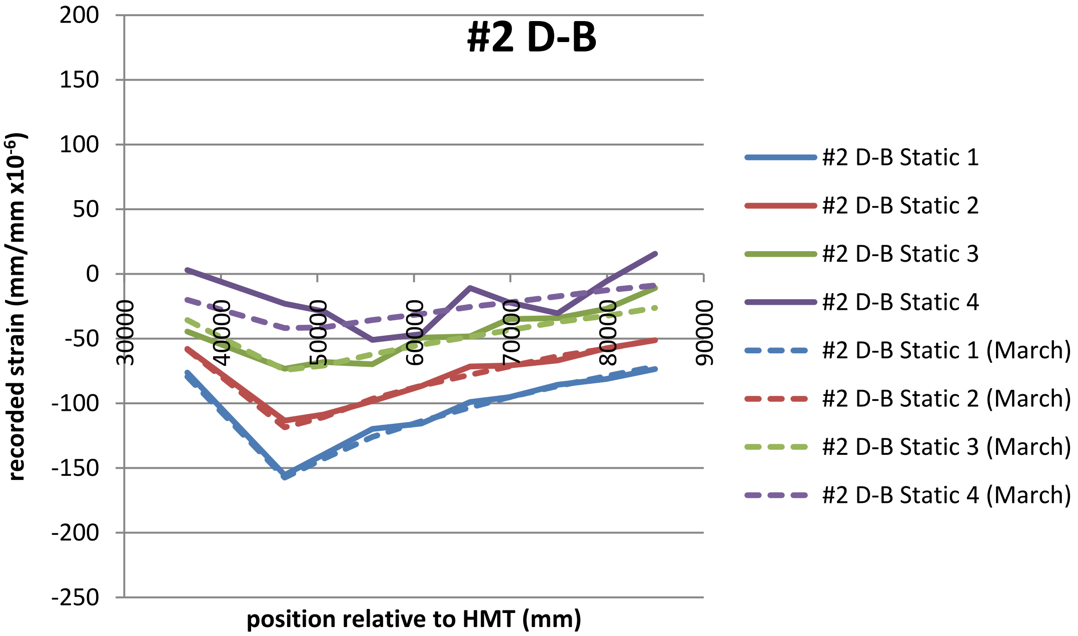
#2 D-B
200
150
100
50
0
-50
-100
-150
-200
-250
recorded strain (mm/mm x10^{-6})
30000
40000
50000
60000
70000
80000
90000
position relative to HMT (mm)
#2 D-B Static 1
#2 D-B Static 2
#2 D-B Static 3
#2 D-B Static 4
#2 D-B Static 1 (March)
#2 D-B Static 2 (March)
#2 D-B Static 3 (March)
#2 D-B Static 4 (March)

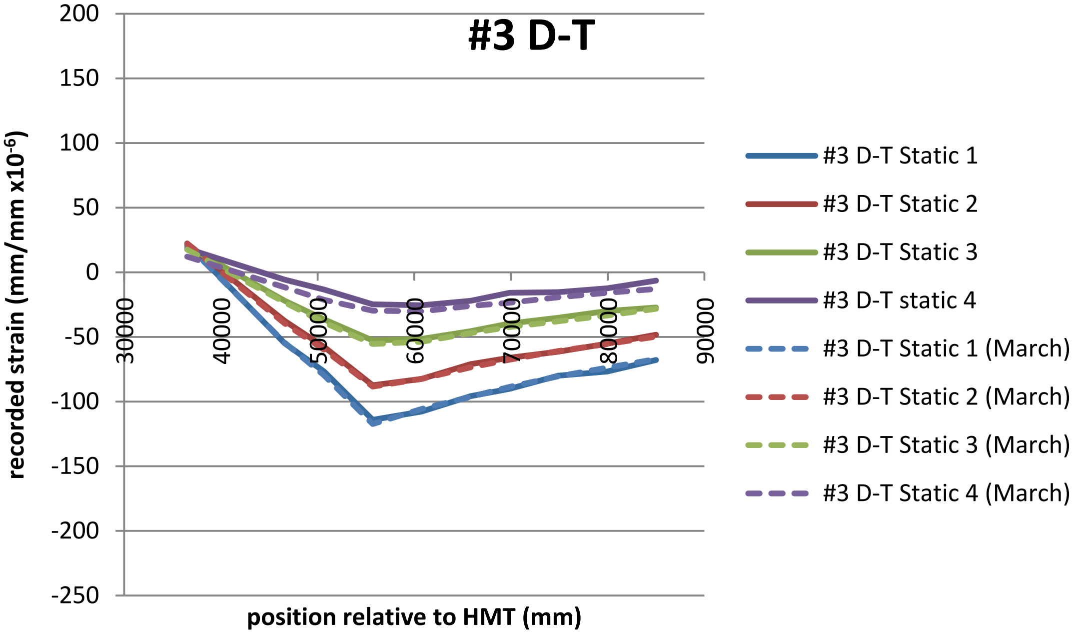
#3 D-T
recorded strain (mm/mm x10^{-6})
200
150
100
50
0
-50
-100
-150
-200
-250
30000
40000
50000
60000
70000
80000
90000
position relative to HMT (mm)
#3 D-T Static 1
#3 D-T Static 2
#3 D-T Static 3
#3 D-T static 4
#3 D-T Static 1 (March)
#3 D-T Static 2 (March)
#3 D-T Static 3 (March)
#3 D-T Static 4 (March)

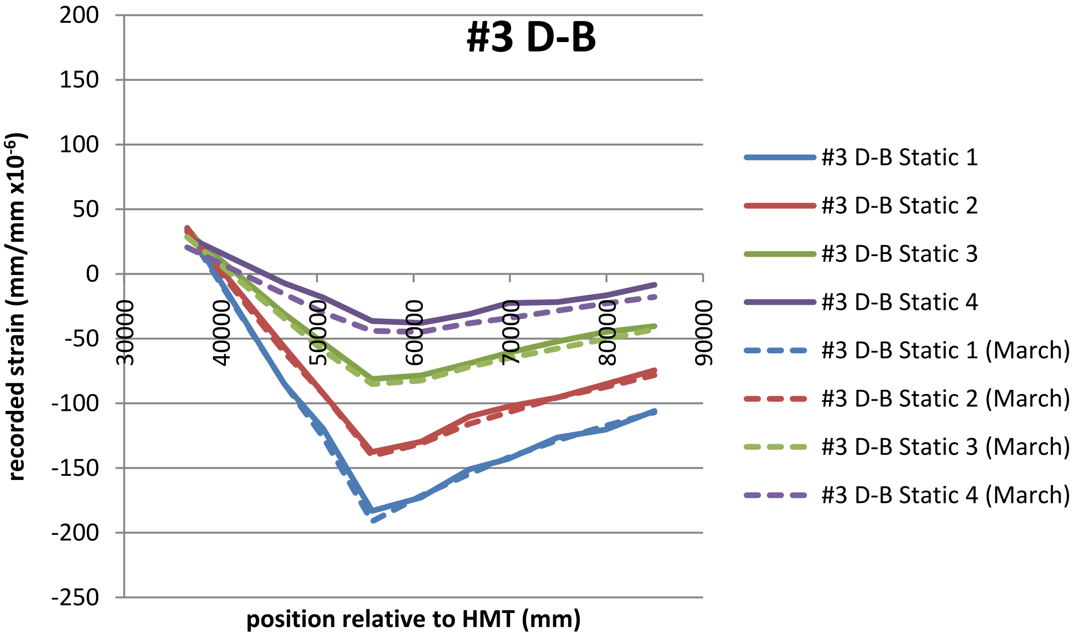
#3 D-B
recorded strain (mm/mm x10^{-6})
200
150
100
50
0
-50
-100
-150
-200
-250
30000
40000
50000
60000
70000
80000
90000
position relative to HMT (mm)
#3 D-B Static 1
#3 D-B Static 2
#3 D-B Static 3
#3 D-B Static 4
#3 D-B Static 1 (March)
#3 D-B Static 2 (March)
#3 D-B Static 3 (March)
#3 D-B Static 4 (March)

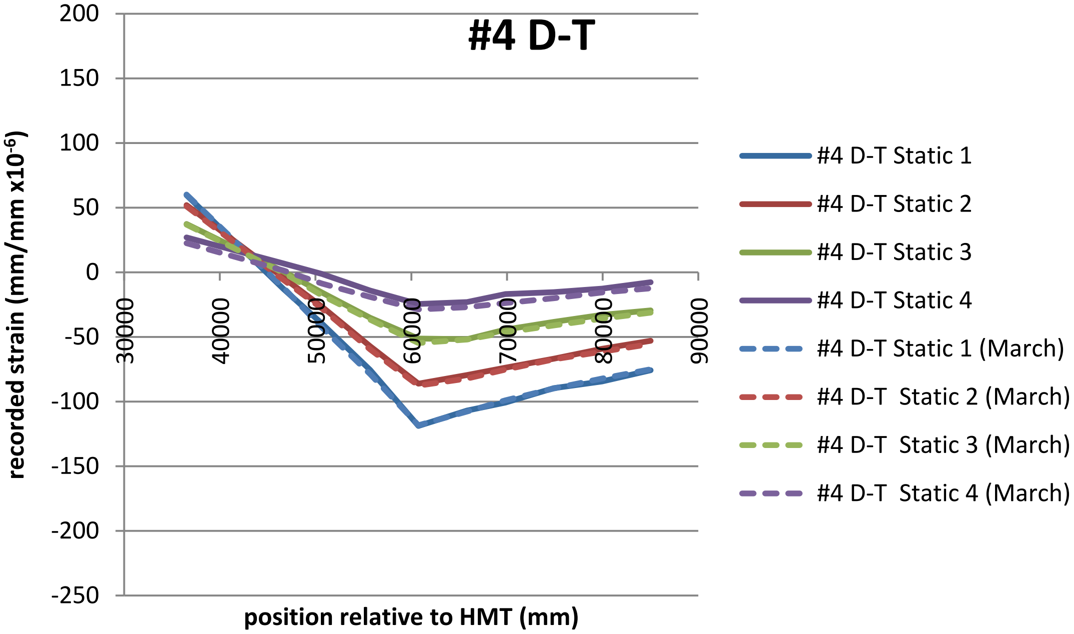
#4 D-T
200
150
100
50
0
-50
-100
-150
-200
-250
recorded strain (mm/mm x10-6)
30000
40000
50000
60000
70000
80000
90000
position relative to HMT (mm)
#4 D-T Static 1
#4 D-T Static 2
#4 D-T Static 3
#4 D-T Static 4
#4 D-T Static 1 (March)
#4 D-T Static 2 (March)
#4 D-T Static 3 (March)
#4 D-T Static 4 (March)

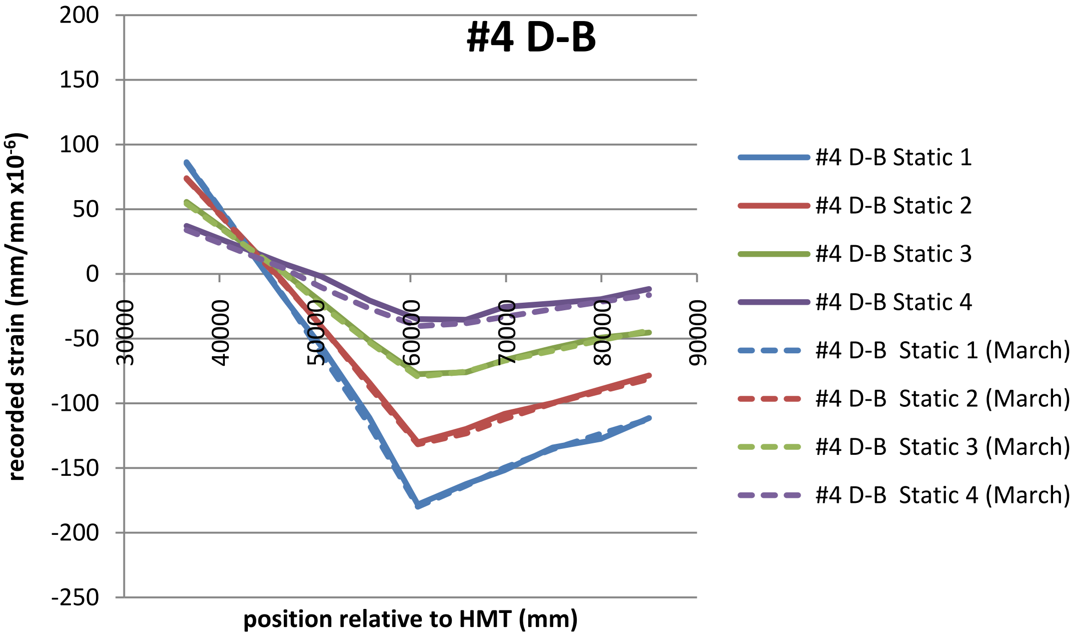
#4 D-B
200
150
100
50
0
-50
-100
-150
-200
-250
recorded strain (mm/mm x10-6)
30000
40000
50000
60000
70000
80000
90000
position relative to HMT (mm)
#4 D-B Static 1
#4 D-B Static 2
#4 D-B Static 3
#4 D-B Static 4
#4 D-B Static 1 (March)
#4 D-B Static 2 (March)
#4 D-B Static 3 (March)
#4 D-B Static 4 (March)

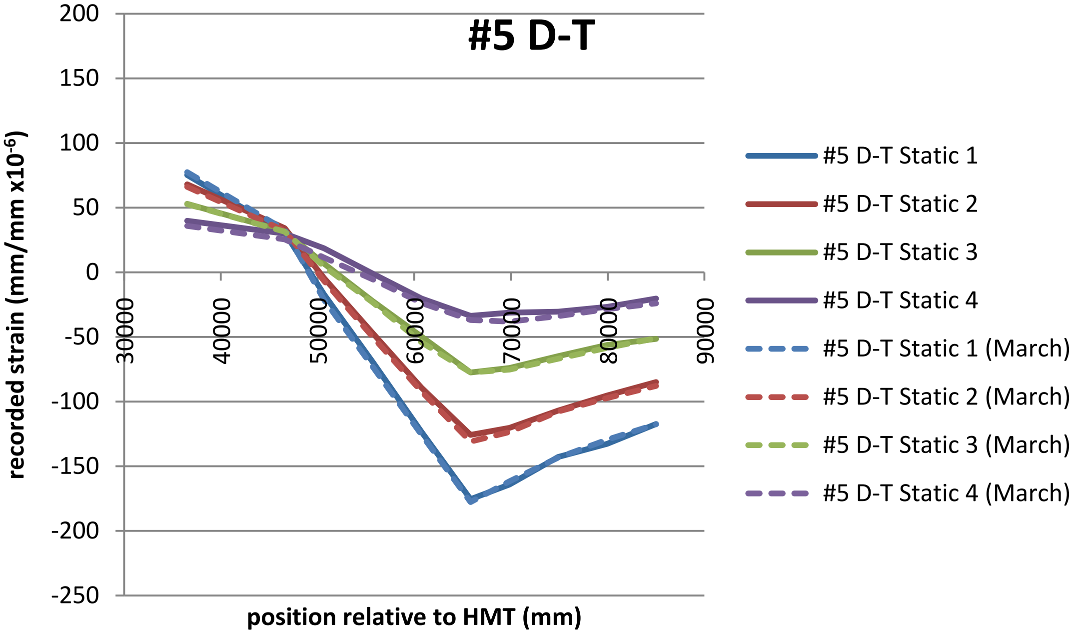
#5 D-T
recorded strain (mm/mm x10^{-6})
200
150
100
50
0
-50
-100
-150
-200
-250
30000
40000
50000
60000
70000
80000
90000
position relative to HMT (mm)
#5 D-T Static 1
#5 D-T Static 2
#5 D-T Static 3
#5 D-T Static 4
#5 D-T Static 1 (March)
#5 D-T Static 2 (March)
#5 D-T Static 3 (March)
#5 D-T Static 4 (March)

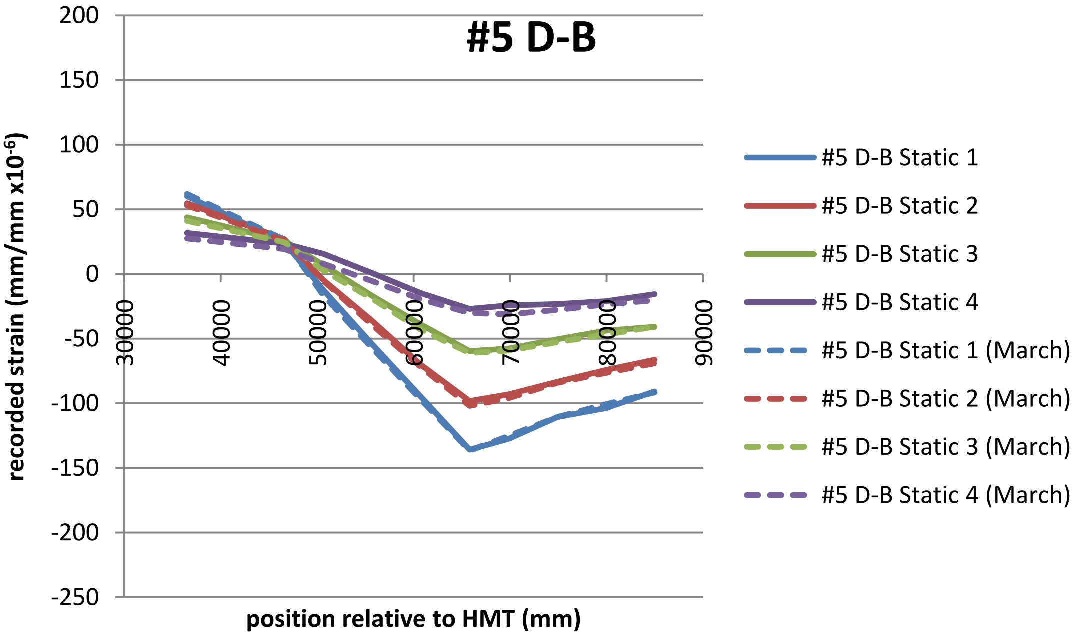
#5 D-B
recorded strain (mm/mm x10^{-6})
200
150
100
50
0
-50
-100
-150
-200
-250
30000
40000
50000
60000
70000
80000
90000
position relative to HMT (mm)
#5 D-B Static 1
#5 D-B Static 2
#5 D-B Static 3
#5 D-B Static 4
#5 D-B Static 1 (March)
#5 D-B Static 2 (March)
#5 D-B Static 3 (March)
#5 D-B Static 4 (March)

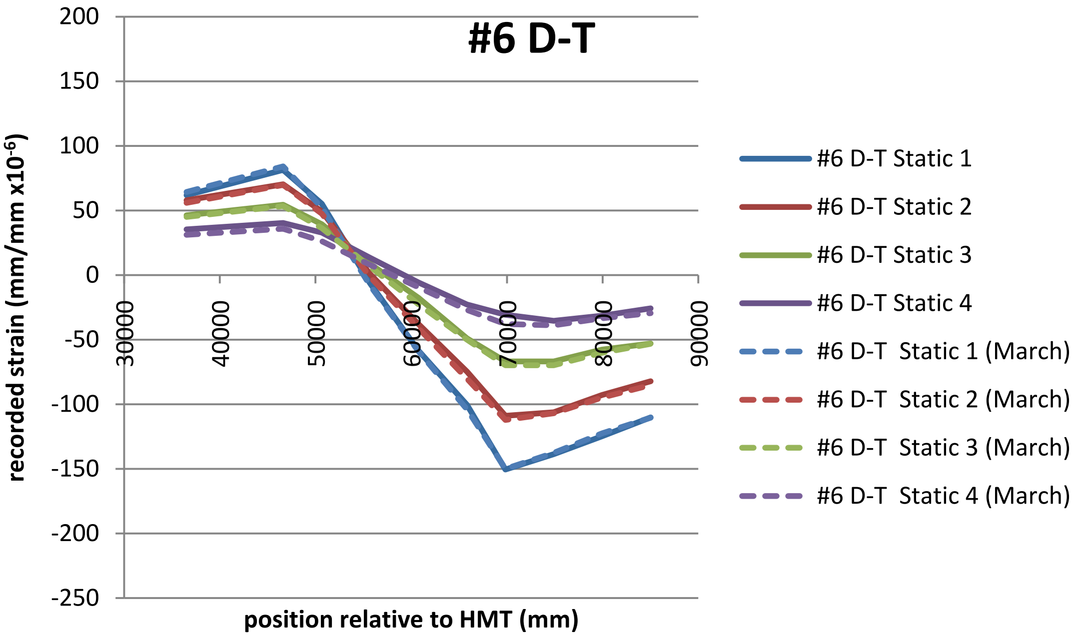
#6 D-T
200
150
100
50
0
-50
-100
-150
-200
-250
recorded strain (mm/mm x10-6)
30000
40000
50000
60000
70000
80000
90000
position relative to HMT (mm)
#6 D-T Static 1
#6 D-T Static 2
#6 D-T Static 3
#6 D-T Static 4
#6 D-T Static 1 (March)
#6 D-T Static 2 (March)
#6 D-T Static 3 (March)
#6 D-T Static 4 (March)

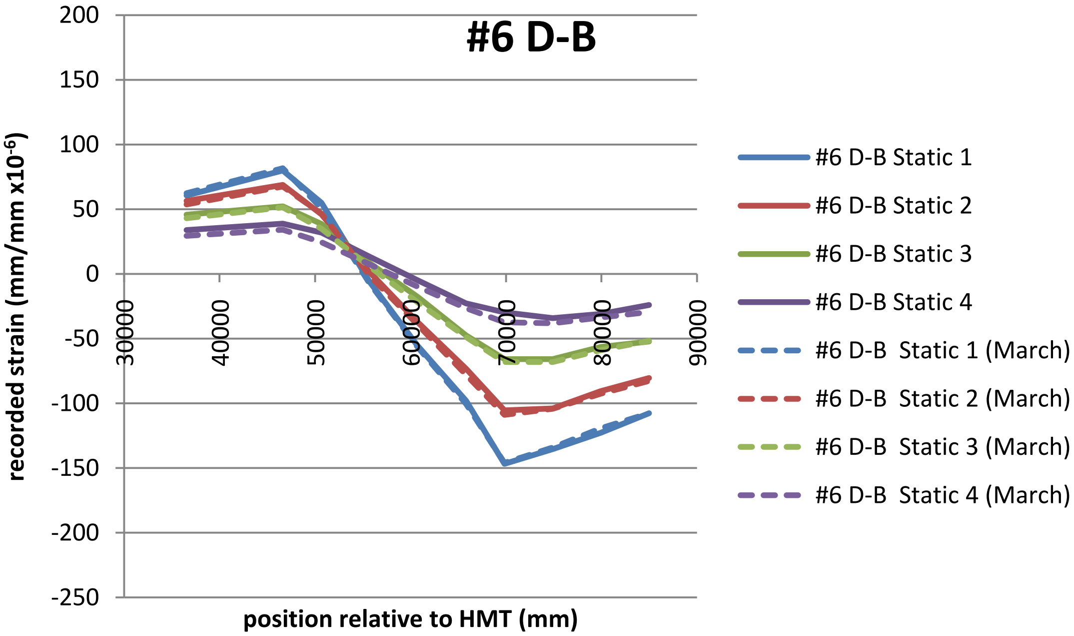
#6 D-B
200
150
100
50
0
-50
-100
-150
-200
-250
recorded strain (mm/mm x10-6)
30000
40000
50000
60000
70000
80000
90000
position relative to HMT (mm)
#6 D-B Static 1
#6 D-B Static 2
#6 D-B Static 3
#6 D-B Static 4
#6 D-B Static 1 (March)
#6 D-B Static 2 (March)
#6 D-B Static 3 (March)
#6 D-B Static 4 (March)

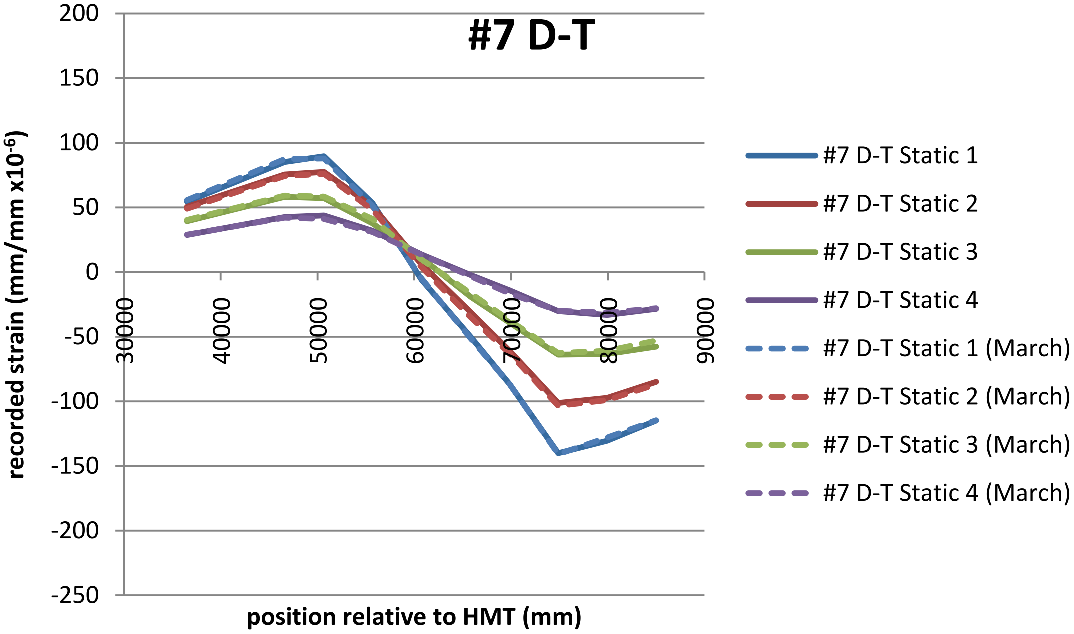
#7 D-T
200
150
100
50
0
-50
-100
-150
-200
-250
recorded strain (mm/mm x10⁻⁶)
30000
40000
50000
60000
70000
80000
90000
position relative to HMT (mm)
#7 D-T Static 1
#7 D-T Static 2
#7 D-T Static 3
#7 D-T Static 4
#7 D-T Static 1 (March)
#7 D-T Static 2 (March)
#7 D-T Static 3 (March)
#7 D-T Static 4 (March)

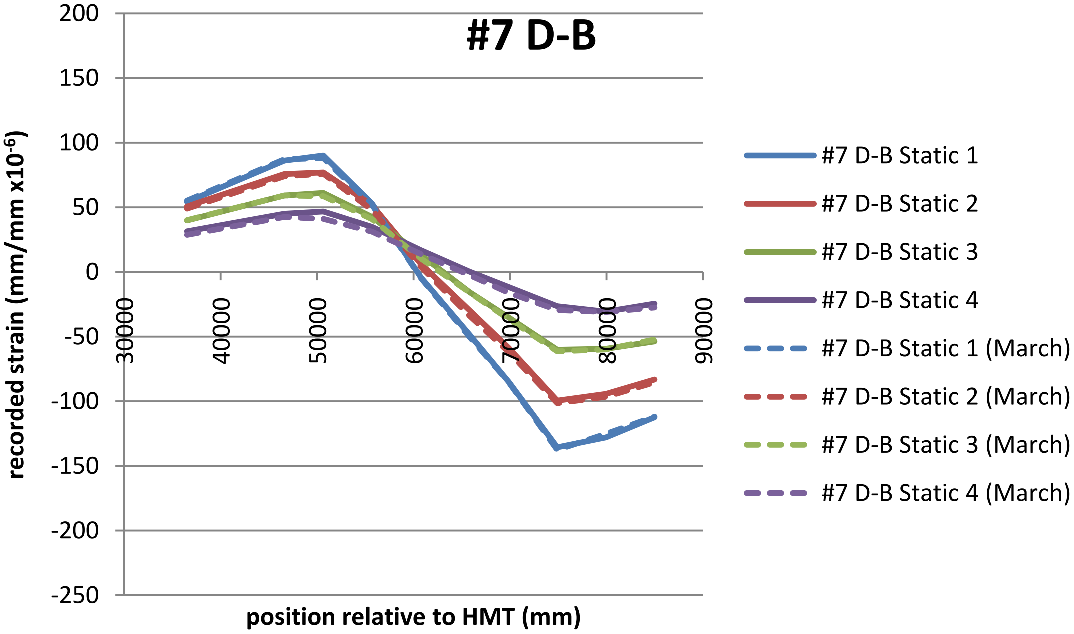
#7 D-B
200
150
100
50
0
-50
-100
-150
-200
-250
recorded strain (mm/mm x10⁻⁶)
30000
40000
50000
60000
70000
80000
90000
position relative to HMT (mm)
#7 D-B Static 1
#7 D-B Static 2
#7 D-B Static 3
#7 D-B Static 4
#7 D-B Static 1 (March)
#7 D-B Static 2 (March)
#7 D-B Static 3 (March)
#7 D-B Static 4 (March)

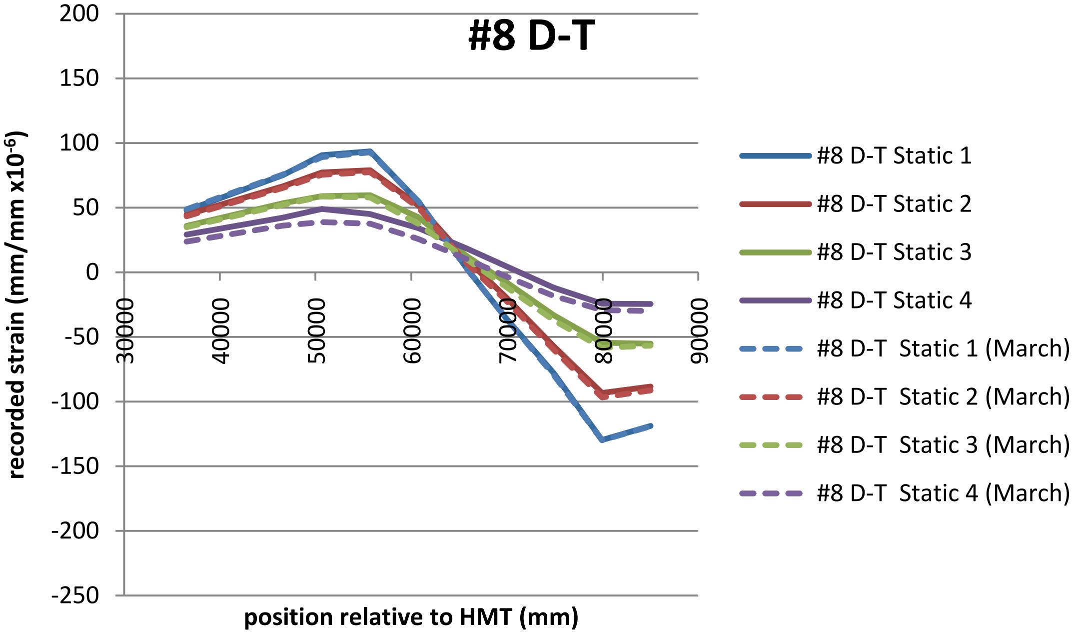
#8 D-T
200
150
100
50
0
-50
-100
-150
-200
-250
recorded strain (mm/mm x10-6)
30000
40000
50000
60000
70000
80000
90000
position relative to HMT (mm)
#8 D-T Static 1
#8 D-T Static 2
#8 D-T Static 3
#8 D-T Static 4
#8 D-T Static 1 (March)
#8 D-T Static 2 (March)
#8 D-T Static 3 (March)
#8 D-T Static 4 (March)

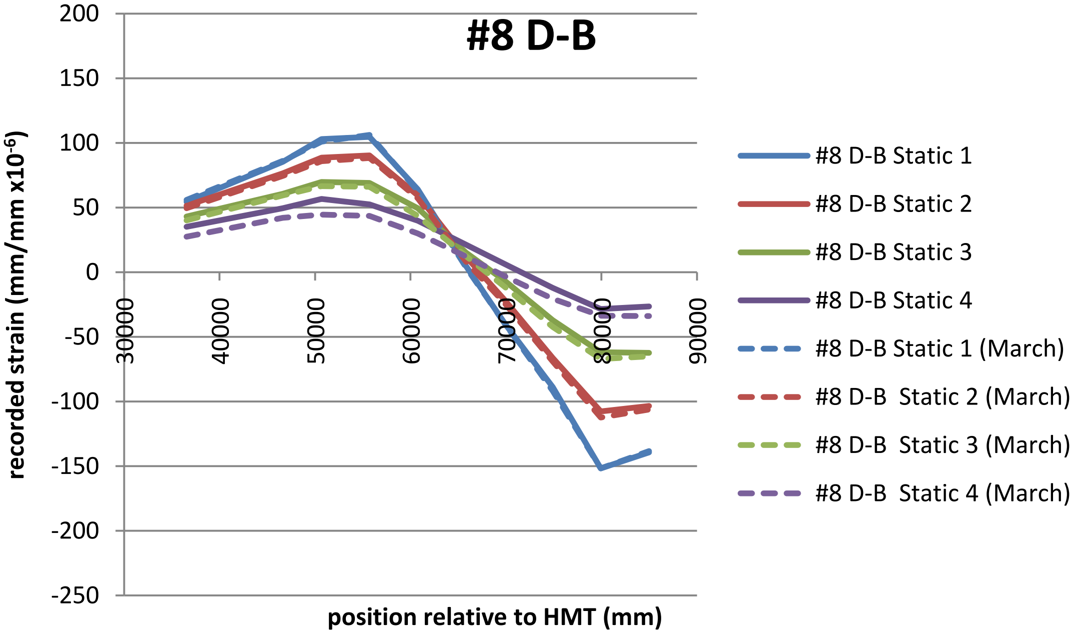
#8 D-B
200
150
100
50
0
-50
-100
-150
-200
-250
recorded strain (mm/mm x10-6)
30000
40000
50000
60000
70000
80000
90000
position relative to HMT (mm)
#8 D-B Static 1
#8 D-B Static 2
#8 D-B Static 3
#8 D-B Static 4
#8 D-B Static 1 (March)
#8 D-B Static 2 (March)
#8 D-B Static 3 (March)
#8 D-B Static 4 (March)

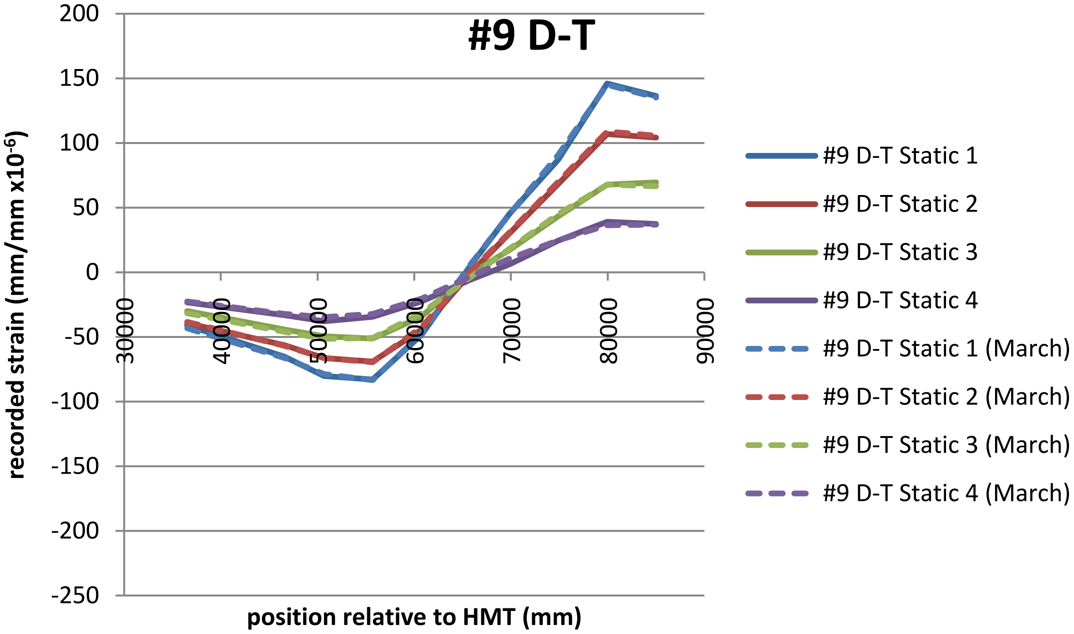
#9 D-T
recorded strain (mm/mm x10^{-6})
200
150
100
50
0
-50
-100
-150
-200
-250
30000
40000
50000
60000
70000
80000
90000
position relative to HMT (mm)
#9 D-T Static 1
#9 D-T Static 2
#9 D-T Static 3
#9 D-T Static 4
#9 D-T Static 1 (March)
#9 D-T Static 2 (March)
#9 D-T Static 3 (March)
#9 D-T Static 4 (March)

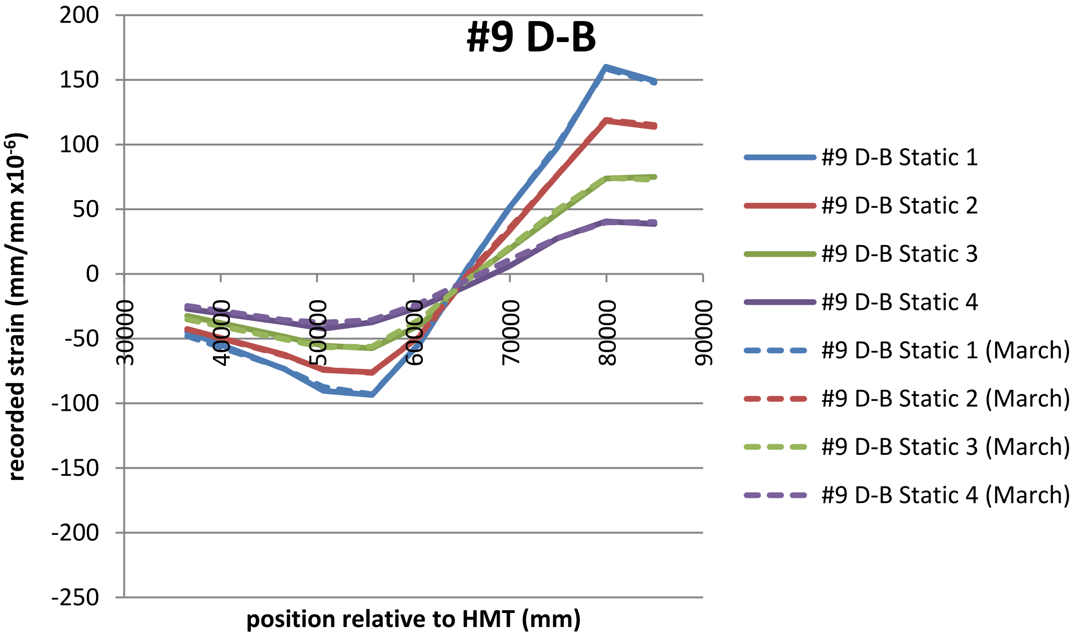
#9 D-B
recorded strain (mm/mm x10^{-6})
200
150
100
50
0
-50
-100
-150
-200
-250
30000
40000
50000
60000
70000
80000
90000
position relative to HMT (mm)
#9 D-B Static 1
#9 D-B Static 2
#9 D-B Static 3
#9 D-B Static 4
#9 D-B Static 1 (March)
#9 D-B Static 2 (March)
#9 D-B Static 3 (March)
#9 D-B Static 4 (March)

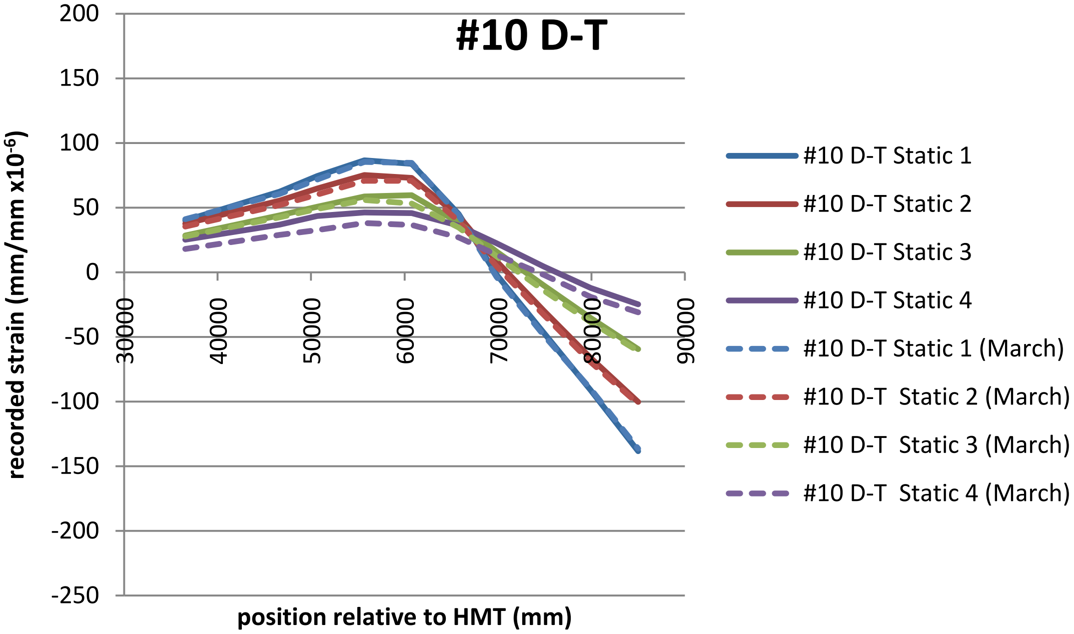
#10 D-T
recorded strain (mm/mm x10^{-6})
200
150
100
50
0
-50
-100
-150
-200
-250
30000
40000
50000
60000
70000
80000
90000
position relative to HMT (mm)
#10 D-T Static 1
#10 D-T Static 2
#10 D-T Static 3
#10 D-T Static 4
#10 D-T Static 1 (March)
#10 D-T Static 2 (March)
#10 D-T Static 3 (March)
#10 D-T Static 4 (March)

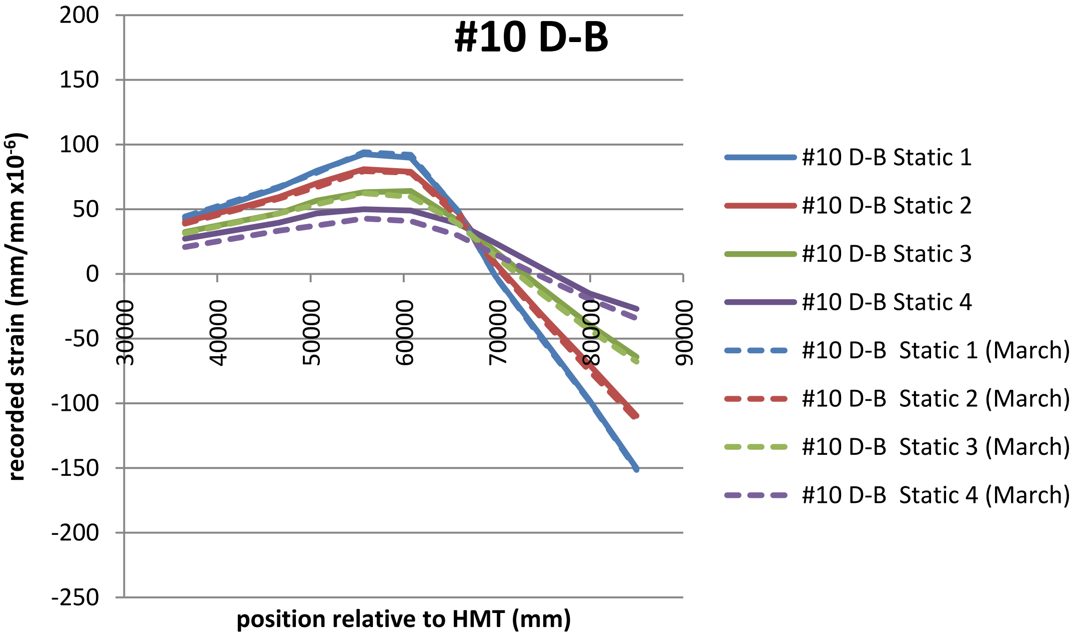
#10 D-B
recorded strain (mm/mm x10^{-6})
200
150
100
50
0
-50
-100
-150
-200
-250
30000
40000
50000
60000
70000
80000
90000
position relative to HMT (mm)
#10 D-B Static 1
#10 D-B Static 2
#10 D-B Static 3
#10 D-B Static 4
#10 D-B Static 1 (March)
#10 D-B Static 2 (March)
#10 D-B Static 3 (March)
#10 D-B Static 4 (March)

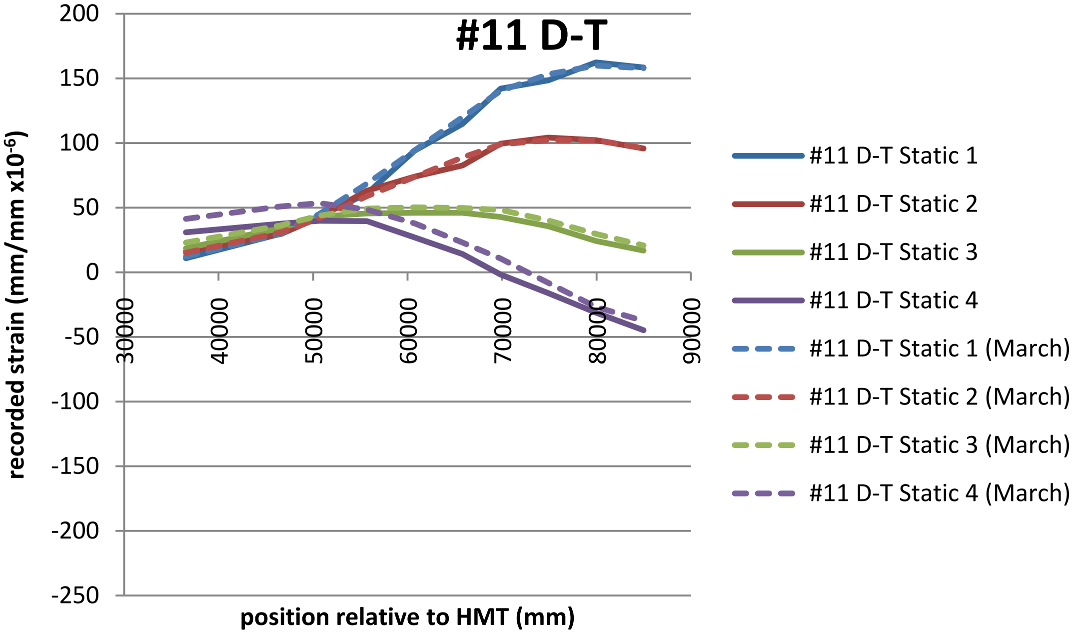
#11 D-T
recorded strain (mm/mm x10^{-6})
200
150
100
50
0
-50
-100
-150
-200
-250
30000
40000
50000
60000
70000
80000
90000
position relative to HMT (mm)
#11 D-T Static 1
#11 D-T Static 2
#11 D-T Static 3
#11 D-T Static 4
#11 D-T Static 1 (March)
#11 D-T Static 2 (March)
#11 D-T Static 3 (March)
#11 D-T Static 4 (March)

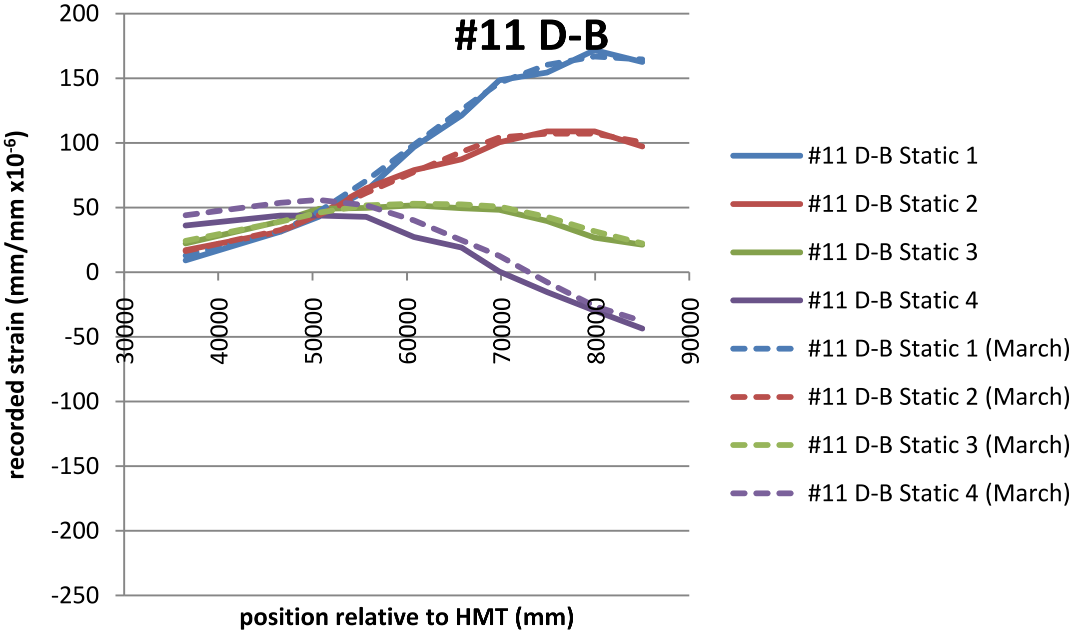
#11 D-B
recorded strain (mm/mm x10^{-6})
200
150
100
50
0
-50
-100
-150
-200
-250
30000
40000
50000
60000
70000
80000
90000
position relative to HMT (mm)
#11 D-B Static 1
#11 D-B Static 2
#11 D-B Static 3
#11 D-B Static 4
#11 D-B Static 1 (March)
#11 D-B Static 2 (March)
#11 D-B Static 3 (March)
#11 D-B Static 4 (March)

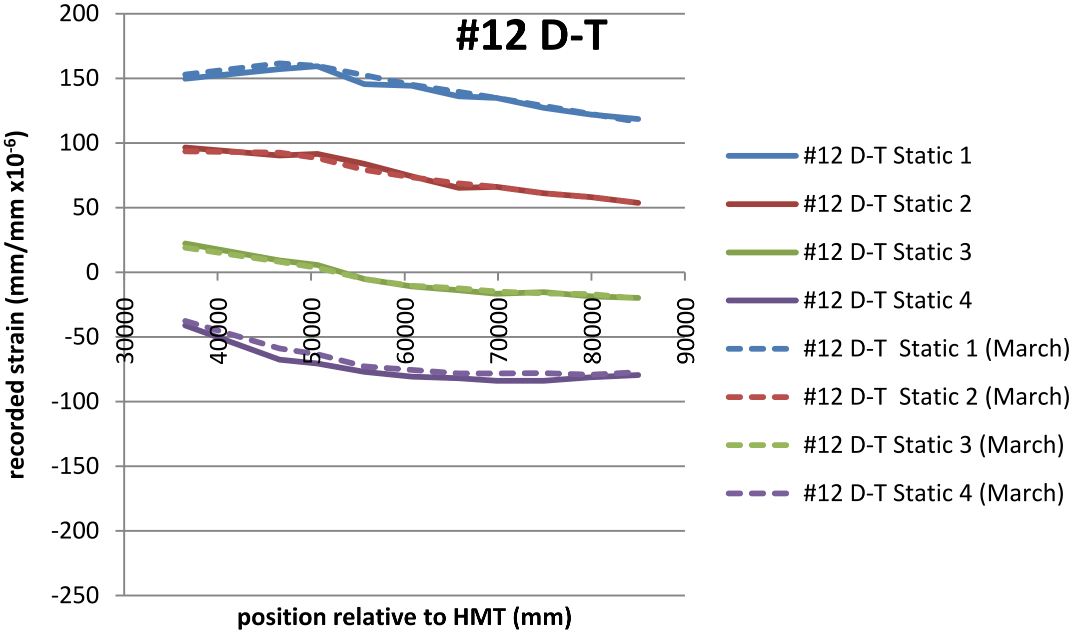
#12 D-T
recorded strain (mm/mm x10^{-6})
200
150
100
50
0
-50
-100
-150
-200
-250
30000
40000
50000
60000
70000
80000
90000
position relative to HMT (mm)
#12 D-T Static 1
#12 D-T Static 2
#12 D-T Static 3
#12 D-T Static 4
#12 D-T Static 1 (March)
#12 D-T Static 2 (March)
#12 D-T Static 3 (March)
#12 D-T Static 4 (March)

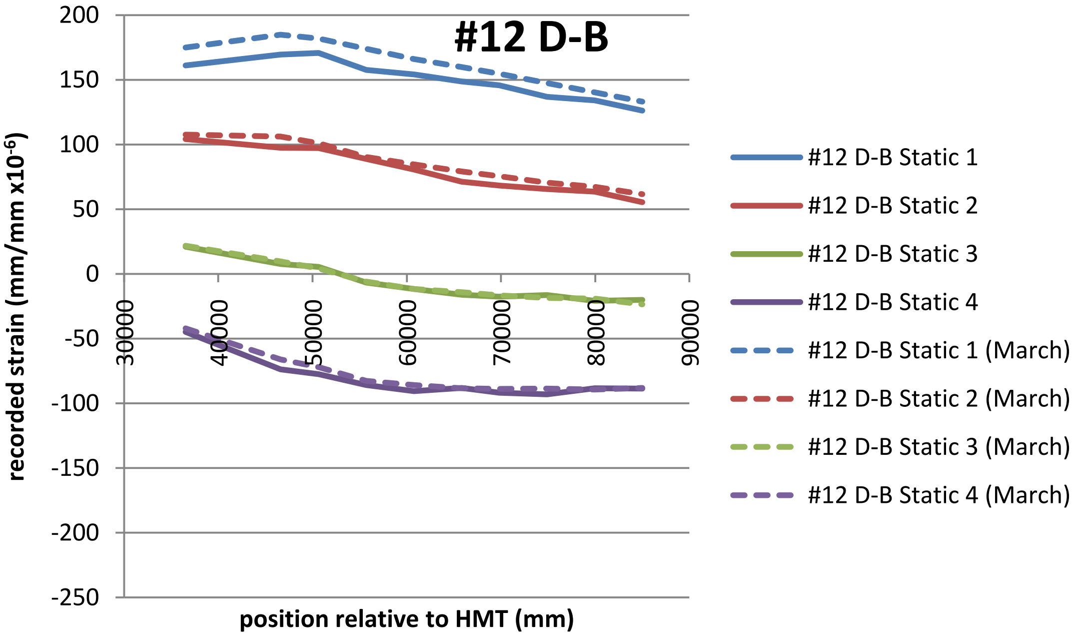
#12 D-B
recorded strain (mm/mm x10^{-6})
200
150
100
50
0
-50
-100
-150
-200
-250
30000
40000
50000
60000
70000
80000
90000
position relative to HMT (mm)
#12 D-B Static 1
#12 D-B Static 2
#12 D-B Static 3
#12 D-B Static 4
#12 D-B Static 1 (March)
#12 D-B Static 2 (March)
#12 D-B Static 3 (March)
#12 D-B Static 4 (March)

Appendix II – Influence Lines From Slow Speed Tests

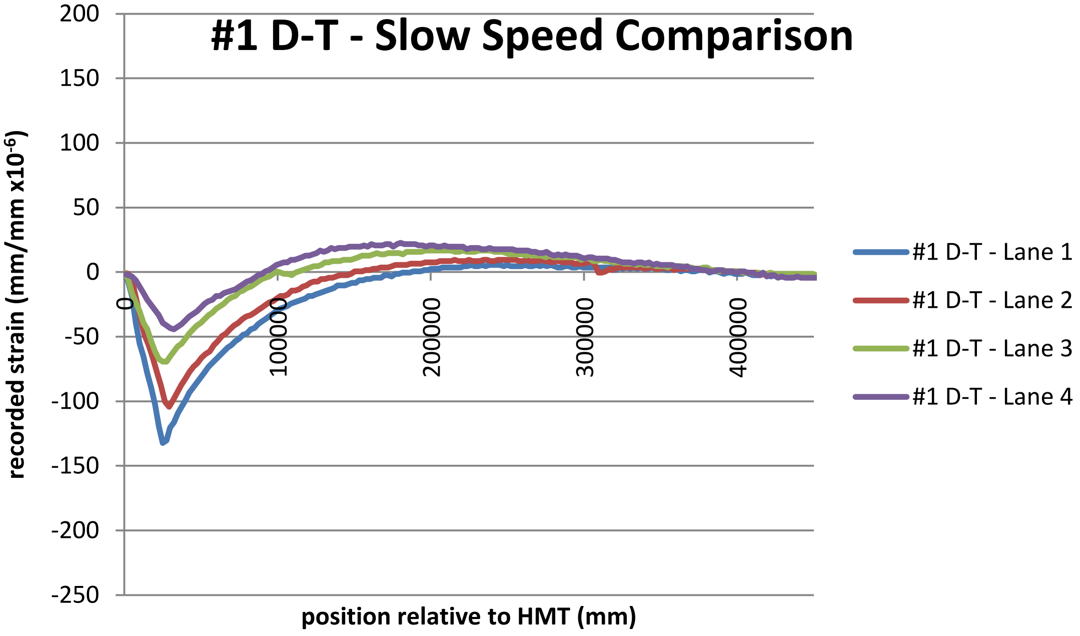

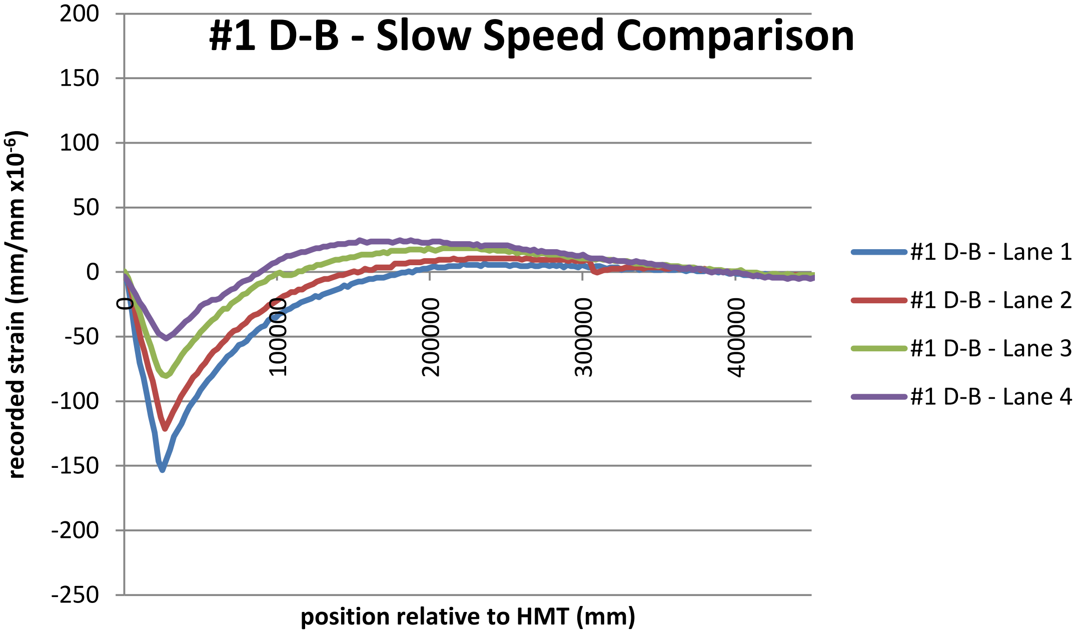

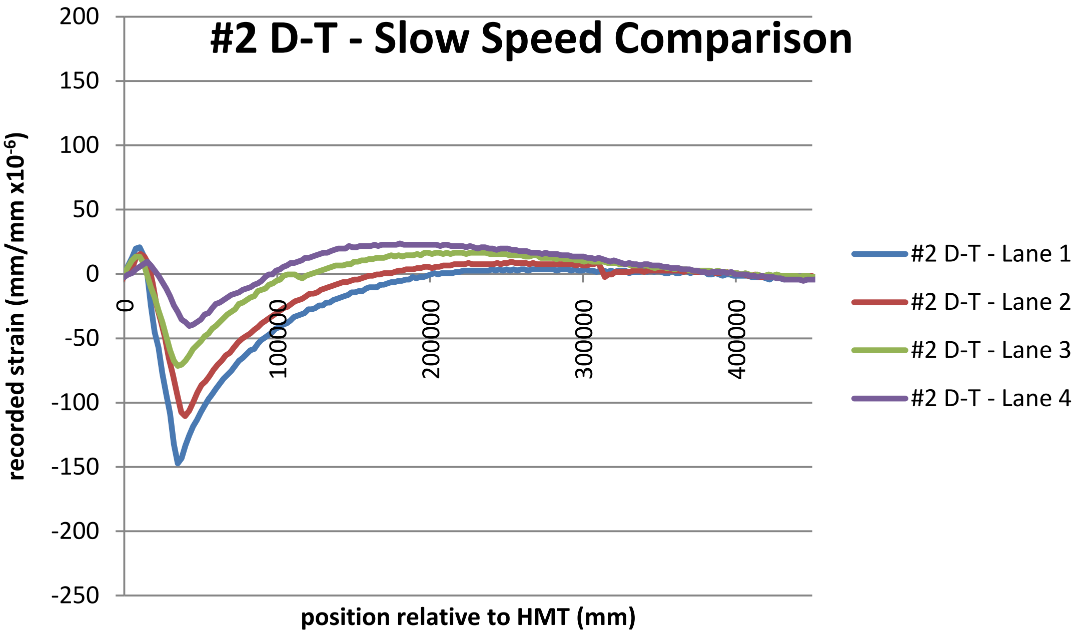
#2 D-T - Slow Speed Comparison
recorded strain (mm/mm x10^{-6})
200
150
100
50
0
-50
-100
-150
-200
-250
0
100000
200000
300000
400000
position relative to HMT (mm)
#2 D-T - Lane 1
#2 D-T - Lane 2
#2 D-T - Lane 3
#2 D-T - Lane 4

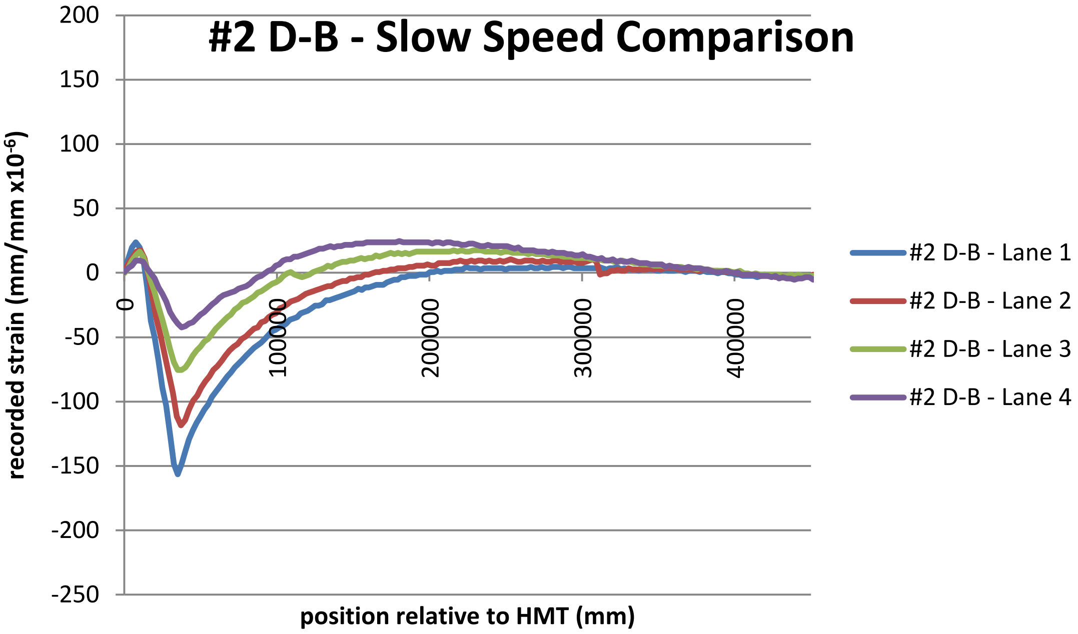
#2 D-B - Slow Speed Comparison
recorded strain (mm/mm x10^{-6})
200
150
100
50
0
-50
-100
-150
-200
-250
0
100000
200000
300000
400000
position relative to HMT (mm)
#2 D-B - Lane 1
#2 D-B - Lane 2
#2 D-B - Lane 3
#2 D-B - Lane 4

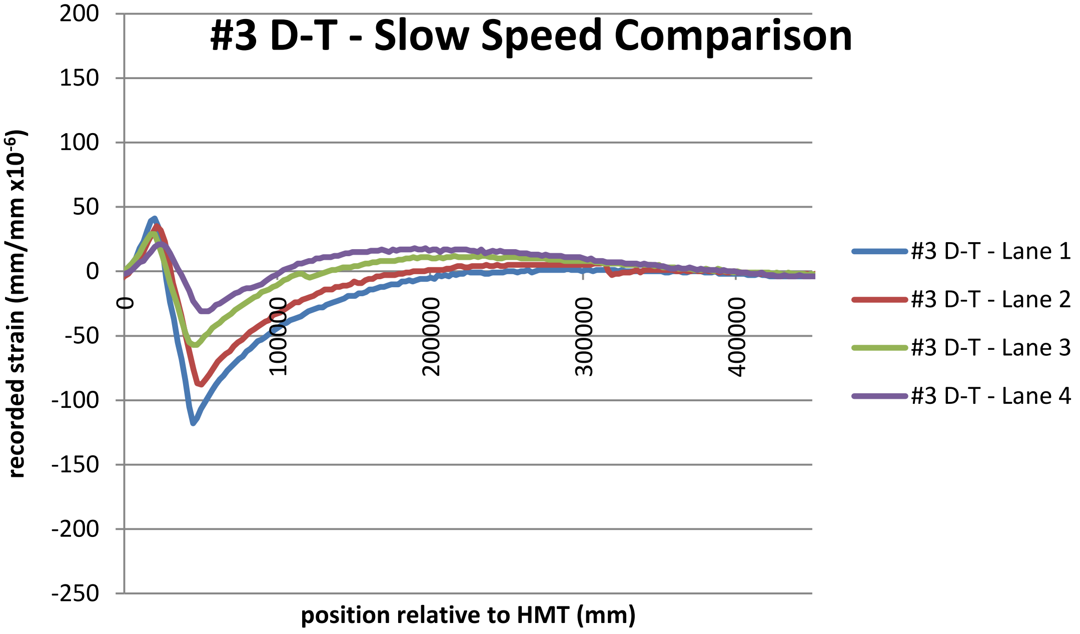
#3 D-T - Slow Speed Comparison
recorded strain (mm/mm x10-6)
200
150
100
50
0
-50
-100
-150
-200
-250
0
100000
200000
300000
400000
position relative to HMT (mm)
#3 D-T - Lane 1
#3 D-T - Lane 2
#3 D-T - Lane 3
#3 D-T - Lane 4

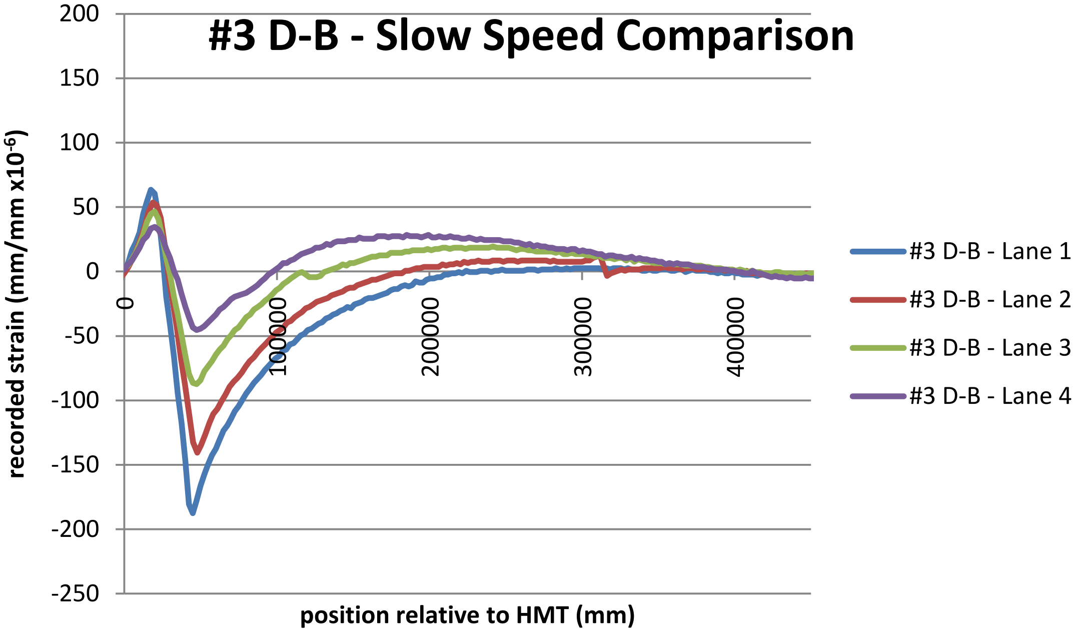
#3 D-B - Slow Speed Comparison
recorded strain (mm/mm x10-6)
200
150
100
50
0
-50
-100
-150
-200
-250
0
100000
200000
300000
400000
position relative to HMT (mm)
#3 D-B - Lane 1
#3 D-B - Lane 2
#3 D-B - Lane 3
#3 D-B - Lane 4

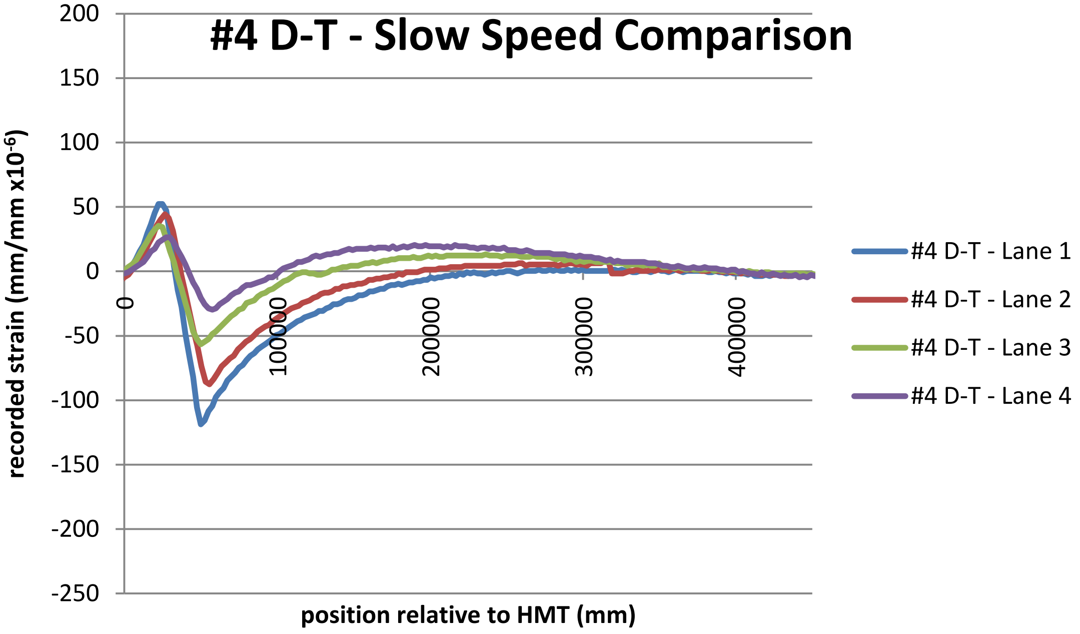
#4 D-T - Slow Speed Comparison
recorded strain (mm/mm x10-6)
200
150
100
50
0
-50
-100
-150
-200
-250
0
100000
200000
300000
400000
position relative to HMT (mm)
#4 D-T - Lane 1
#4 D-T - Lane 2
#4 D-T - Lane 3
#4 D-T - Lane 4

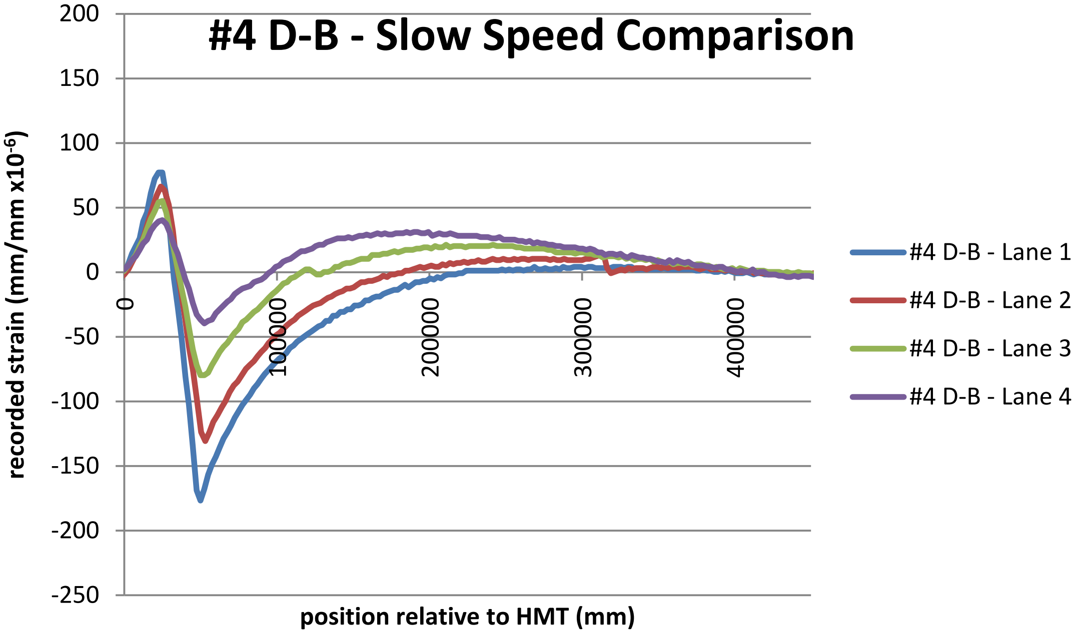
#4 D-B - Slow Speed Comparison
recorded strain (mm/mm x10-6)
200
150
100
50
0
-50
-100
-150
-200
-250
0
100000
200000
300000
400000
position relative to HMT (mm)
#4 D-B - Lane 1
#4 D-B - Lane 2
#4 D-B - Lane 3
#4 D-B - Lane 4

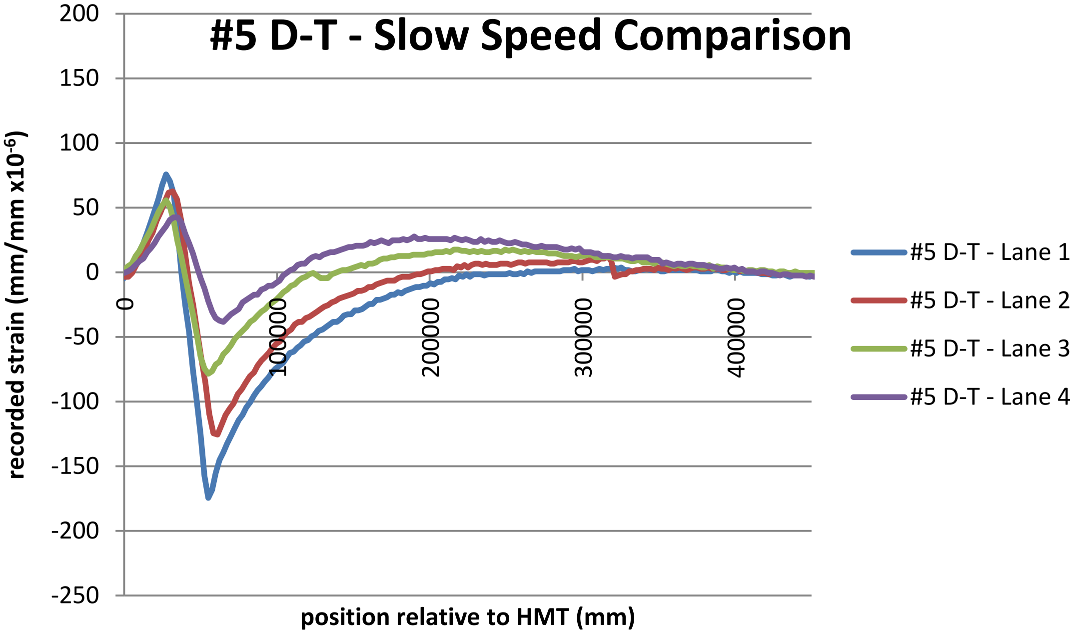
#5 D-T - Slow Speed Comparison
200
150
100
50
0
-50
-100
-150
-200
-250
recorded strain (mm/mm x10-6)
0
100000
200000
300000
400000
position relative to HMT (mm)
#5 D-T - Lane 1
#5 D-T - Lane 2
#5 D-T - Lane 3
#5 D-T - Lane 4

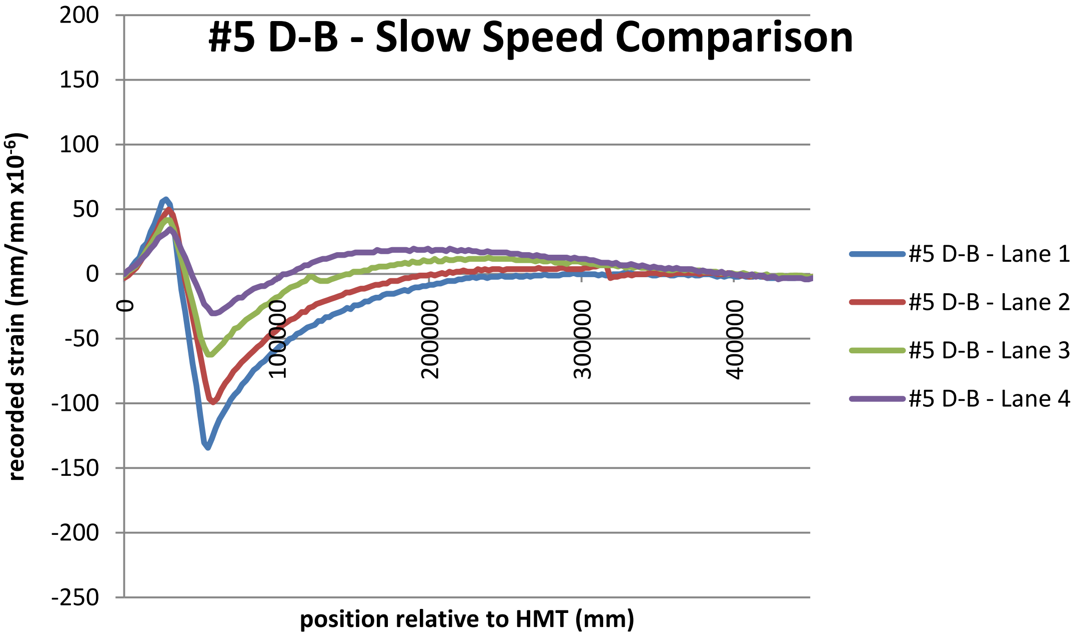
#5 D-B - Slow Speed Comparison
200
150
100
50
0
-50
-100
-150
-200
-250
recorded strain (mm/mm x10-6)
0
100000
200000
300000
400000
position relative to HMT (mm)
#5 D-B - Lane 1
#5 D-B - Lane 2
#5 D-B - Lane 3
#5 D-B - Lane 4

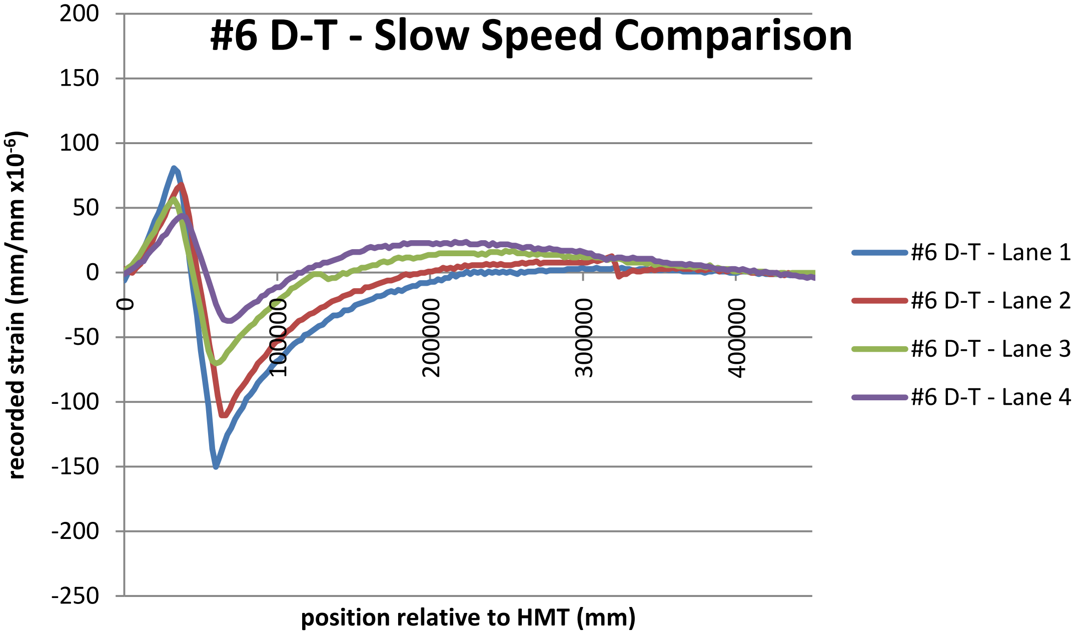
#6 D-T - Slow Speed Comparison
200
150
100
50
0
-50
-100
-150
-200
-250
recorded strain (mm/mm x10⁻⁶)
0
100000
200000
300000
400000
position relative to HMT (mm)
#6 D-T - Lane 1
#6 D-T - Lane 2
#6 D-T - Lane 3
#6 D-T - Lane 4

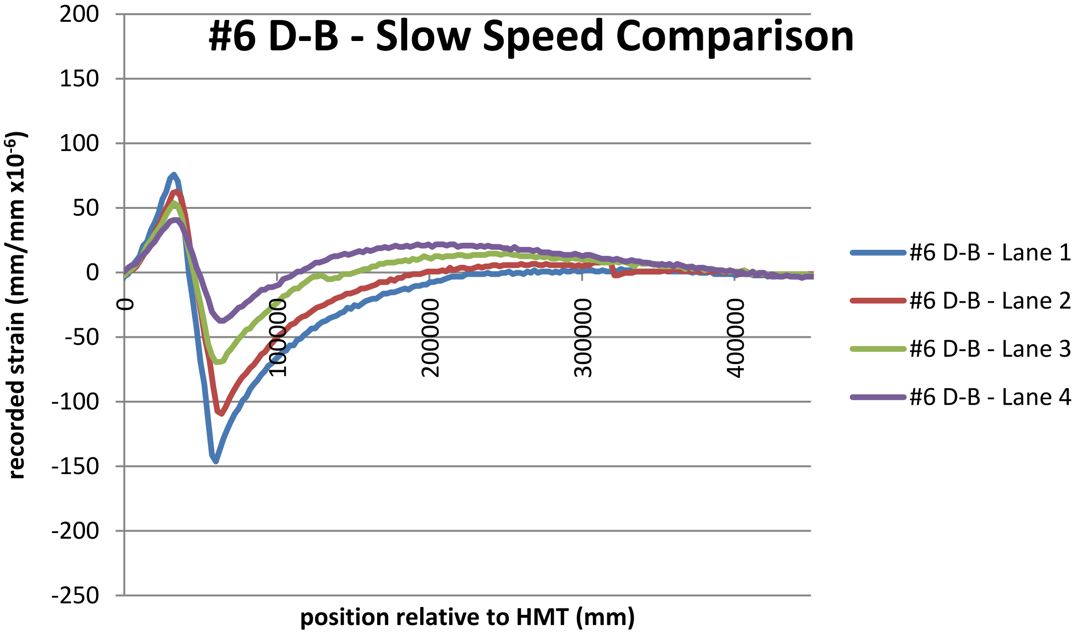
#6 D-B - Slow Speed Comparison
200
150
100
50
0
-50
-100
-150
-200
-250
recorded strain (mm/mm x10⁻⁶)
0
100000
200000
300000
400000
position relative to HMT (mm)
#6 D-B - Lane 1
#6 D-B - Lane 2
#6 D-B - Lane 3
#6 D-B - Lane 4

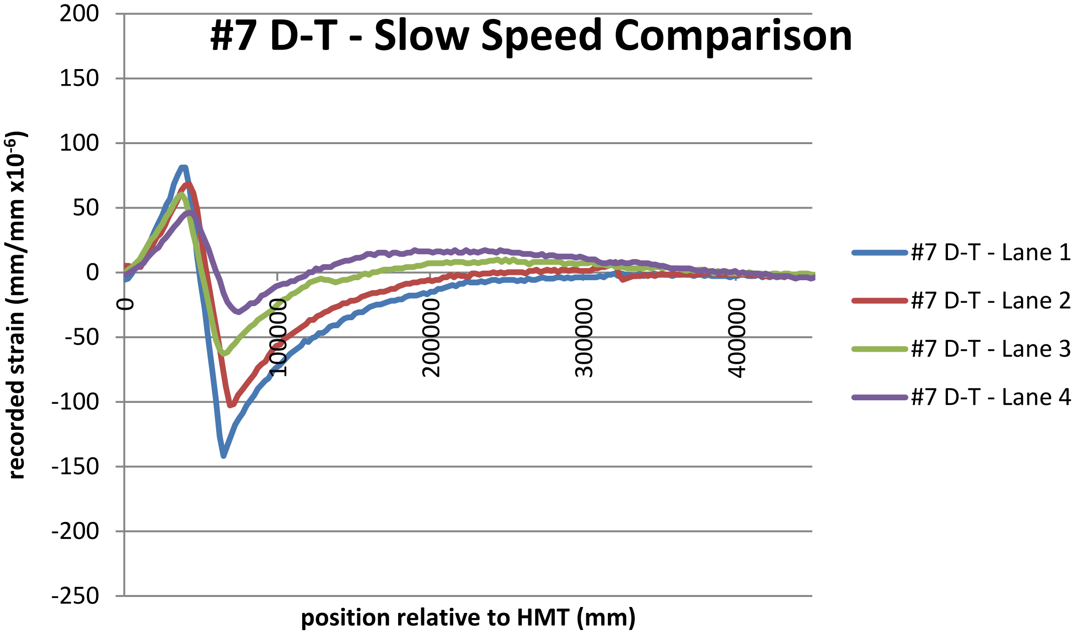
#7 D-T - Slow Speed Comparison
recorded strain (mm/mm x10^{-6})
200
150
100
50
0
-50
-100
-150
-200
-250
0
100000
200000
300000
400000
position relative to HMT (mm)
#7 D-T - Lane 1
#7 D-T - Lane 2
#7 D-T - Lane 3
#7 D-T - Lane 4

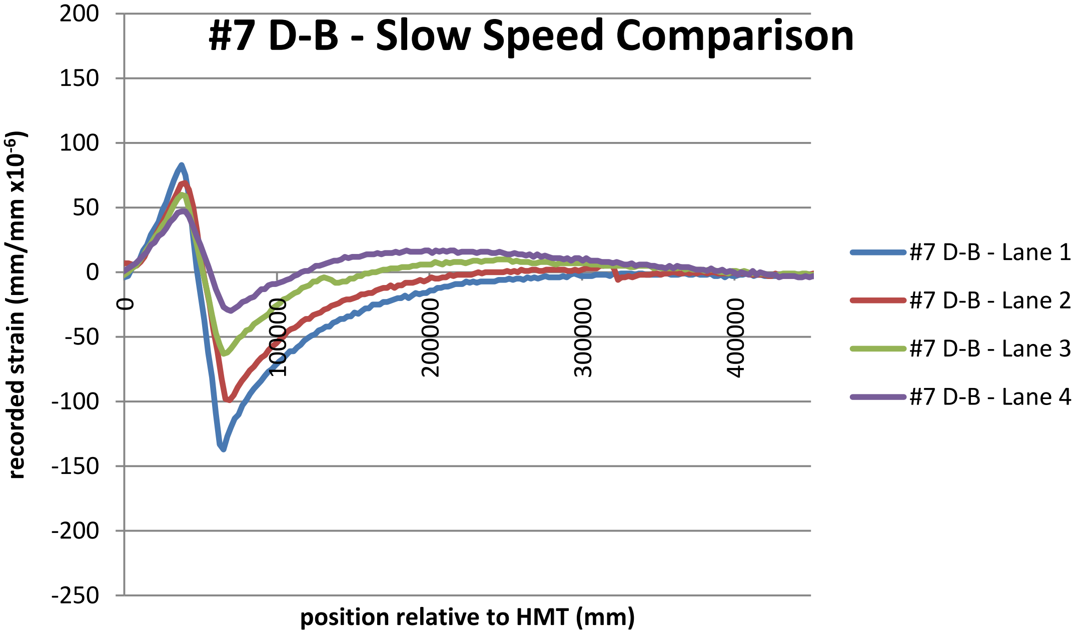
#7 D-B - Slow Speed Comparison
recorded strain (mm/mm x10^{-6})
200
150
100
50
0
-50
-100
-150
-200
-250
0
100000
200000
300000
400000
position relative to HMT (mm)
#7 D-B - Lane 1
#7 D-B - Lane 2
#7 D-B - Lane 3
#7 D-B - Lane 4

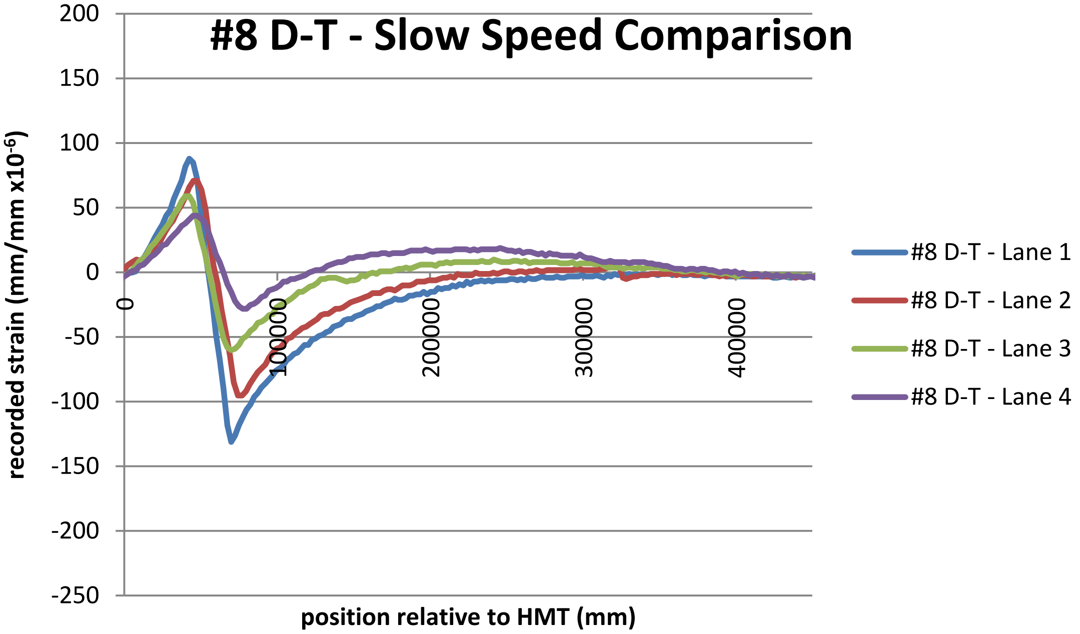
#8 D-T - Slow Speed Comparison
200
150
100
50
0
-50
-100
-150
-200
-250
recorded strain (mm/mm x10^{-6})
0
100000
200000
300000
400000
position relative to HMT (mm)
#8 D-T - Lane 1
#8 D-T - Lane 2
#8 D-T - Lane 3
#8 D-T - Lane 4

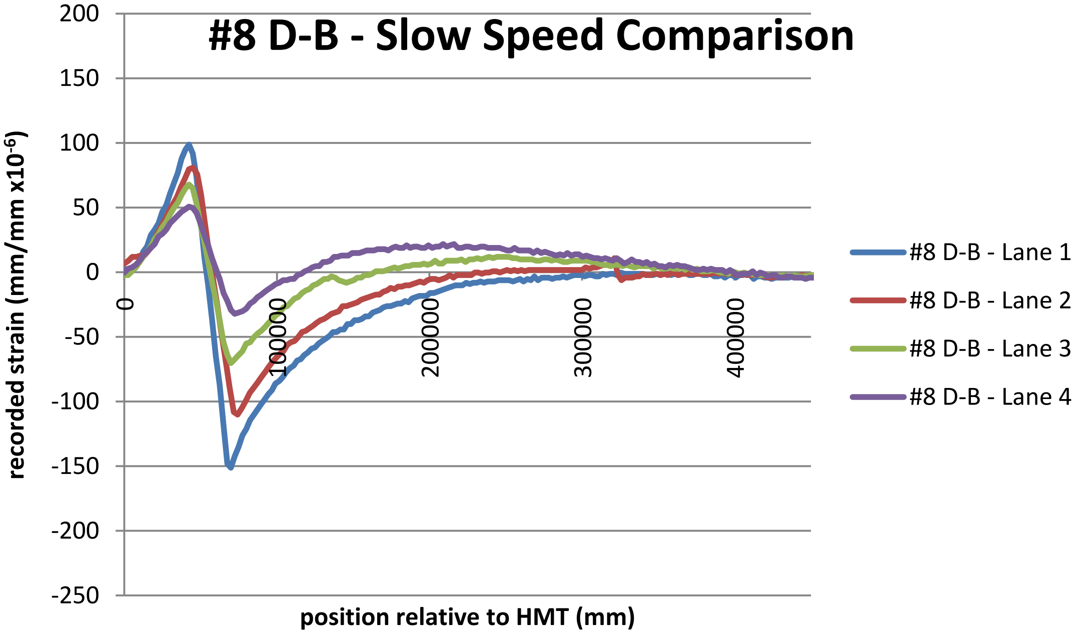
#8 D-B - Slow Speed Comparison
200
150
100
50
0
-50
-100
-150
-200
-250
recorded strain (mm/mm x10^{-6})
0
100000
200000
300000
400000
position relative to HMT (mm)
#8 D-B - Lane 1
#8 D-B - Lane 2
#8 D-B - Lane 3
#8 D-B - Lane 4

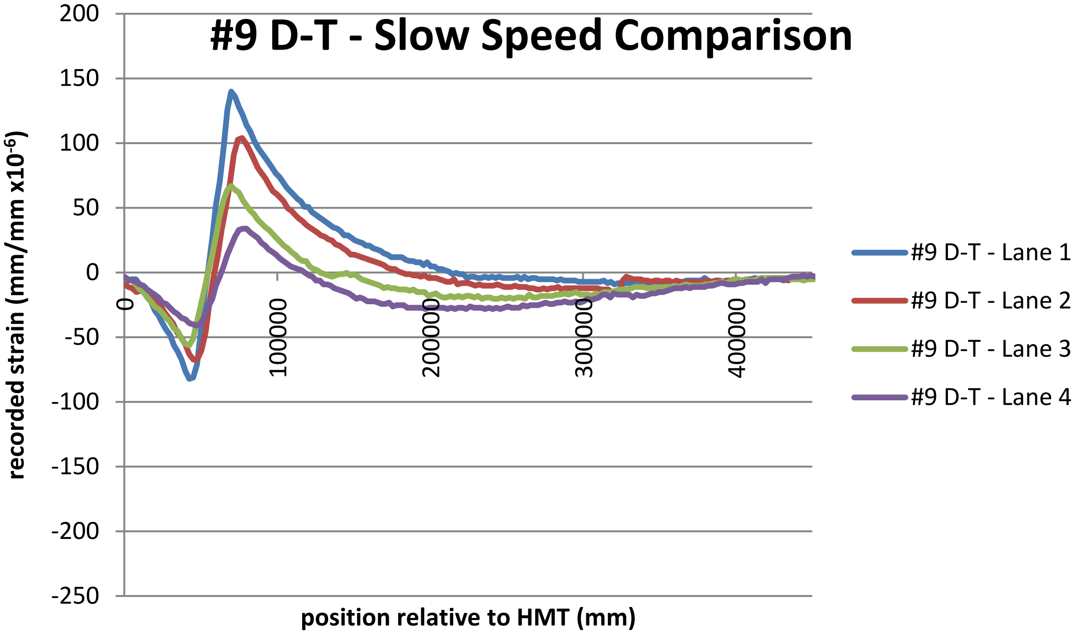
#9 D-T - Slow Speed Comparison
recorded strain (mm/mm x10⁻⁶)
200
150
100
50
0
-50
-100
-150
-200
-250
0
100000
200000
300000
400000
position relative to HMT (mm)
#9 D-T - Lane 1
#9 D-T - Lane 2
#9 D-T - Lane 3
#9 D-T - Lane 4

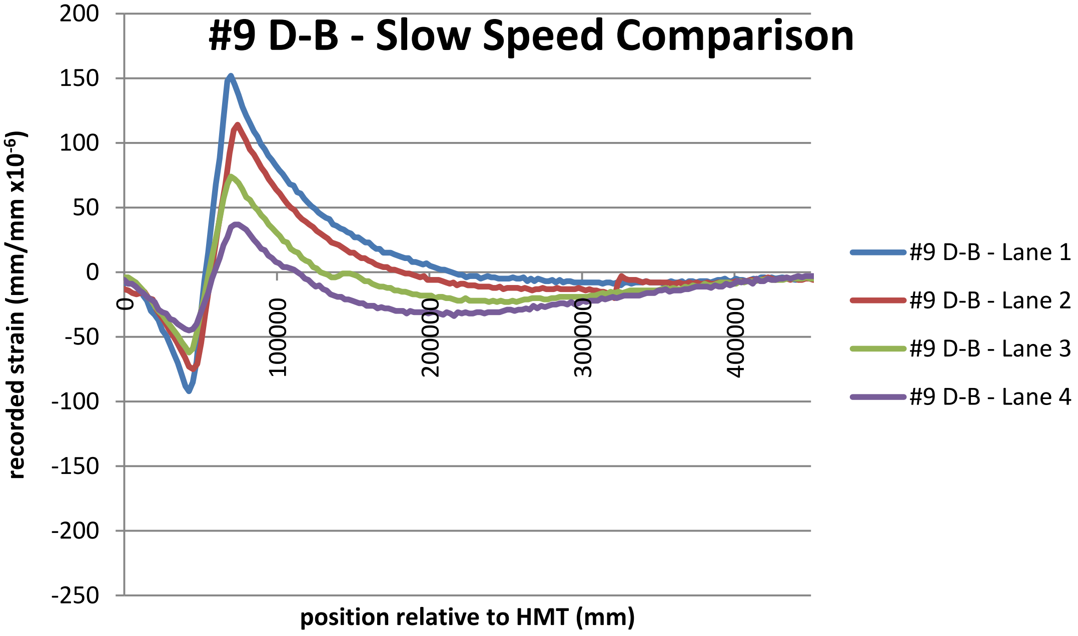
#9 D-B - Slow Speed Comparison
recorded strain (mm/mm x10⁻⁶)
200
150
100
50
0
-50
-100
-150
-200
-250
0
100000
200000
300000
400000
position relative to HMT (mm)
#9 D-B - Lane 1
#9 D-B - Lane 2
#9 D-B - Lane 3
#9 D-B - Lane 4

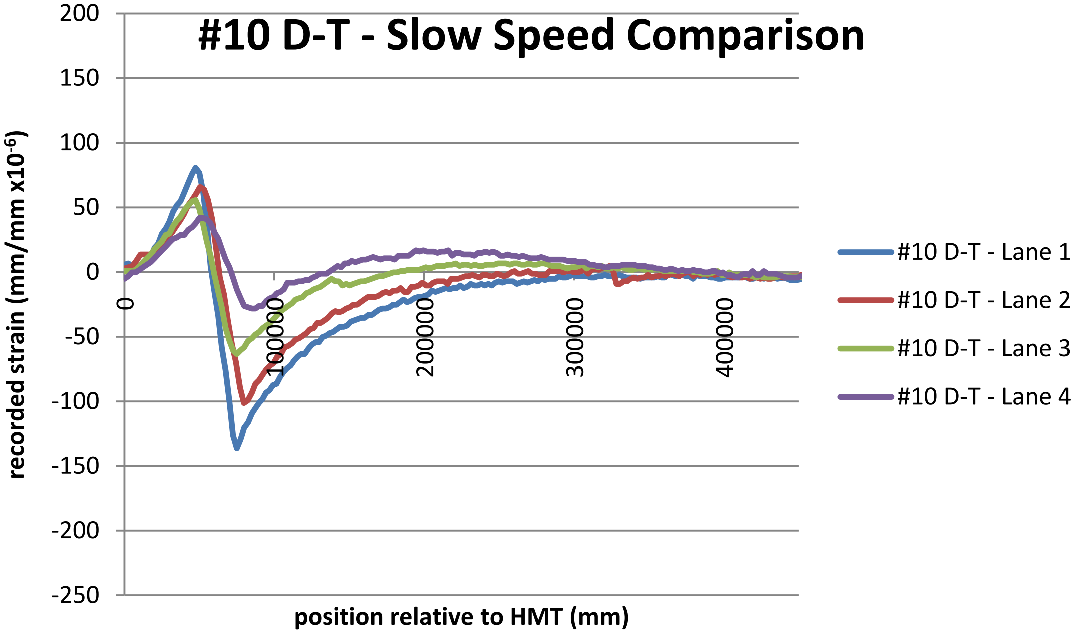
#10 D-T - Slow Speed Comparison
200
150
100
50
0
-50
-100
-150
-200
-250
recorded strain (mm/mm x10^{-6})
0
100000
200000
300000
400000
position relative to HMT (mm)
#10 D-T - Lane 1
#10 D-T - Lane 2
#10 D-T - Lane 3
#10 D-T - Lane 4

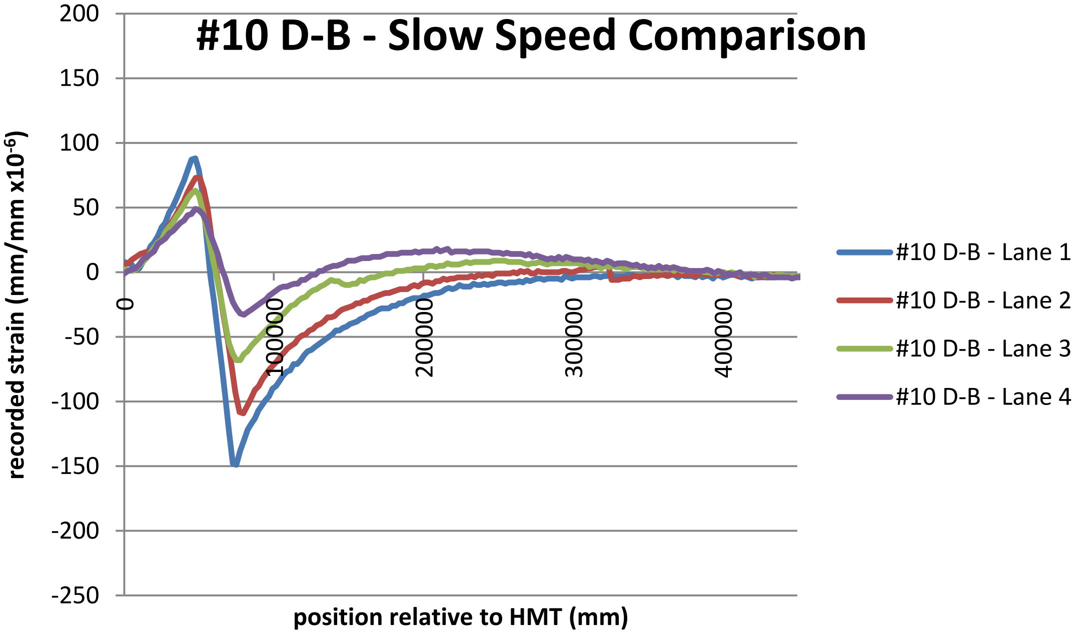
#10 D-B - Slow Speed Comparison
200
150
100
50
0
-50
-100
-150
-200
-250
recorded strain (mm/mm x10^{-6})
0
100000
200000
300000
400000
position relative to HMT (mm)
#10 D-B - Lane 1
#10 D-B - Lane 2
#10 D-B - Lane 3
#10 D-B - Lane 4

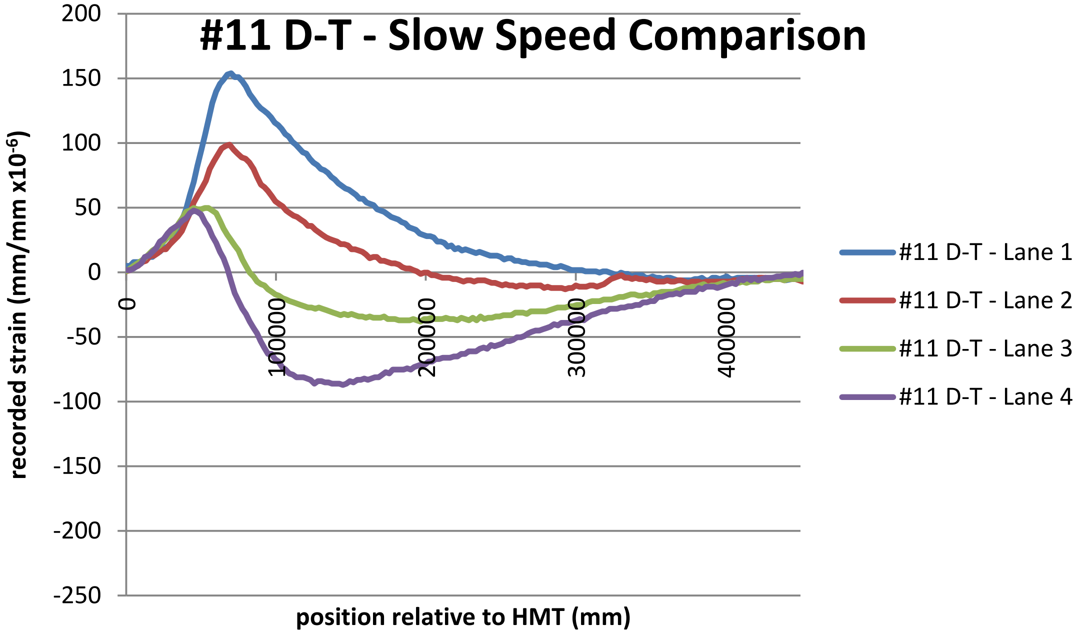
#11 D-T - Slow Speed Comparison
recorded strain (mm/mm x10-6)
200
150
100
50
0
-50
-100
-150
-200
-250
0
100000
200000
300000
400000
position relative to HMT (mm)
#11 D-T - Lane 1
#11 D-T - Lane 2
#11 D-T - Lane 3
#11 D-T - Lane 4

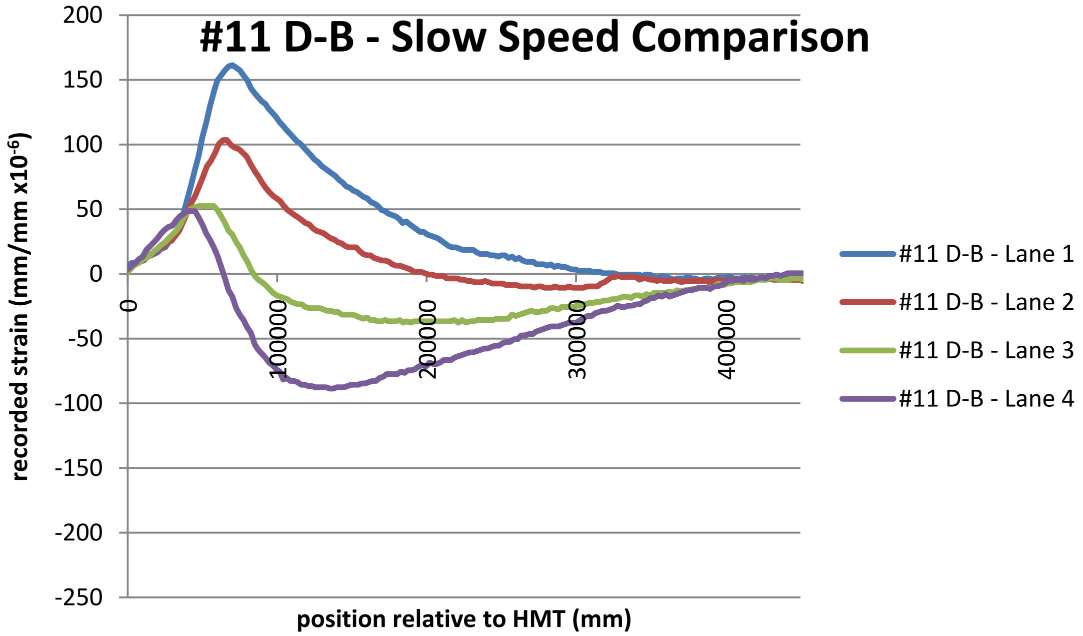
#11 D-B - Slow Speed Comparison
recorded strain (mm/mm x10-6)
200
150
100
50
0
-50
-100
-150
-200
-250
0
100000
200000
300000
400000
position relative to HMT (mm)
#11 D-B - Lane 1
#11 D-B - Lane 2
#11 D-B - Lane 3
#11 D-B - Lane 4

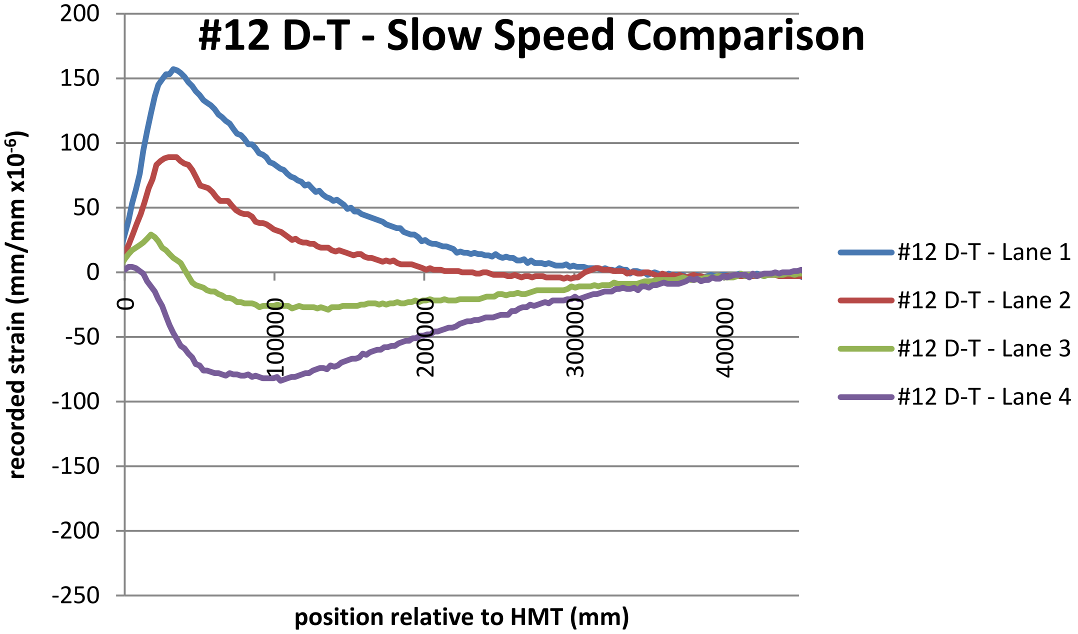
#12 D-T - Slow Speed Comparison
200
150
100
50
0
-50
-100
-150
-200
-250
recorded strain (mm/mm x10^{-6})
0
100000
200000
300000
400000
position relative to HMT (mm)
#12 D-T - Lane 1
#12 D-T - Lane 2
#12 D-T - Lane 3
#12 D-T - Lane 4

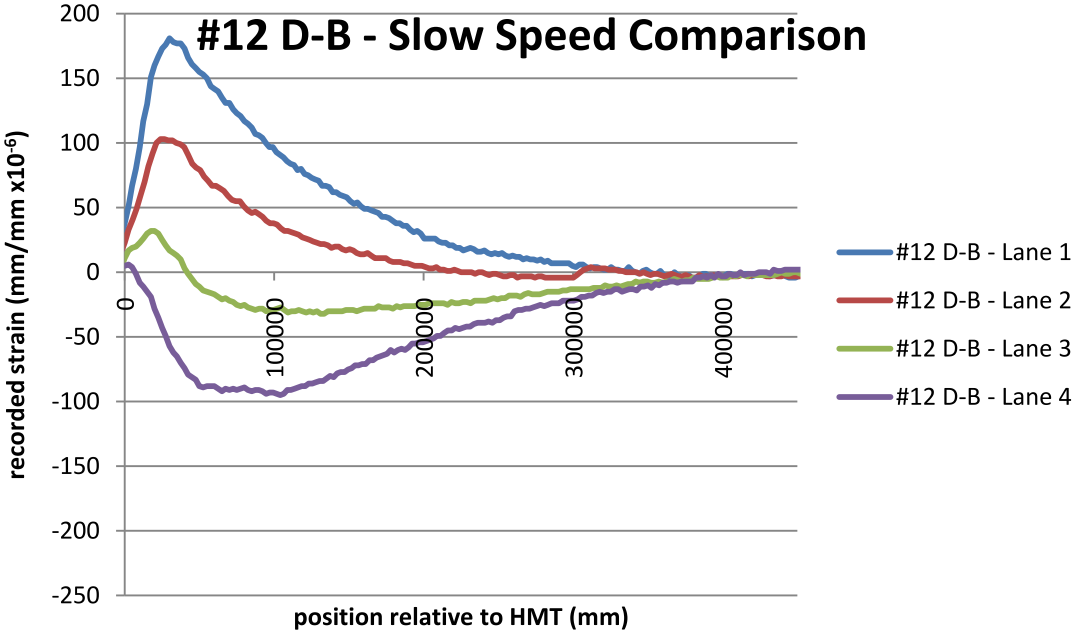
#12 D-B - Slow Speed Comparison
200
150
100
50
0
-50
-100
-150
-200
-250
recorded strain (mm/mm x10^{-6})
0
100000
200000
300000
400000
position relative to HMT (mm)
#12 D-B - Lane 1
#12 D-B - Lane 2
#12 D-B - Lane 3
#12 D-B - Lane 4

Appendix III – Gauge Comparison March 2010 – Numerical Model

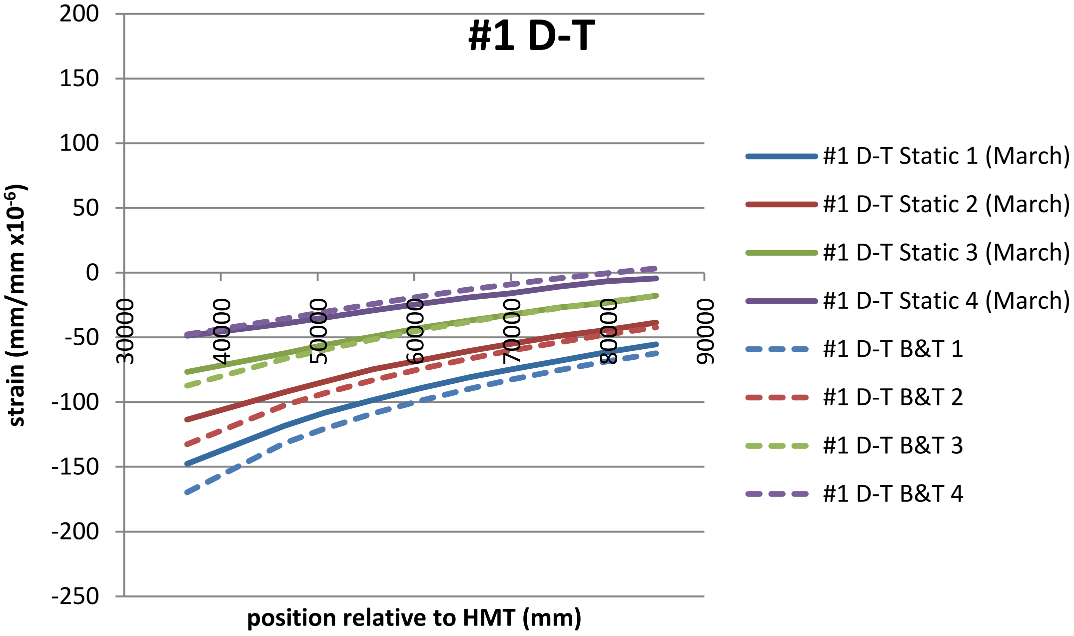

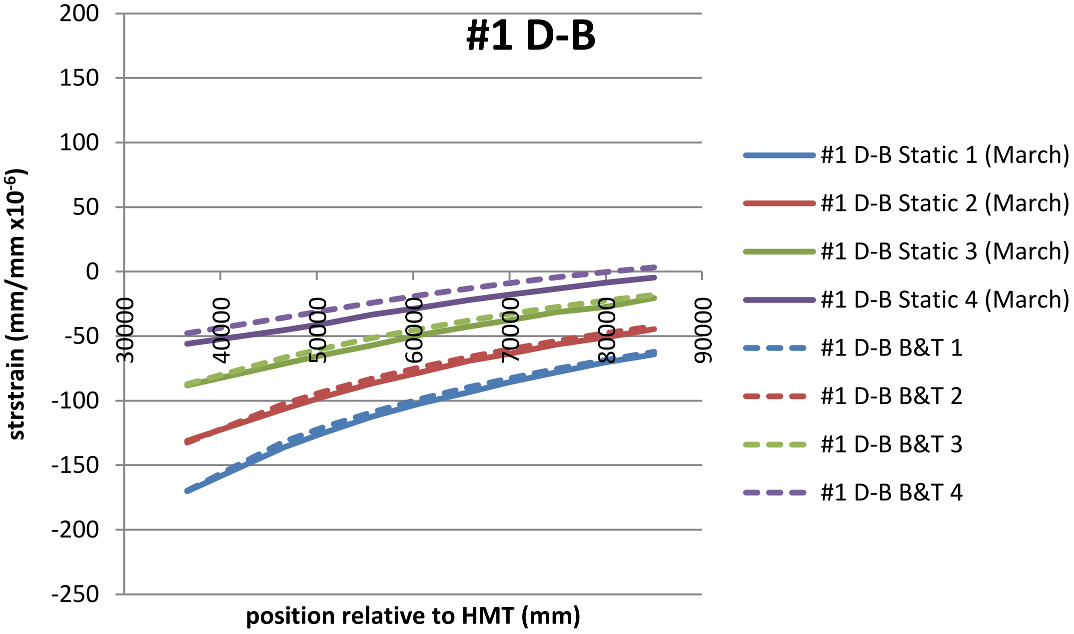

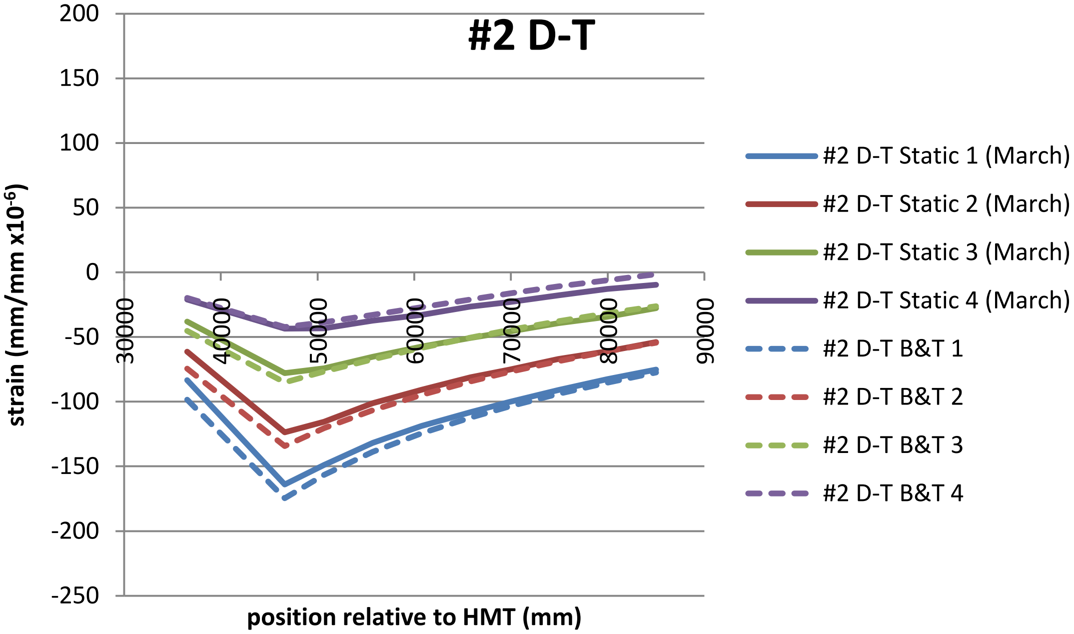
#2 D-T
strain (mm/mm x10^-6)
200
150
100
50
0
-50
-100
-150
-200
-250
30000
40000
50000
60000
70000
80000
90000
position relative to HMT (mm)
#2 D-T Static 1 (March)
#2 D-T Static 2 (March)
#2 D-T Static 3 (March)
#2 D-T Static 4 (March)
#2 D-T B&T 1
#2 D-T B&T 2
#2 D-T B&T 3
#2 D-T B&T 4

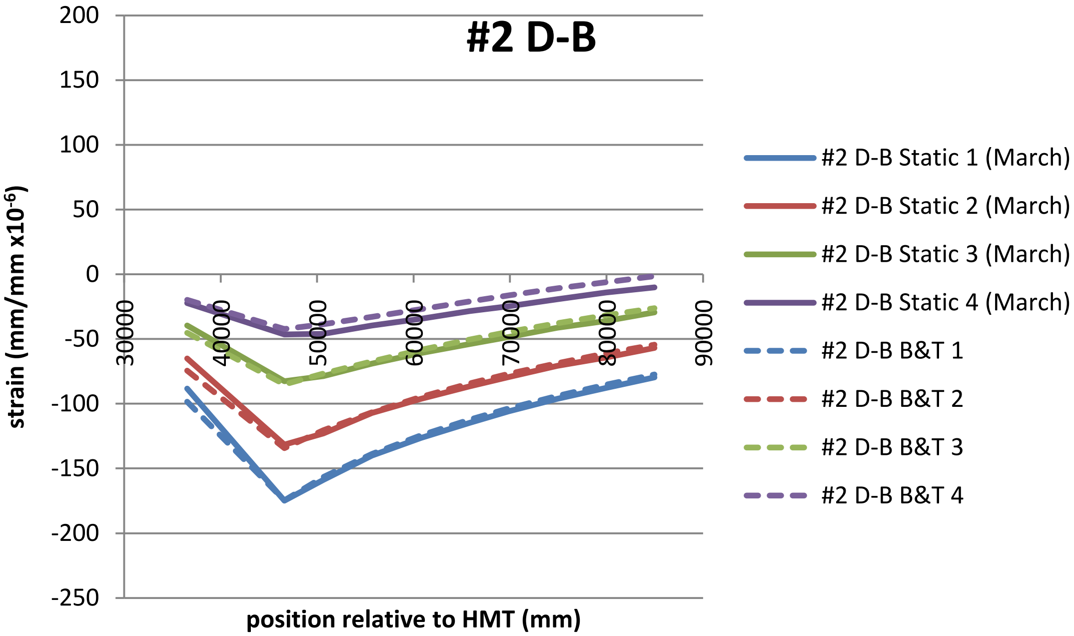
#2 D-B
strain (mm/mm x10^-6)
200
150
100
50
0
-50
-100
-150
-200
-250
30000
40000
50000
60000
70000
80000
90000
position relative to HMT (mm)
#2 D-B Static 1 (March)
#2 D-B Static 2 (March)
#2 D-B Static 3 (March)
#2 D-B Static 4 (March)
#2 D-B B&T 1
#2 D-B B&T 2
#2 D-B B&T 3
#2 D-B B&T 4

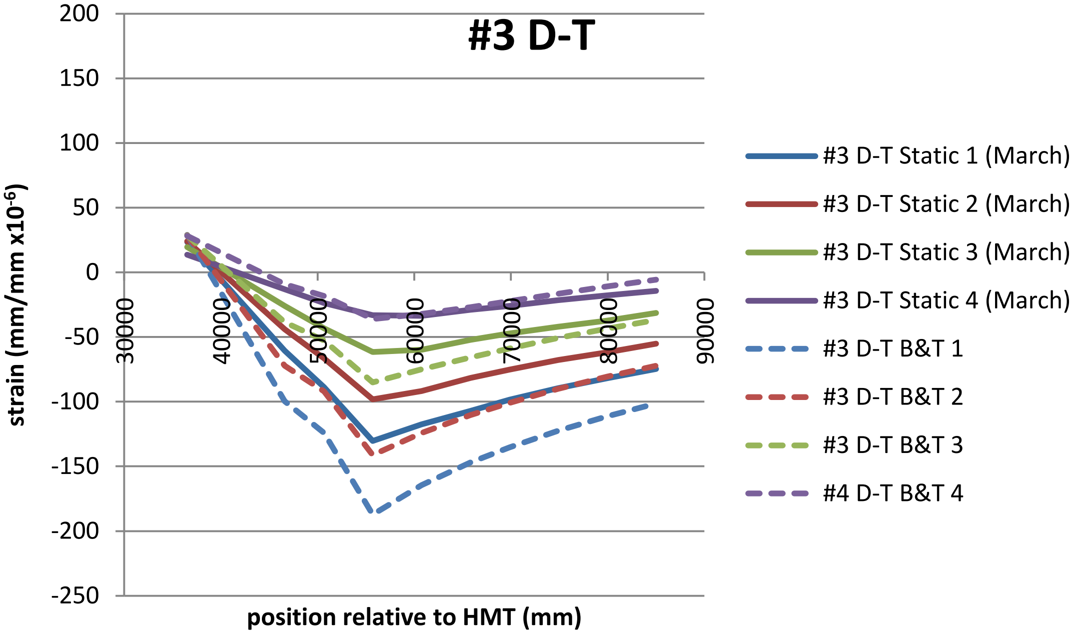
#3 D-T
200
150
100
50
0
-50
-100
-150
-200
-250
strain (mm/mm x10-6)
30000
40000
50000
60000
70000
80000
90000
position relative to HMT (mm)
#3 D-T Static 1 (March)
#3 D-T Static 2 (March)
#3 D-T Static 3 (March)
#3 D-T Static 4 (March)
#3 D-T B&T 1
#3 D-T B&T 2
#3 D-T B&T 3
#4 D-T B&T 4

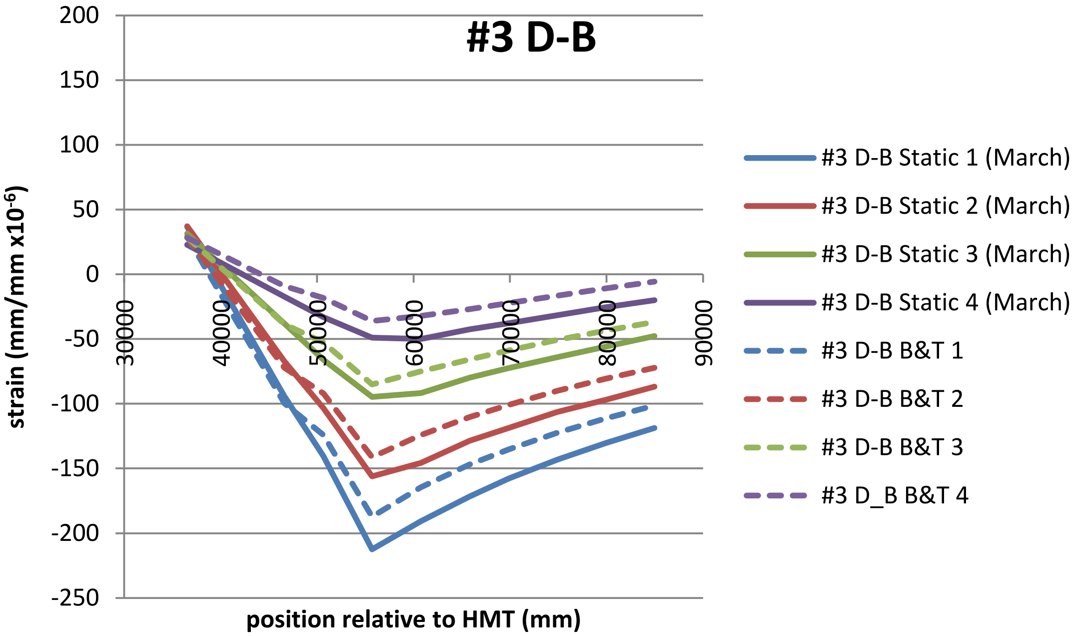
#3 D-B
200
150
100
50
0
-50
-100
-150
-200
-250
strain (mm/mm x10-6)
30000
40000
50000
60000
70000
80000
90000
position relative to HMT (mm)
#3 D-B Static 1 (March)
#3 D-B Static 2 (March)
#3 D-B Static 3 (March)
#3 D-B Static 4 (March)
#3 D-B B&T 1
#3 D-B B&T 2
#3 D-B B&T 3
#3 D_B B&T 4

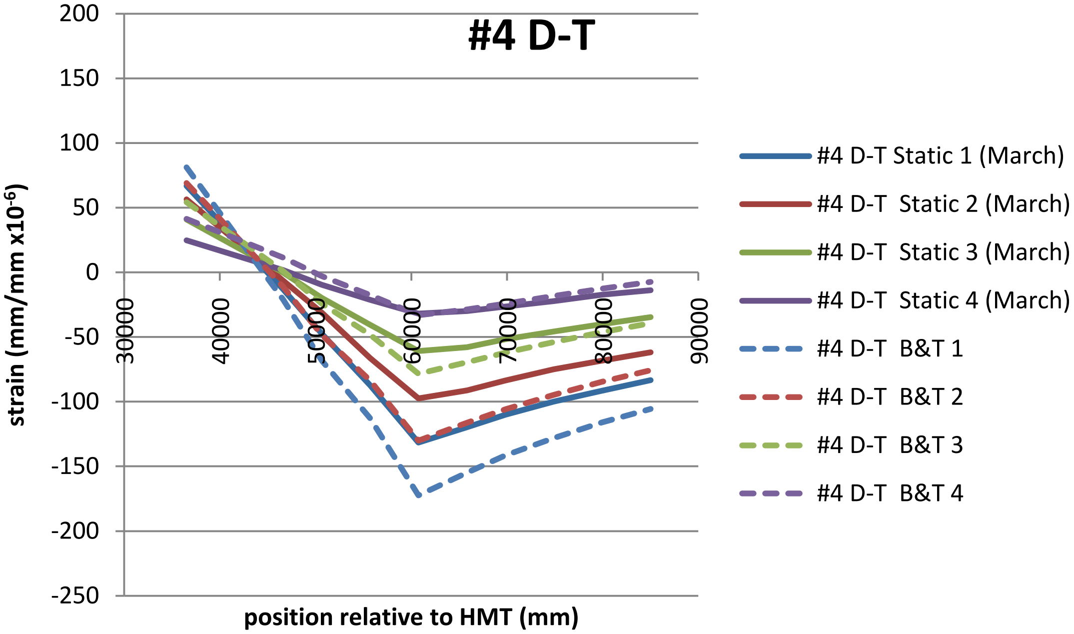
#4 D-T
strain (mm/mm x10^{-6})
200
150
100
50
0
-50
-100
-150
-200
-250
30000
40000
50000
60000
70000
80000
90000
position relative to HMT (mm)
#4 D-T Static 1 (March)
#4 D-T Static 2 (March)
#4 D-T Static 3 (March)
#4 D-T Static 4 (March)
#4 D-T B&T 1
#4 D-T B&T 2
#4 D-T B&T 3
#4 D-T B&T 4

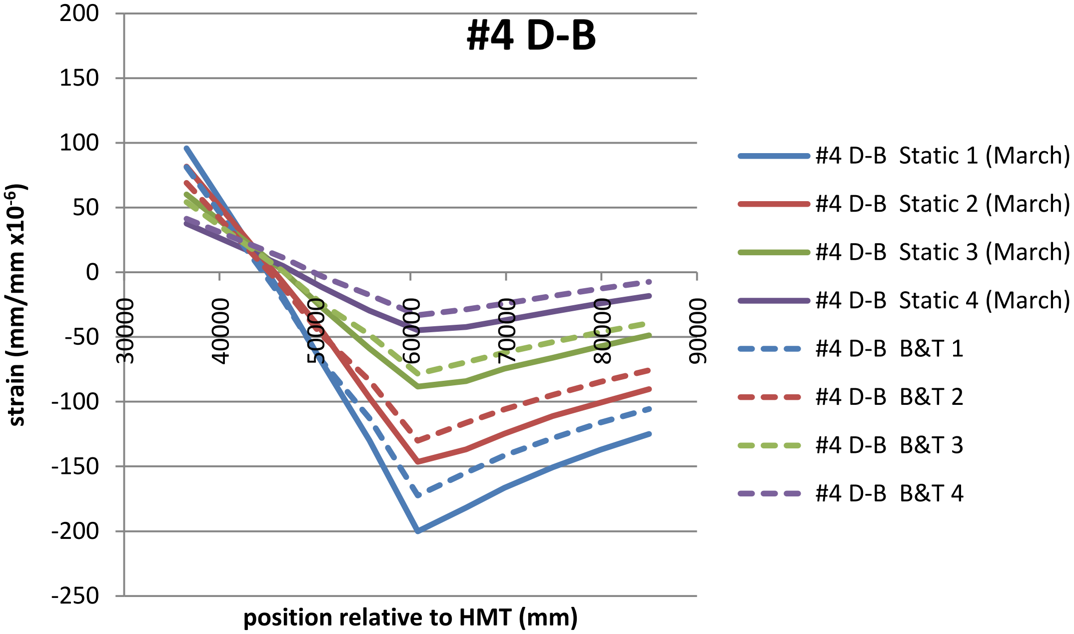
#4 D-B
strain (mm/mm x10^{-6})
200
150
100
50
0
-50
-100
-150
-200
-250
30000
40000
50000
60000
70000
80000
90000
position relative to HMT (mm)
#4 D-B Static 1 (March)
#4 D-B Static 2 (March)
#4 D-B Static 3 (March)
#4 D-B Static 4 (March)
#4 D-B B&T 1
#4 D-B B&T 2
#4 D-B B&T 3
#4 D-B B&T 4

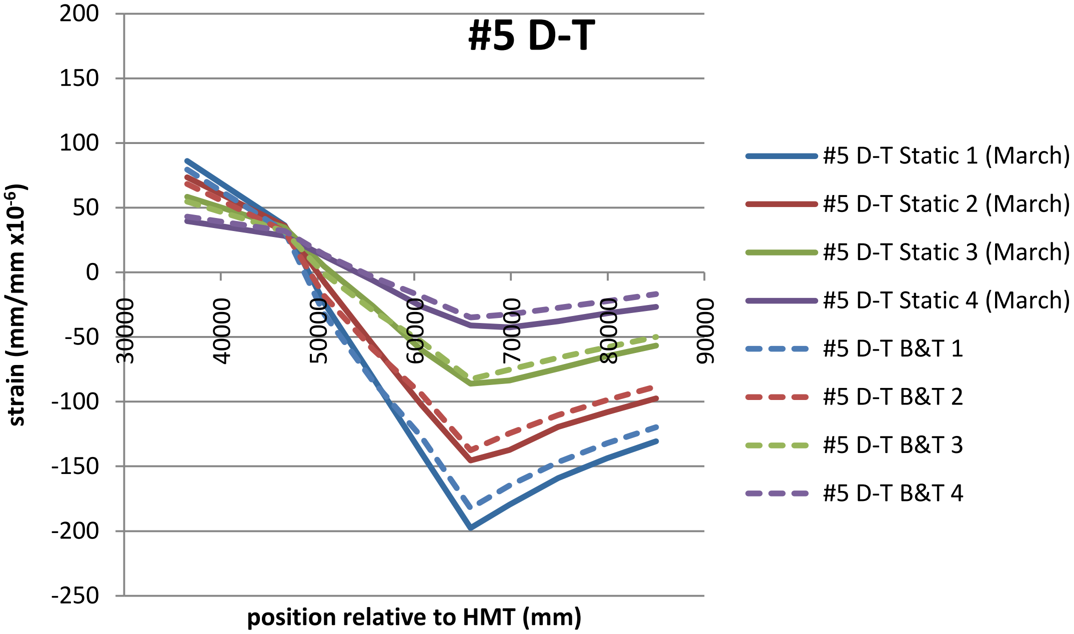
#5 D-T
strain (mm/mm x10-6)
200
150
100
50
0
-50
-100
-150
-200
-250
30000
40000
50000
60000
70000
80000
90000
position relative to HMT (mm)
#5 D-T Static 1 (March)
#5 D-T Static 2 (March)
#5 D-T Static 3 (March)
#5 D-T Static 4 (March)
#5 D-T B&T 1
#5 D-T B&T 2
#5 D-T B&T 3
#5 D-T B&T 4

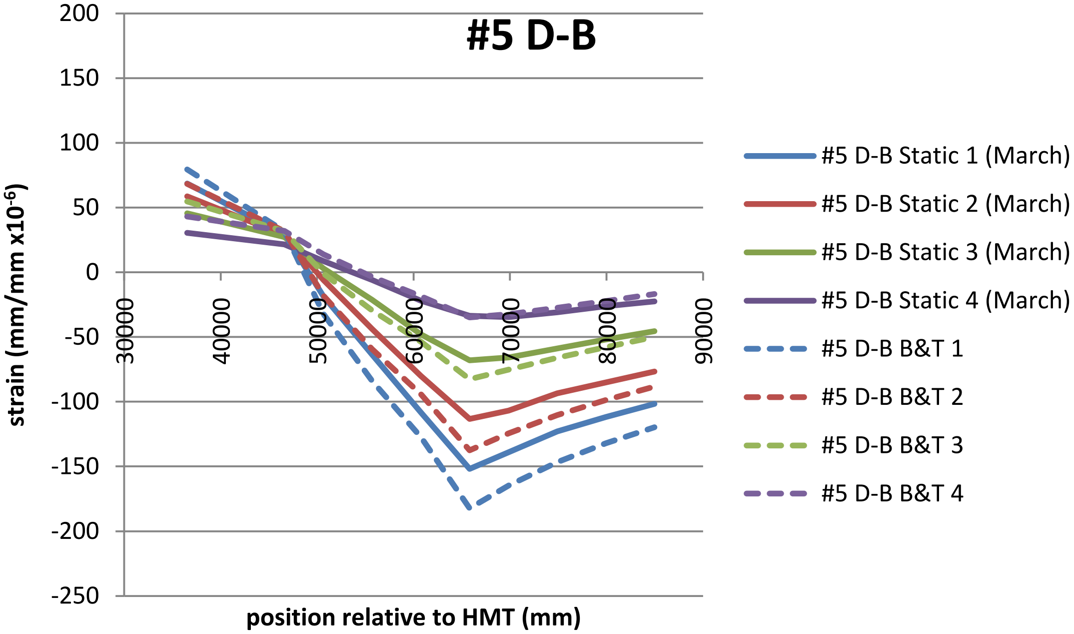
#5 D-B
strain (mm/mm x10-6)
200
150
100
50
0
-50
-100
-150
-200
-250
30000
40000
50000
60000
70000
80000
90000
position relative to HMT (mm)
#5 D-B Static 1 (March)
#5 D-B Static 2 (March)
#5 D-B Static 3 (March)
#5 D-B Static 4 (March)
#5 D-B B&T 1
#5 D-B B&T 2
#5 D-B B&T 3
#5 D-B B&T 4

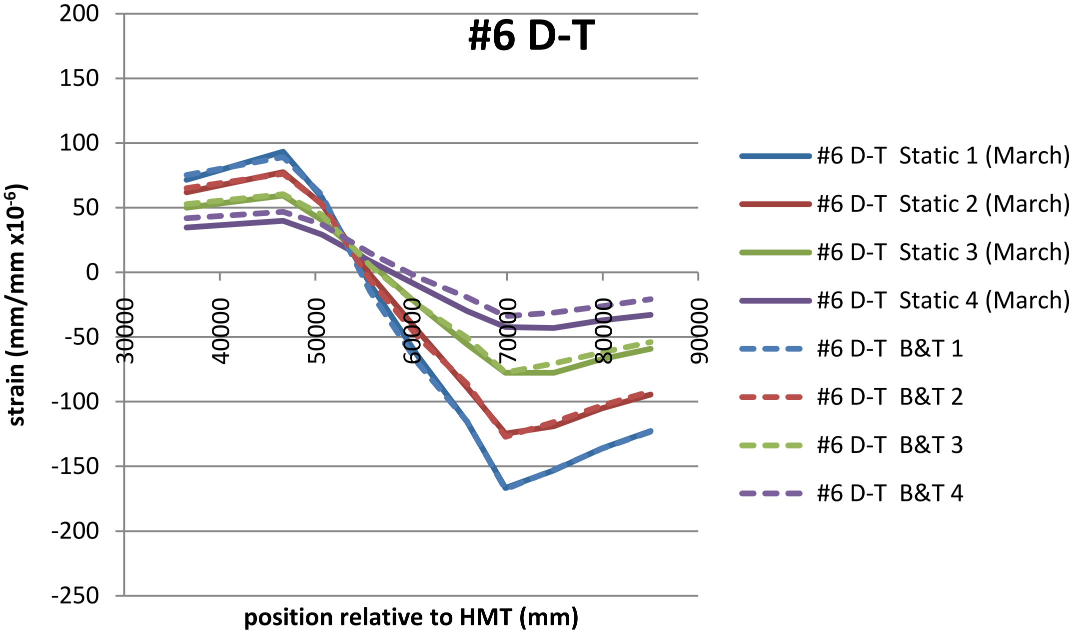
#6 D-T
strain (mm/mm x10⁻⁶)
200
150
100
50
0
-50
-100
-150
-200
-250
30000
40000
50000
60000
70000
80000
90000
position relative to HMT (mm)
#6 D-T Static 1 (March)
#6 D-T Static 2 (March)
#6 D-T Static 3 (March)
#6 D-T Static 4 (March)
#6 D-T B&T 1
#6 D-T B&T 2
#6 D-T B&T 3
#6 D-T B&T 4

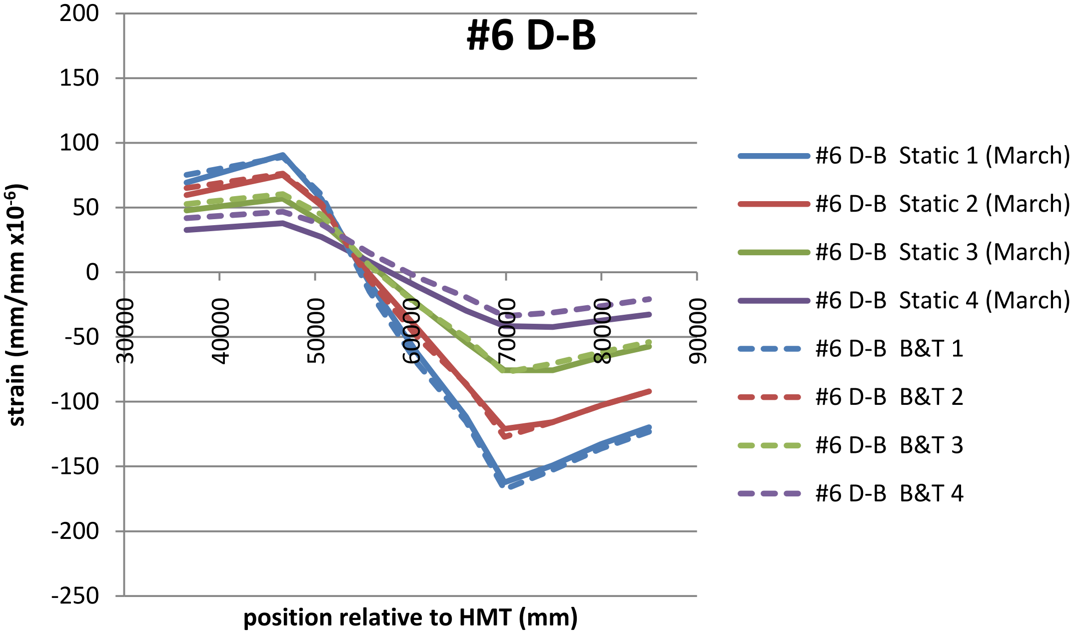
#6 D-B
strain (mm/mm x10⁻⁶)
200
150
100
50
0
-50
-100
-150
-200
-250
30000
40000
50000
60000
70000
80000
90000
position relative to HMT (mm)
#6 D-B Static 1 (March)
#6 D-B Static 2 (March)
#6 D-B Static 3 (March)
#6 D-B Static 4 (March)
#6 D-B B&T 1
#6 D-B B&T 2
#6 D-B B&T 3
#6 D-B B&T 4

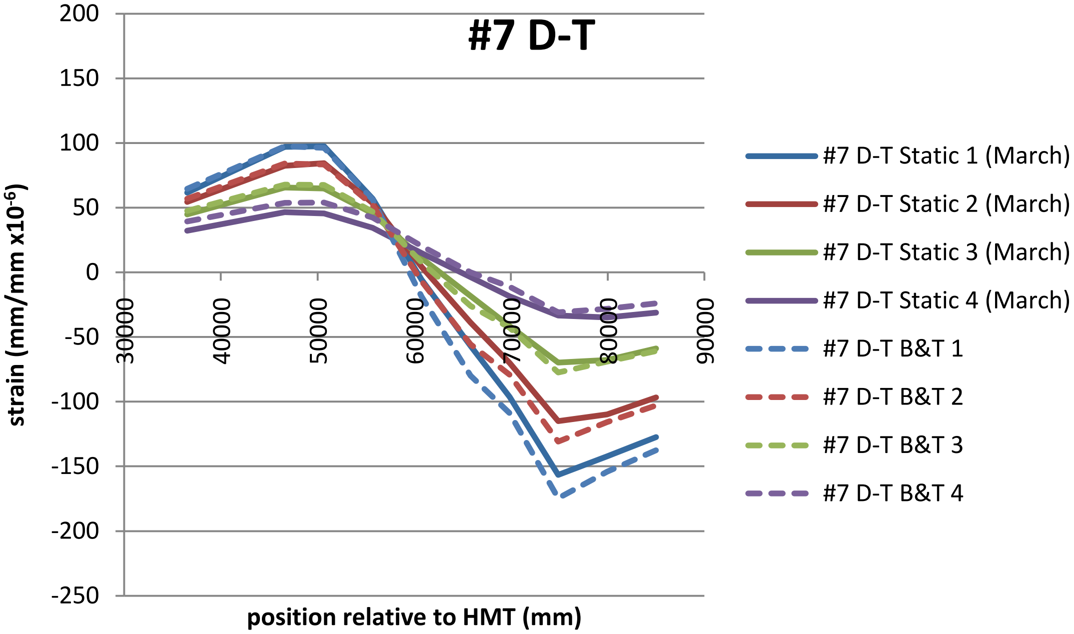
#7 D-T
strain (mm/mm x10^-6)
200
150
100
50
0
-50
-100
-150
-200
-250
30000
40000
50000
60000
70000
80000
90000
position relative to HMT (mm)
#7 D-T Static 1 (March)
#7 D-T Static 2 (March)
#7 D-T Static 3 (March)
#7 D-T Static 4 (March)
#7 D-T B&T 1
#7 D-T B&T 2
#7 D-T B&T 3
#7 D-T B&T 4

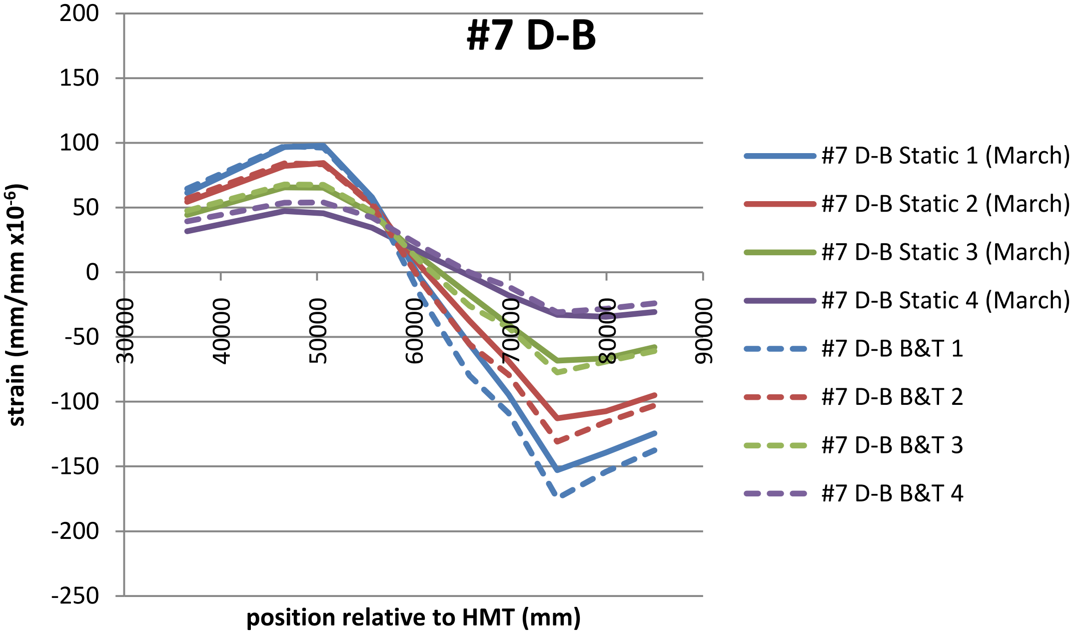
#7 D-B
strain (mm/mm x10^-6)
200
150
100
50
0
-50
-100
-150
-200
-250
30000
40000
50000
60000
70000
80000
90000
position relative to HMT (mm)
#7 D-B Static 1 (March)
#7 D-B Static 2 (March)
#7 D-B Static 3 (March)
#7 D-B Static 4 (March)
#7 D-B B&T 1
#7 D-B B&T 2
#7 D-B B&T 3
#7 D-B B&T 4

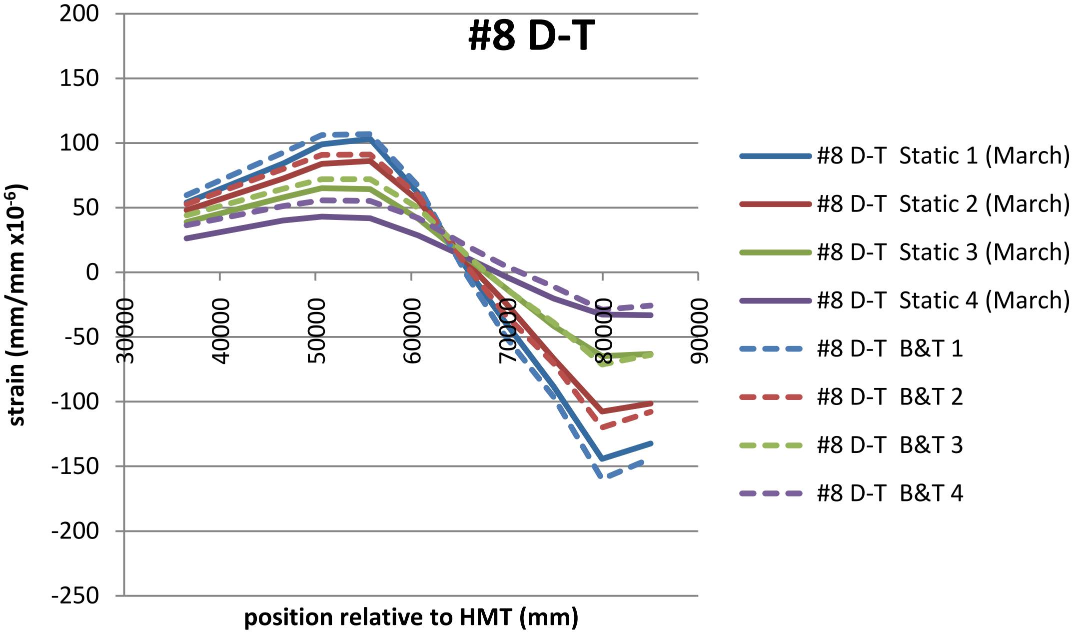
#8 D-T
200
150
100
50
0
-50
-100
-150
-200
-250
strain (mm/mm x10-6)
30000
40000
50000
60000
70000
80000
90000
position relative to HMT (mm)
#8 D-T Static 1 (March)
#8 D-T Static 2 (March)
#8 D-T Static 3 (March)
#8 D-T Static 4 (March)
#8 D-T B&T 1
#8 D-T B&T 2
#8 D-T B&T 3
#8 D-T B&T 4

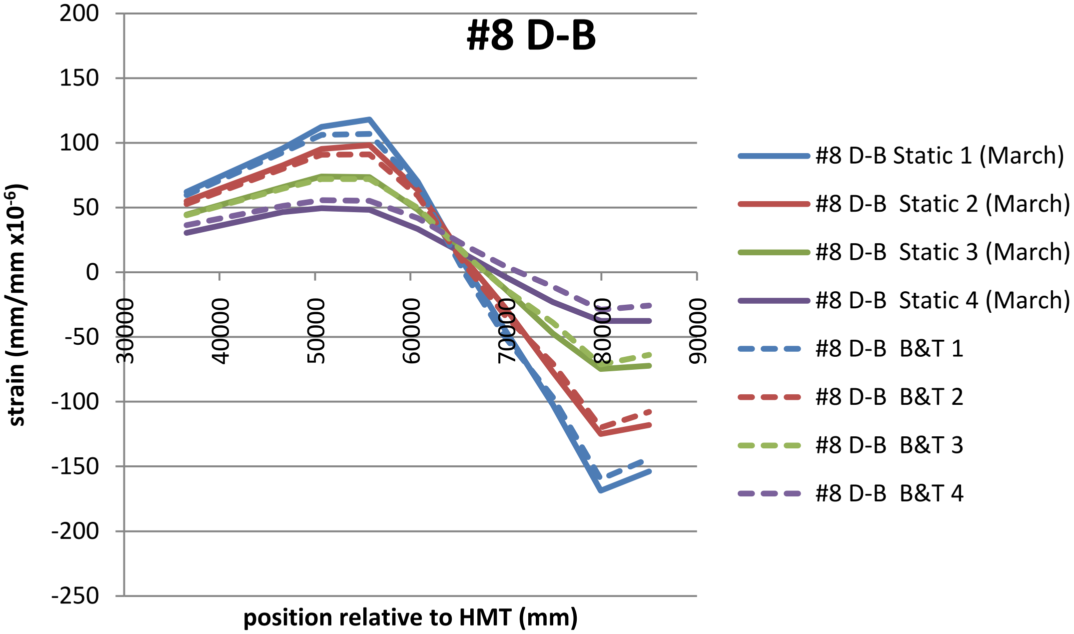
#8 D-B
200
150
100
50
0
-50
-100
-150
-200
-250
strain (mm/mm x10-6)
30000
40000
50000
60000
70000
80000
90000
position relative to HMT (mm)
#8 D-B Static 1 (March)
#8 D-B Static 2 (March)
#8 D-B Static 3 (March)
#8 D-B Static 4 (March)
#8 D-B B&T 1
#8 D-B B&T 2
#8 D-B B&T 3
#8 D-B B&T 4

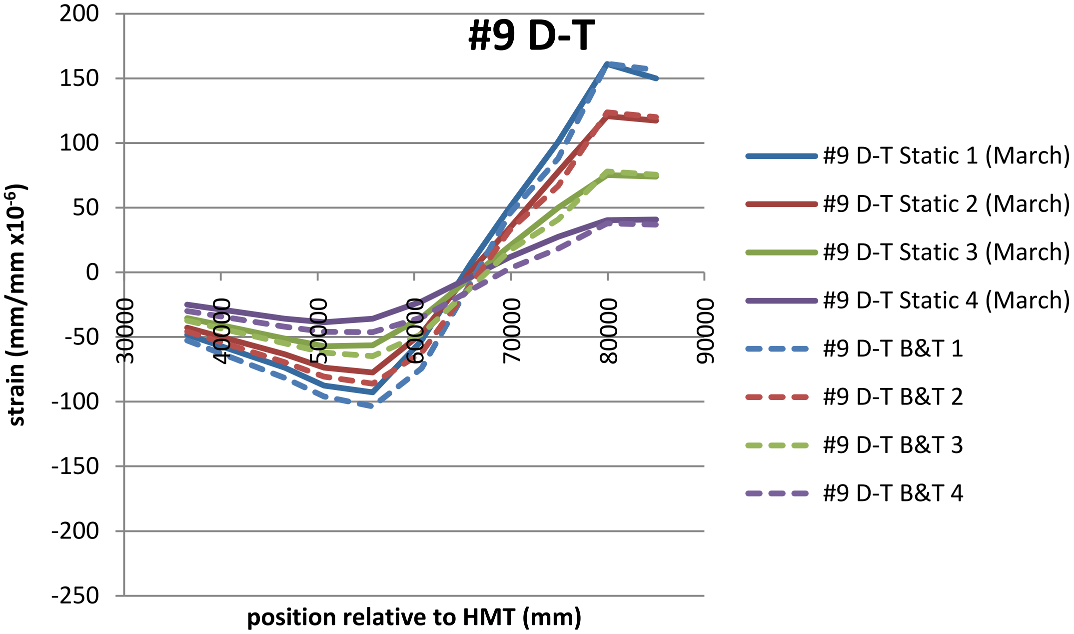
#9 D-T
strain (mm/mm x10^{-6})
200
150
100
50
0
-50
-100
-150
-200
-250
30000
40000
50000
60000
70000
80000
90000
position relative to HMT (mm)
#9 D-T Static 1 (March)
#9 D-T Static 2 (March)
#9 D-T Static 3 (March)
#9 D-T Static 4 (March)
#9 D-T B&T 1
#9 D-T B&T 2
#9 D-T B&T 3
#9 D-T B&T 4

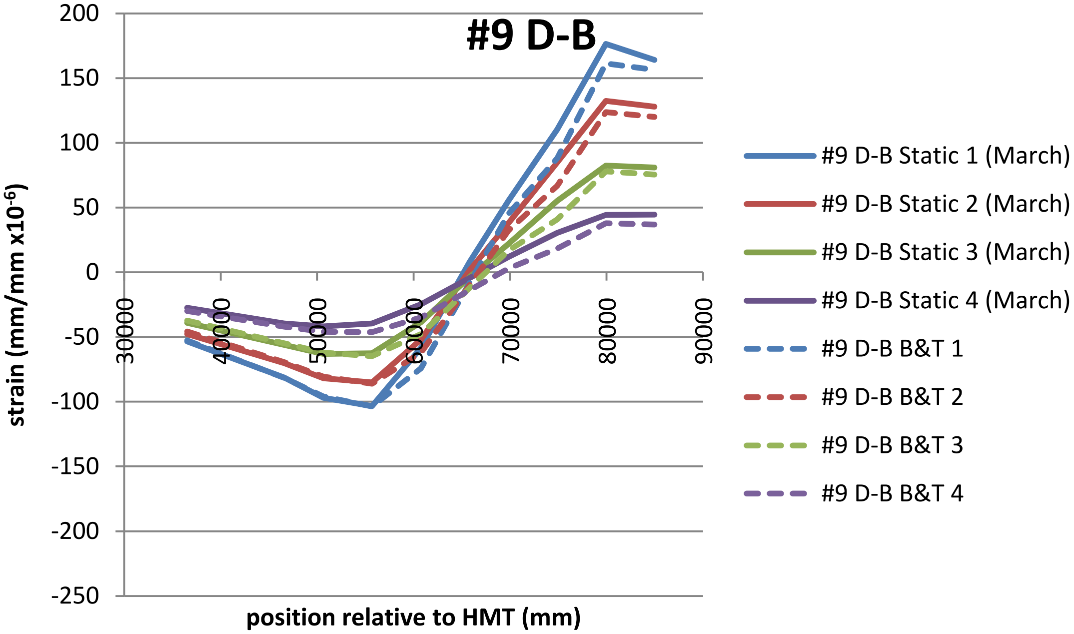
#9 D-B
strain (mm/mm x10^{-6})
200
150
100
50
0
-50
-100
-150
-200
-250
30000
40000
50000
60000
70000
80000
90000
position relative to HMT (mm)
#9 D-B Static 1 (March)
#9 D-B Static 2 (March)
#9 D-B Static 3 (March)
#9 D-B Static 4 (March)
#9 D-B B&T 1
#9 D-B B&T 2
#9 D-B B&T 3
#9 D-B B&T 4

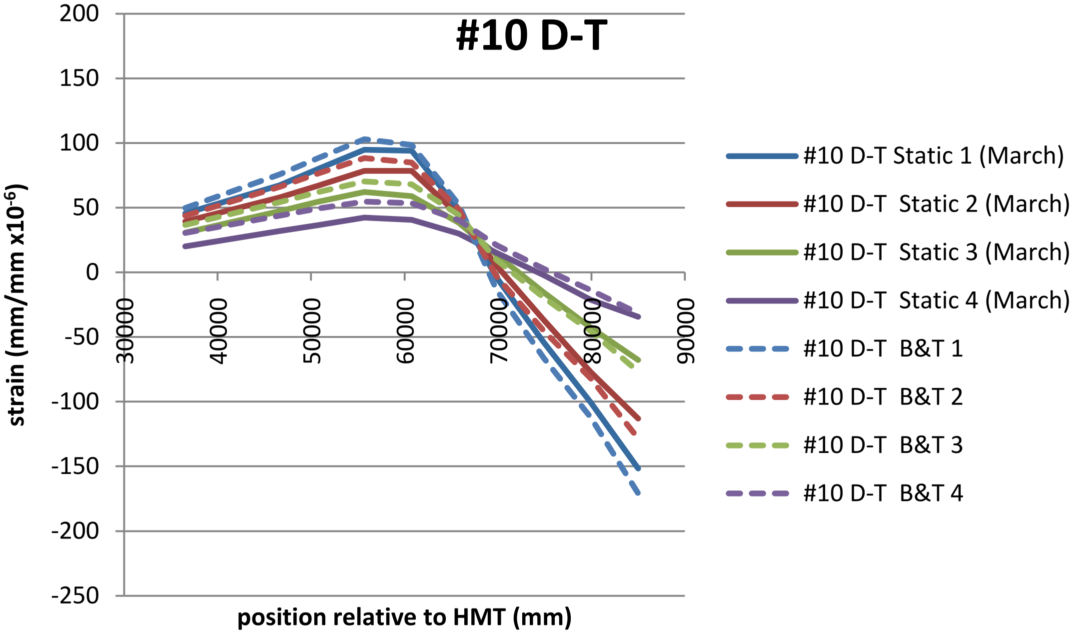
#10 D-T
strain (mm/mm x10^{-6})
200
150
100
50
0
-50
-100
-150
-200
-250
30000
40000
50000
60000
70000
80000
90000
position relative to HMT (mm)
#10 D-T Static 1 (March)
#10 D-T Static 2 (March)
#10 D-T Static 3 (March)
#10 D-T Static 4 (March)
#10 D-T B&T 1
#10 D-T B&T 2
#10 D-T B&T 3
#10 D-T B&T 4

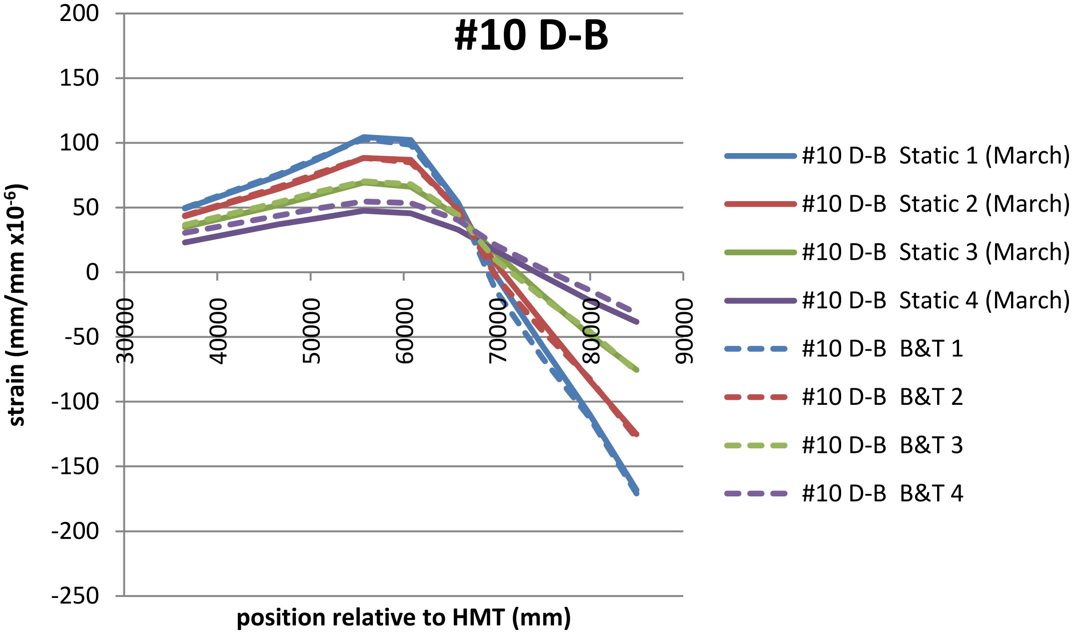
#10 D-B
strain (mm/mm x10^{-6})
200
150
100
50
0
-50
-100
-150
-200
-250
30000
40000
50000
60000
70000
80000
90000
position relative to HMT (mm)
#10 D-B Static 1 (March)
#10 D-B Static 2 (March)
#10 D-B Static 3 (March)
#10 D-B Static 4 (March)
#10 D-B B&T 1
#10 D-B B&T 2
#10 D-B B&T 3
#10 D-B B&T 4

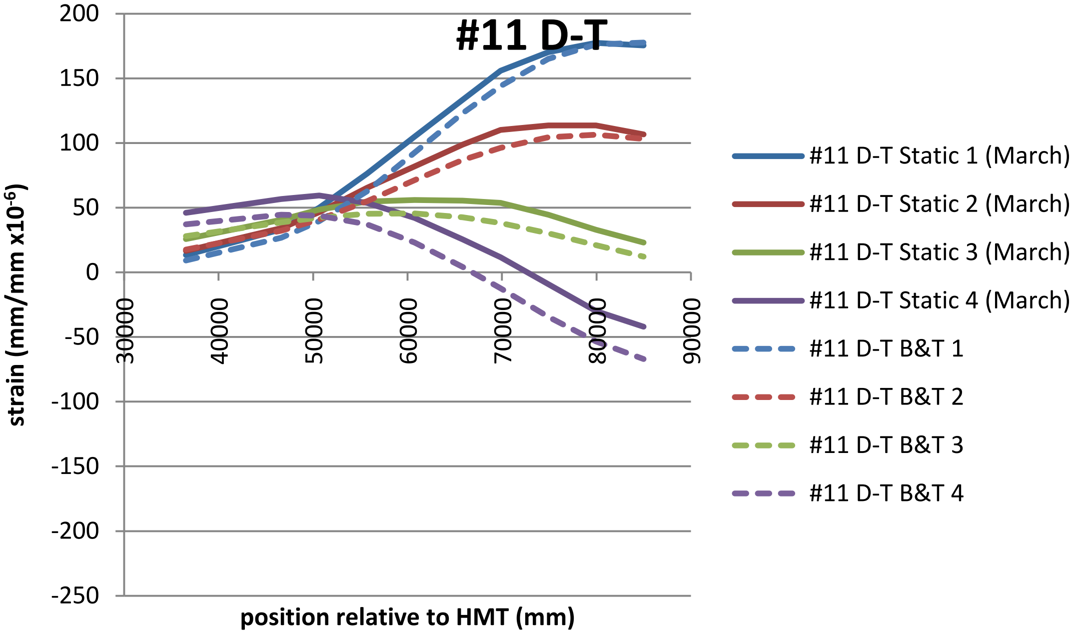
#11 D-T
strain (mm/mm x10^{-6})
200
150
100
50
0
-50
-100
-150
-200
-250
30000
40000
50000
60000
70000
80000
90000
position relative to HMT (mm)
#11 D-T Static 1 (March)
#11 D-T Static 2 (March)
#11 D-T Static 3 (March)
#11 D-T Static 4 (March)
#11 D-T B&T 1
#11 D-T B&T 2
#11 D-T B&T 3
#11 D-T B&T 4

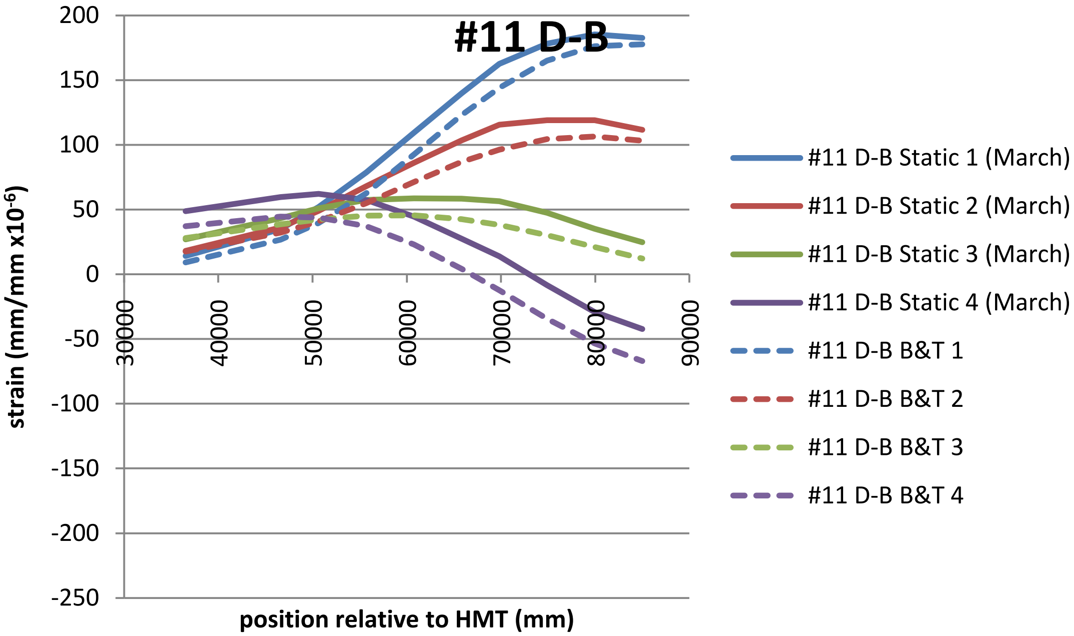
#11 D-B
strain (mm/mm x10^{-6})
200
150
100
50
0
-50
-100
-150
-200
-250
30000
40000
50000
60000
70000
80000
90000
position relative to HMT (mm)
#11 D-B Static 1 (March)
#11 D-B Static 2 (March)
#11 D-B Static 3 (March)
#11 D-B Static 4 (March)
#11 D-B B&T 1
#11 D-B B&T 2
#11 D-B B&T 3
#11 D-B B&T 4

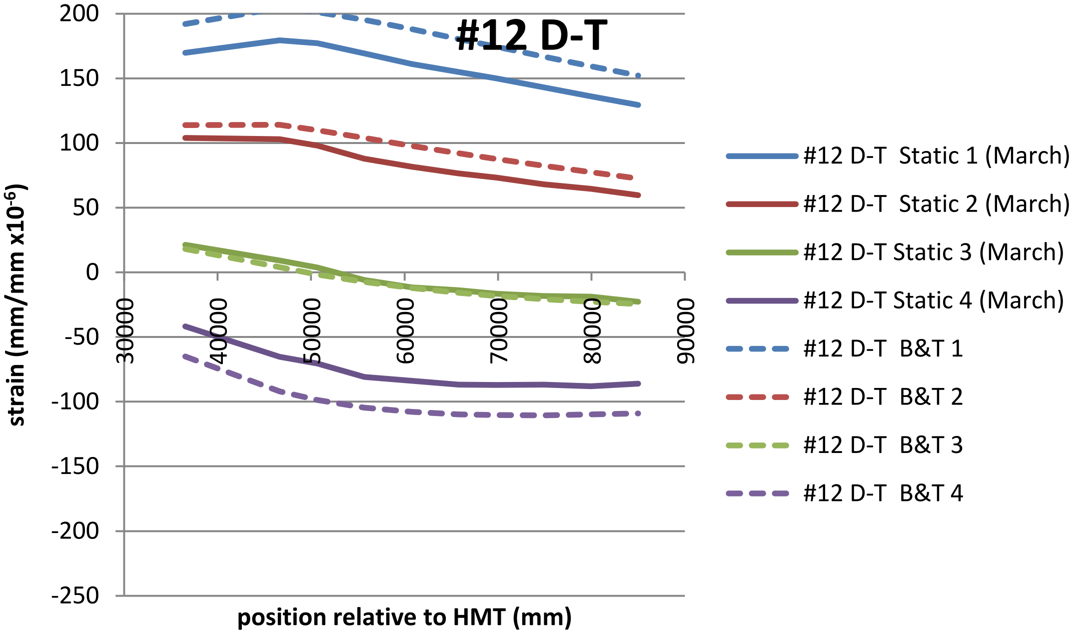
#12 D-T
strain (mm/mm x10^{-6})
200
150
100
50
0
-50
-100
-150
-200
-250
30000
40000
50000
60000
70000
80000
90000
position relative to HMT (mm)
#12 D-T Static 1 (March)
#12 D-T Static 2 (March)
#12 D-T Static 3 (March)
#12 D-T Static 4 (March)
#12 D-T B&T 1
#12 D-T B&T 2
#12 D-T B&T 3
#12 D-T B&T 4

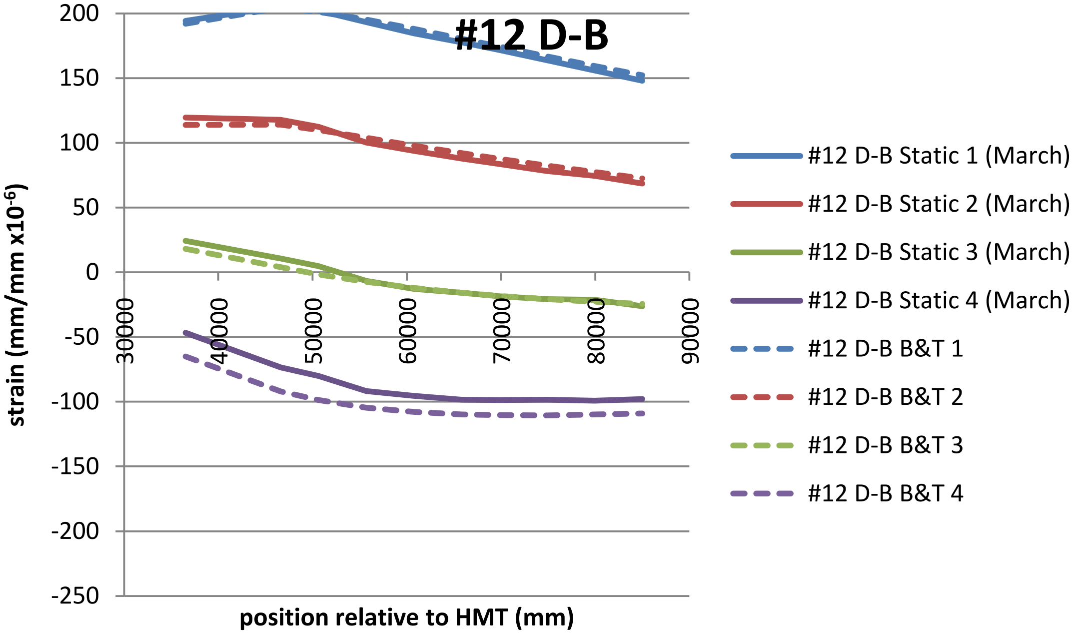
#12 D-B
strain (mm/mm x10^{-6})
200
150
100
50
0
-50
-100
-150
-200
-250
30000
40000
50000
60000
70000
80000
90000
position relative to HMT (mm)
#12 D-B Static 1 (March)
#12 D-B Static 2 (March)
#12 D-B Static 3 (March)
#12 D-B Static 4 (March)
#12 D-B B&T 1
#12 D-B B&T 2
#12 D-B B&T 3
#12 D-B B&T 4

Appendix IV – Long-Term Data Histograms

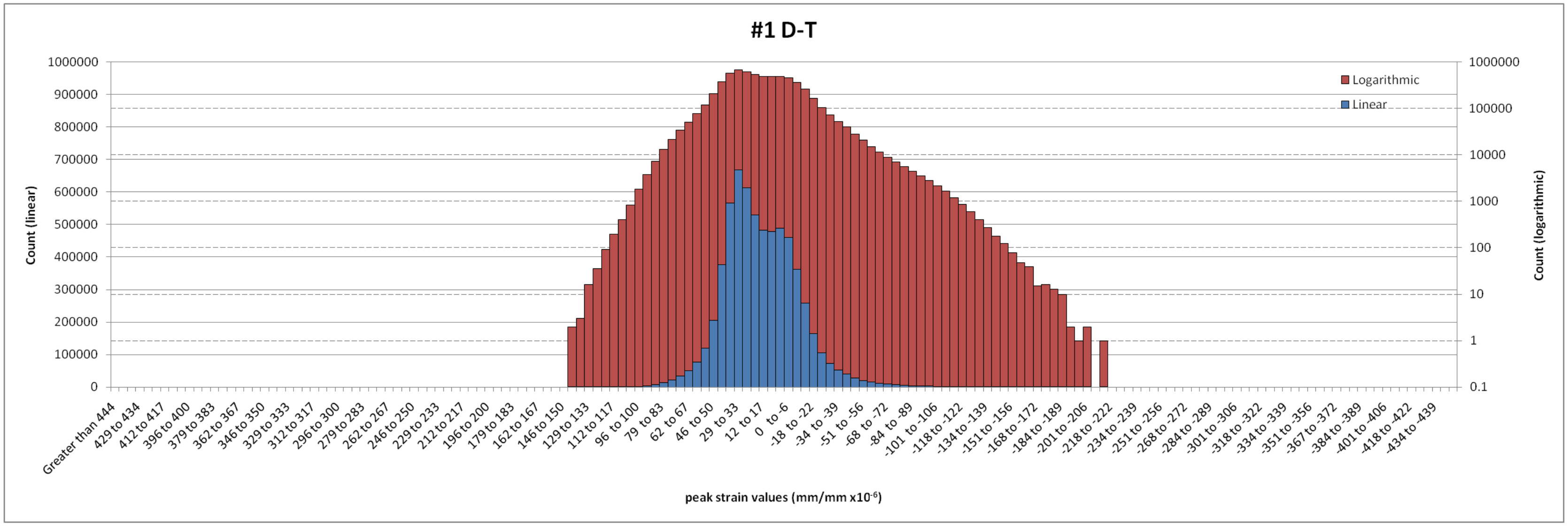
#1 D-T
Logarithmic
Linear
Count (linear)
1000000
900000
800000
700000
600000
500000
400000
300000
200000
100000
0
Count (logarithmic)
1000000
100000
10000
1000
100
10
1
0.1
Greater than 444
429 to 434
412 to 417
396 to 400
379 to 383
362 to 367
346 to 350
329 to 333
312 to 317
296 to 300
279 to 283
262 to 267
246 to 250
229 to 233
212 to 217
196 to 200
179 to 183
162 to 167
146 to 150
129 to 133
112 to 117
96 to 100
79 to 83
62 to 67
46 to 50
29 to 33
12 to 17
0 to -6
-18 to -22
-34 to -39
-51 to -56
-68 to -72
-84 to -89
-101 to -106
-118 to -122
-134 to -139
-151 to -156
-168 to -172
-184 to -189
-201 to -206
-218 to -222
-234 to -239
-251 to -256
-268 to -272
-284 to -289
-301 to -306
-318 to -322
-334 to -339
-351 to -356
-367 to -372
-384 to -389
-401 to -406
-418 to -422
-434 to -439
peak strain values (mm/mm x10⁻⁶)

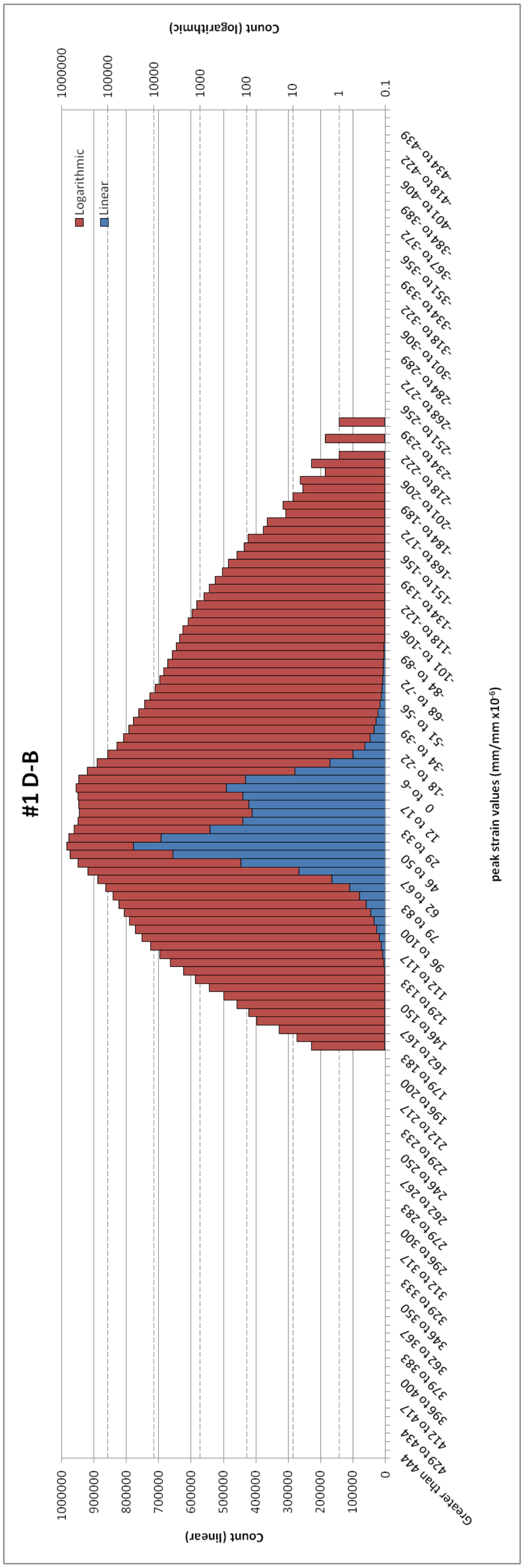
#1 D-B
Logarithmic
Linear
Count (logarithmic)
1000000
100000
10000
1000
100
10
1
0.1
Count (linear)
1000000
900000
800000
700000
600000
500000
400000
300000
200000
100000
0
peak strain values (mm/mm x10⁻⁶)
-434 to -439
-418 to -422
-401 to -406
-384 to -389
-367 to -372
-351 to -356
-334 to -339
-318 to -322
-301 to -306
-284 to -289
-268 to -272
-251 to -256
-234 to -239
-218 to -222
-201 to -206
-184 to -189
-168 to -172
-151 to -156
-134 to -139
-118 to -122
-101 to -106
-84 to -89
-68 to -72
-51 to -56
-34 to -39
-18 to -22
to -6
0
12 to 17
29 to 33
46 to 50
62 to 67
79 to 83
96 to 100
112 to 117
129 to 133
146 to 150
162 to 167
179 to 183
196 to 200
212 to 217
229 to 233
246 to 250
262 to 267
279 to 283
296 to 300
312 to 317
329 to 333
346 to 350
362 to 367
379 to 383
396 to 400
412 to 417
429 to 434
Greater than 444

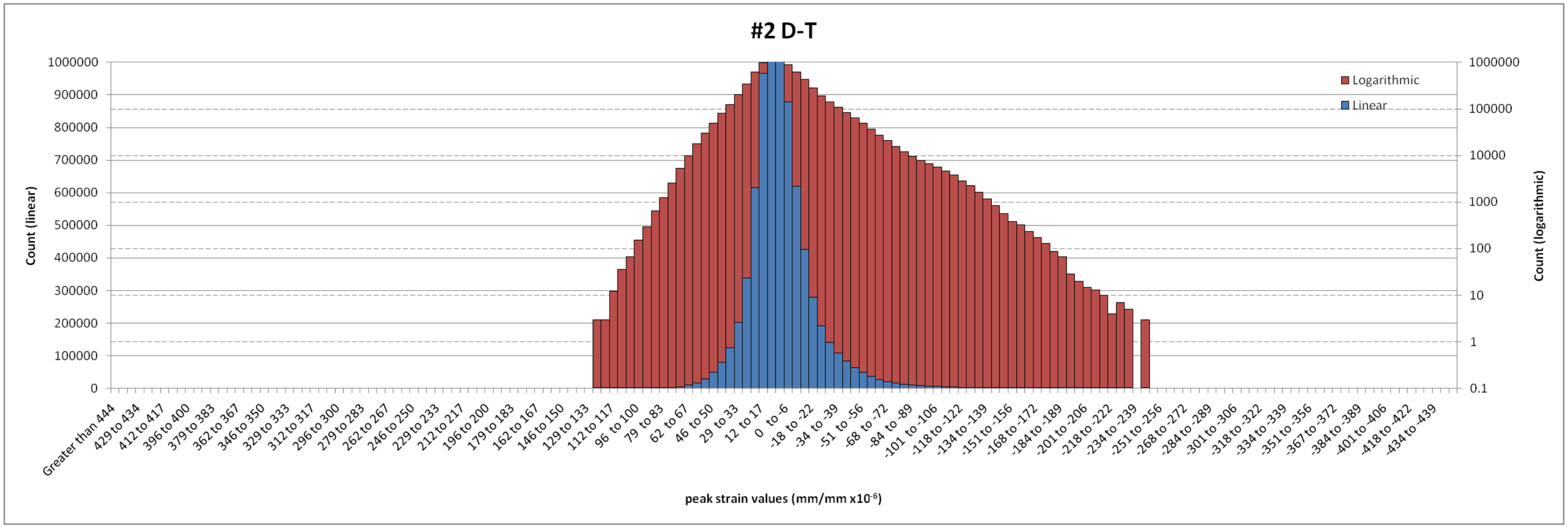
#2 D-T
Count (linear)
1000000
900000
800000
700000
600000
500000
400000
300000
200000
100000
0
Count (logarithmic)
1000000
100000
10000
1000
100
10
1
0.1
Logarithmic
Linear
Greater than 444
429 to 434
412 to 417
396 to 400
379 to 383
362 to 367
346 to 350
329 to 333
312 to 317
296 to 300
279 to 283
262 to 267
246 to 250
229 to 233
212 to 217
196 to 200
179 to 183
162 to 167
146 to 150
129 to 133
112 to 117
96 to 100
79 to 83
62 to 67
46 to 50
29 to 33
12 to 17
0 to -6
-18 to -22
-34 to -39
-51 to -56
-68 to -72
-84 to -89
-101 to -106
-118 to -122
-134 to -139
-151 to -156
-168 to -172
-184 to -189
-201 to -206
-218 to -222
-234 to -239
-251 to -256
-268 to -272
-284 to -289
-301 to -306
-318 to -322
-334 to -339
-351 to -356
-367 to -372
-384 to -389
-401 to -406
-418 to -422
-434 to -439
peak strain values (mm/mm x10⁻⁶)

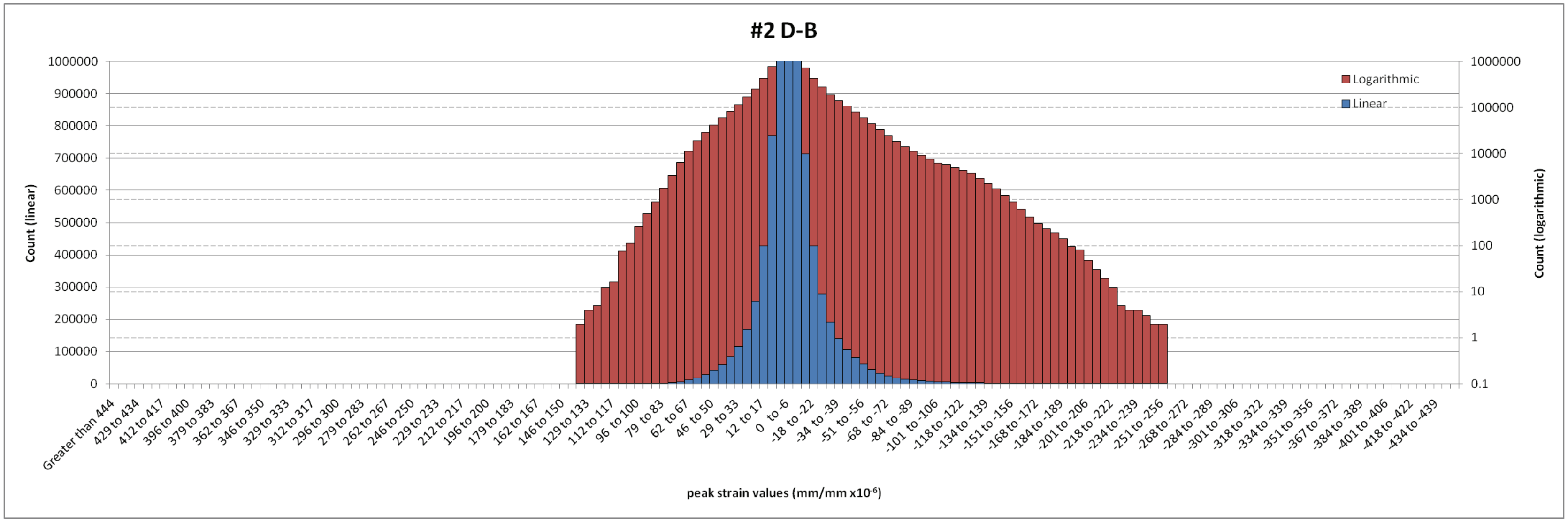
#2 D-B
Count (linear)
1000000
900000
800000
700000
600000
500000
400000
300000
200000
100000
0
Count (logarithmic)
1000000
100000
10000
1000
100
10
1
0.1
Logarithmic
Linear
Greater than 444
429 to 434
412 to 417
396 to 400
379 to 383
362 to 367
346 to 350
329 to 333
312 to 317
296 to 300
279 to 283
262 to 267
246 to 250
229 to 233
212 to 217
196 to 200
179 to 183
162 to 167
146 to 150
129 to 133
112 to 117
96 to 100
79 to 83
62 to 67
46 to 50
29 to 33
12 to 17
0 to -6
-18 to -22
-34 to -39
-51 to -56
-68 to -72
-84 to -89
-101 to -106
-118 to -122
-134 to -139
-151 to -156
-168 to -172
-184 to -189
-201 to -206
-218 to -222
-234 to -239
-251 to -256
-268 to -272
-284 to -289
-301 to -306
-318 to -322
-334 to -339
-351 to -356
-367 to -372
-384 to -389
-401 to -406
-418 to -422
-434 to -439
peak strain values (mm/mm x10^{-6})

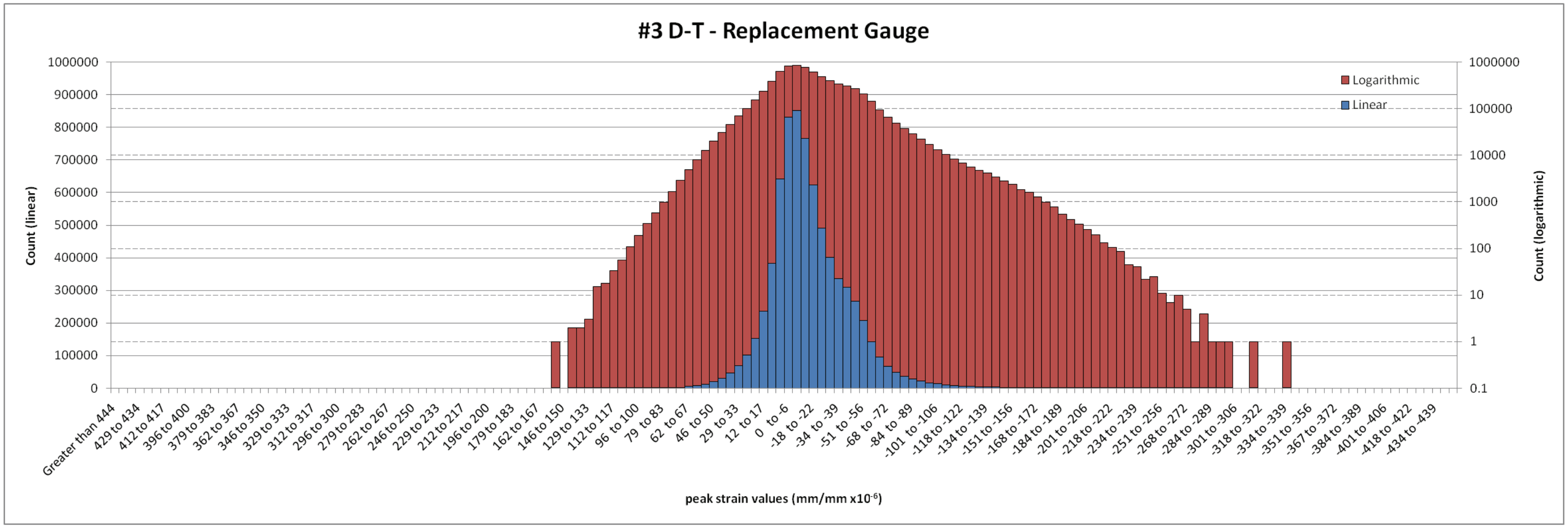
#3 D-T - Replacement Gauge
Count (linear)
1000000
900000
800000
700000
600000
500000
400000
300000
200000
100000
0
Count (logarithmic)
1000000
100000
10000
1000
100
10
1
0.1
Logarithmic
Linear
Greater than 444
429 to 434
412 to 417
396 to 400
379 to 383
362 to 367
346 to 350
329 to 333
312 to 317
296 to 300
279 to 283
262 to 267
246 to 250
229 to 233
212 to 217
196 to 200
179 to 183
162 to 167
146 to 150
129 to 133
112 to 117
96 to 100
79 to 83
62 to 67
46 to 50
29 to 33
12 to 17
0 to -6
-18 to -22
-34 to -39
-51 to -56
-68 to -72
-84 to -89
-101 to -106
-118 to -122
-134 to -139
-151 to -156
-168 to -172
-184 to -189
-201 to -206
-218 to -222
-234 to -239
-251 to -256
-268 to -272
-284 to -289
-301 to -306
-318 to -322
-334 to -339
-351 to -356
-367 to -372
-384 to -389
-401 to -406
-418 to -422
-434 to -439
peak strain values (mm/mm x10-6)

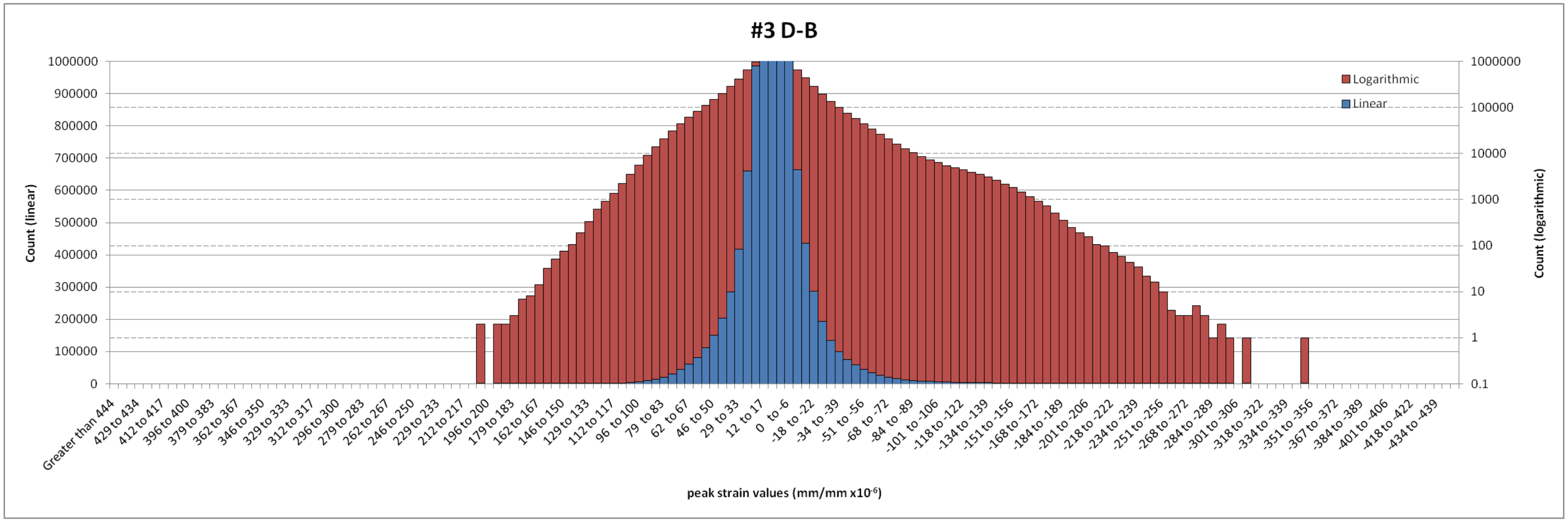
#3 D-B
Logarithmic
Linear
Count (linear)
1000000
900000
800000
700000
600000
500000
400000
300000
200000
100000
0
Count (logarithmic)
1000000
100000
10000
1000
100
10
1
0.1
peak strain values (mm/mm x10^{-6})
Greater than 444
429 to 434
412 to 417
396 to 400
379 to 383
362 to 367
346 to 350
329 to 333
312 to 317
296 to 300
279 to 283
262 to 267
246 to 250
229 to 233
212 to 217
196 to 200
179 to 183
162 to 167
146 to 150
129 to 133
112 to 117
96 to 100
79 to 83
62 to 67
46 to 50
29 to 33
12 to 17
0 to -6
-18 to -22
-34 to -39
-51 to -56
-68 to -72
-84 to -89
-101 to -106
-118 to -122
-134 to -139
-151 to -156
-168 to -172
-184 to -189
-201 to -206
-218 to -222
-234 to -239
-251 to -256
-268 to -272
-284 to -289
-301 to -306
-318 to -322
-334 to -339
-351 to -356
-367 to -372
-384 to -389
-401 to -406
-418 to -422
-434 to -439

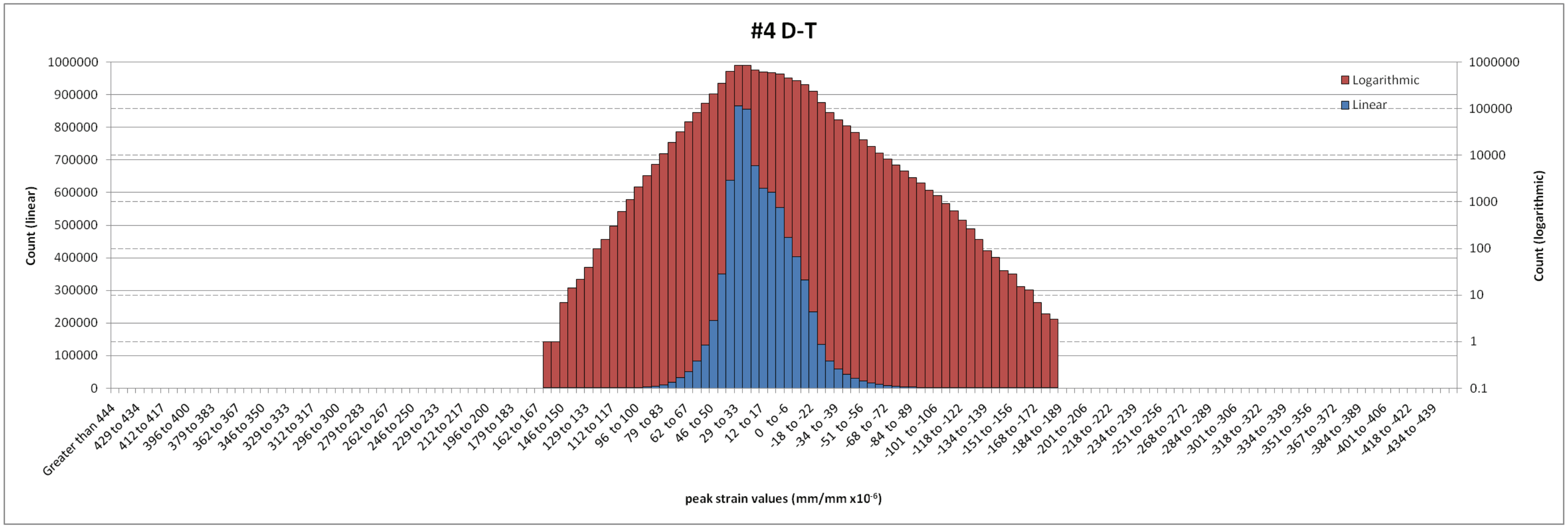
#4 D-T
Count (linear)
1000000
900000
800000
700000
600000
500000
400000
300000
200000
100000
0
Count (logarithmic)
1000000
100000
10000
1000
100
10
1
0.1
Logarithmic
Linear
Greater than 444
429 to 434
412 to 417
396 to 400
379 to 383
362 to 367
346 to 350
329 to 333
312 to 317
296 to 300
279 to 283
262 to 267
246 to 250
229 to 233
212 to 217
196 to 200
179 to 183
162 to 167
146 to 150
129 to 133
112 to 117
96 to 100
79 to 83
62 to 67
46 to 50
29 to 33
12 to 17
0 to -6
-18 to -22
-34 to -39
-51 to -56
-68 to -72
-84 to -89
-101 to -106
-118 to -122
-134 to -139
-151 to -156
-168 to -172
-184 to -189
-201 to -206
-218 to -222
-234 to -239
-251 to -256
-268 to -272
-284 to -289
-301 to -306
-318 to -322
-334 to -339
-351 to -356
-367 to -372
-384 to -389
-401 to -406
-418 to -422
-434 to -439
peak strain values (mm/mm x10⁻⁶)

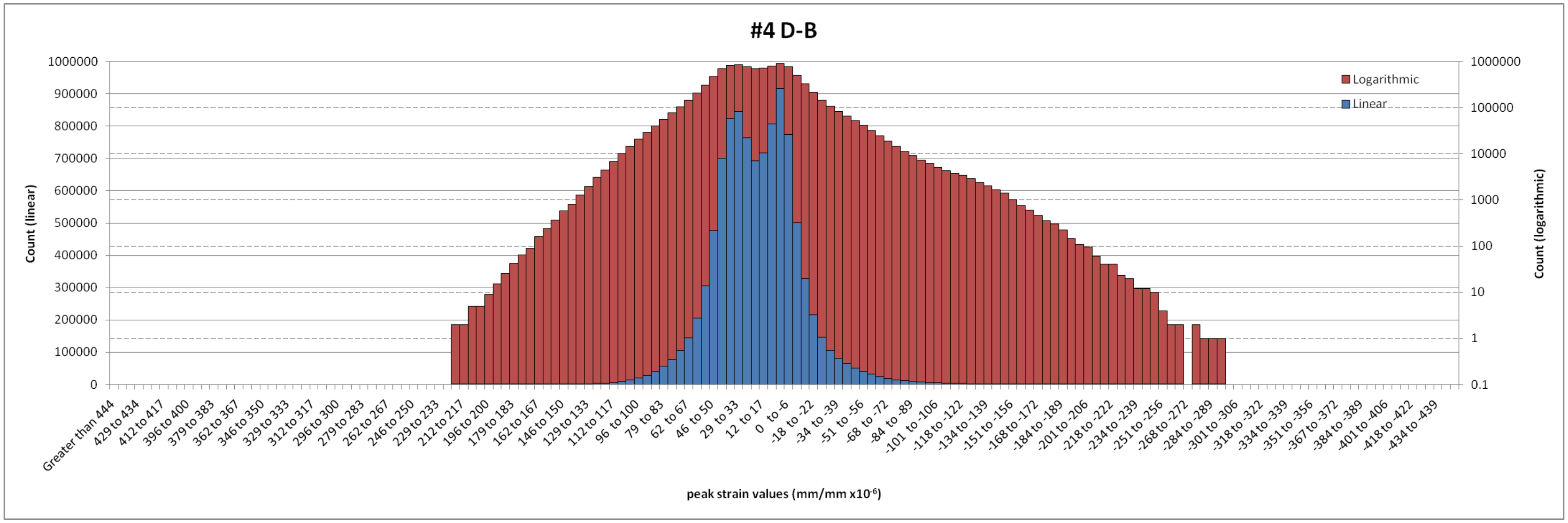
#4 D-B
Logarithmic
Linear
Count (linear)
1000000
900000
800000
700000
600000
500000
400000
300000
200000
100000
0
Count (logarithmic)
1000000
100000
10000
1000
100
10
1
0.1
Greater than 444
429 to 434
412 to 417
396 to 400
379 to 383
362 to 367
346 to 350
329 to 333
312 to 317
296 to 300
279 to 283
262 to 267
246 to 250
229 to 233
212 to 217
196 to 200
179 to 183
162 to 167
146 to 150
129 to 133
112 to 117
96 to 100
79 to 83
62 to 67
46 to 50
29 to 33
12 to 17
0 to -6
-18 to -22
-34 to -39
-51 to -56
-68 to -72
-84 to -89
-101 to -106
-118 to -122
-134 to -139
-151 to -156
-168 to -172
-184 to -189
-201 to -206
-218 to -222
-234 to -239
-251 to -256
-268 to -272
-284 to -289
-301 to -306
-318 to -322
-334 to -339
-351 to -356
-367 to -372
-384 to -389
-401 to -406
-418 to -422
-434 to -439
peak strain values (mm/mm x10^{-6})

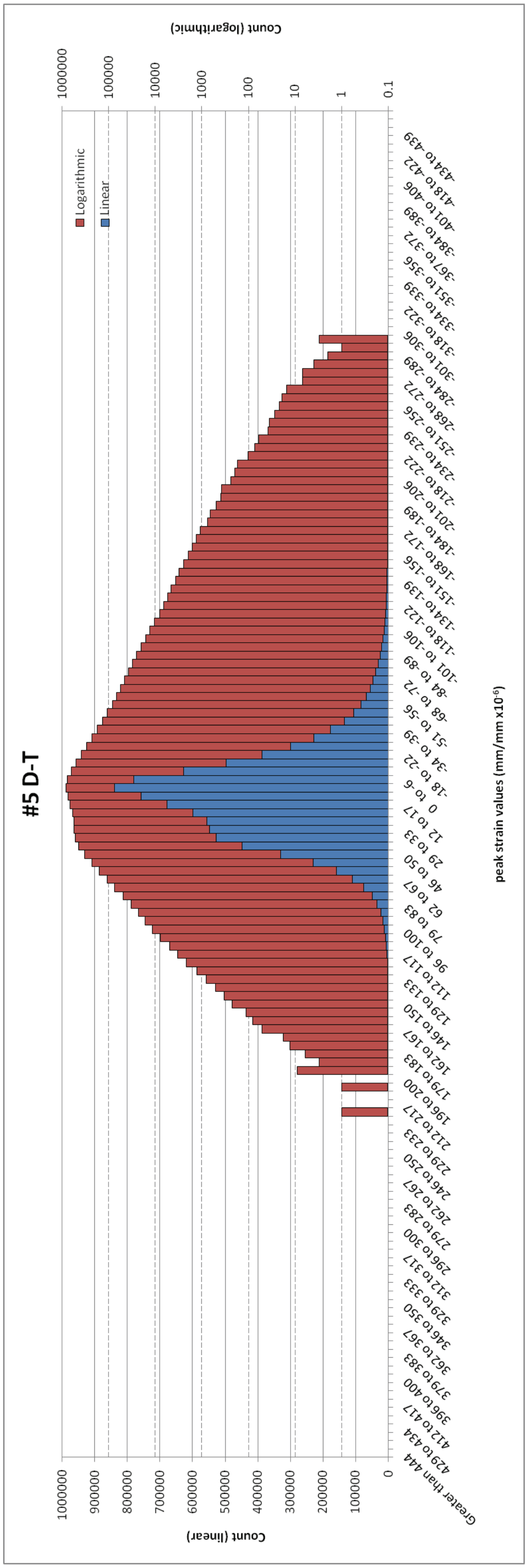
#5 D-T
Count (logarithmic)
Count (linear)
peak strain values (mm/mm x10-6)
Logarithmic
Linear
1000000
100000
10000
1000
100
10
1
0.1
1000000
900000
800000
700000
600000
500000
400000
300000
200000
100000
0
Greater than 444
429 to 434
412 to 417
396 to 400
379 to 383
362 to 367
346 to 350
329 to 333
312 to 317
296 to 300
279 to 283
262 to 267
246 to 250
229 to 233
212 to 217
196 to 200
179 to 183
162 to 167
146 to 150
129 to 133
112 to 117
96 to 100
79 to 83
62 to 67
46 to 50
29 to 33
12 to 17
0 to -6
-18 to -22
-34 to -39
-51 to -56
-68 to -72
-84 to -89
-101 to -106
-118 to -122
-134 to -139
-151 to -156
-168 to -172
-184 to -189
-201 to -206
-218 to -222
-234 to -239
-251 to -256
-268 to -272
-284 to -289
-301 to -306
-318 to -322
-334 to -339
-351 to -356
-367 to -372
-384 to -389
-401 to -406
-418 to -422
-434 to -439

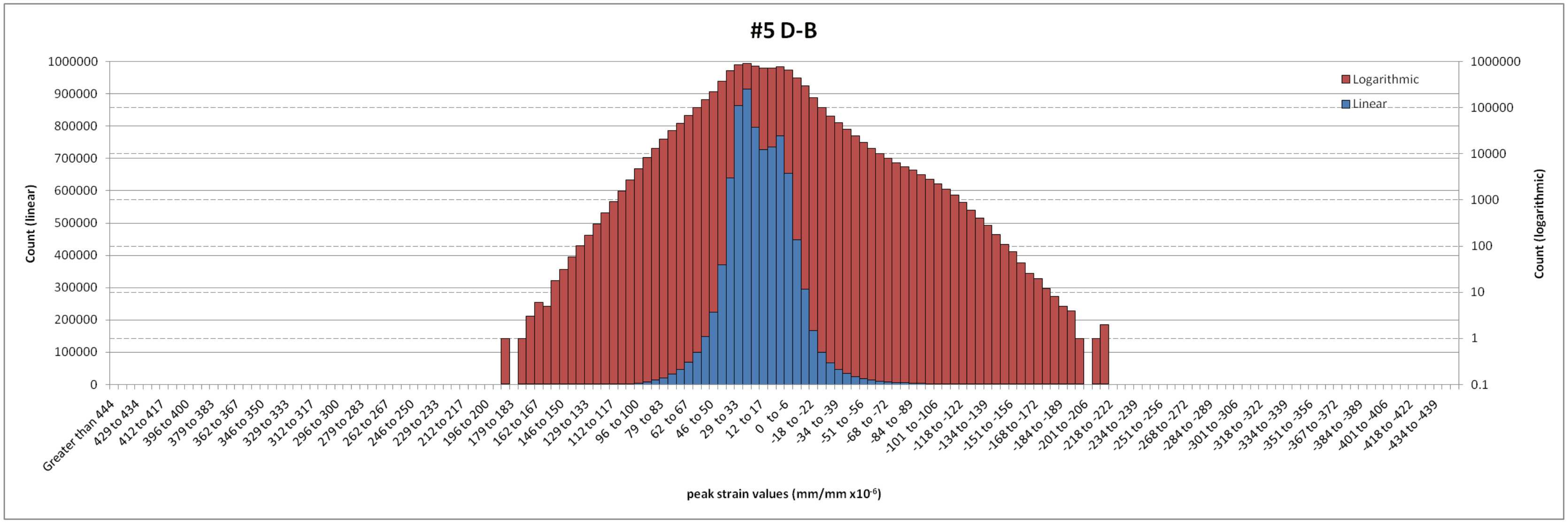
#5 D-B
Count (linear)
1000000
900000
800000
700000
600000
500000
400000
300000
200000
100000
0
Count (logarithmic)
1000000
100000
10000
1000
100
10
1
0.1
Logarithmic
Linear
Greater than 444
429 to 434
412 to 417
396 to 400
379 to 383
362 to 367
346 to 350
329 to 333
312 to 317
296 to 300
279 to 283
262 to 267
246 to 250
229 to 233
212 to 217
196 to 200
179 to 183
162 to 167
146 to 150
129 to 133
112 to 117
96 to 100
79 to 83
62 to 67
46 to 50
29 to 33
12 to 17
0 to -6
-18 to -22
-34 to -39
-51 to -56
-68 to -72
-84 to -89
-101 to -106
-118 to -122
-134 to -139
-151 to -156
-168 to -172
-184 to -189
-201 to -206
-218 to -222
-234 to -239
-251 to -256
-268 to -272
-284 to -289
-301 to -306
-318 to -322
-334 to -339
-351 to -356
-367 to -372
-384 to -389
-401 to -406
-418 to -422
-434 to -439
peak strain values (mm/mm x10^{-6})

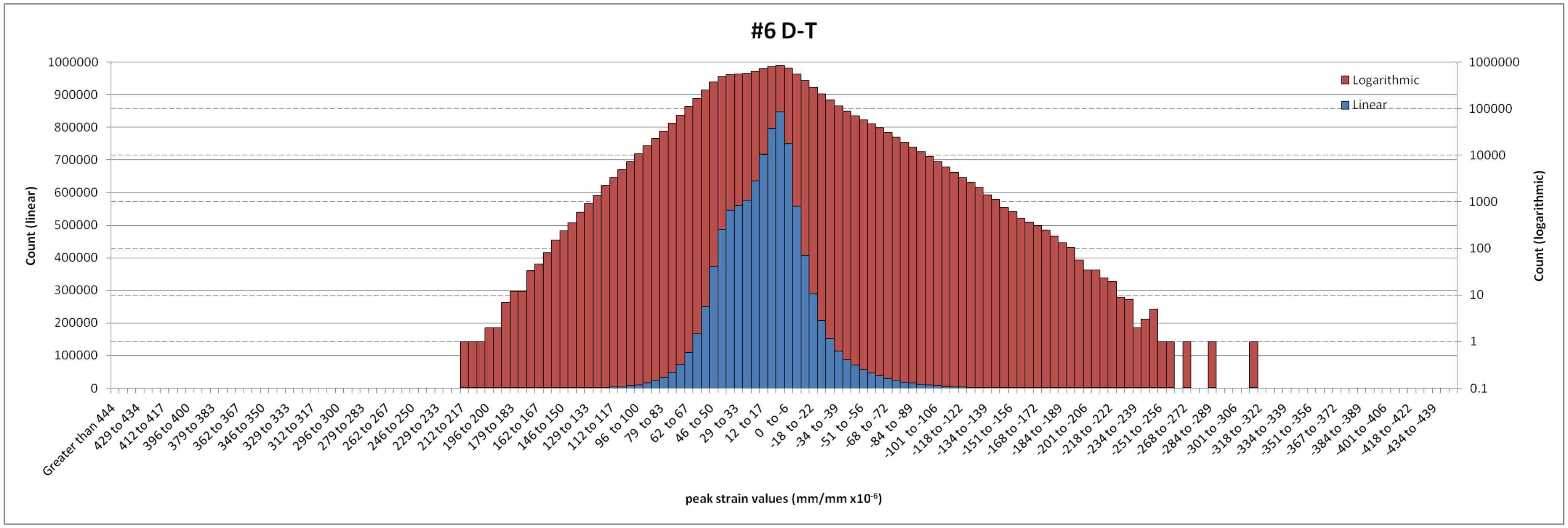
#6 D-T
Logarithmic
Linear
Count (linear)
1000000
900000
800000
700000
600000
500000
400000
300000
200000
100000
0
Count (logarithmic)
1000000
100000
10000
1000
100
10
1
0.1
Greater than 444
429 to 434
412 to 417
396 to 400
379 to 383
362 to 367
346 to 350
329 to 333
312 to 317
296 to 300
279 to 283
262 to 267
246 to 250
229 to 233
212 to 217
196 to 200
179 to 183
162 to 167
146 to 150
129 to 133
112 to 117
96 to 100
79 to 83
62 to 67
46 to 50
29 to 33
12 to 17
0 to -6
-18 to -22
-34 to -39
-51 to -56
-68 to -72
-84 to -89
-101 to -106
-118 to -122
-134 to -139
-151 to -156
-168 to -172
-184 to -189
-201 to -206
-218 to -222
-234 to -239
-251 to -256
-268 to -272
-284 to -289
-301 to -306
-318 to -322
-334 to -339
-351 to -356
-367 to -372
-384 to -389
-401 to -406
-418 to -422
-434 to -439
peak strain values (mm/mm x10-6)

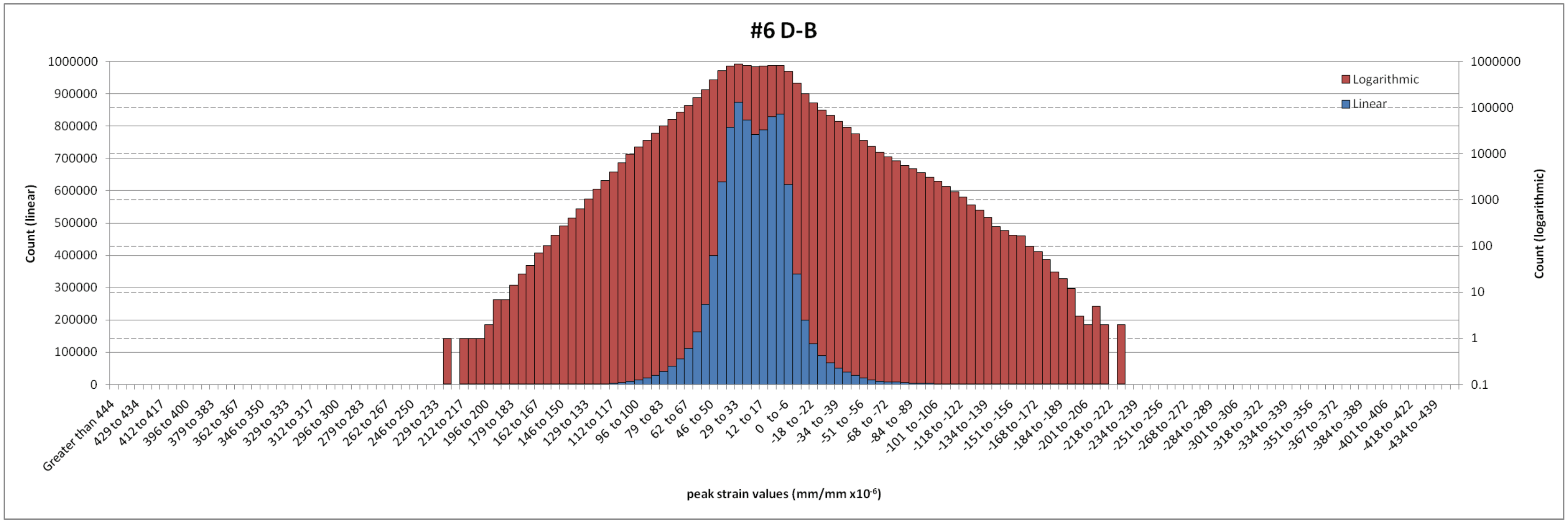
#6 D-B
Logarithmic
Linear
Count (linear)
1000000
900000
800000
700000
600000
500000
400000
300000
200000
100000
0
Count (logarithmic)
1000000
100000
10000
1000
100
10
1
0.1
Greater than 444
429 to 434
412 to 417
396 to 400
379 to 383
362 to 367
346 to 350
329 to 333
312 to 317
296 to 300
279 to 283
262 to 267
246 to 250
229 to 233
212 to 217
196 to 200
179 to 183
162 to 167
146 to 150
129 to 133
112 to 117
96 to 100
79 to 83
62 to 67
46 to 50
29 to 33
12 to 17
0 to -6
-18 to -22
-34 to -39
-51 to -56
-68 to -72
-84 to -89
-101 to -106
-118 to -122
-134 to -139
-151 to -156
-168 to -172
-184 to -189
-201 to -206
-218 to -222
-234 to -239
-251 to -256
-268 to -272
-284 to -289
-301 to -306
-318 to -322
-334 to -339
-351 to -356
-367 to -372
-384 to -389
-401 to -406
-418 to -422
-434 to -439
peak strain values (mm/mm x10⁻⁶)

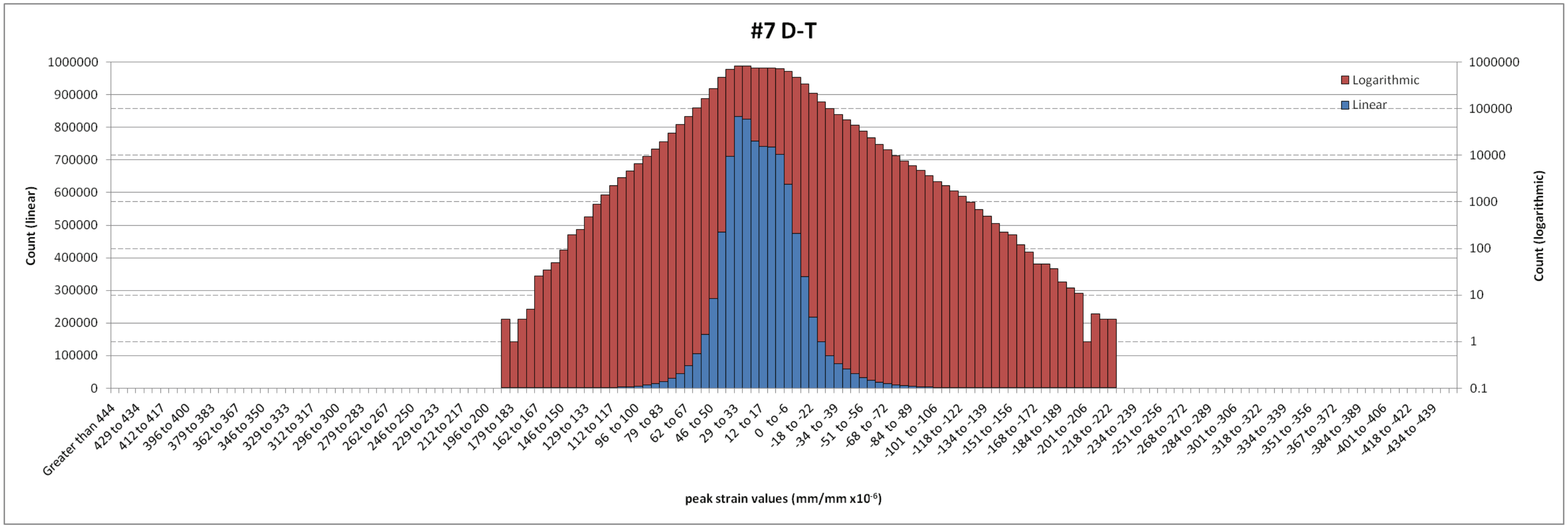
#7 D-T
Count (linear)
1000000
900000
800000
700000
600000
500000
400000
300000
200000
100000
0
Count (logarithmic)
1000000
100000
10000
1000
100
10
1
0.1
Logarithmic
Linear
Greater than 444
429 to 434
412 to 417
396 to 400
379 to 383
362 to 367
346 to 350
329 to 333
312 to 317
296 to 300
279 to 283
262 to 267
246 to 250
229 to 233
212 to 217
196 to 200
179 to 183
162 to 167
146 to 150
129 to 133
112 to 117
96 to 100
79 to 83
62 to 67
46 to 50
29 to 33
12 to 17
0 to -6
-18 to -22
-34 to -39
-51 to -56
-68 to -72
-84 to -89
-101 to -106
-118 to -122
-134 to -139
-151 to -156
-168 to -172
-184 to -189
-201 to -206
-218 to -222
-234 to -239
-251 to -256
-268 to -272
-284 to -289
-301 to -306
-318 to -322
-334 to -339
-351 to -356
-367 to -372
-384 to -389
-401 to -406
-418 to -422
-434 to -439
peak strain values (mm/mm x10^{-6})

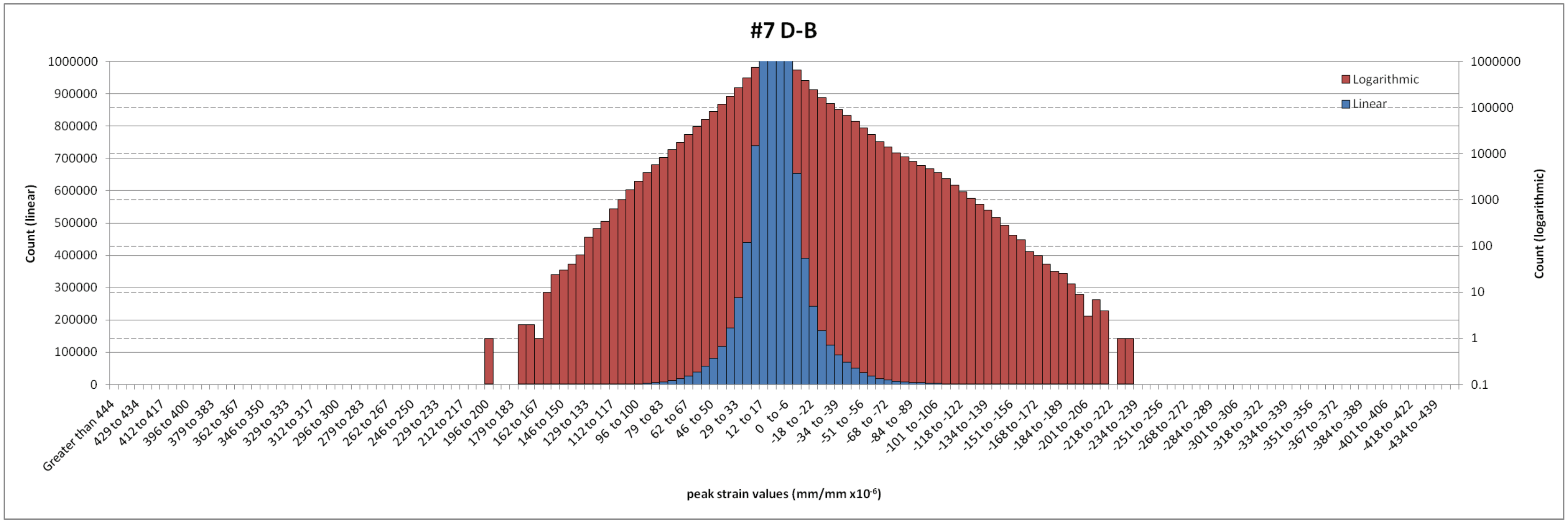
#7 D-B
Logarithmic
Linear
Count (linear)
Count (logarithmic)
peak strain values (mm/mm x10^{-6})
1000000
900000
800000
700000
600000
500000
400000
300000
200000
100000
0
1000000
100000
10000
1000
100
10
1
0.1
Greater than 444
429 to 434
412 to 417
396 to 400
379 to 383
362 to 367
346 to 350
329 to 333
312 to 317
296 to 300
279 to 283
262 to 267
246 to 250
229 to 233
212 to 217
196 to 200
179 to 183
162 to 167
146 to 150
129 to 133
112 to 117
96 to 100
79 to 83
62 to 67
46 to 50
29 to 33
12 to 17
0 to -6
-18 to -22
-34 to -39
-51 to -56
-68 to -72
-84 to -89
-101 to -106
-118 to -122
-134 to -139
-151 to -156
-168 to -172
-184 to -189
-201 to -206
-218 to -222
-234 to -239
-251 to -256
-268 to -272
-284 to -289
-301 to -306
-318 to -322
-334 to -339
-351 to -356
-367 to -372
-384 to -389
-401 to -406
-418 to -422
-434 to -439

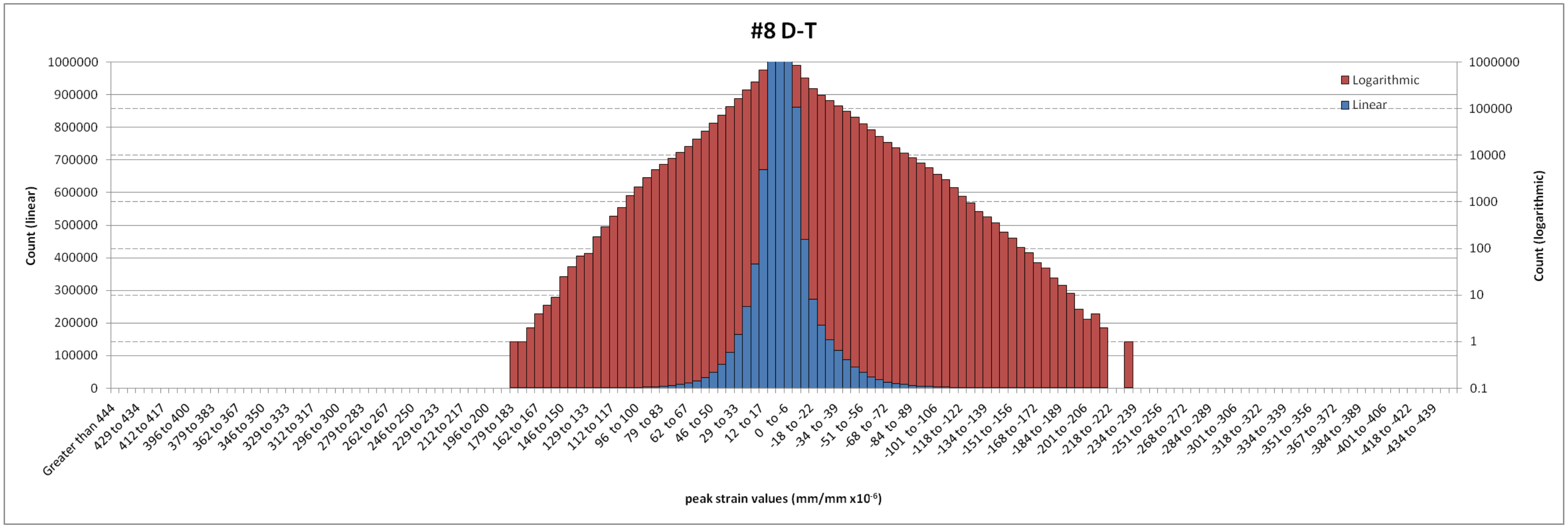
#8 D-T
Logarithmic
Linear
Count (linear)
1000000
900000
800000
700000
600000
500000
400000
300000
200000
100000
0
Count (logarithmic)
1000000
100000
10000
1000
100
10
1
0.1
Greater than 444
429 to 434
412 to 417
396 to 400
379 to 383
362 to 367
346 to 350
329 to 333
312 to 317
296 to 300
279 to 283
262 to 267
246 to 250
229 to 233
212 to 217
196 to 200
179 to 183
162 to 167
146 to 150
129 to 133
112 to 117
96 to 100
79 to 83
62 to 67
46 to 50
29 to 33
12 to 17
0 to -6
-18 to -22
-34 to -39
-51 to -56
-68 to -72
-84 to -89
-101 to -106
-118 to -122
-134 to -139
-151 to -156
-168 to -172
-184 to -189
-201 to -206
-218 to -222
-234 to -239
-251 to -256
-268 to -272
-284 to -289
-301 to -306
-318 to -322
-334 to -339
-351 to -356
-367 to -372
-384 to -389
-401 to -406
-418 to -422
-434 to -439
peak strain values (mm/mm x10^{-6})

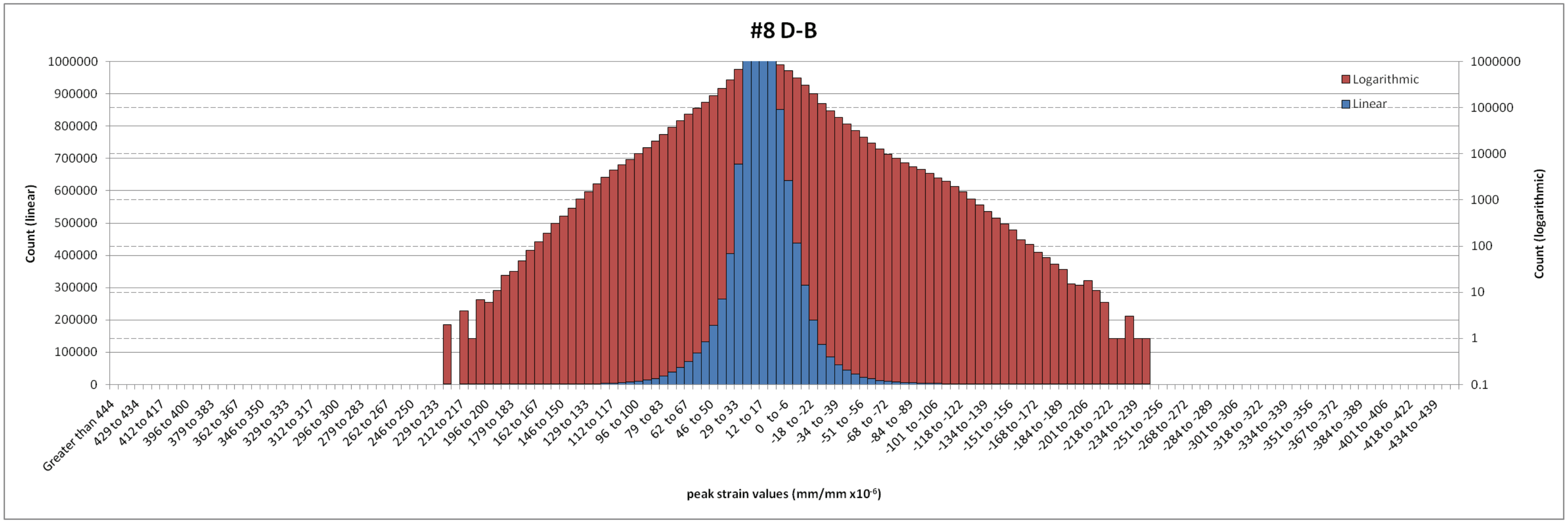
#8 D-B
Logarithmic
Linear
Count (linear)
1000000
900000
800000
700000
600000
500000
400000
300000
200000
100000
0
Count (logarithmic)
1000000
100000
10000
1000
100
10
1
0.1
Greater than 444
429 to 434
412 to 417
396 to 400
379 to 383
362 to 367
346 to 350
329 to 333
312 to 317
296 to 300
279 to 283
262 to 267
246 to 250
229 to 233
212 to 217
196 to 200
179 to 183
162 to 167
146 to 150
129 to 133
112 to 117
96 to 100
79 to 83
62 to 67
46 to 50
29 to 33
12 to 17
0 to -6
-18 to -22
-34 to -39
-51 to -56
-68 to -72
-84 to -89
-101 to -106
-118 to -122
-134 to -139
-151 to -156
-168 to -172
-184 to -189
-201 to -206
-218 to -222
-234 to -239
-251 to -256
-268 to -272
-284 to -289
-301 to -306
-318 to -322
-334 to -339
-351 to -356
-367 to -372
-384 to -389
-401 to -406
-418 to -422
-434 to -439
peak strain values (mm/mm x10⁻⁶)

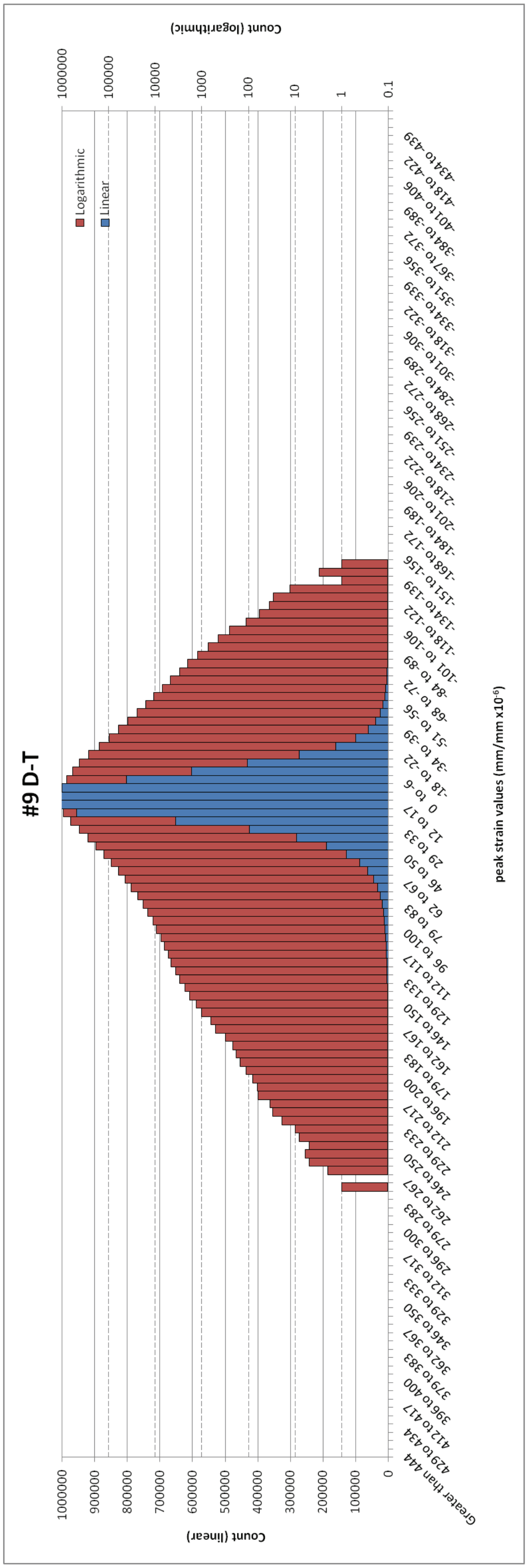
#9 D-T
Logarithmic
Linear
Count (linear)
1000000
900000
800000
700000
600000
500000
400000
300000
200000
100000
0
Count (logarithmic)
1000000
100000
10000
1000
100
10
1
0.1
peak strain values (mm/mm x10^{-6})
Greater than 444
429 to 434
412 to 417
396 to 400
379 to 383
362 to 367
346 to 350
329 to 333
312 to 317
296 to 300
279 to 283
262 to 267
246 to 250
229 to 233
212 to 217
196 to 200
179 to 183
162 to 167
146 to 150
129 to 133
112 to 117
96 to 100
79 to 83
62 to 67
46 to 50
29 to 33
12 to 17
0
to -6
-18 to -22
-34 to -39
-51 to -56
-68 to -72
-84 to -89
-101 to -106
-118to -122
-134to -139
-151to -156
-168to -172
-184to -189
-201to -206
-218to -222
-234to -239
-251to -256
-268to -272
-284to -289
-301to -306
-318to -322
-334to -339
-351to -356
-367to -372
-384to -389
-401to -406
-418to -422
-434to -439

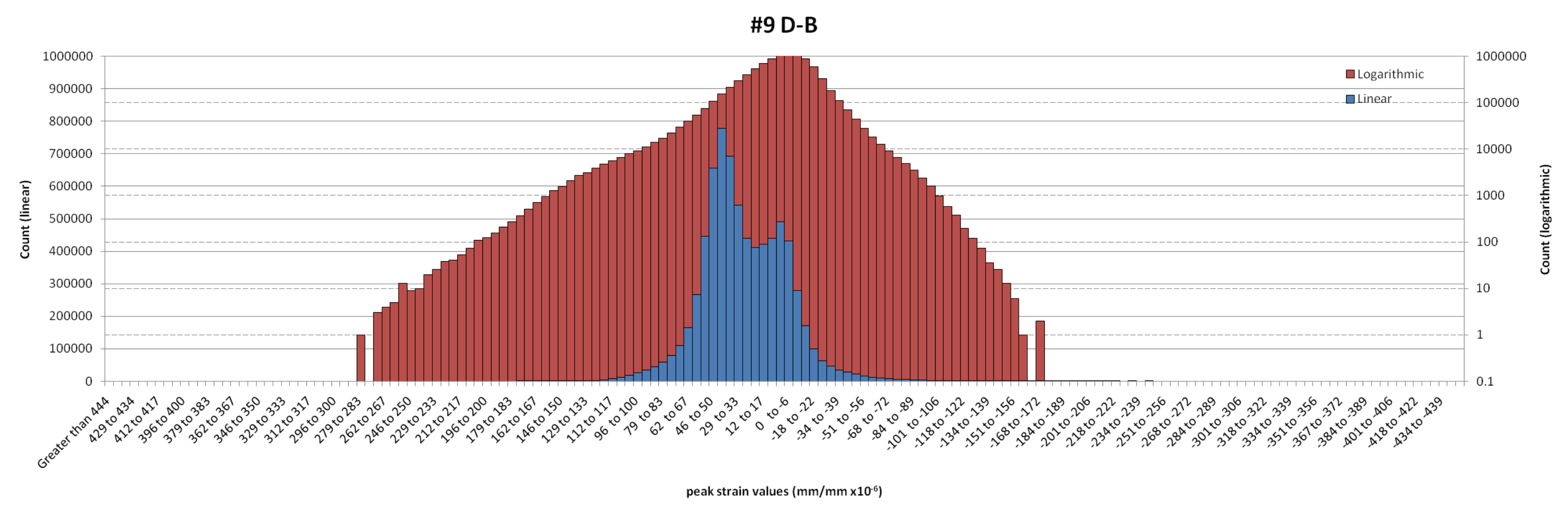
#9 D-B
Logarithmic
Linear
Count (linear)
1000000
900000
800000
700000
600000
500000
400000
300000
200000
100000
0
Count (logarithmic)
1000000
100000
10000
1000
100
10
1
0.1
Greater than 444
429 to 434
412 to 417
396 to 400
379 to 383
362 to 367
346 to 350
329 to 333
312 to 317
296 to 300
279 to 283
262 to 267
246 to 250
229 to 233
212 to 217
196 to 200
179 to 183
162 to 167
146 to 150
129 to 133
112 to 117
96 to 100
79 to 83
62 to 67
46 to 50
29 to 33
12 to 17
0 to -6
-18 to -22
-34 to -39
-51 to -56
-68 to -72
-84 to -89
-101 to -106
-118 to -122
-134 to -139
-151 to -156
-168 to -172
-184 to -189
-201 to -206
-218 to -222
-234 to -239
-251 to -256
-268 to -272
-284 to -289
-301 to -306
-318 to -322
-334 to -339
-351 to -356
-367 to -372
-384 to -389
-401 to -406
-418 to -422
-434 to -439
peak strain values (mm/mm x10^{-6})

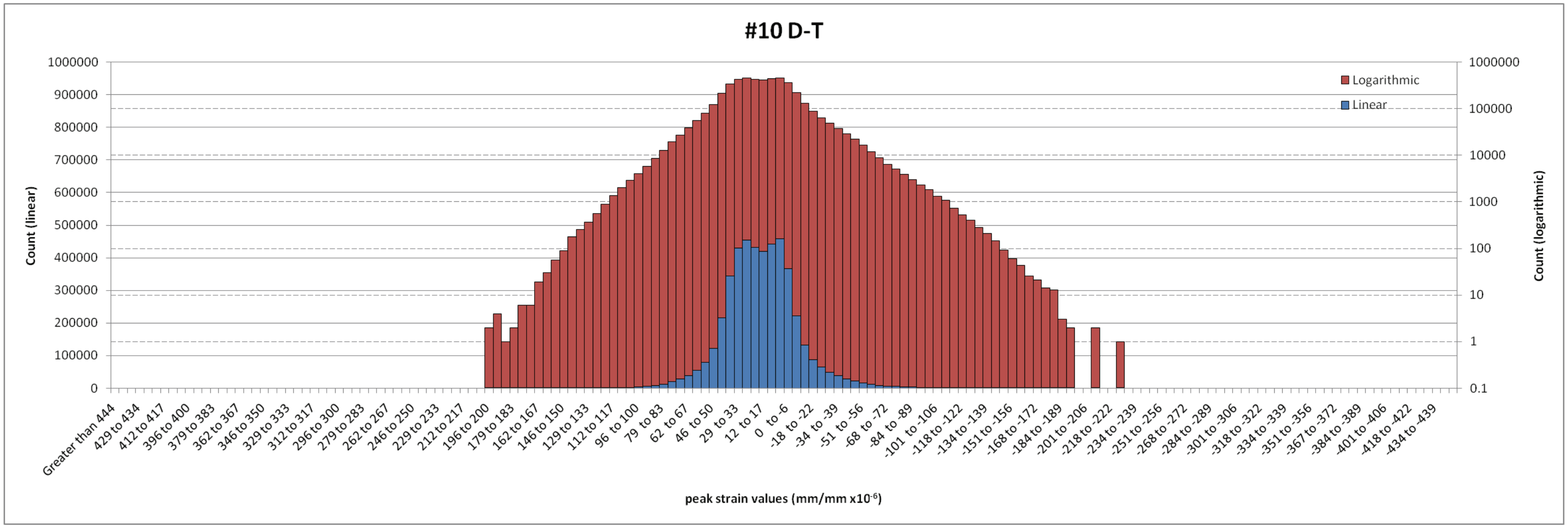
#10 D-T
Logarithmic
Linear
Count (linear)
1000000
900000
800000
700000
600000
500000
400000
300000
200000
100000
0
Count (logarithmic)
1000000
100000
10000
1000
100
10
1
0.1
Greater than 444
429 to 434
412 to 417
396 to 400
379 to 383
362 to 367
346 to 350
329 to 333
312 to 317
296 to 300
279 to 283
262 to 267
246 to 250
229 to 233
212 to 217
196 to 200
179 to 183
162 to 167
146 to 150
129 to 133
112 to 117
96 to 100
79 to 83
62 to 67
46 to 50
29 to 33
12 to 17
0 to -6
-18 to -22
-34 to -39
-51 to -56
-68 to -72
-84 to -89
-101 to -106
-118 to -122
-134 to -139
-151 to -156
-168 to -172
-184 to -189
-201 to -206
-218 to -222
-234 to -239
-251 to -256
-268 to -272
-284 to -289
-301 to -306
-318 to -322
-334 to -339
-351 to -356
-367 to -372
-384 to -389
-401 to -406
-418 to -422
-434 to -439
peak strain values (mm/mm x10^{-6})

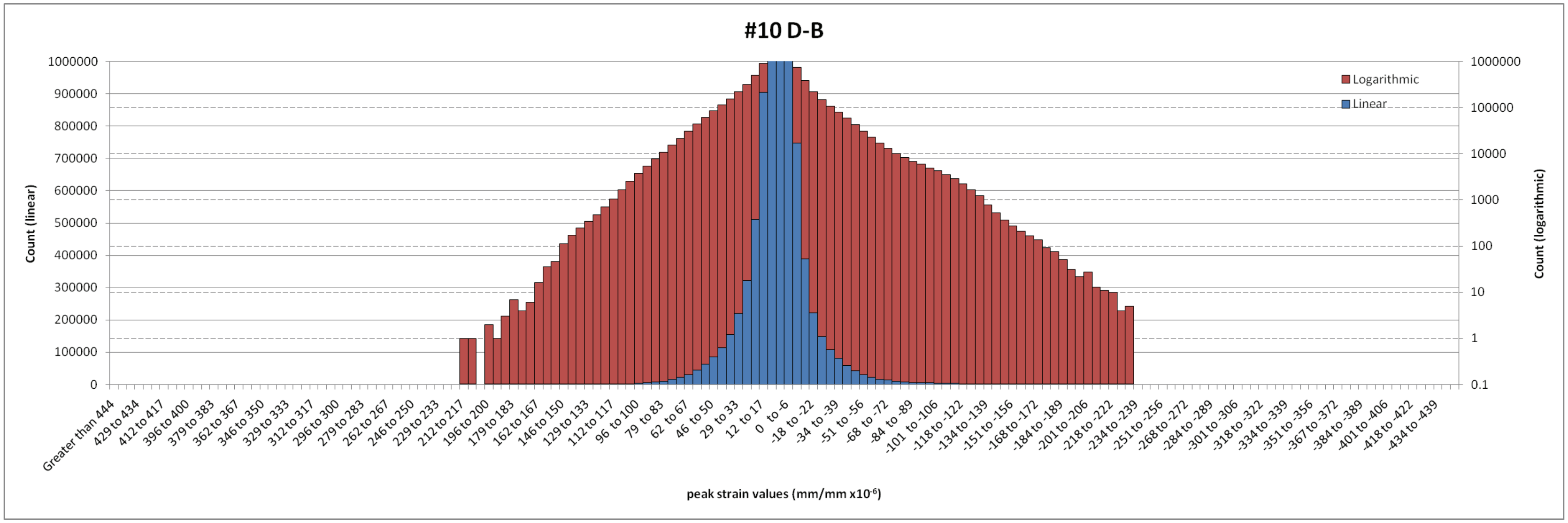
#10 D-B
Logarithmic
Linear
Count (linear)
1000000
900000
800000
700000
600000
500000
400000
300000
200000
100000
0
Count (logarithmic)
1000000
100000
10000
1000
100
10
1
0.1
Greater than 444
429 to 434
412 to 417
396 to 400
379 to 383
362 to 367
346 to 350
329 to 333
312 to 317
296 to 300
279 to 283
262 to 267
246 to 250
229 to 233
212 to 217
196 to 200
179 to 183
162 to 167
146 to 150
129 to 133
112 to 117
96 to 100
79 to 83
62 to 67
46 to 50
29 to 33
12 to 17
0 to -6
-18 to -22
-34 to -39
-51 to -56
-68 to -72
-84 to -89
-101 to -106
-118 to -122
-134 to -139
-151 to -156
-168 to -172
-184 to -189
-201 to -206
-218 to -222
-234 to -239
-251 to -256
-268 to -272
-284 to -289
-301 to -306
-318 to -322
-334 to -339
-351 to -356
-367 to -372
-384 to -389
-401 to -406
-418 to -422
-434 to -439
peak strain values (mm/mm x10⁻⁶)

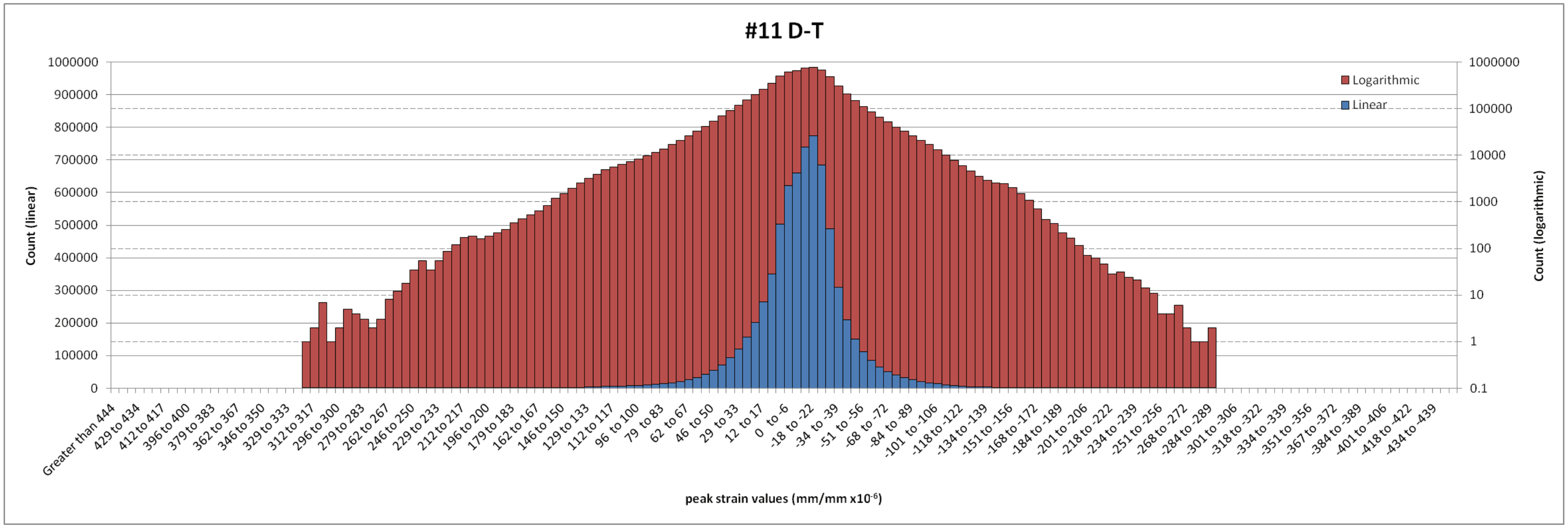
#11 D-T
Count (linear)
1000000
900000
800000
700000
600000
500000
400000
300000
200000
100000
0
Count (logarithmic)
1000000
100000
10000
1000
100
10
1
0.1
Logarithmic
Linear
peak strain values (mm/mm x10^{-6})
Greater than 444
429 to 434
412 to 417
396 to 400
379 to 383
362 to 367
346 to 350
329 to 333
312 to 317
296 to 300
279 to 283
262 to 267
246 to 250
229 to 233
212 to 217
196 to 200
179 to 183
162 to 167
146 to 150
129 to 133
112 to 117
96 to 100
79 to 83
62 to 67
46 to 50
29 to 33
12 to 17
0 to -6
-18 to -22
-34 to -39
-51 to -56
-68 to -72
-84 to -89
-101 to -106
-118 to -122
-134 to -139
-151 to -156
-168 to -172
-184 to -189
-201 to -206
-218 to -222
-234 to -239
-251 to -256
-268 to -272
-284 to -289
-301 to -306
-318 to -322
-334 to -339
-351 to -356
-367 to -372
-384 to -389
-401 to -406
-418 to -422
-434 to -439

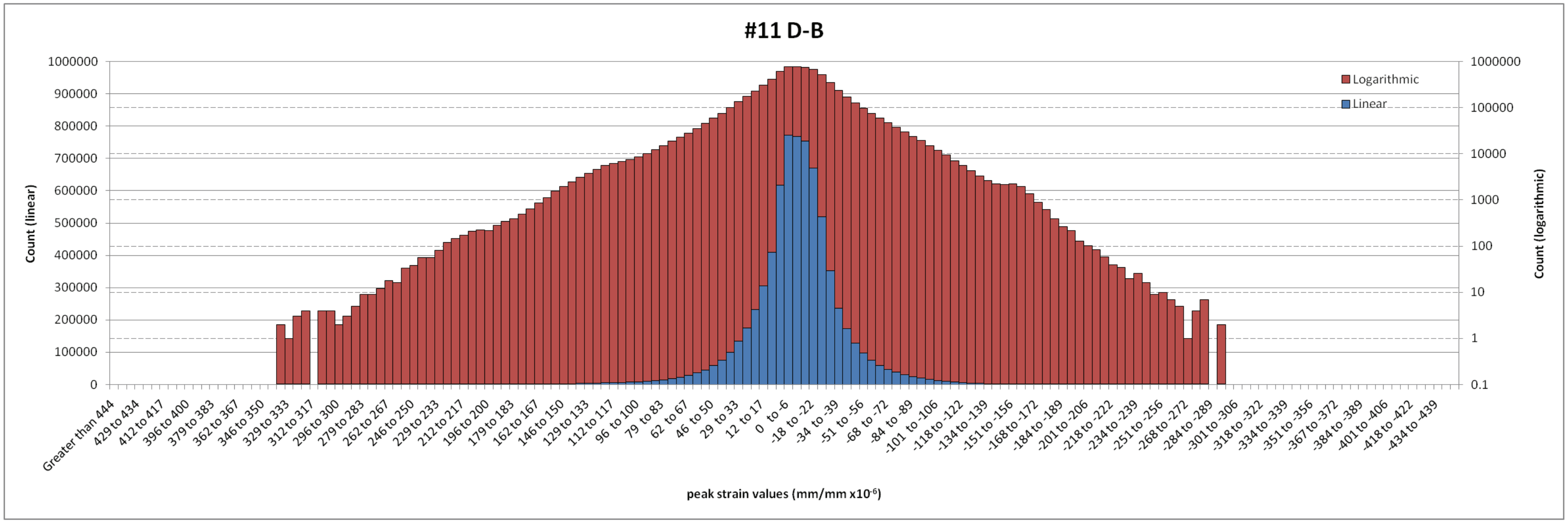
#11 D-B
Logarithmic
Linear
Count (linear)
1000000
900000
800000
700000
600000
500000
400000
300000
200000
100000
0
Count (logarithmic)
1000000
100000
10000
1000
100
10
1
0.1
Greater than 444
429 to 434
412 to 417
396 to 400
379 to 383
362 to 367
346 to 350
329 to 333
312 to 317
296 to 300
279 to 283
262 to 267
246 to 250
229 to 233
212 to 217
196 to 200
179 to 183
162 to 167
146 to 150
129 to 133
112 to 117
96 to 100
79 to 83
62 to 67
46 to 50
29 to 33
12 to 17
0 to -6
-18 to -22
-34 to -39
-51 to -56
-68 to -72
-84 to -89
-101 to -106
-118 to -122
-134 to -139
-151 to -156
-168 to -172
-184 to -189
-201 to -206
-218 to -222
-234 to -239
-251 to -256
-268 to -272
-284 to -289
-301 to -306
-318 to -322
-334 to -339
-351 to -356
-367 to -372
-384 to -389
-401 to -406
-418 to -422
-434 to -439
peak strain values (mm/mm x10^{-6})

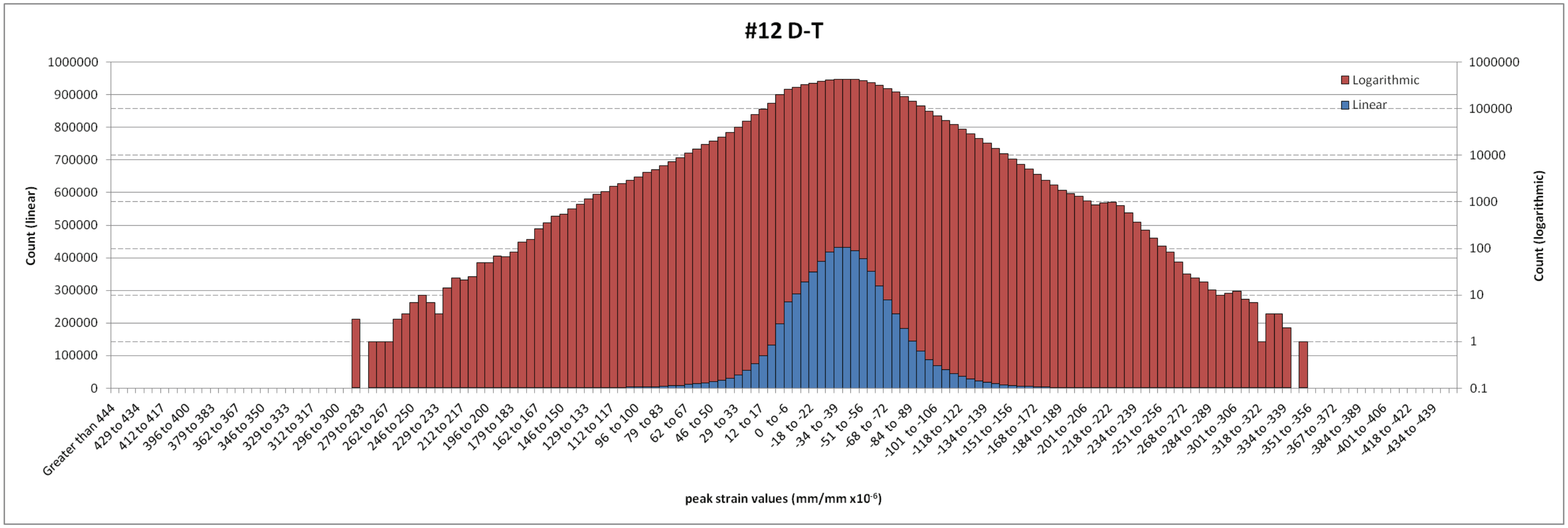
#12 D-T
Count (linear)
1000000
900000
800000
700000
600000
500000
400000
300000
200000
100000
0
Count (logarithmic)
1000000
100000
10000
1000
100
10
1
0.1
Logarithmic
Linear
Greater than 444
429 to 434
412 to 417
396 to 400
379 to 383
362 to 367
346 to 350
329 to 333
312 to 317
296 to 300
279 to 283
262 to 267
246 to 250
229 to 233
212 to 217
196 to 200
179 to 183
162 to 167
146 to 150
129 to 133
112 to 117
96 to 100
79 to 83
62 to 67
46 to 50
29 to 33
12 to 17
0 to -6
-18 to -22
-34 to -39
-51 to -56
-68 to -72
-84 to -89
-101 to -106
-118 to -122
-134 to -139
-151 to -156
-168 to -172
-184 to -189
-201 to -206
-218 to -222
-234 to -239
-251 to -256
-268 to -272
-284 to -289
-301 to -306
-318 to -322
-334 to -339
-351 to -356
-367 to -372
-384 to -389
-401 to -406
-418 to -422
-434 to -439
peak strain values (mm/mm x10^{-6})

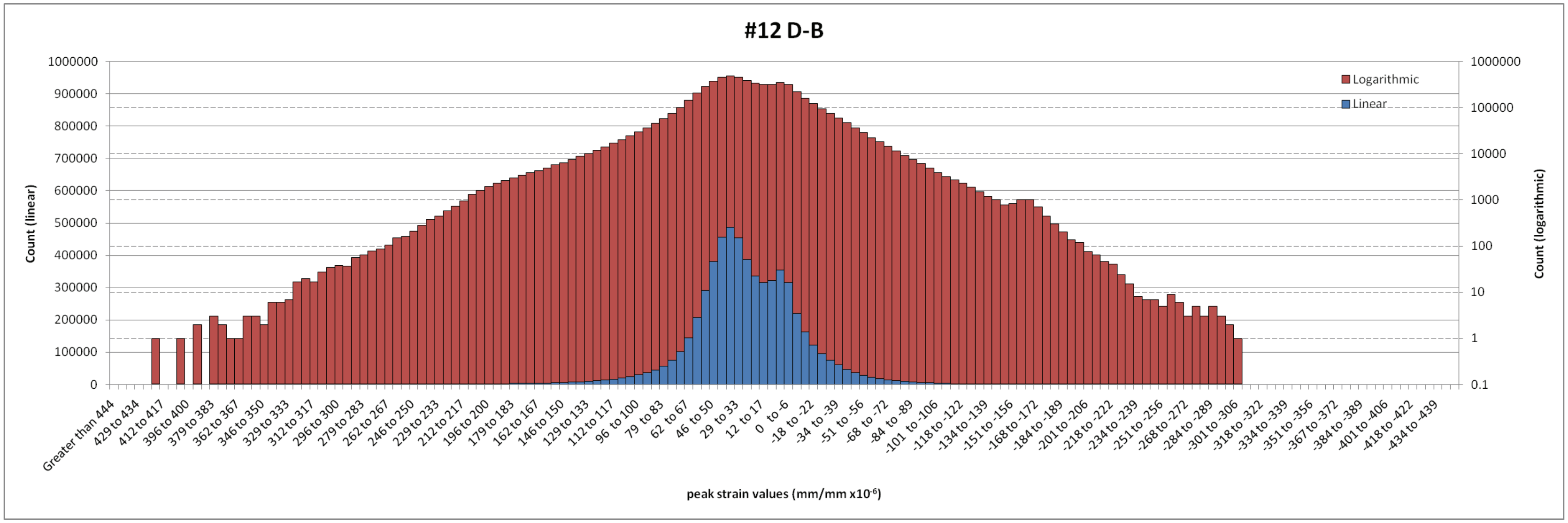
#12 D-B
Logarithmic
Linear
Count (linear)
1000000
900000
800000
700000
600000
500000
400000
300000
200000
100000
0
Count (logarithmic)
1000000
100000
10000
1000
100
10
1
0.1
Greater than 444
429 to 434
412 to 417
396 to 400
379 to 383
362 to 367
346 to 350
329 to 333
312 to 317
296 to 300
279 to 283
262 to 267
246 to 250
229 to 233
212 to 217
196 to 200
179 to 183
162 to 167
146 to 150
129 to 133
112 to 117
96 to 100
79 to 83
62 to 67
46 to 50
29 to 33
12 to 17
0 to -6
-18 to -22
-34 to -39
-51 to -56
-68 to -72
-84 to -89
-101 to -106
-118 to -122
-134 to -139
-151 to -156
-168 to -172
-184 to -189
-201 to -206
-218 to -222
-234 to -239
-251 to -256
-268 to -272
-284 to -289
-301 to -306
-318 to -322
-334 to -339
-351 to -356
-367 to -372
-384 to -389
-401 to -406
-418 to -422
-434 to -439
peak strain values (mm/mm x10⁻⁶)

Appendix V – Peak Gauge Pair Examination

The figures shown in this appendix are plots of unprocessed data collected from the MacKay Bridge. These figures provide an illustration of the characteristic shape of the peak pair events for each gauge. During the post-processing phase, several corrections are made to the data:

Zero correction is applied as described in Section 10.2.1.

Temperature correction is applied as described in Section 10.2.2.

Data filter and peak selection are applied as described in Section 10.2.3.

Gauge type correction factor is applied as described in Chapter 6.

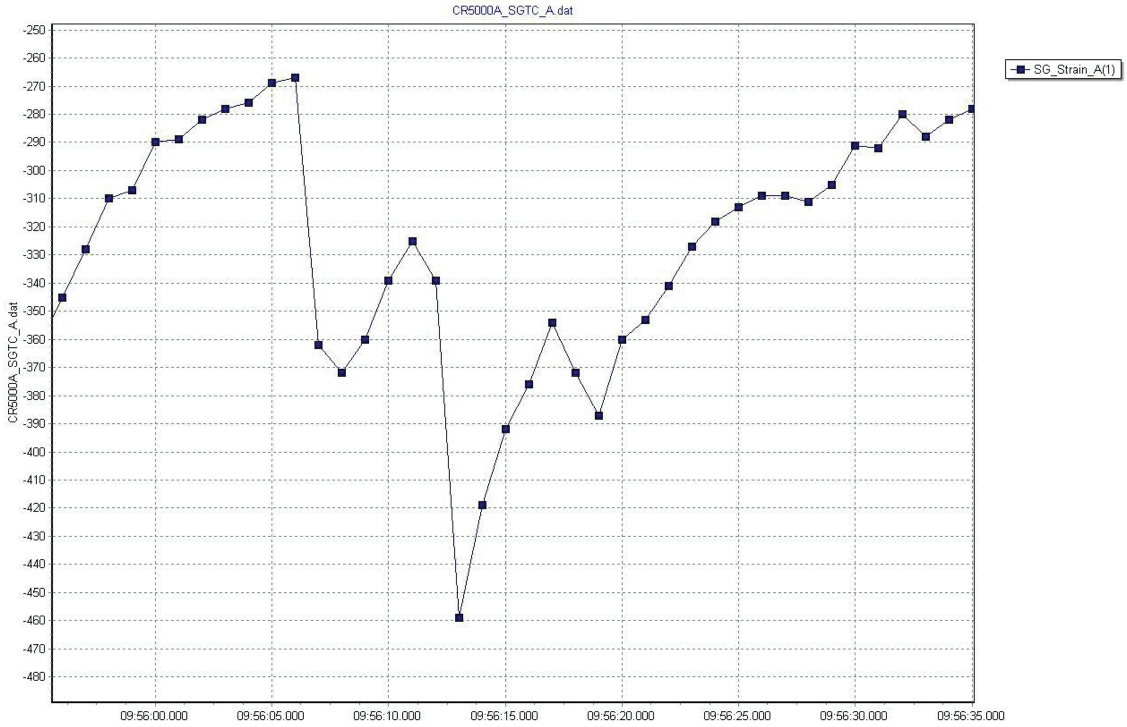
CR5000A_SGTC_A.dat
CR5000A_SGTC_A.dat
-250
-260
-270
-280
-290
-300
-310
-320
-330
-340
-350
-360
-370
-380
-390
-400
-410
-420
-430
-440
-450
-460
-470
-480
09:56:00.000
09:56:05.000
09:56:10.000
09:56:15.000
09:56:20.000
09:56:25.000
09:56:30.000
09:56:35.000
SG_Strain_A(1)

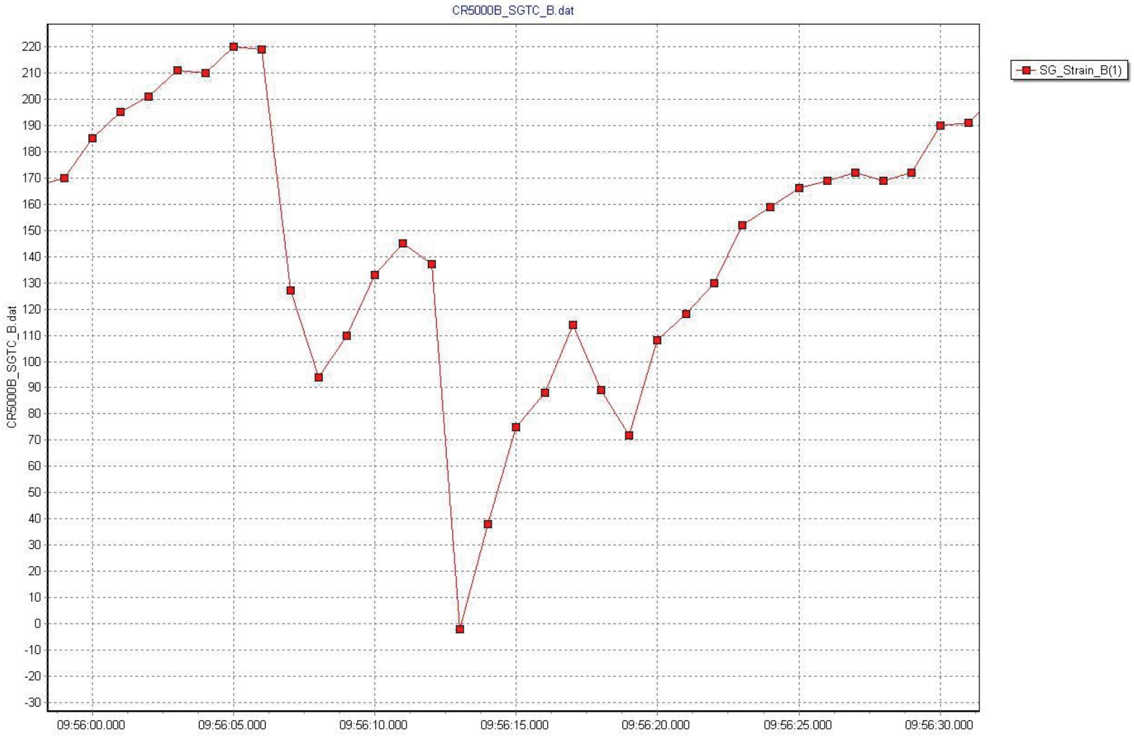
CR5000B_SGTC_B.dat
CR5000B_SGTC_B.dat
220
210
200
190
180
170
160
150
140
130
120
110
100
90
80
70
60
50
40
30
20
10
0
-10
-20
-30
09:56:00.000
09:56:05.000
09:56:10.000
09:56:15.000
09:56:20.000
09:56:25.000
09:56:30.000
SG_Strain_B(1)

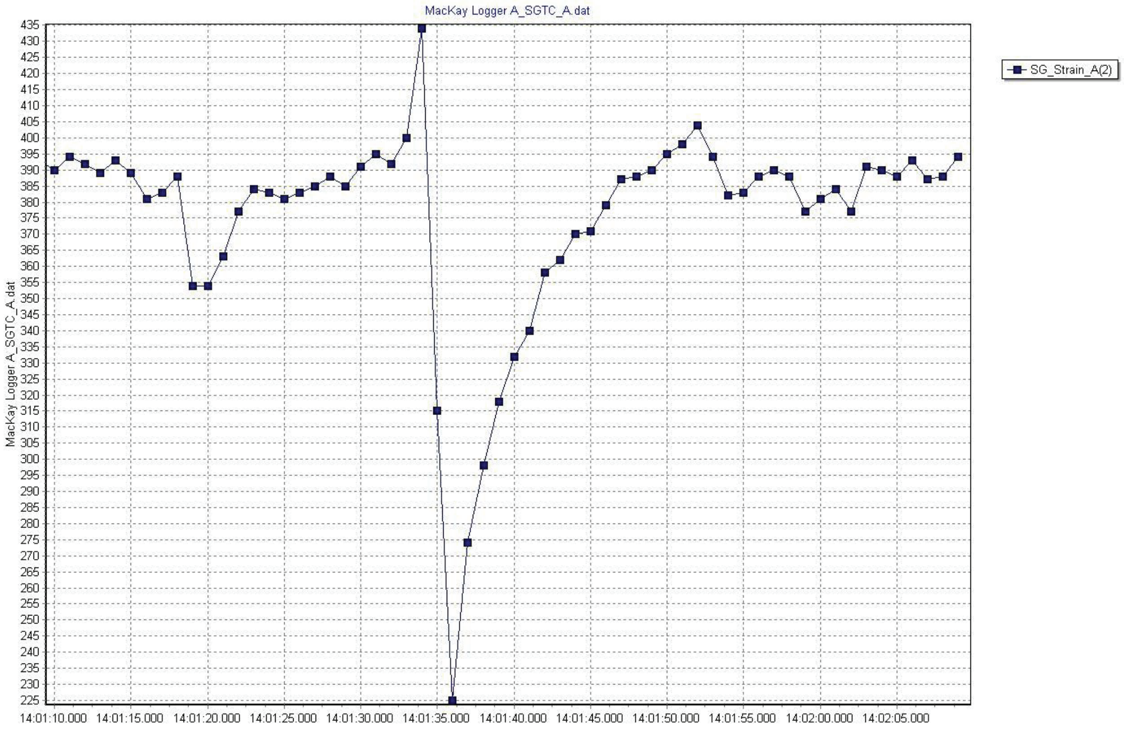
MacKay Logger A_SGTC_A.dat
SG_Strain_A(2)
MacKay Logger A_SGTC_A.dat
435
430
425
420
415
410
405
400
395
390
385
380
375
370
365
360
355
350
345
340
335
330
325
320
315
310
305
300
295
290
285
280
275
270
265
260
255
250
245
240
235
230
225
14:01:10.000
14:01:15.000
14:01:20.000
14:01:25.000
14:01:30.000
14:01:35.000
14:01:40.000
14:01:45.000
14:01:50.000
14:01:55.000
14:02:00.000
14:02:05.000

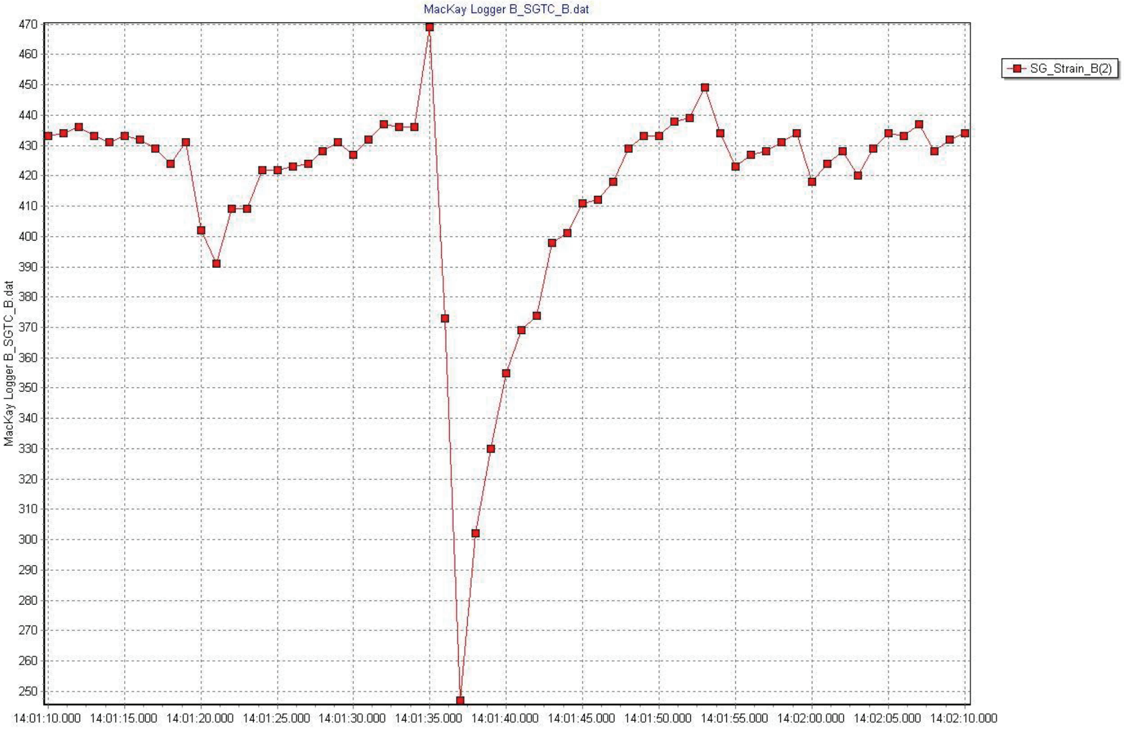
MacKay Logger B_SGTC_B.dat
SG_Strain_B(2)
MacKay Logger B_SGTC_B.dat
470
460
450
440
430
420
410
400
390
380
370
360
350
340
330
320
310
300
290
280
270
260
250
14:01:10.000
14:01:15.000
14:01:20.000
14:01:25.000
14:01:30.000
14:01:35.000
14:01:40.000
14:01:45.000
14:01:50.000
14:01:55.000
14:02:00.000
14:02:05.000
14:02:10.000

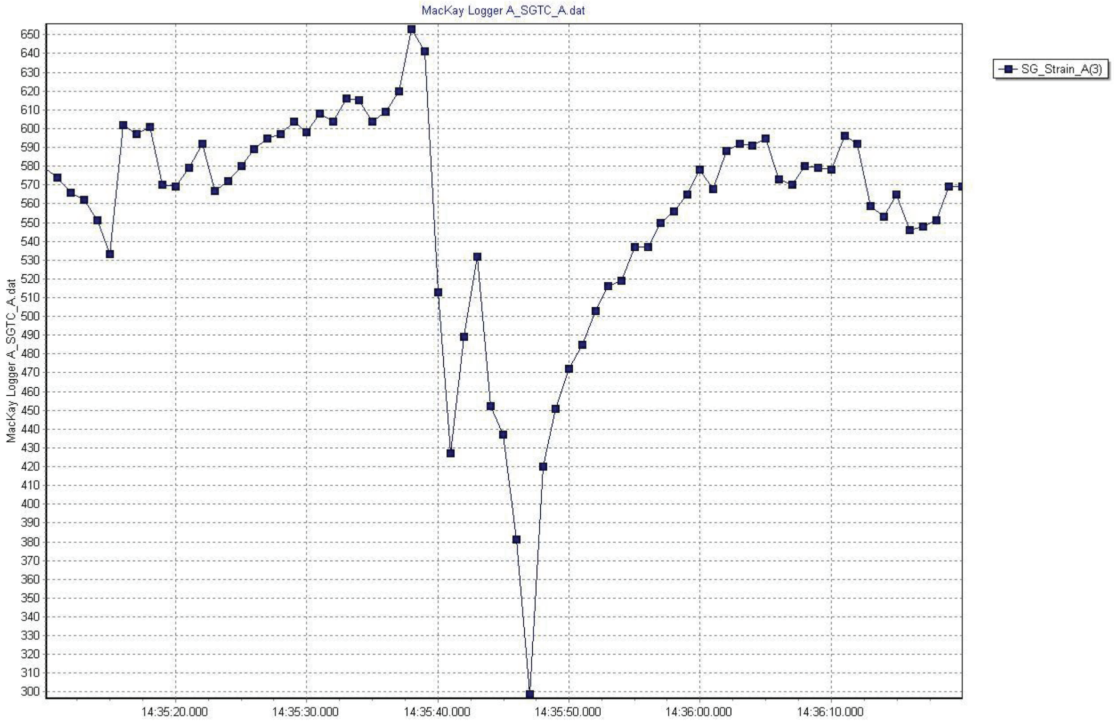
MacKay Logger A_SGTC_A.dat
MacKay Logger A_SGTC_A.dat
SG_Strain_A(3)
650
640
630
620
610
600
590
580
570
560
550
540
530
520
510
500
490
480
470
460
450
440
430
420
410
400
390
380
370
360
350
340
330
320
310
300
14:35:20.000
14:35:30.000
14:35:40.000
14:35:50.000
14:36:00.000
14:36:10.000

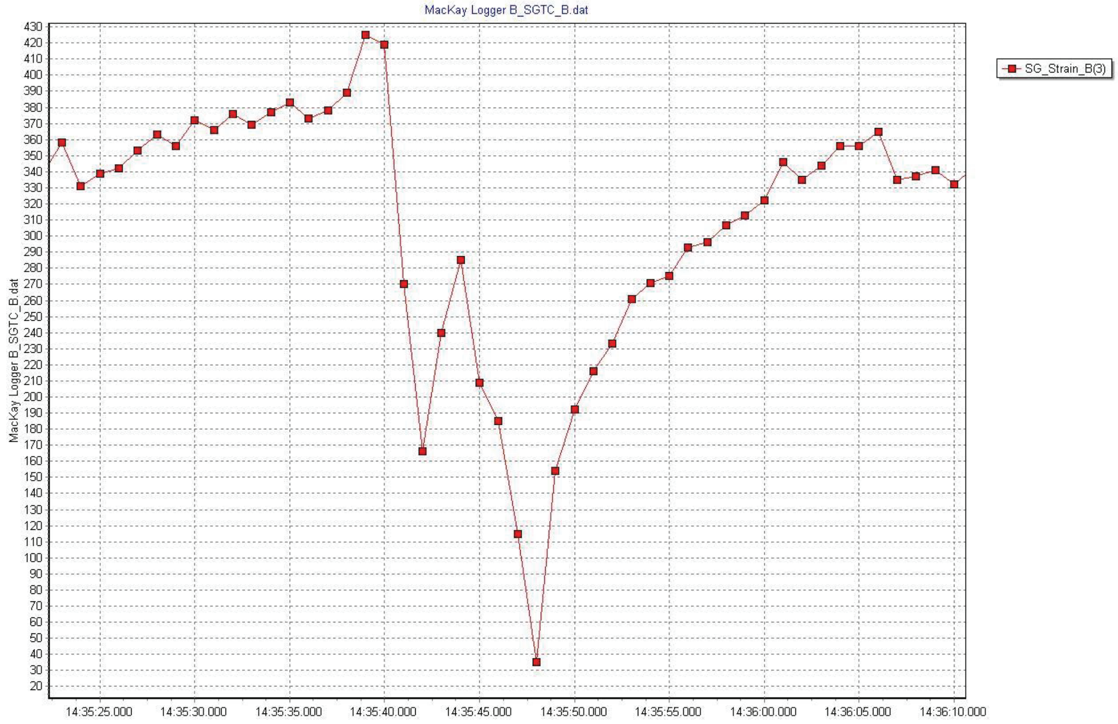
MacKay Logger B_SGTC_B.dat
MacKay Logger B_SGTC_B.dat
SG_Strain_B(3)
430
420
410
400
390
380
370
360
350
340
330
320
310
300
290
280
270
260
250
240
230
220
210
200
190
180
170
160
150
140
130
120
110
100
90
80
70
60
50
40
30
20
14:35:25.000
14:35:30.000
14:35:35.000
14:35:40.000
14:35:45.000
14:35:50.000
14:35:55.000
14:36:00.000
14:36:05.000
14:36:10.000

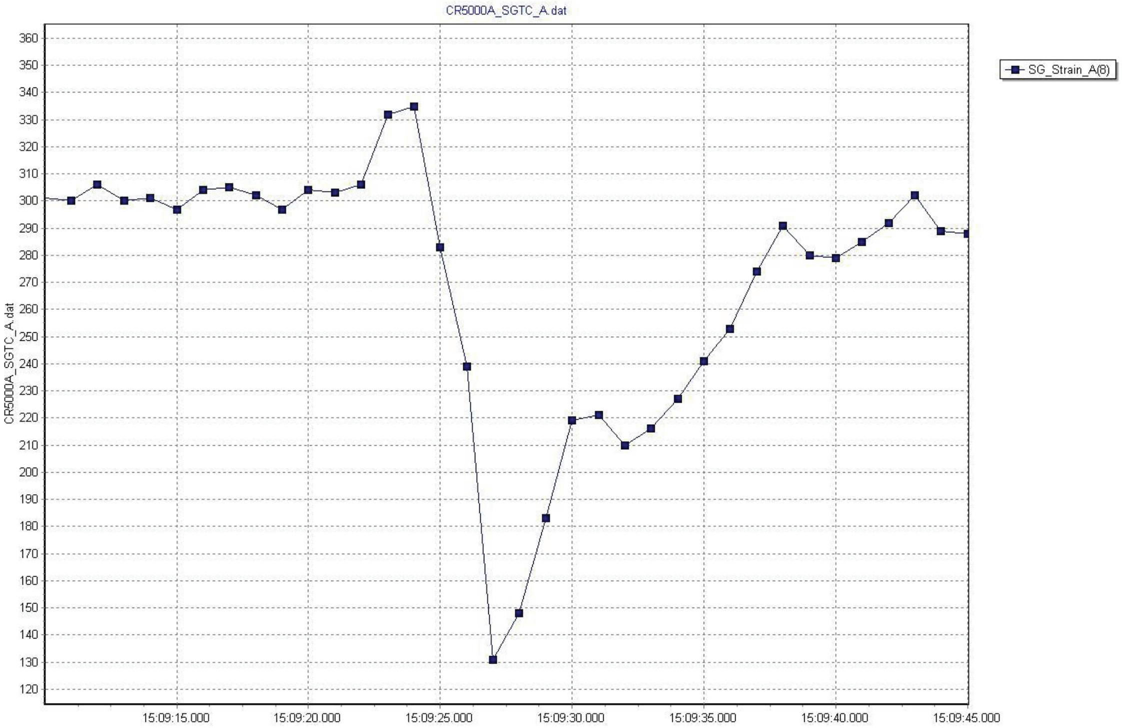
CR5000A_SGTC_A.dat
SG_Strain_A(8)
CR5000A_SGTC_A.dat
360
350
340
330
320
310
300
290
280
270
260
250
240
230
220
210
200
190
180
170
160
150
140
130
120
15:09:15.000
15:09:20.000
15:09:25.000
15:09:30.000
15:09:35.000
15:09:40.000
15:09:45.000

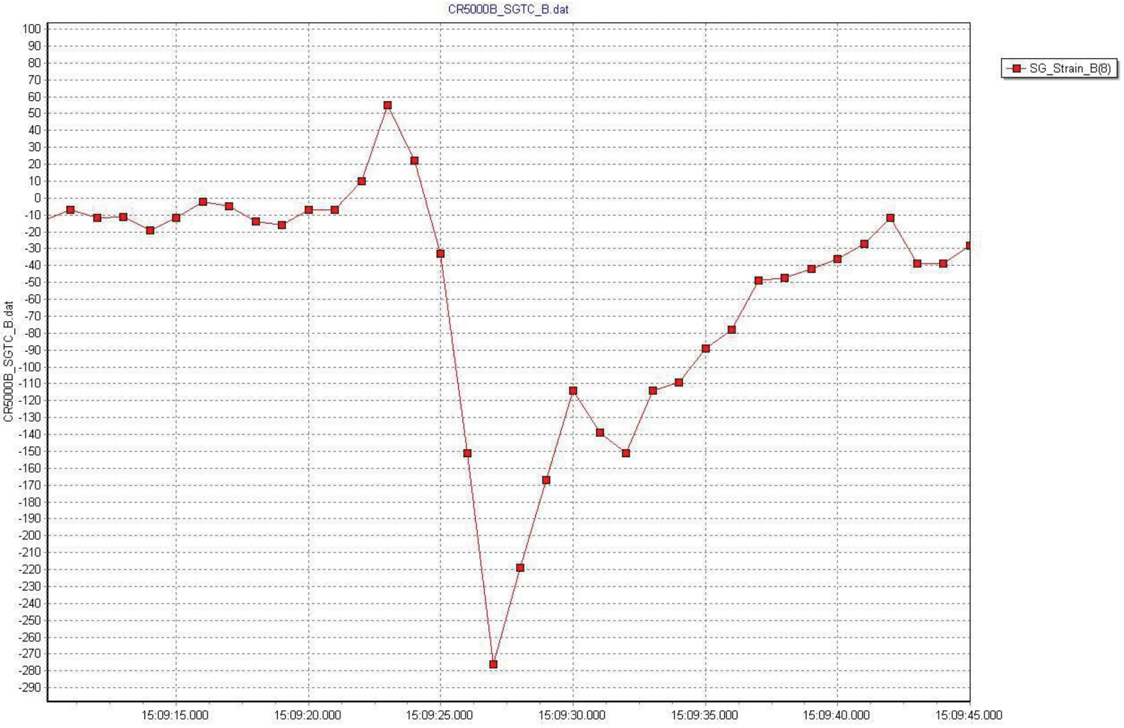
CR5000B_SGTC_B.dat
SG_Strain_B(8)
CR5000B_SGTC_B.dat
100
90
80
70
60
50
40
30
20
10
0
-10
-20
-30
-40
-50
-60
-70
-80
-90
-100
-110
-120
-130
-140
-150
-160
-170
-180
-190
-200
-210
-220
-230
-240
-250
-260
-270
-280
-290
15:09:15.000
15:09:20.000
15:09:25.000
15:09:30.000
15:09:35.000
15:09:40.000
15:09:45.000

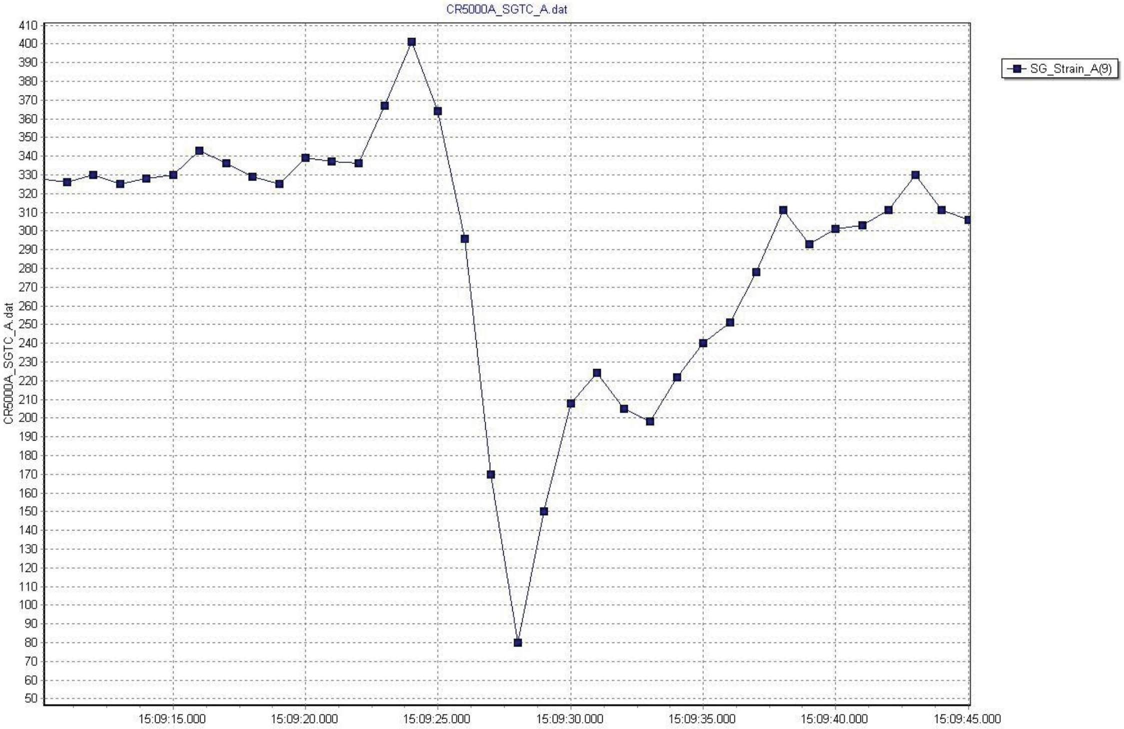
CR5000A_SGTC_A.dat
SG_Strain_A(9)
CR5000A_SGTC_A.dat
410
400
390
380
370
360
350
340
330
320
310
300
290
280
270
260
250
240
230
220
210
200
190
180
170
160
150
140
130
120
110
100
90
80
70
60
50
15:09:15.000
15:09:20.000
15:09:25.000
15:09:30.000
15:09:35.000
15:09:40.000
15:09:45.000

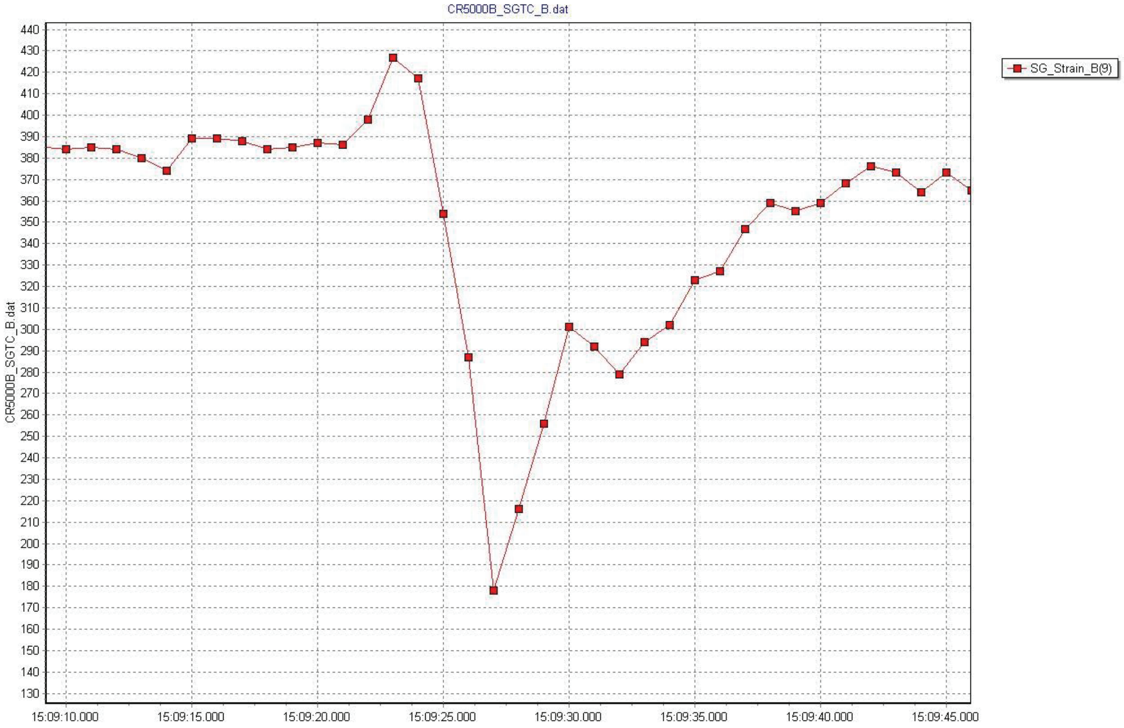
CR5000B_SGTC_B.dat
SG_Strain_B(9)
CR5000B_SGTC_B.dat
440
430
420
410
400
390
380
370
360
350
340
330
320
310
300
290
280
270
260
250
240
230
220
210
200
190
180
170
160
150
140
130
15:09:10.000
15:09:15.000
15:09:20.000
15:09:25.000
15:09:30.000
15:09:35.000
15:09:40.000
15:09:45.000

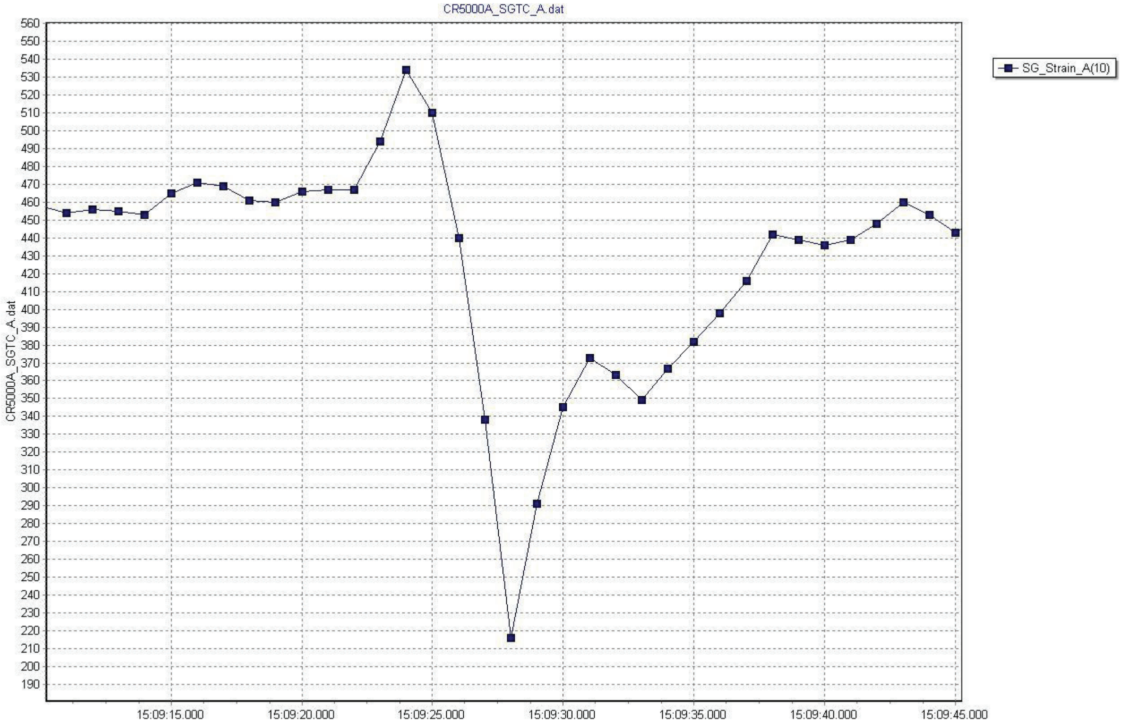
CR5000A_SGTC_A.dat
CR5000A_SGTC_A.dat
SG_Strain_A(10)
560
550
540
530
520
510
500
490
480
470
460
450
440
430
420
410
400
390
380
370
360
350
340
330
320
310
300
290
280
270
260
250
240
230
220
210
200
190
15:09:15.000
15:09:20.000
15:09:25.000
15:09:30.000
15:09:35.000
15:09:40.000
15:09:45.000

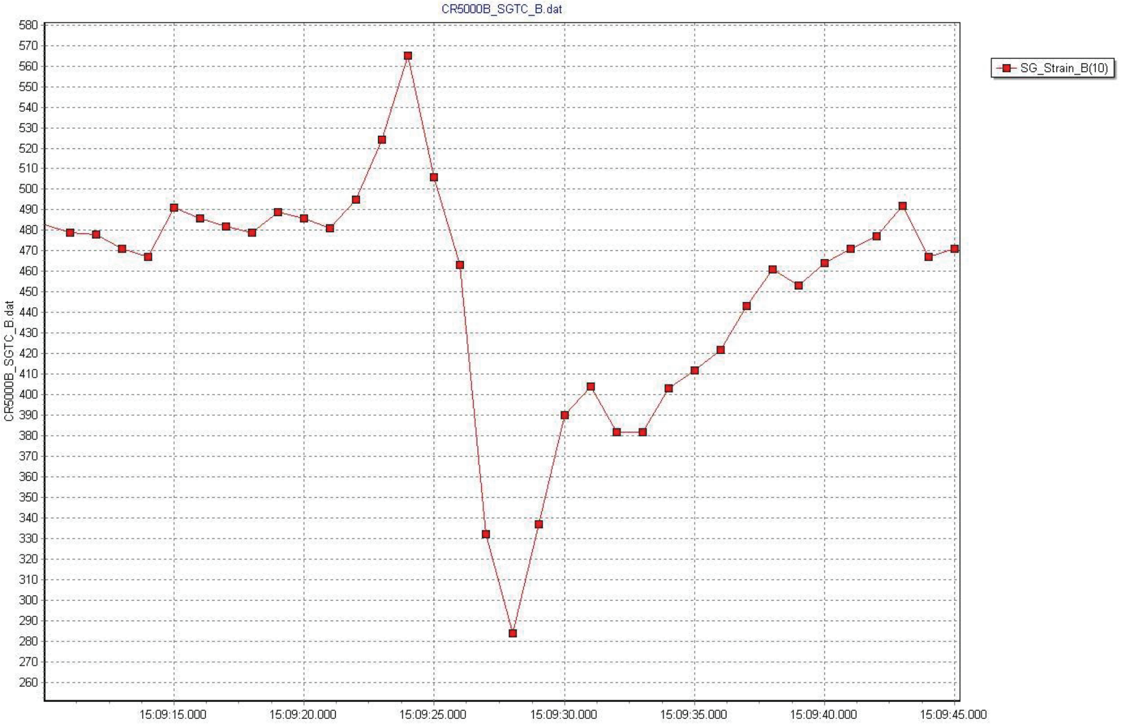
CR5000B_SGTC_B.dat
CR5000B_SGTC_B.dat
SG_Strain_B(10)
580
570
560
550
540
530
520
510
500
490
480
470
460
450
440
430
420
410
400
390
380
370
360
350
340
330
320
310
300
290
280
270
260
15:09:15.000
15:09:20.000
15:09:25.000
15:09:30.000
15:09:35.000
15:09:40.000
15:09:45.000

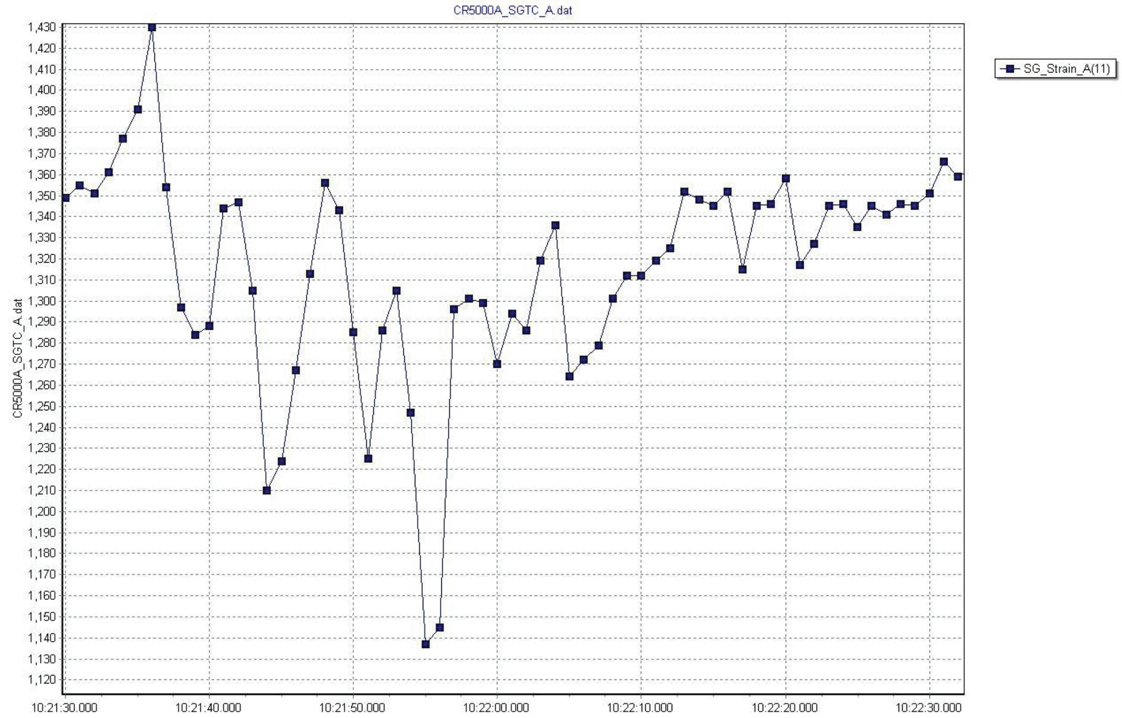
CR5000A_SGTC_A.dat
CR5000A_SGTC_A.dat
1,430
1,420
1,410
1,400
1,390
1,380
1,370
1,360
1,350
1,340
1,330
1,320
1,310
1,300
1,290
1,280
1,270
1,260
1,250
1,240
1,230
1,220
1,210
1,200
1,190
1,180
1,170
1,160
1,150
1,140
1,130
1,120
10:21:30.000
10:21:40.000
10:21:50.000
10:22:00.000
10:22:10.000
10:22:20.000
10:22:30.000
SG_Strain_A(11)

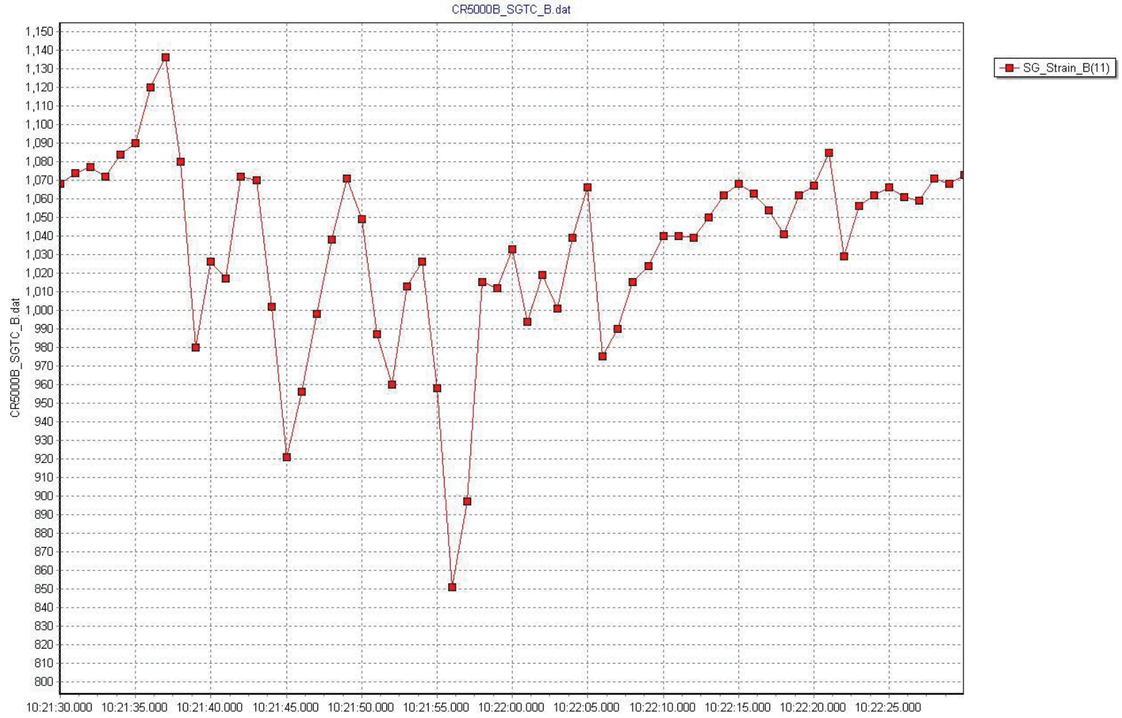
CR5000B_SGTC_B.dat
CR5000B_SGTC_B.dat
1,150
1,140
1,130
1,120
1,110
1,100
1,090
1,080
1,070
1,060
1,050
1,040
1,030
1,020
1,010
1,000
990
980
970
960
950
940
930
920
910
900
890
880
870
860
850
840
830
820
810
800
10:21:30.000
10:21:35.000
10:21:40.000
10:21:45.000
10:21:50.000
10:21:55.000
10:22:00.000
10:22:05.000
10:22:10.000
10:22:15.000
10:22:20.000
10:22:25.000
SG_Strain_B(11)

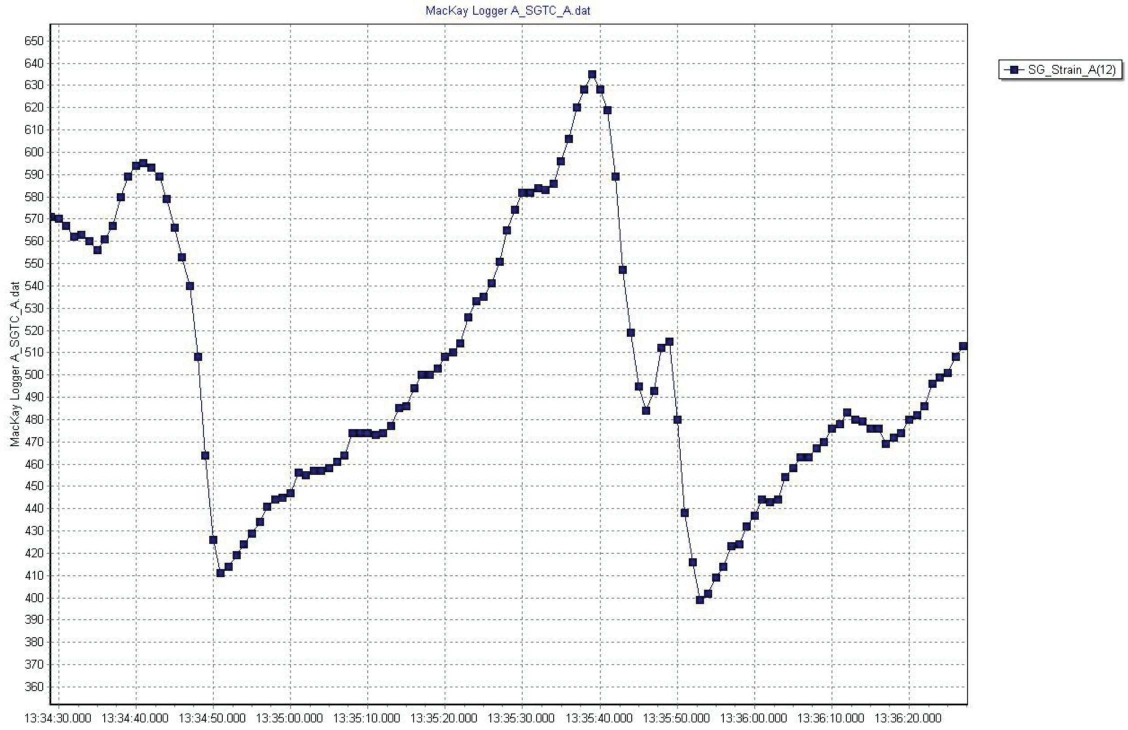
MacKay Logger A_SGTC_A.dat
MacKay Logger A_SGTC_A.dat
SG_Strain_A(12)
650
640
630
620
610
600
590
580
570
560
550
540
530
520
510
500
490
480
470
460
450
440
430
420
410
400
390
380
370
360
13:34:30.000
13:34:40.000
13:34:50.000
13:35:00.000
13:35:10.000
13:35:20.000
13:35:30.000
13:35:40.000
13:35:50.000
13:36:00.000
13:36:10.000
13:36:20.000

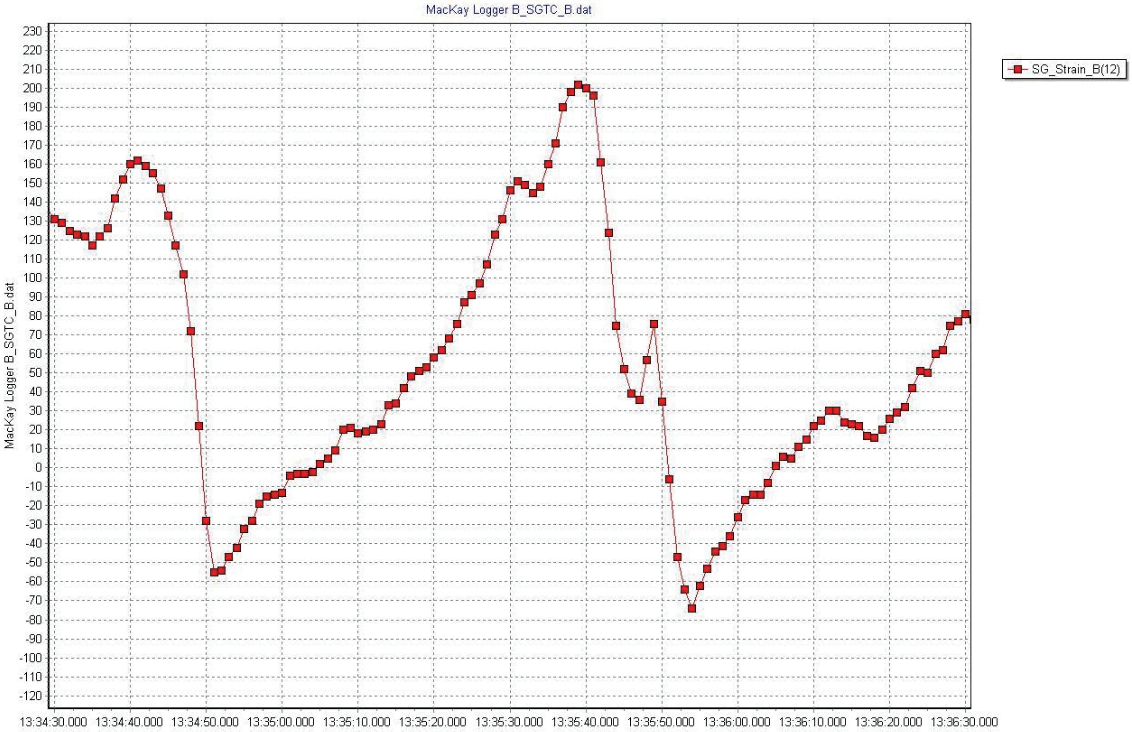
MacKay Logger B_SGTC_B.dat
MacKay Logger B_SGTC_B.dat
SG_Strain_B(12)
230
220
210
200
190
180
170
160
150
140
130
120
110
100
90
80
70
60
50
40
30
20
10
0
-10
-20
-30
-40
-50
-60
-70
-80
-90
-100
-110
-120
13:34:30.000
13:34:40.000
13:34:50.000
13:35:00.000
13:35:10.000
13:35:20.000
13:35:30.000
13:35:40.000
13:35:50.000
13:36:00.000
13:36:10.000
13:36:20.000
13:36:30.000

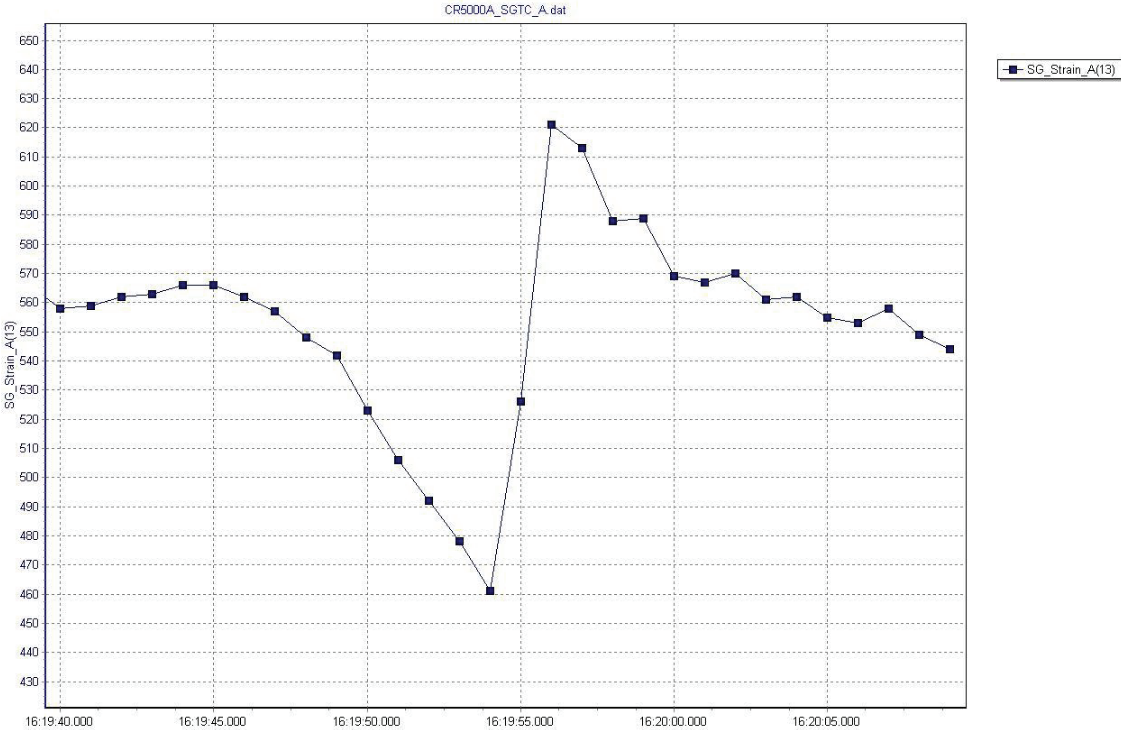
CR5000A_SGTC_A.dat
SG_Strain_A(13)
SG_Strain_A(13)
650
640
630
620
610
600
590
580
570
560
550
540
530
520
510
500
490
480
470
460
450
440
430
16:19:40.000
16:19:45.000
16:19:50.000
16:19:55.000
16:20:00.000
16:20:05.000

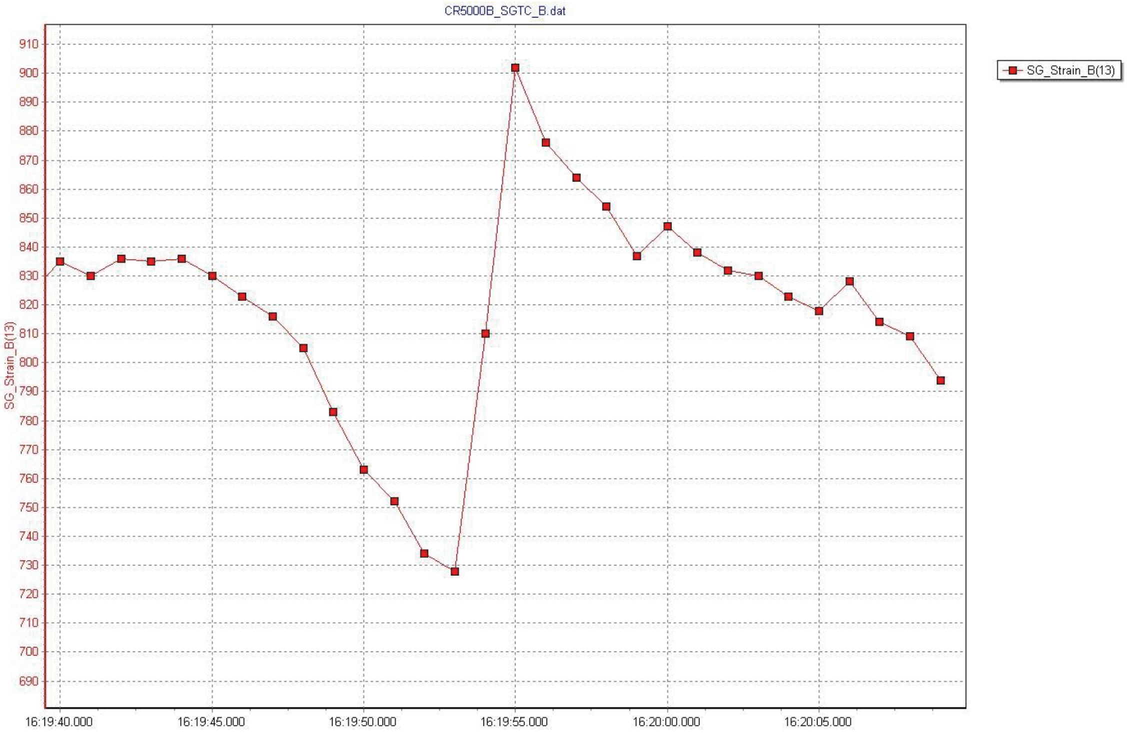
CR5000B_SGTC_B.dat
SG_Strain_B(13)
SG_Strain_B(13)
910
900
890
880
870
860
850
840
830
820
810
800
790
780
770
760
750
740
730
720
710
700
690
16:19:40.000
16:19:45.000
16:19:50.000
16:19:55.000
16:20:00.000
16:20:05.000

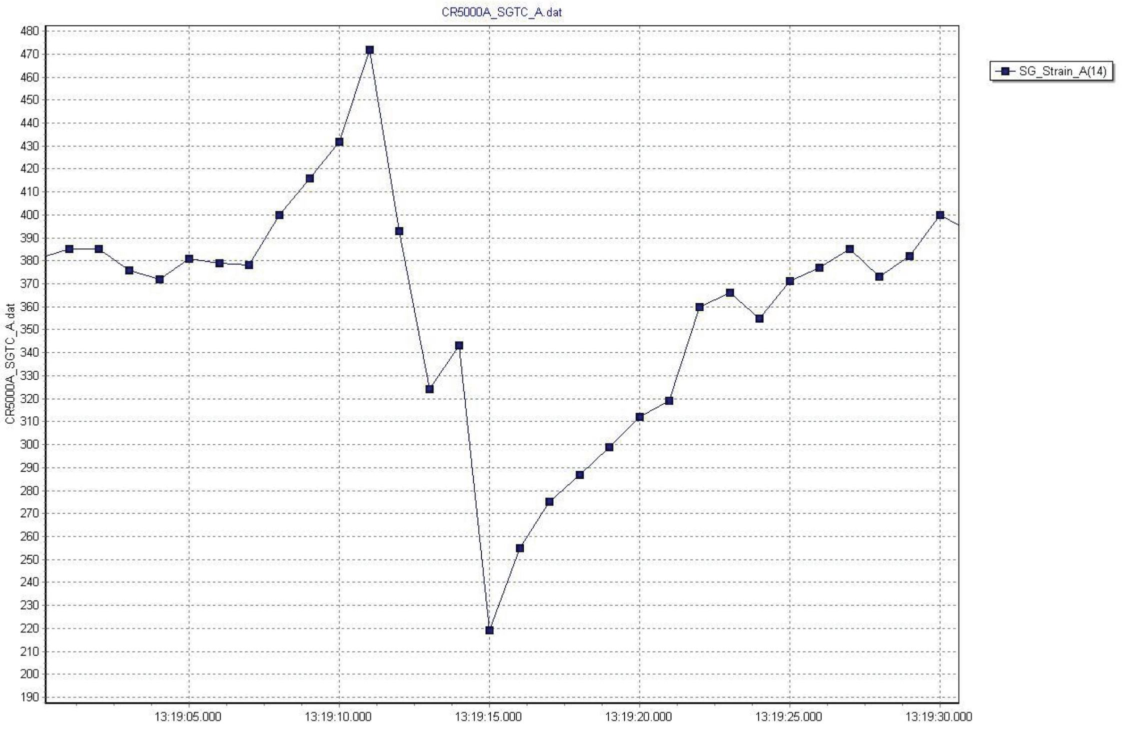
CR5000A_SGTC_A.dat
SG_Strain_A(14)
CR5000A_SGTC_A.dat
480
470
460
450
440
430
420
410
400
390
380
370
360
350
340
330
320
310
300
290
280
270
260
250
240
230
220
210
200
190
13:19:05.000
13:19:10.000
13:19:15.000
13:19:20.000
13:19:25.000
13:19:30.000

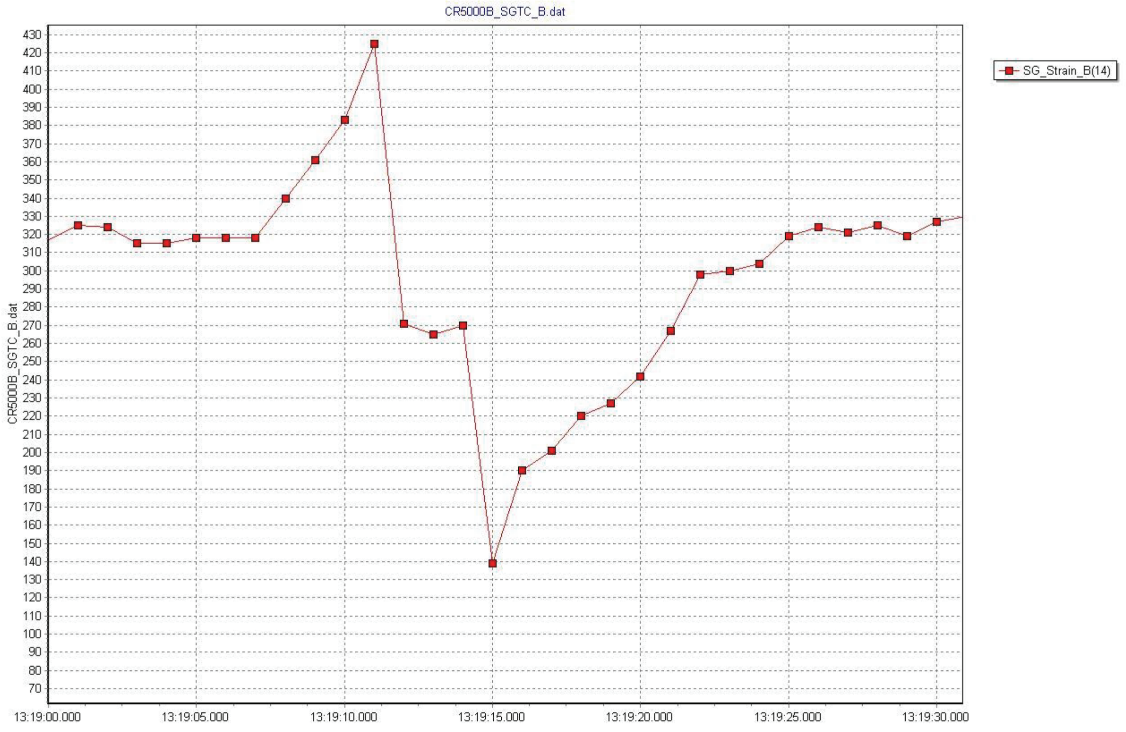
CR5000B_SGTC_B.dat
SG_Strain_B(14)
CR5000B_SGTC_B.dat
430
420
410
400
390
380
370
360
350
340
330
320
310
300
290
280
270
260
250
240
230
220
210
200
190
180
170
160
150
140
130
120
110
100
90
80
70
13:19:00.000
13:19:05.000
13:19:10.000
13:19:15.000
13:19:20.000
13:19:25.000
13:19:30.000

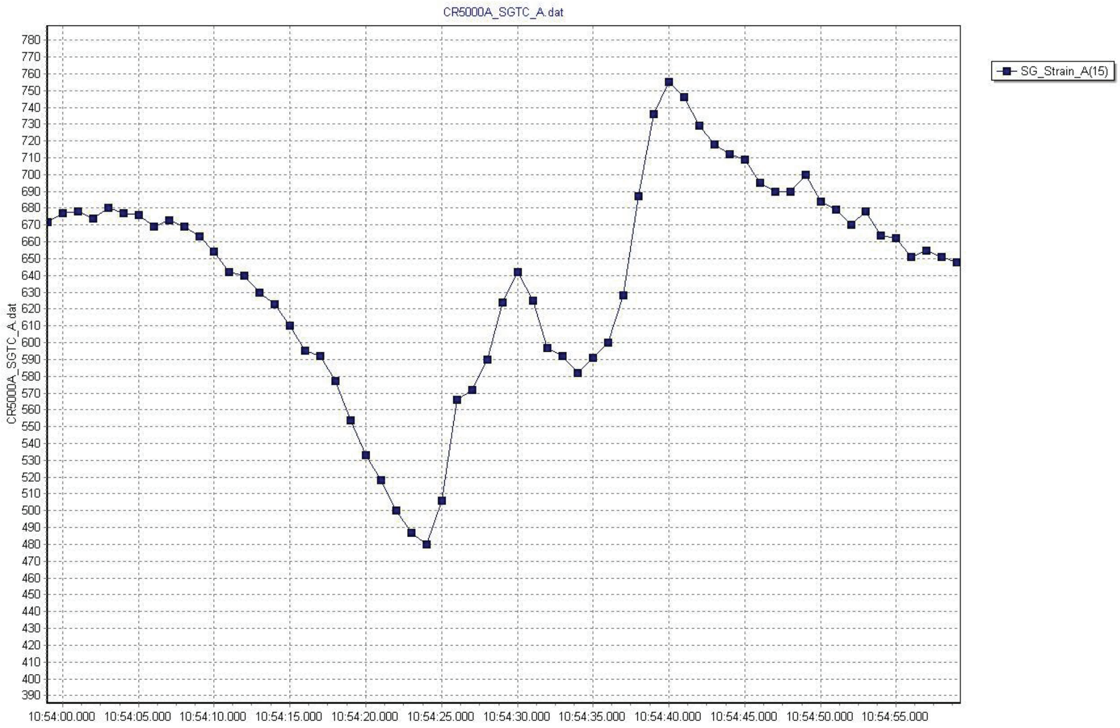
CR5000A_SGTC_A.dat
CR5000A_SGTC_A.dat
SG_Strain_A(15)
780
770
760
750
740
730
720
710
700
690
680
670
660
650
640
630
620
610
600
590
580
570
560
550
540
530
520
510
500
490
480
470
460
450
440
430
420
410
400
390
10:54:00.000
10:54:05.000
10:54:10.000
10:54:15.000
10:54:20.000
10:54:25.000
10:54:30.000
10:54:35.000
10:54:40.000
10:54:45.000
10:54:50.000
10:54:55.000

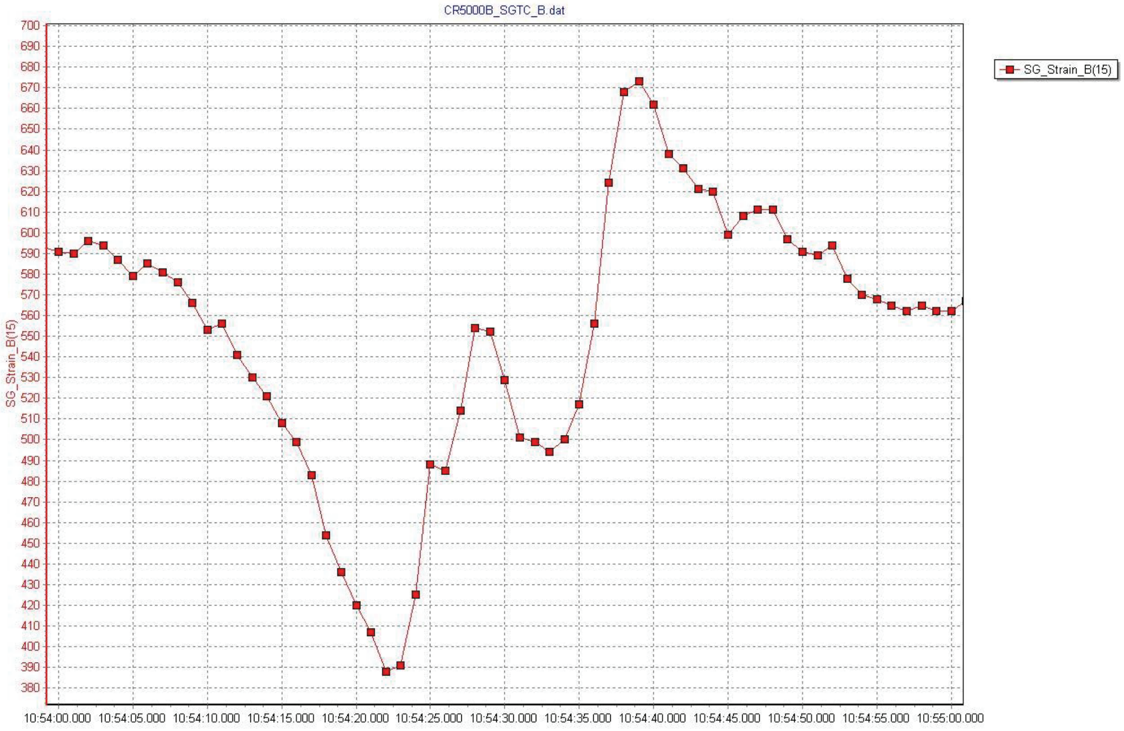
CR5000B_SGTC_B.dat
SG_Strain_B(15)
SG_Strain_B(15)
700
690
680
670
660
650
640
630
620
610
600
590
580
570
560
550
540
530
520
510
500
490
480
470
460
450
440
430
420
410
400
390
380
10:54:00.000
10:54:05.000
10:54:10.000
10:54:15.000
10:54:20.000
10:54:25.000
10:54:30.000
10:54:35.000
10:54:40.000
10:54:45.000
10:54:50.000
10:54:55.000
10:55:00.000

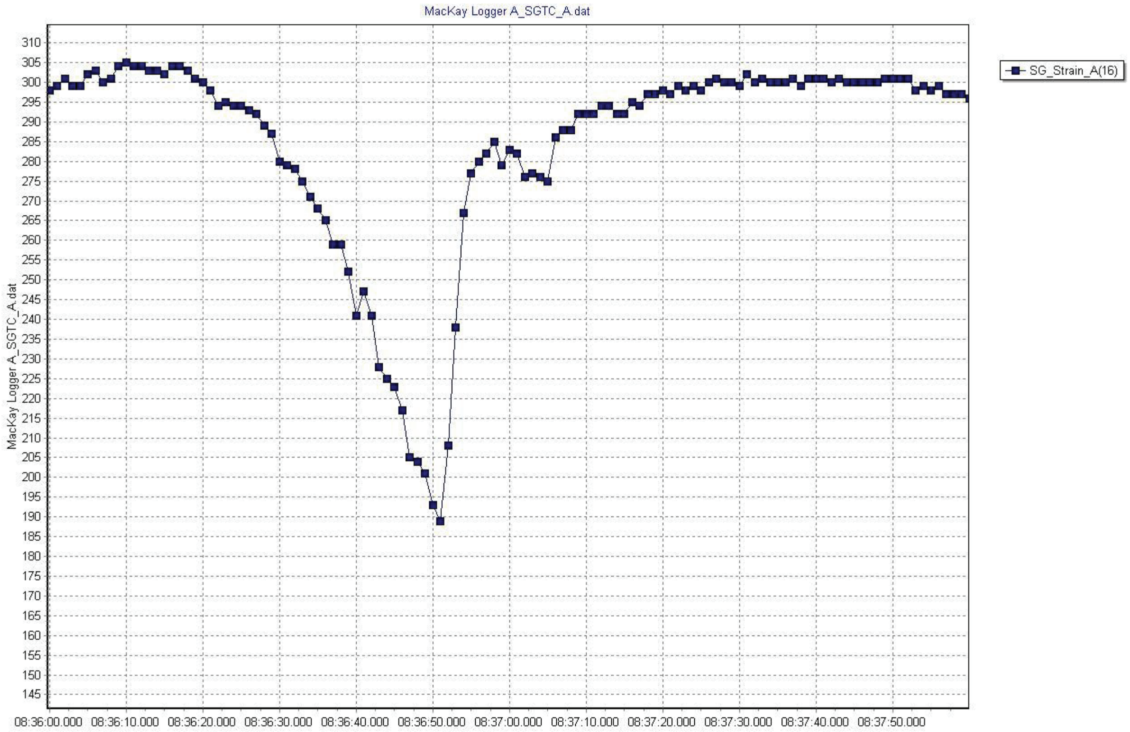
MacKay Logger A_SGTC_A.dat
MacKay Logger A_SGTC_A.dat
SG_Strain_A(16)
310
305
300
295
290
285
280
275
270
265
260
255
250
245
240
235
230
225
220
215
210
205
200
195
190
185
180
175
170
165
160
155
150
145
08:36:00.000
08:36:10.000
08:36:20.000
08:36:30.000
08:36:40.000
08:36:50.000
08:37:00.000
08:37:10.000
08:37:20.000
08:37:30.000
08:37:40.000
08:37:50.000

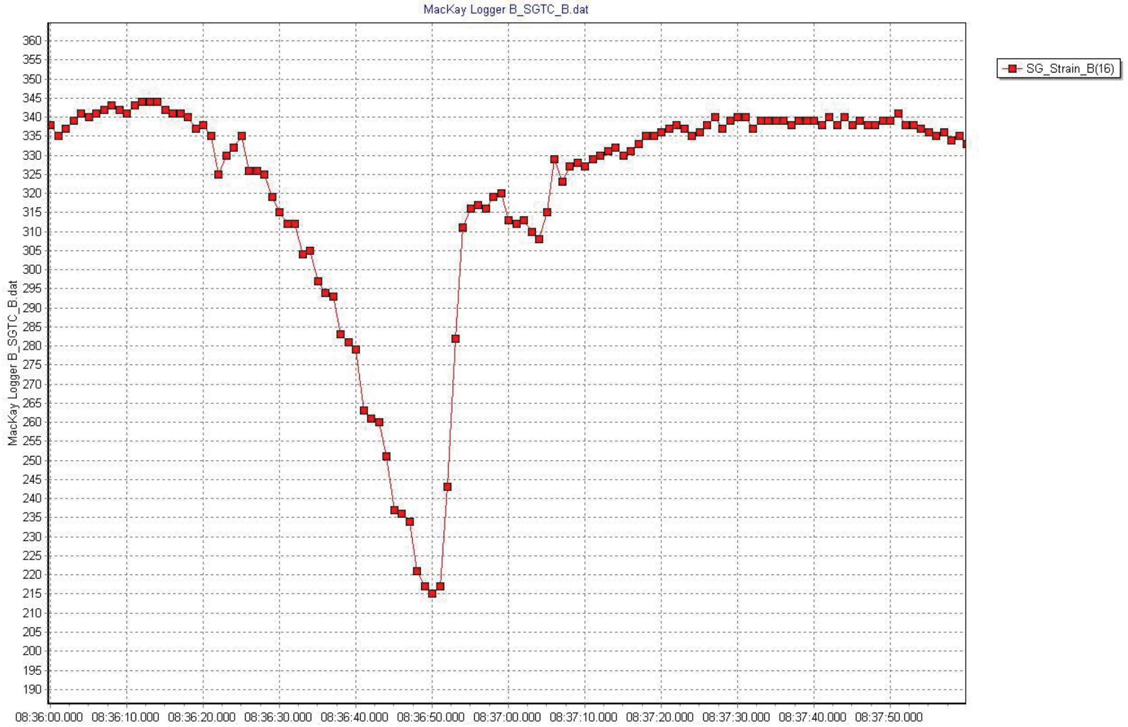
MacKay Logger B_SGTC_B.dat
MacKay Logger B_SGTC_B.dat
SG_Strain_B(16)
360
355
350
345
340
335
330
325
320
315
310
305
300
295
290
285
280
275
270
265
260
255
250
245
240
235
230
225
220
215
210
205
200
195
190
08:36:00.000
08:36:10.000
08:36:20.000
08:36:30.000
08:36:40.000
08:36:50.000
08:37:00.000
08:37:10.000
08:37:20.000
08:37:30.000
08:37:40.000
08:37:50.000

Appendix VI – Influence Zones From Calibration Test Data

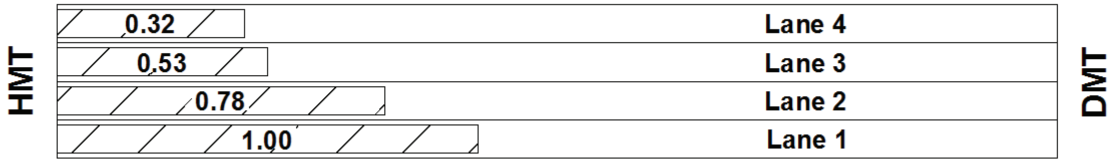

Diagonal #1

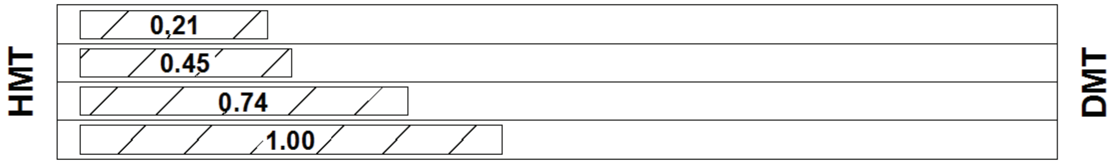

Diagonal #2

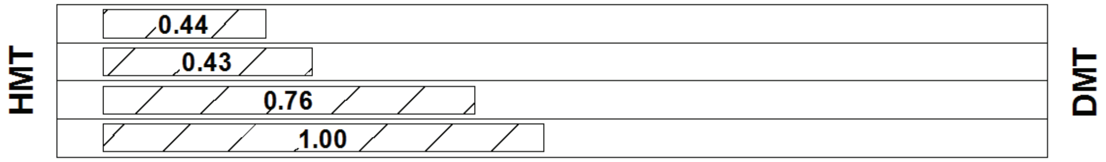

Diagonal #3

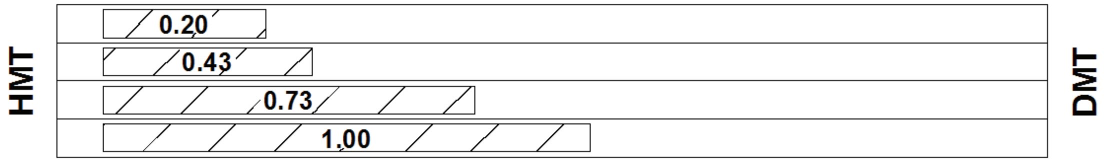

Diagonal #4

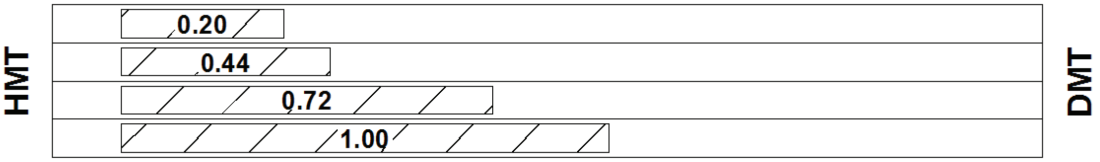

Diagonal #5

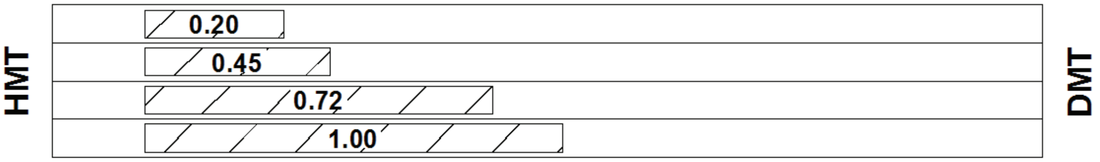

Diagonal #6

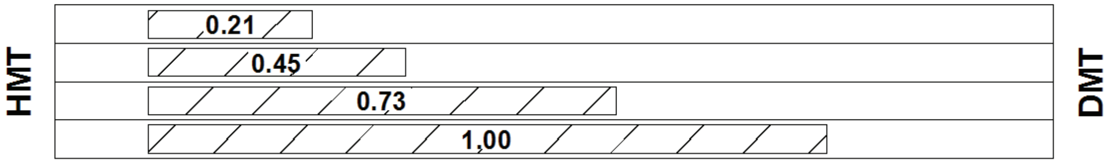

Diagonal #7

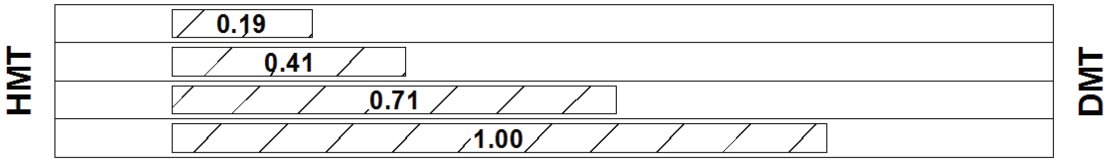

Diagonal #8

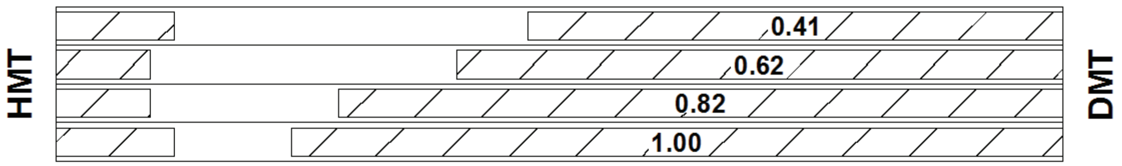

Diagonal #9

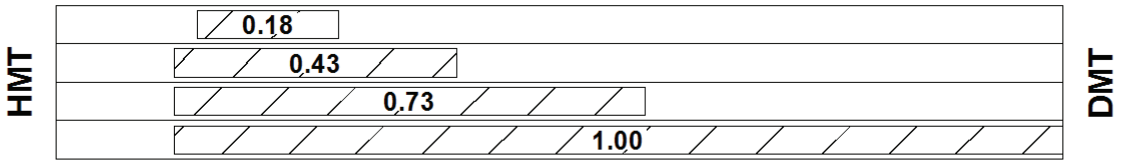

Diagonal #10

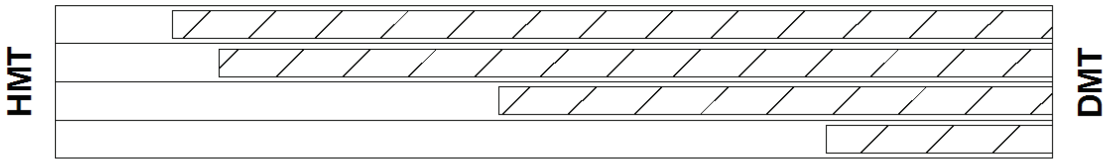

Diagonal #11

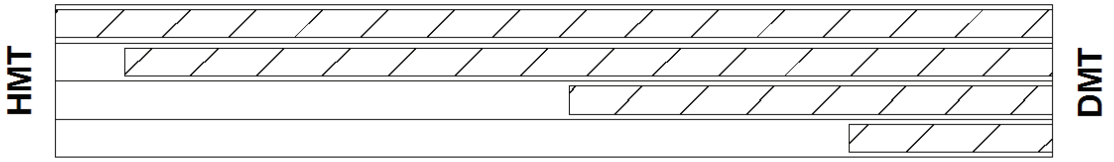

Diagonal #12

Appendix VII – Summary of Detailed Calculations for CHBDC Live Load

CHBDC Lane Load	9.0 kN/m
CHBDC CL-625 Truck	625 kN
CHBDC Live Load factor	1.0 (unfactored)

Number of lanes loaded	Multilane Modification Factor
1	1.00
2	0.90
3	0.80
4	0.70
5	0.60
6 or more	0.55

Calibration Truck	569 kN
Weldable Gauge Type Correction Factor	1.11 (1/0.90)

	Recorded Peak Calibration Strain (με)				Calculated Area Under Curve (με·m)			
	Lane 1	**Lane 2**	**Lane 3**	**Lane 4**	**Lane 1**	**Lane 2**	**Lane 3**	**Lane 4**
Diagonal #1	-140	-115.0	-75.0	-50.0	-7850	-5788	-2988	-1913
Diagonal #2	-155	-115.0	-75.0	-40.0	-8425	-5975	-2938	-1588
Diagonal #3	-155	-115.0	-70.0	-40.0	-9100	-6213	-2800	-1375
Diagonal #4	-150	-110.0	-70.0	-35.0	-9550	-6325	-2738	-1225
Diagonal #5	-155	-115.0	-75.0	-35.0	-9075	-6175	-2513	-1313
Diagonal #6	-150	-110.0	-70.0	-40.0	-8313	-5725	-2625	-1625
Diagonal #7	-140	-100.0	-65.0	-30.0	-8975	-6125	-2525	-1275
Diagonal #8	-140	-105.0	-65.0	-30.0	-9013	-6063	-2425	-1238
Diagonal #9	-85	-70.0	-60.0	-40.0	-3310	-3619	-5699	-7195
Diagonal #10	-145	-105.0	-70.0	-35.0	-10085	-6425	-3063	-1313
Diagonal #11	-5	-10.0	-40.0	-85.0	-243	-1368	-8148	-16681
Diagonal #12	-5	-5.0	-30.0	-90.0	-218	-518	-6926	-17773

Apply GTCF and normalize based on calibration truck

	Normalized Peak Calibration Strain (με/kN)				Normalized Area Under Curve (με·m/kN)			
	Lane 1	Lane 2	Lane 3	Lane 4	Lane 1	Lane 2	Lane 3	Lane 4
Diagonal #1	-0.273	-0.225	-0.146	-0.098	-15.329	-11.302	-5.835	-3.736
Diagonal #2	-0.303	-0.225	-0.146	-0.078	-16.452	-11.668	-5.737	-3.101
Diagonal #3	-0.303	-0.225	-0.137	-0.078	-17.770	-12.132	-5.468	-2.685
Diagonal #4	-0.293	-0.215	-0.137	-0.068	-18.649	-12.351	-5.347	-2.392
Diagonal #5	-0.303	-0.225	-0.146	-0.068	-17.721	-12.058	-4.907	-2.564
Diagonal #6	-0.293	-0.215	-0.137	-0.078	-16.233	-11.179	-5.126	-3.173
Diagonal #7	-0.273	-0.195	-0.127	-0.059	-17.526	-11.961	-4.931	-2.490
Diagonal #8	-0.273	-0.205	-0.127	-0.059	-17.600	-11.839	-4.735	-2.417
Diagonal #9	-0.166	-0.137	-0.117	-0.078	-6.464	-7.067	-11.129	-14.050
Diagonal #10	-0.283	-0.205	-0.137	-0.068	-19.693	-12.546	-5.981	-2.564
Diagonal #11	-0.010	-0.020	-0.078	-0.166	-0.475	-2.671	-15.911	-32.574
Diagonal #12	-0.010	-0.010	-0.059	-0.176	-0.426	-1.012	-13.525	-34.706

Apply Unfactored Lane Load to Normalized Area Under Curve, and Unfactored CHBDC Truck Load Normalized Peak Calibration Strain. Try various lane combinations to achieve greatest load for each diagonal.

	1 Lane	2 Lanes	3 Lanes	4 Lanes
Diagonal #1	-275	-440	-492	-488
Diagonal #2	-299	-465	-513	-496
Diagonal #3	-311	-479	-520	-499
Diagonal #4	-314	-480	-519	-494
Diagonal #5	-311	-478	-519	-494
Diagonal #6	-293	-451	-492	-478
Diagonal #7	-294	-450	-486	-461
Diagonal #8	-295	-454	-488	-463
Diagonal #9	-141	-246	-345	-418
	-166	-292	-365	-418
Diagonal #10	-319	-481	-525	-500
Diagonal #11	-376	-503	-474	-421
Diagonal #12	-400	-496	-452	-402

Appendix VIII – Gumbel Probability Plots

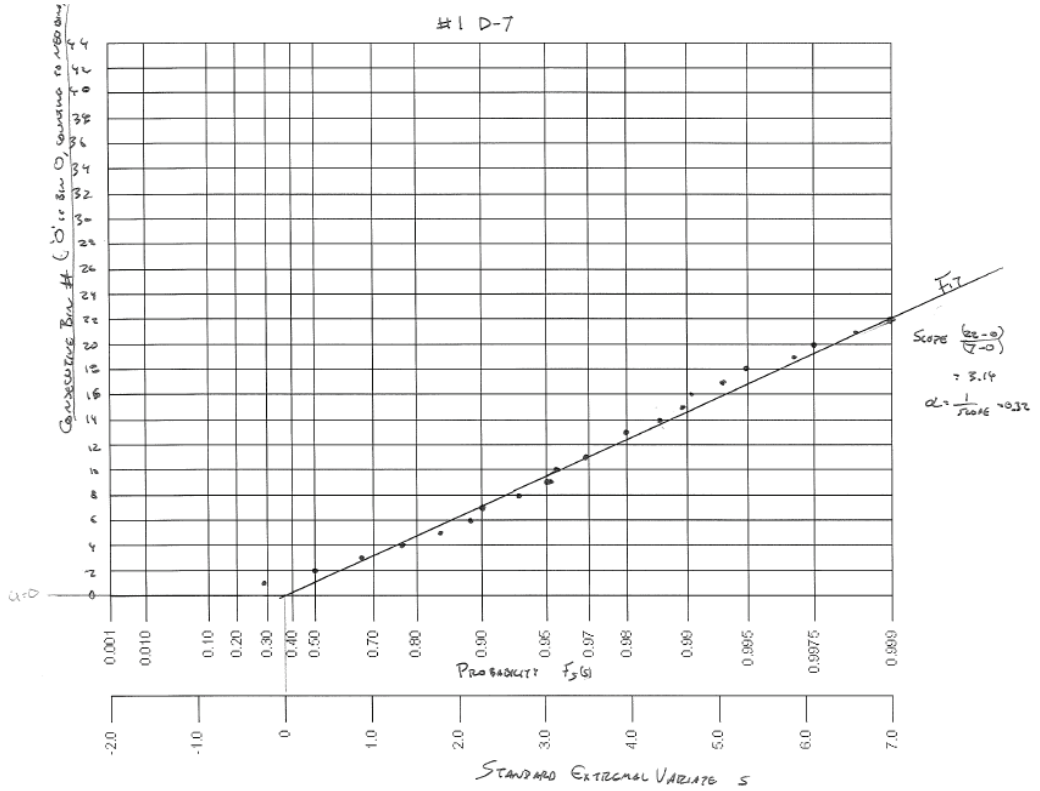

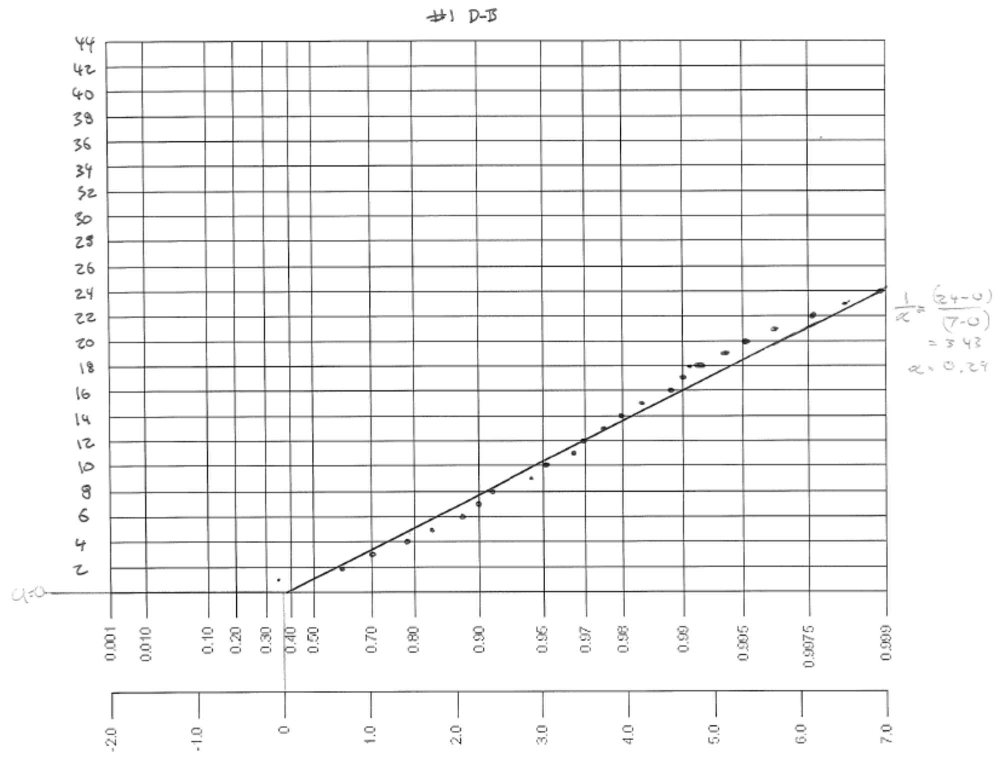

#2 D-T

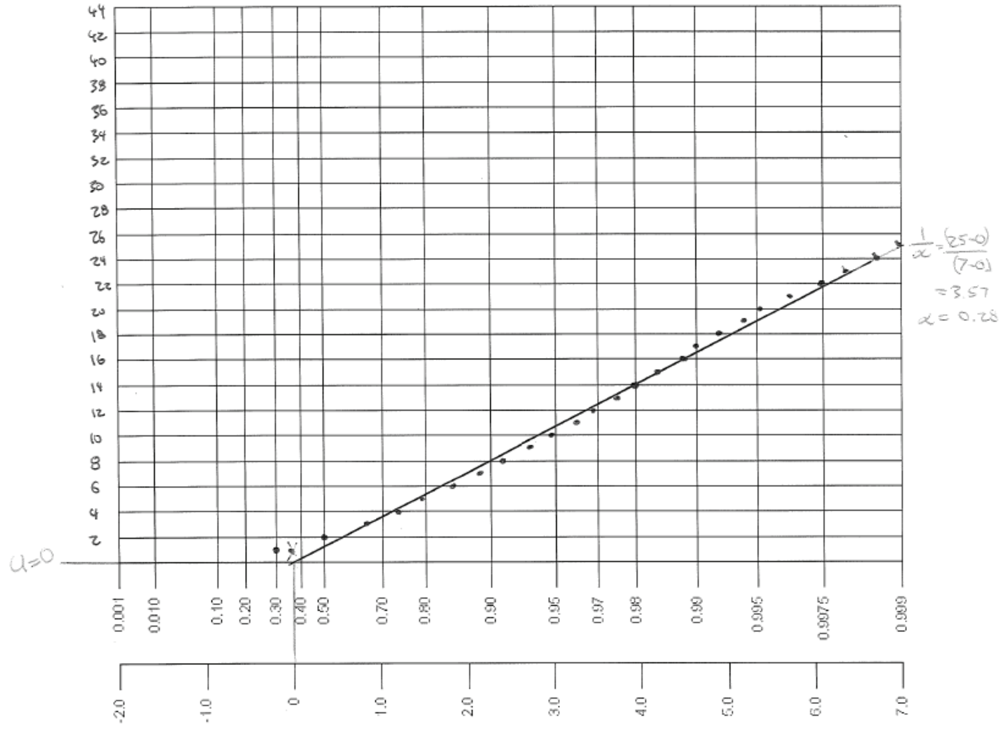
44
42
40
38
36
34
32
30
28
26
24
22
20
18
16
14
12
10
8
6
4
2
u=0
0.001
0.010
0.10
0.20
0.30
0.40
0.50
0.70
0.80
0.90
0.95
0.97
0.98
0.99
0.995
0.9975
0.999
-2.0
-1.0
0
1.0
2.0
3.0
4.0
5.0
6.0
7.0
$\frac{1}{\alpha}=\frac{(25-0)}{(7-0)}$
$=3.57$
$\alpha=0.28$

#2 D-B

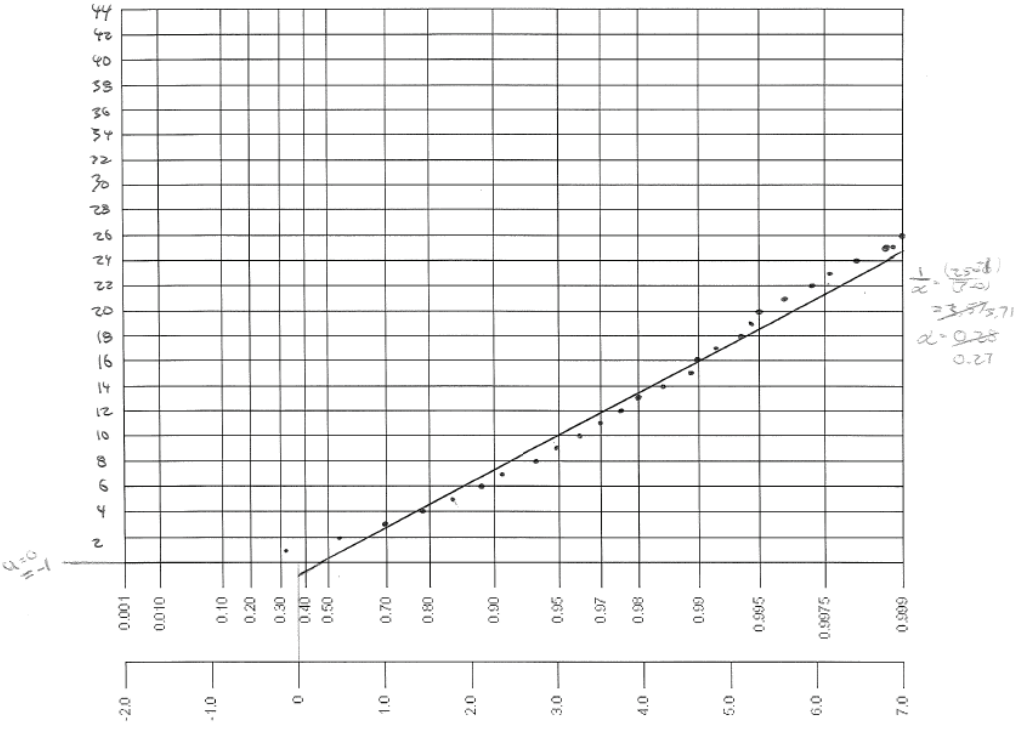
44
42
40
38
36
34
32
30
28
26
24
22
20
18
16
14
12
10
8
6
4
2
u=0
=-1
0.001
0.010
0.10
0.20
0.30
0.40
0.50
0.70
0.80
0.90
0.95
0.97
0.98
0.99
0.995
0.9975
0.999
-2.0
-1.0
0
1.0
2.0
3.0
4.0
5.0
6.0
7.0
$\frac{1}{\alpha}=\frac{(25+1)}{(7-0)}$
$=$ ~~3.57~~ 3.71
$\alpha=$ ~~0.28~~
0.27

#3 D-T

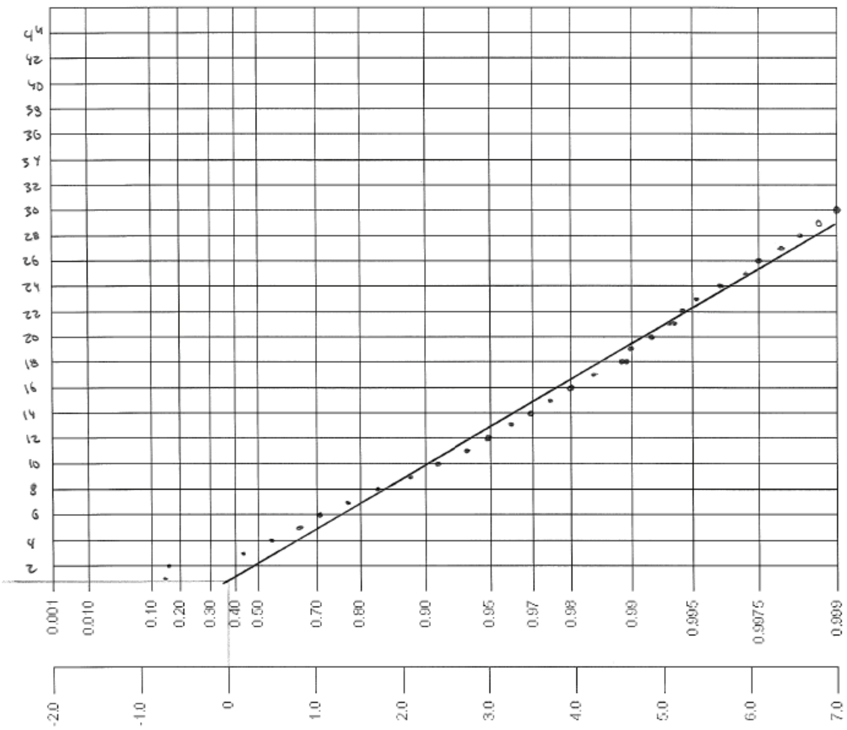

$\frac{1}{\alpha} = \frac{(29-1)}{(7-0)}$

$= 4$

$\alpha = 0.25$

u=1

#3 D-B

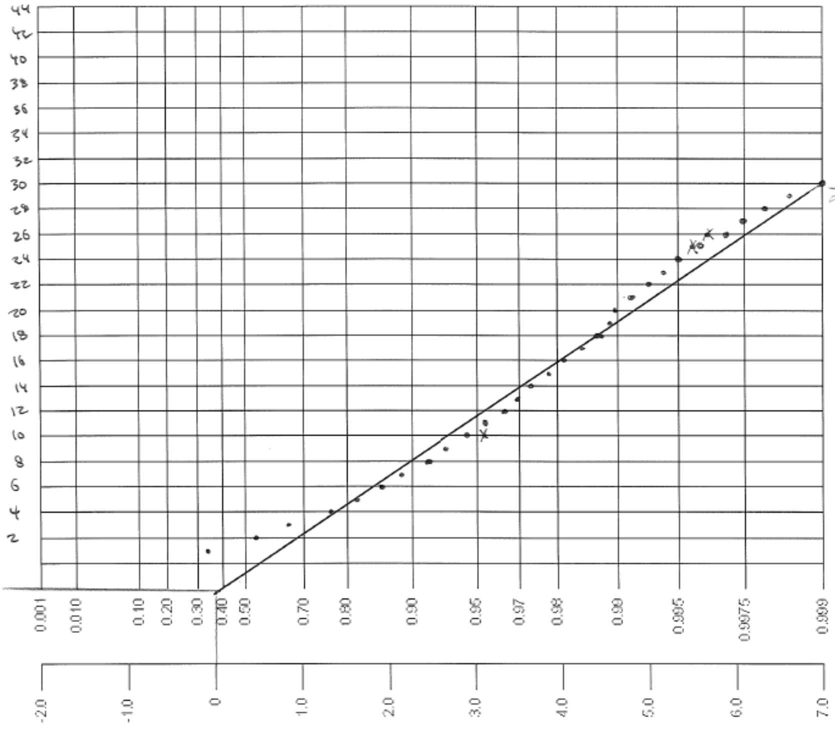

$\frac{1}{\alpha} = \frac{(30-2)}{(7-0)}$

$= 4.57$

$\alpha = 0.22$

u=2

#4D-T

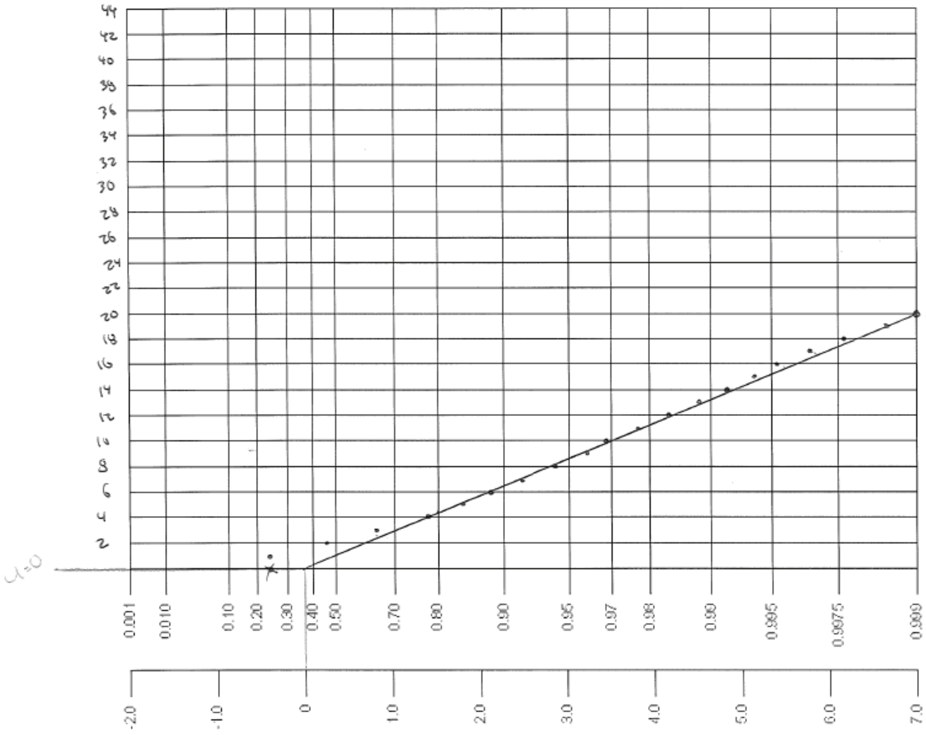

$\frac{1}{\alpha} = \frac{(20-0)}{(7-0)}$

$= 2.86$

$\alpha = 0.35$

#4D-B

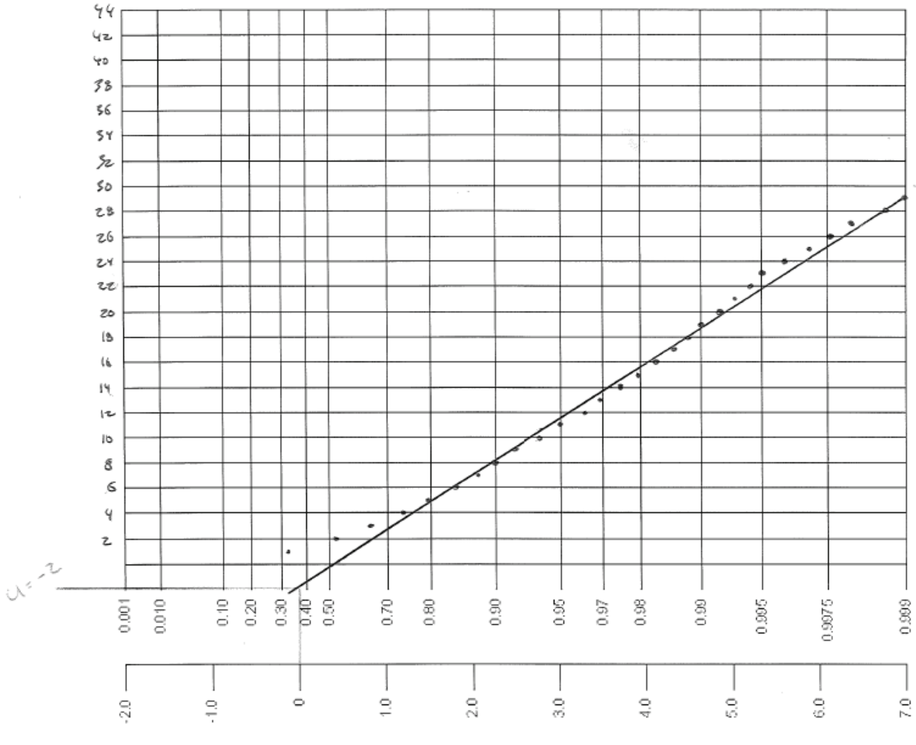

$\frac{1}{\alpha} = \frac{(29 - -2)}{(7-0)}$

$= 4.43$

$\alpha = 0.23$

#5 D-T

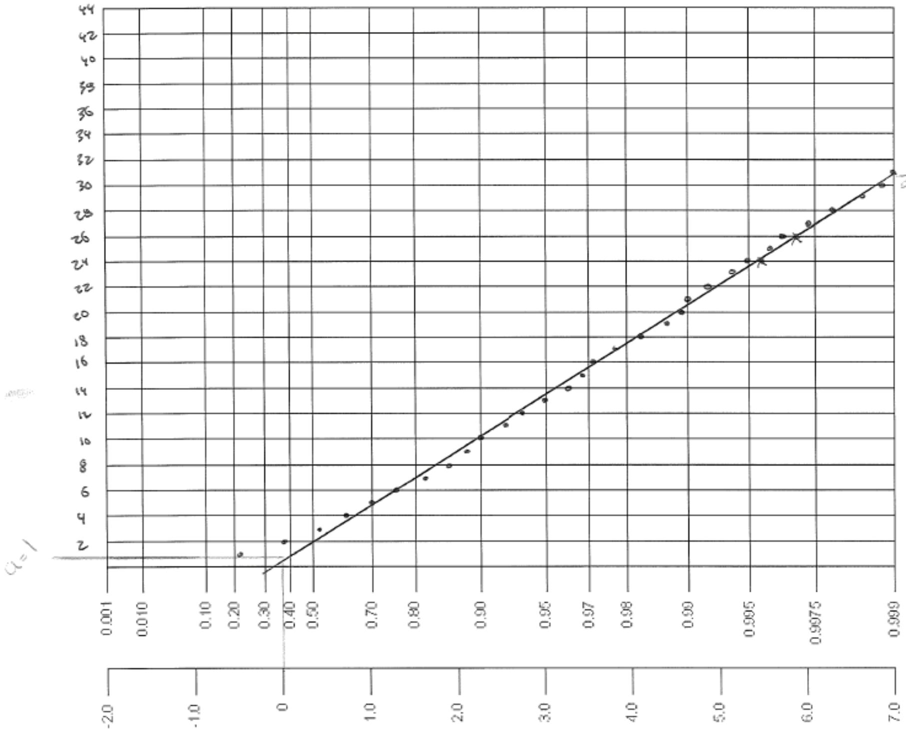

$\frac{1}{\alpha} = \frac{(31-1)}{(7-0)}$

$= 4.29$

$\alpha = 0.23$

#5D-B

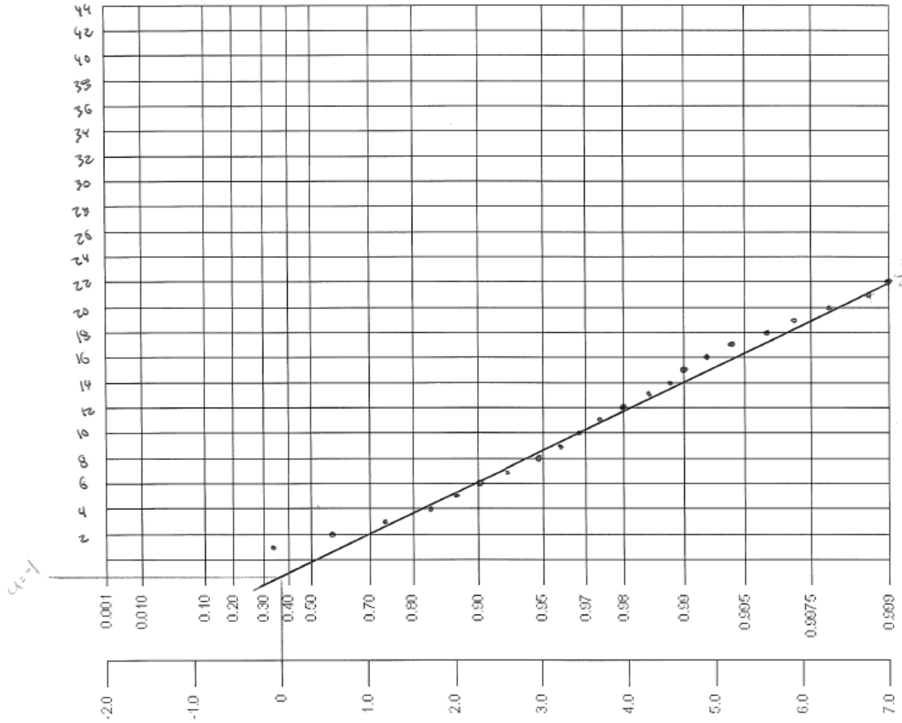

$\frac{1}{\alpha} = \frac{(22 - -1)}{(7-0)}$

$= 3.29$

$\alpha = 0.30$

#6. D-T

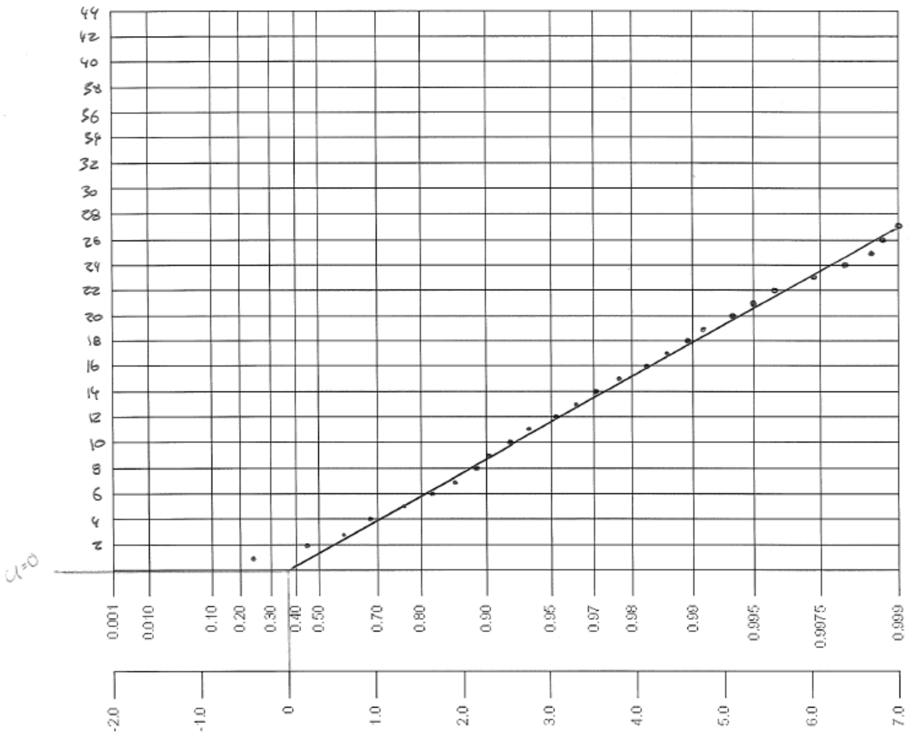

$\frac{1}{\alpha} = \frac{(25-0)}{(7-0)}$

$= 3.57$

$\alpha = 0.28$

#6 D-B

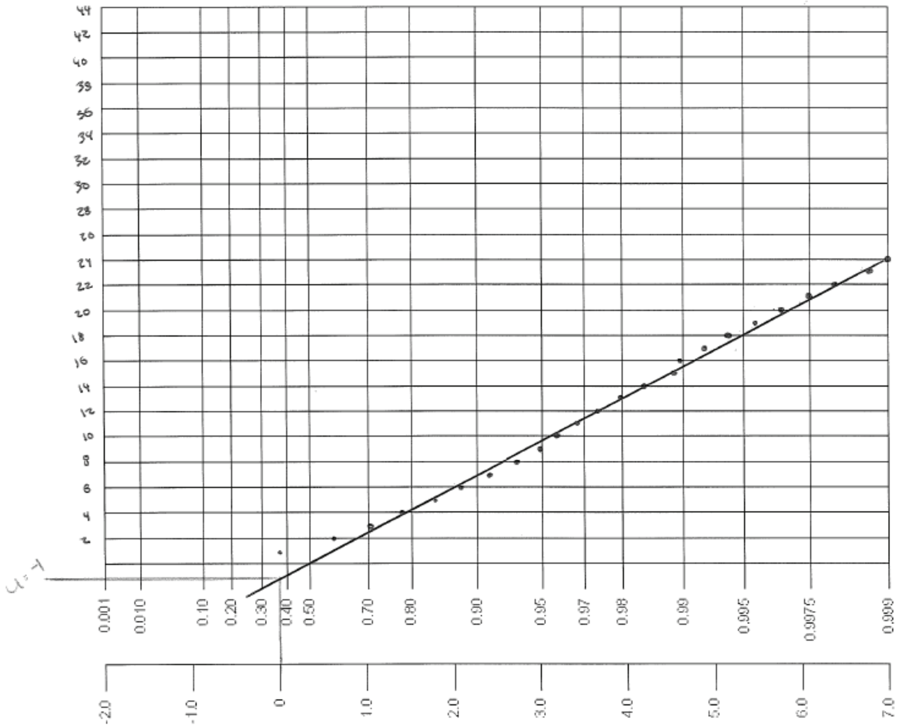

$\frac{1}{\alpha} = \frac{(24 - -1)}{(7-0)}$

$= 3.57$

$\alpha = 0.28$

#7 D-T

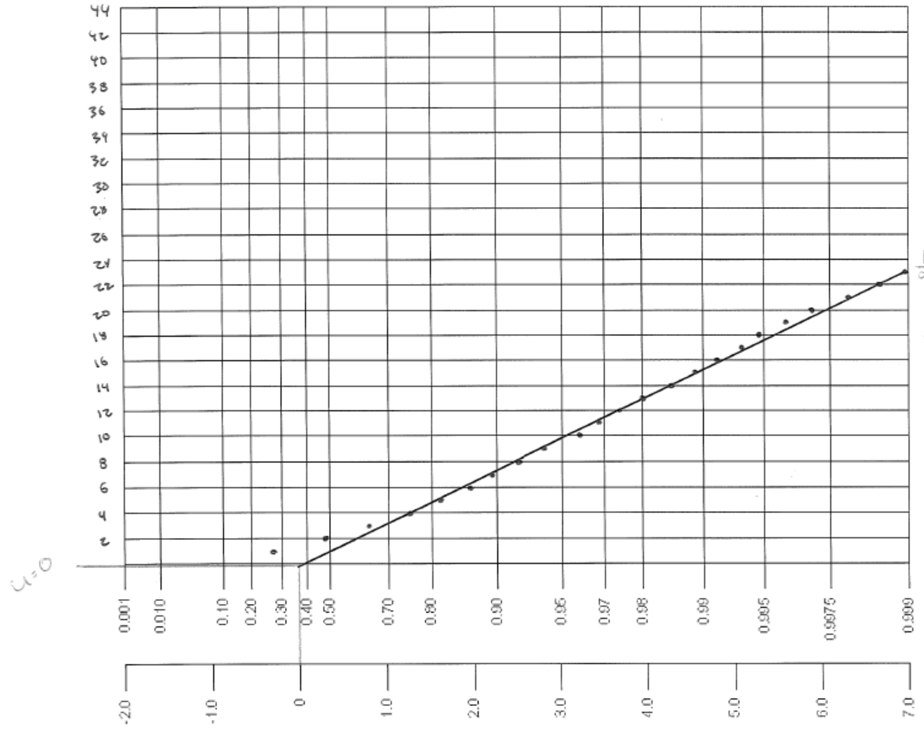

$\frac{1}{\alpha} = \frac{(23-0)}{(7-0)}$

$= 3.3$

$\alpha = 0.30$

#7 D-B

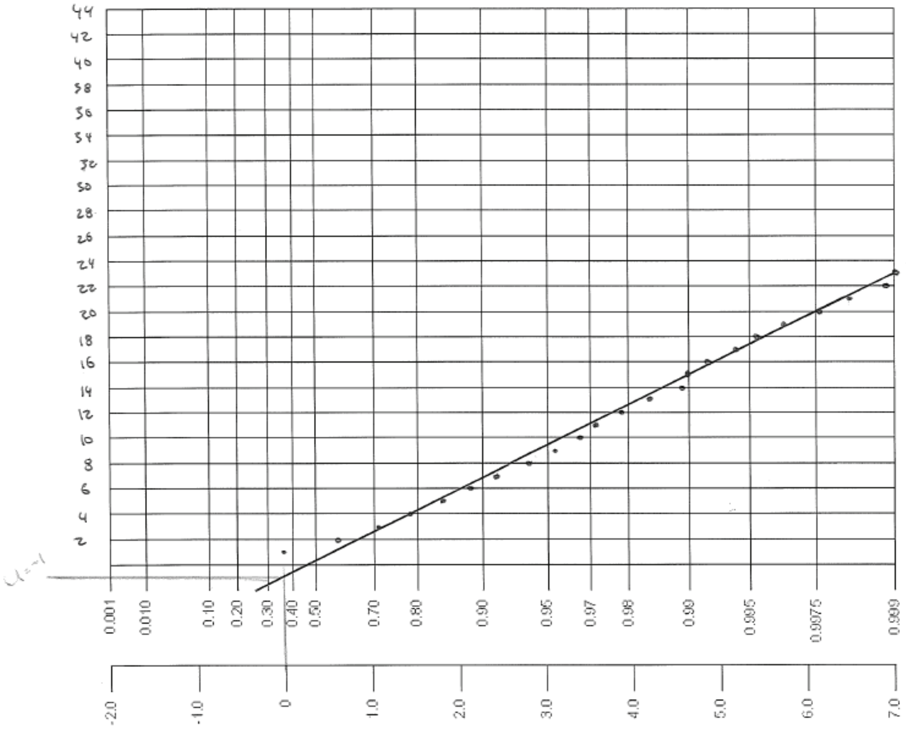

$\frac{1}{\alpha} = \frac{(23- -1)}{(7-0)}$

$= 3.43$

$\alpha = 0.29$

#8 D-T

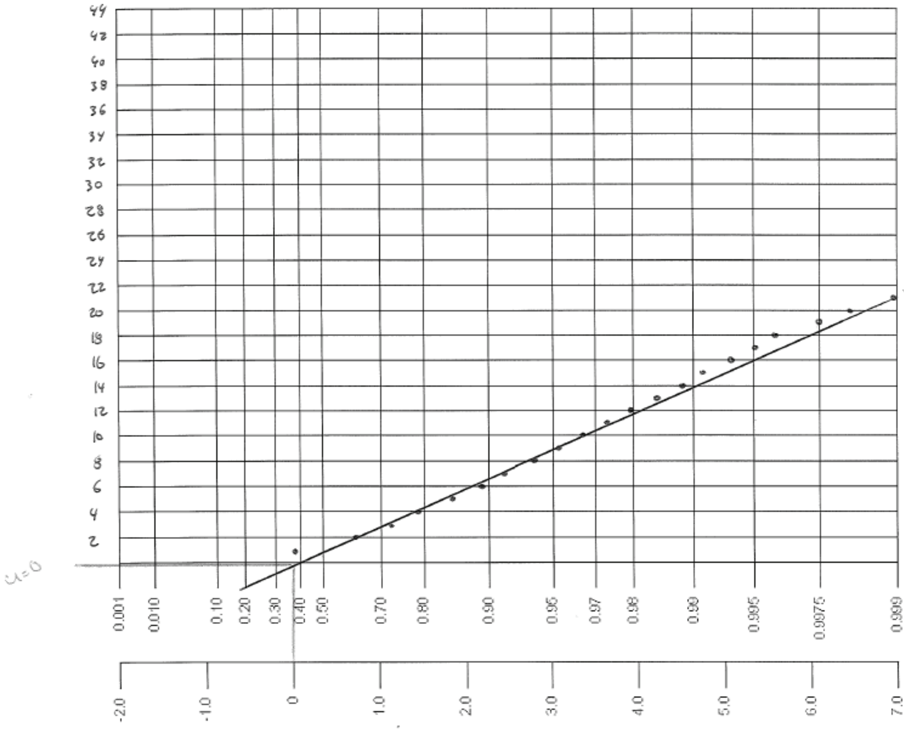

$\frac{1}{\alpha} = \frac{(21-0)}{(7-0)}$

$= 3.0$

$\alpha = 0.33$

#8 D-B

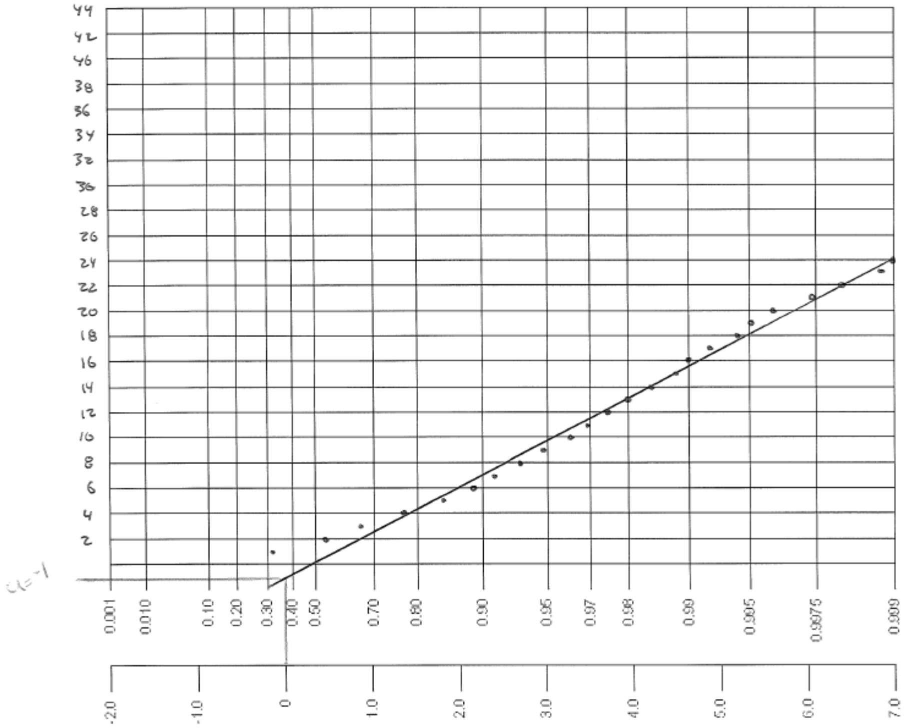

$\frac{1}{\alpha} = \frac{(24-1)}{(7-0)}$

$= 3.57$

$\alpha = 0.28$

#9 D-T

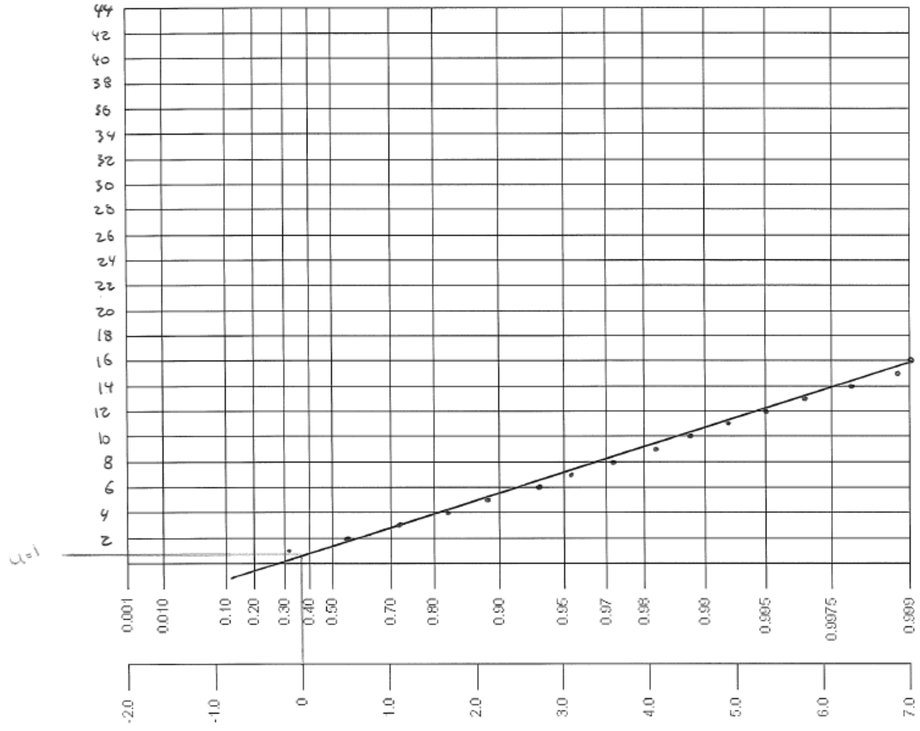

$\frac{1}{\alpha} = \frac{(16-1)}{(7-0)}$

$= 2.14$

$\alpha = 0.47$

#9 D-B

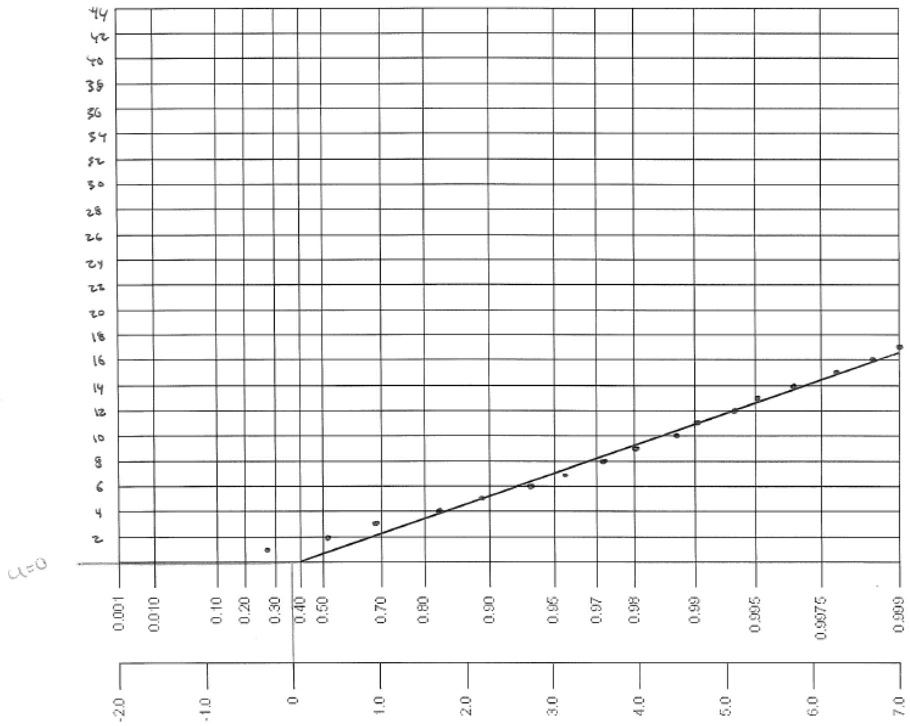

$\frac{1}{\alpha} = \frac{(17-0)}{(7-0)}$

$= 2.43$

$\alpha = 0.41$

#10 D-T

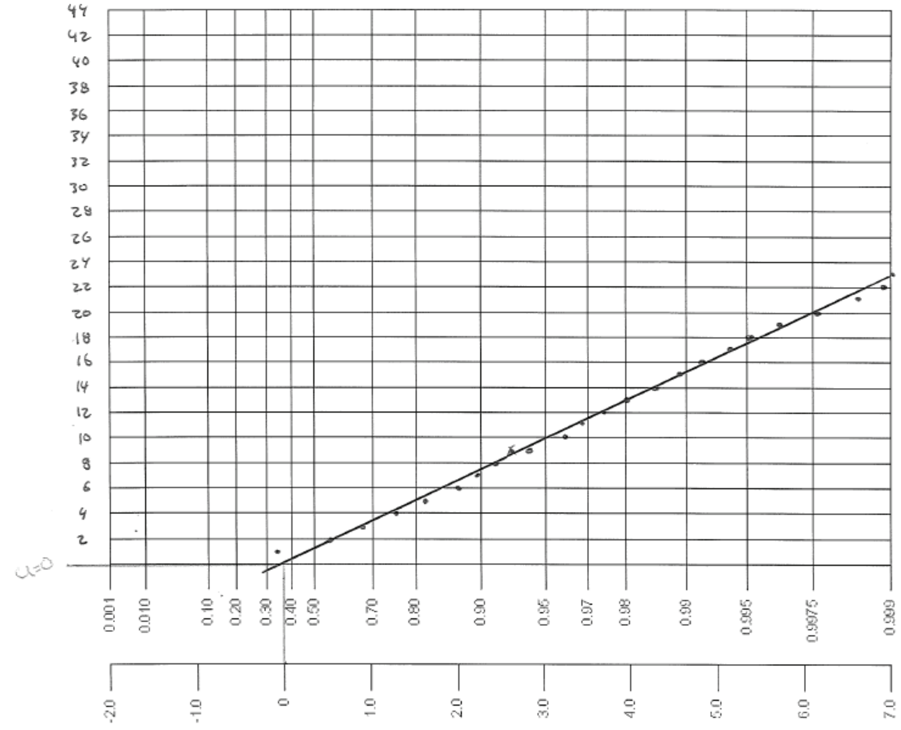

$\frac{1}{\alpha} = \frac{(23-0)}{(7-0)}$

$= 3.29$

$\alpha = 0.30$

#10 D-B

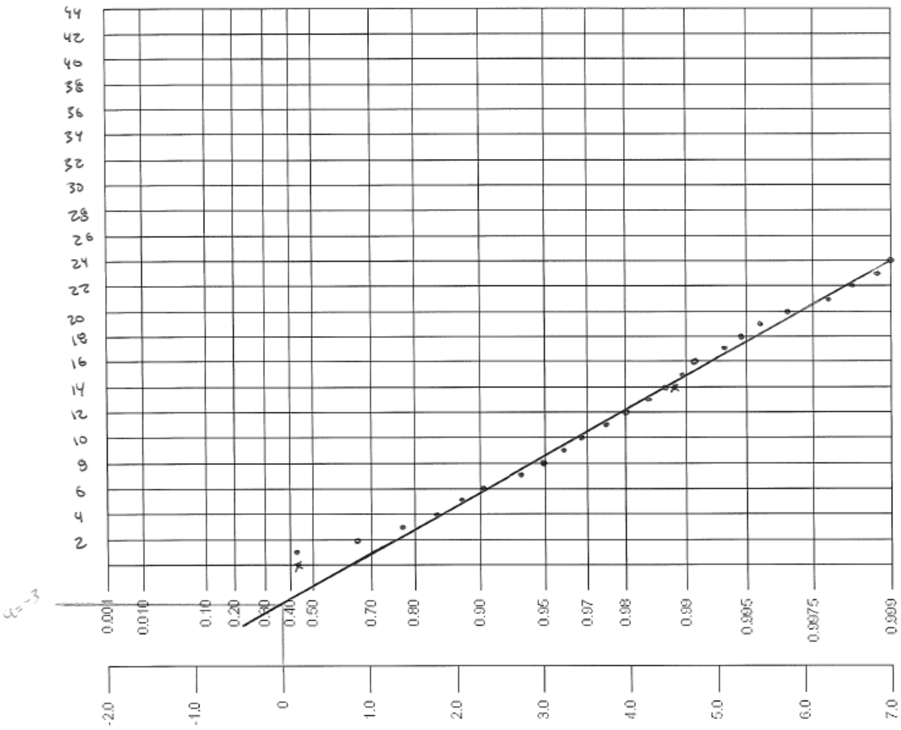

$\frac{1}{\alpha} = \frac{(24 - -3)}{(7-0)}$

$= 3.86$

$\alpha = 0.26$

#11 D-T

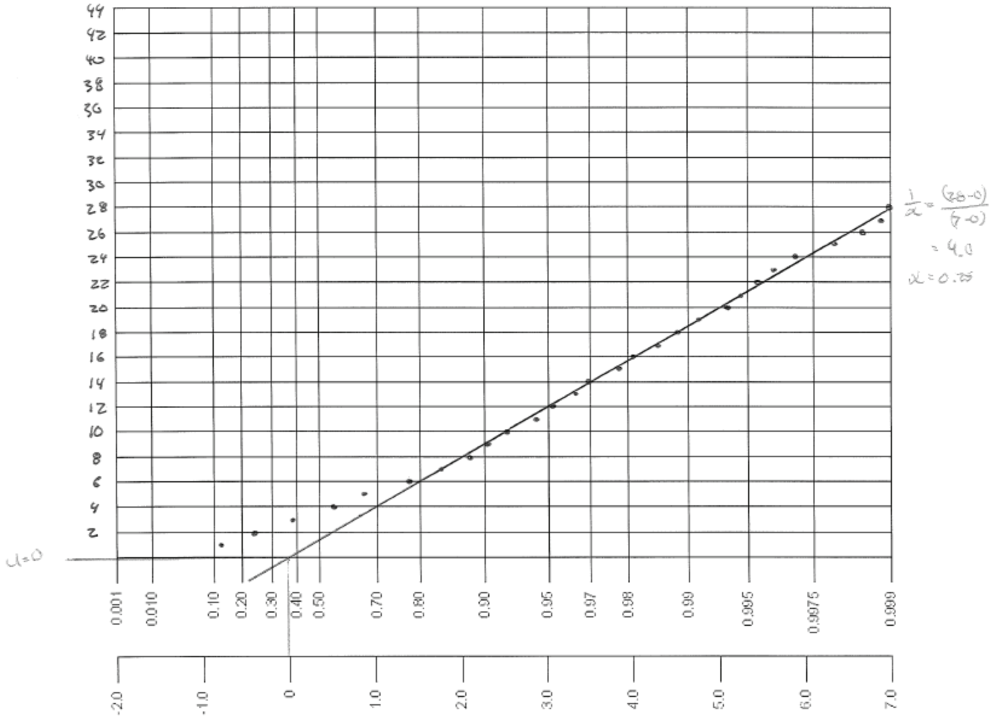
44
42
40
38
36
34
32
30
28
26
24
22
20
18
16
14
12
10
8
6
4
2
u=0
0.001
0.010
0.10
0.20
0.30
0.40
0.50
0.70
0.80
0.90
0.95
0.97
0.98
0.99
0.995
0.9975
0.999
-2.0
-1.0
0
1.0
2.0
3.0
4.0
5.0
6.0
7.0
$\frac{1}{\alpha} = \frac{(28-0)}{(7-0)}$
$= 4.0$
$\alpha = 0.25$

#11 D-B

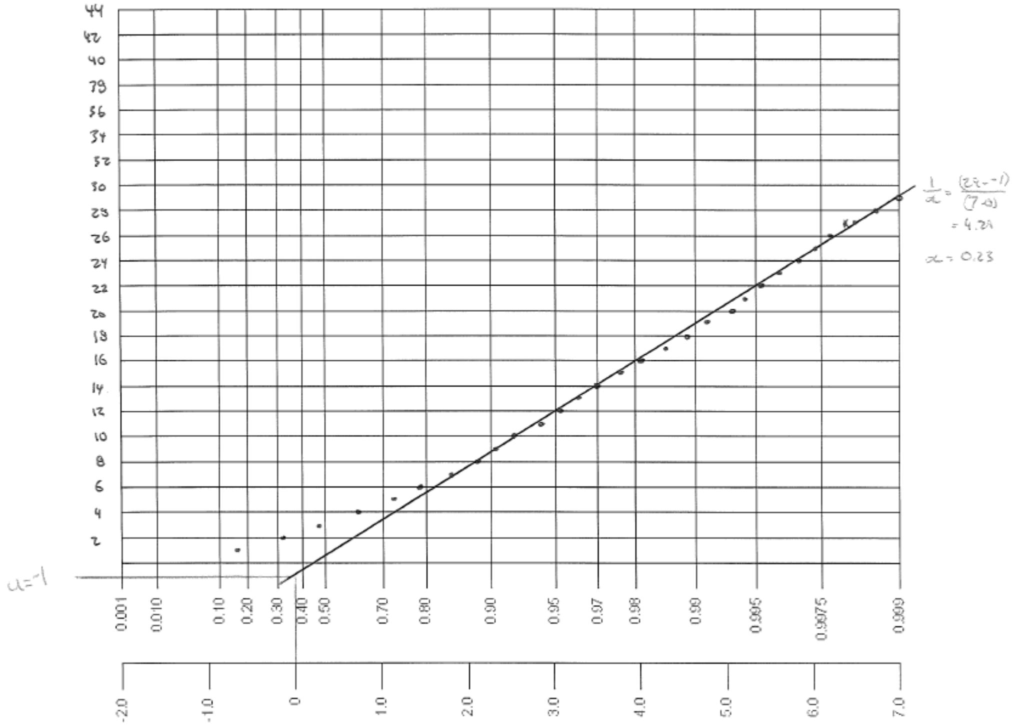
44
42
40
38
36
34
32
30
28
26
24
22
20
18
16
14
12
10
8
6
4
2
u=-1
0.001
0.010
0.10
0.20
0.30
0.40
0.50
0.70
0.80
0.90
0.95
0.97
0.98
0.99
0.995
0.9975
0.999
-2.0
-1.0
0
1.0
2.0
3.0
4.0
5.0
6.0
7.0
$\frac{1}{\alpha} = \frac{(29--1)}{(7-0)}$
$= 4.29$
$\alpha = 0.23$

#12 D-7

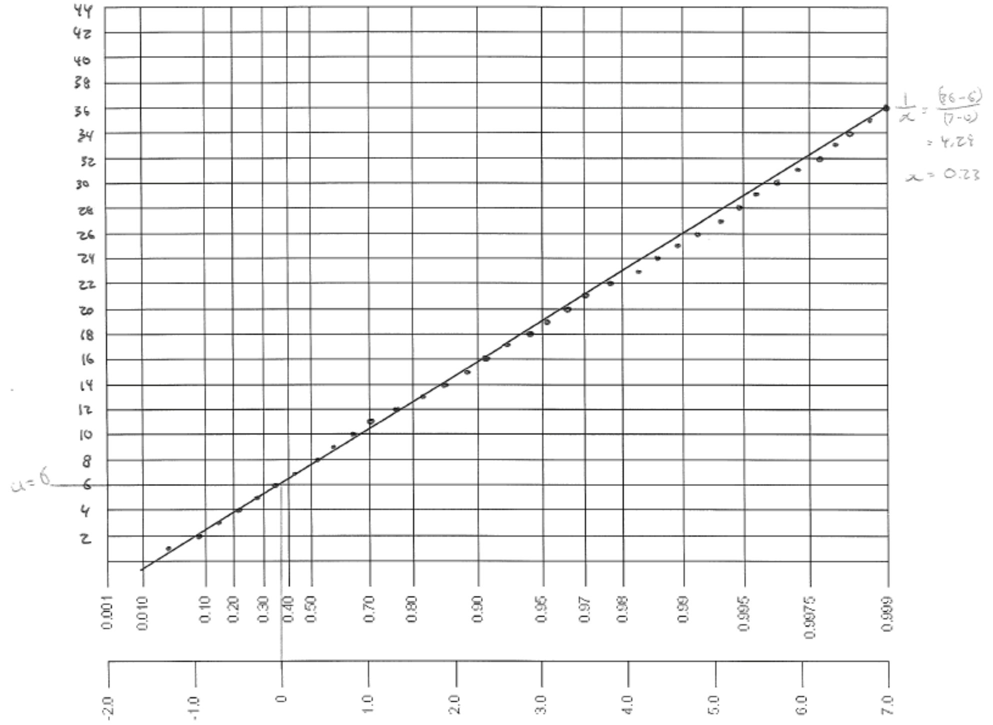

44
42
40
38
36
34
32
30
28
26
24
22
20
18
16
14
12
10
8
6
4
2
u=6
0.001
0.010
0.10
0.20
0.30
0.40
0.50
0.70
0.80
0.90
0.95
0.97
0.98
0.99
0.995
0.9975
0.999
-2.0
-1.0
0
1.0
2.0
3.0
4.0
5.0
6.0
7.0
$\frac{1}{\alpha} = \frac{(36-6)}{(7-0)}$
$= 4.28$
$\alpha = 0.23$

#12 D-B

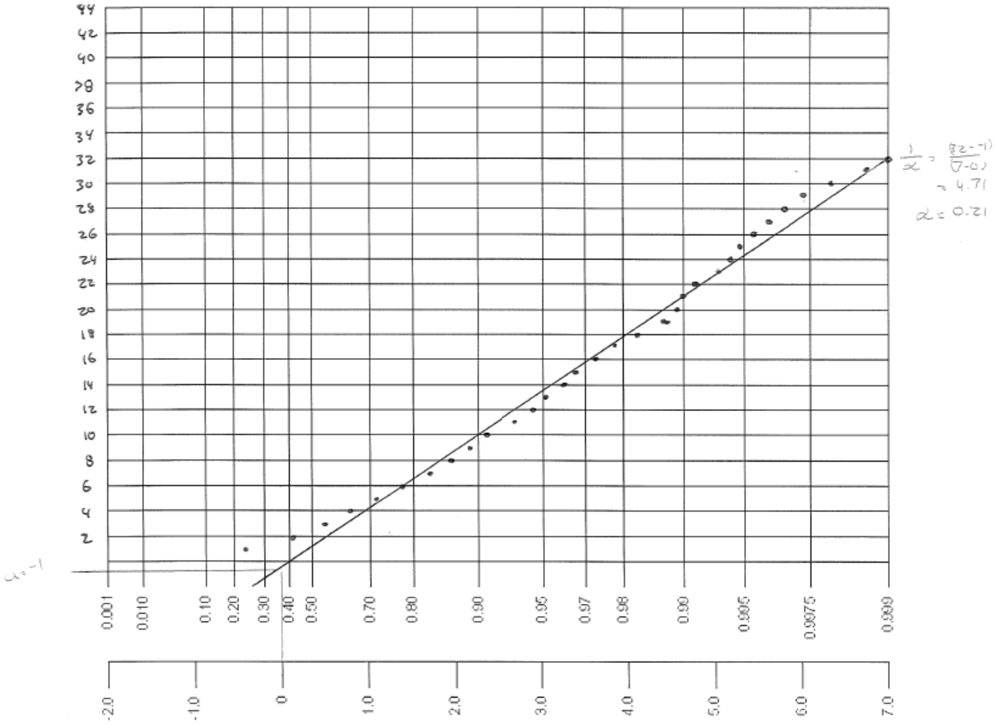

44
42
40
38
36
34
32
30
28
26
24
22
20
18
16
14
12
10
8
6
4
2
u=-1
0.001
0.010
0.10
0.20
0.30
0.40
0.50
0.70
0.80
0.90
0.95
0.97
0.98
0.99
0.995
0.9975
0.999
-2.0
-1.0
0
1.0
2.0
3.0
4.0
5.0
6.0
7.0
$\frac{1}{\alpha} = \frac{(32 - -1)}{(7-0)}$
$= 4.71$
$\alpha = 0.21$